AD_____

Award Number: DAMD17-02-1-0110

TITLE: “The Role of Nuclear Receptor Coactivators in Recurrent Prostate Cancer”

PRINCIPAL INVESTIGATOR: Elizabeth M. Wilson, Ph.D.

CONTRACTING ORGANIZATION: University of North Carolina at Chapel Hill
Chapel Hill, North Carolina 27599-1350

REPORT DATE: February 2006

TYPE OF REPORT: Final

PREPARED FOR: U.S. Army Medical Research and Materiel Command
Fort Detrick, Maryland 21702-5012

REPORT DOCUMENTATION PAGE

Form Approved
OMB No. 0704-0188

1. REPORT DATE *(DD-MM-YYYY)*	**2. REPORT TYPE**	**3. DATES COVERED** *(From - To)*
01-02-2006	Final	1 Feb 2002 – 31 Jan 2006

4. TITLE AND SUBTITLE

"The Role of Nuclear Receptor Coactivators in Recurrent Prostate Cancer"

5a. CONTRACT NUMBER

5b. GRANT NUMBER
DAMD17-02-1-0110

5c. PROGRAM ELEMENT NUMBER

6. AUTHOR(S)

Elizabeth M. Wilson, Ph.D.

E-Mail: emw@med.unc.edu

5d. PROJECT NUMBER

5e. TASK NUMBER

5f. WORK UNIT NUMBER

7. PERFORMING ORGANIZATION NAME(S) AND ADDRESS(ES)

University of North Carolina at Chapel Hill
Chapel Hill, North Carolina 27599-1350

8. PERFORMING ORGANIZATION REPORT NUMBER

9. SPONSORING / MONITORING AGENCY NAME(S) AND ADDRESS(ES)
U.S. Army Medical Research and Materiel Command
Fort Detrick, Maryland 21702-5012

10. SPONSOR/MONITOR'S ACRONYM(S)

11. SPONSOR/MONITOR'S REPORT NUMBER(S)

12. DISTRIBUTION / AVAILABILITY STATEMENT
Approved for Public Release; Distribution Unlimited

13. SUPPLEMENTARY NOTES

14. ABSTRACT
See page 4 of this document.

15. SUBJECT TERMS - See page 4 of this document .

16. SECURITY CLASSIFICATION OF:			**17. LIMITATION OF ABSTRACT**	**18. NUMBER OF PAGES**	**19a. NAME OF RESPONSIBLE PERSON**
a. REPORT	**b. ABSTRACT**	**c. THIS PAGE**			USAMRMC
U	U	U	UU	83	**19b. TELEPHONE NUMBER** *(include area code)*

Standard Form 298 (Rev. 8-98)
Prescribed by ANSI Std. Z39.18

Table of Contents

Abstract

The purpose of our studies supported by this DOD award has been to characterize the signaling pathways and interacting proteins that contribute to increased androgen receptor (AR) mediated gene activation in recurrent prostate cancer. We have followed up our previous studies on the AR by focusing on the EGF and heregulin-induced signaling pathways. We have used traditional yeast two hybrid screening methods to identify two key regulatory proteins that interact with AR. In collaborative studies with Dr. James Mohler, the levels of several androgen metabolites were determined in prostate cancer tissue specimens. In collaboration with Robert Gampe at GlaxoSmithKline, we determined the structural basis for F*XX*LF and L*XX*LL motif binding to AR AF2 in the ligand binding domain. In collaboration with Dr. Shelly Earp, we determined the presence of HER2 and HER3 receptors in the CWR-R1 prostate cancer cell line derived from the CWR22 recurrent human xenograft propagated in nude mice. We established the functional basis for an AR mutation in prostate cancer that involves increased AR recruitment of the SRC/p160 coactivators. Previously we reported increased levels of SRC1 and TIF2 in prostate cancer specimens obtained after recurrent growth following androgen ablation therapy. As outlined below, our studies have led to several important conclusions regarding AR function in prostate cancer cells. Importantly, the work has set the stage for our continued experiments designed to understand AR functional activity in prostate cancer.

Subject terms/keywords

androgen receptor, coactivators, EGF, prostate cancer, F*XX*LF motif, L*XX*LL motif, HER2, HER3, CHIP, MAGE-11, dominant negative

Introduction

The objective of our studies has been to understand how the androgen receptor (AR) contributes to prostate cancer development and progression. In particular, we have performed studies to determine the role of EGF and heregulin-induced signaling pathways in AR transcriptional activity. We have sought to identify key AR interacting proteins that are modulated by MAP kinase signaling and determine how they increase AR activity in prostate cancer. Our statement of work was to:

1. Further evaluate the expression of SRC1 and TIF2 in androgen dependent and recurrent prostate cancer specimens and the CWR22 human prostate cancer xenograft model using quantitative immunohistochemistry.
2. Establish the effects of SRC1 and TIF2 overexpression and phosphorylation on AR function.
3. Identify the kinase signaling pathways involved in SRC1 and TIF2 phosphorylation and determine their growth promoting effects on prostate cancer cells.

During the funding period of this DOD Award, Christopher Gregory, the original grantee, left UNC Chapel Hill for a position in industry. The grant was reassigned by the US Army Medical Research and Materiel Command to Elizabeth M. Wilson, who carried on the project and who is submitting this final progress report. The work aims expanded somewhat during this transition to include AR interacting proteins that are influenced by SRC1 and TIF2 and are impacted by the EGF and heregulin-induced signaling pathways. There was a no-cost extension of the funding period from January 2005 through January 2006.

Body

Mechanism of EGF-induced increase in androgen receptor (AR) function–Growth of normal and neoplastic prostate is mediated by the AR. AR is highly expressed in recurrent prostate cancer cells

that proliferate despite reduced circulating androgen. We investigated the mechanisms involved in epidermal growth factor (EGF)-induced increase in AR transcriptional activity in recurrent prostate cancer cells. We showed that EGF and heregulin increase AR transactivation in the presence of androgen by increasing TIF2 phosphorylation mediated through MAP kinase signaling pathways. The response was blocked by IRESSA and GW2016, inhibitors of ErbB1 and ErbB2. EGF signaling increased coimmunoprecipitation of TIF2 and AR, and AR transactivation and its stimulation by EGF was reduced by siRNA inhibition of TIF2 expression. The data suggest that recurrent prostate cancer establishes an autocrine loop for TGFα/EGF and EGF receptors that is recapitulated in the recurrent CWR22 xenograft and CWR22-R1 cell line and that these signaling pathways increase AR transactivation in recurrent prostate cancer.

Gregory CW, Fei X, Ponguta LA, He B, Bill HM, French FS, Wilson EM 2004 Epidermal growth factor increases coactivation of the androgen receptor in recurrent prostate cancer. ***J Biol Chem*** 279:7119-7130

Androgen levels in recurrent prostate cancer tissue–Prostate cancer that recurs after androgen deprivation therapy grows in the absence of testicular androgens. The concept of complete androgen blockade has recently come into question based on poor survival of men with advanced prostate cancer and high levels of expression of AR and AR regulated genes. The androgen axis was evaluated in tissue specimens of recurrent prostate cancer after androgen deprivation therapy and in benign prostate specimens. Immunohistochemical analysis was performed using antigen-retrieval, monoclonal AR antibody and automated digital video image analysis. Steroid hormones were assayed in extracts of frozen tissue using RIA. AR immunostaining in recurrent prostate cancer was similar to that of benign prostate. Tissue levels of DHT (1.12 nM), DHEA, DHEA sulfate and androstenedione were lower in recurrent cancer in castrate men than in benign prostate. Tissue levels of testosterone were similar in recurrent prostate cancer (3.25 nM) and benign prostate (3.27 nM). Tissue levels of the androgen regulated gene product PSA, were 1/10 the level in benign prostate, a ratio similar to that described for benign and androgen stimulated prostate cancer reported by others. We concluded that testosterone and DHT occur in recurrent prostate cancer tissue at levels sufficient to activate AR. With prostate cancer recurrence, complete androgen blockade does not significantly alter tissue testosterone levels.

Mohler JL, Gregory CW, Ford OH, Kim D, Weaver CM, Petrusz P, Wilson EM, French FS 2004 The androgen axis in recurrent prostate cancer, ***Clin Can Res*** 10:440-448

A role for HER2 (Erb2) and HER3 (ErbB3) in AR activation–In prostate tumors that recur after androgen withdrawal, AR is highly expressed and transcriptionally active in the absence of testicular androgens. Alternative means of AR activation have been invoked, including regulation by growth factors and their receptors in prostate cancer recurrence. Stimulation by EGF and heregulin activates downstream signaling, including mitogen activated protein kinase and PI3-kinase and Akt pathways. Here we show HER receptor tyrosine kinases 1 through 4 are expressed in CWR-R1 cell line derived from the CWR22 recurrent prostate cancer xenograft. Heregulin activates HER2 (ErbB2) and HER3 (ErbB3) and increases androgen dependent AR activation of reporter genes in CWR-R1 cells. Basal proliferation in the absence of growth factors was inhibited by the HER1 (ErbB1) and HER2 (ErbB2) inhibitor GW572016 (lapatinib) to a greater extent than the HER1 (ErbB1) specific inhibitor ZD1839 (gefitinib), suggesting that low level HER2 and HER3 activation by an autocrine pathway promotes cell proliferation. The data indicate that heregulin signaling through HER2 and HER3 increases AR transactivation and alters growth in a recurrent prostate cancer cell line. Inhibition of low level HER2 signaling may be a potential novel therapeutic strategy in prostate cancer.

Gregory CW, Whang YE, McCall W, Fei X, Liu Y, Ponguta LA, French FS, Wilson EM, Earp HS 2005 Heregulin-induced activation of HER2 and HER3 increases androgen receptor transactivation and CWR-R1 human recurrent prostate cancer cell growth, ***Clin Cancer Res*** 11:1704-1712

Repression of AR function and proliferation of the recurrent prostate cancer CWR-R1 cell line using dominant negatives and RNA interference–Our objective was to inhibit AR and decrease AR transactivation and decrease prostate cancer cell proliferation. We transiently transfected two dominant negative AR mutants (AR122-HDAC-KRAB and ARΔ142-337) and AR siRNA in CWR-R1 prostate cancer cells to determine the effect on DHT and DHT plus EGF-mediated AR transactivation using MMTV- and PSA-luciferase reporter genes. We also targeted AR coactivators TIF2 and SRC1 by transfecting double-stranded siRNAs for RNA interference. We performed cell proliferation assays comparing transfected and untransfected CWR-R1 cells with and without DHT to establish the effects on cell proliferation. We found that the dominant negative AR mutants and AR siRNA repress AR transcriptional activation and inhibit cell proliferation ~50%. Silencing the SRC/p160 coactivators resulted in 75-90% inhibition of DHT and DHT plus EGF-mediated AR transactivation. Our data indicate that proliferation of CWR-R1 cells can be inhibited by directly silencing AR by expressing dominant negative AR protein or AR siRNA and that AR transactivation is decreased by targeting the AR coactivators SRC1 and TIF2.

Ponguta LA, Bill HM, Fei X, Chen Y, Gregory CW 2004 Repression of androgen receptor function and cellular proliferation in the CWR-R1 recurrent prostate cancer cell line with dominant negatives and RNA interference. ***FASEB J*** 18:A935 (Selected for the Chugai Award Lecture and Symposium for Young Investigators, American Society for Investigative Pathology Minisymposium, Experimental Biology Meeting 2004, Washington, DC.)

Identification of CHIP as an AR interacting protein that increases the degradation of AR–The NH_2-terminal sequence of steroid receptors is highly variable between different receptors and among the same receptor from different species. Two activation regions of the AR NH_2-terminal region, AF1 and AF3, lack significant sequence conservation across species. It is likely that the NH_2-terminal activation domains evolved in parallel with their interacting partners. In contrast, the carboxyl-terminal region of steroid receptors, including AF2, is structurally conserved.

To better understand the functional properties of the AR NH_2-terminal domain, we initiated a structure-function study by searching for evolutionarily conserved sequences that predict a critical role in AR function. Our approach was based in part on studies of the AR NH_2-terminal FXXLF motif, which is one of few highly conserved regions in the AR NH_2-terminal domain. A primary sequence homology comparison identified a 14 amino acid conserved region of human AR with the sequence ^{234}AKELCKAVSVSMGL^{247} that is common in AR from all species reported including the lower vertebrates. Presence of the conserved sequence in AR and a homologous sequence in GR and absence from other steroid receptors suggests convergent evolution.

Based on the premise that strict amino acid sequence conservation predicts a site of critical function, we investigated the functional importance of human AR residues 234-247 using a yeast two hybrid screen. CHIP, the carboxyl-terminus of Hsp70-interacting protein, was identified as a binding partner. We found that CHIP functions as a negative regulator of AR transcriptional activity by promoting AR degradation. Our results suggest that the AR NH_2-terminal domain contains an evolutionarily conserved NH_2-terminal signature motif that functions to limit AR transcriptional activity. The conserved motif lacks intrinsic transcriptional activity per se, but contributes to the transcriptional response of a larger region between residues 220-270. The work demonstrates that the combination of comparative sequence alignment and yeast two hybrid screening using short conserved peptides as bait is an effective strategy to probe the structure–function relationships of steroid receptor NH_2-terminal domains and other intrinsically unstructured transcriptional regulatory proteins. CHIP is highly conserved across species and interacts with a sequence that is strictly conserved through the entire AR gene family. Coexpression studies show that CHIP limits AR function most likely through its previously described role in ubiquitylation.

He B, Bai S, Hnat AT, Kalman RI, Minges JT, Patterson C, Wilson EM 2004 An androgen receptor NH_2-terminal signature motif interacts with carboxyl terminus of Hsp70-interacting protein CHIP. ***J Biol Chem*** 279:30643-30653

Identification of MAGE-11 as an AR interacting protein that modulates AR activity–Gene activation by steroid hormone receptors involves the recruitment of the SRC/p160 coactivator L*XX*LL motifs to activation function 2 (AF2) in the ligand binding domain. For AR, AF2 also serves as the interaction site for the AR NH_2-terminal F*XX*LF motif in the androgen dependent NH_2- and carboxyl (N/C) interaction. The relative importance of the AR AF2 site was unclear since the AR F*XX*LF motif interferes with coactivator recruitment by competitive inhibition of L*XX*LL motif binding. Preference for F*XX*LF binding by AF2, but adaptability to coactivator L*XX*LL motif binding, brought into question the role of the SRC/p160 family of coactivators in AR functional activity. These observations led us to postulate the existence of an AR coregulator that binds the AR F*XX*LF motif that could expose the AF2 site to coactivator binding.

We made use of the AR NH_2-terminal F*XX*LF peptide as bait in a yeast two hybrid screen of a human testis library and identified the melanoma antigen gene product, MAGE-11, as a novel AR coregulator that specifically binds the AR NH_2-terminal F*XX*LF motif. The molecular interaction between AR and MAGE-11 in the absence and presence of androgen is supported by their intracellular colocalization, coimmunoprecipitation, GST affinity matrix binding, and by MAGE-11-induced increases in AR transcriptional activity and ligand dissociation. MAGE-11 forms a stable complex with the ligand free AR that results in increased AR stability in the absence of androgen. Increased AR stabilization in the absence of androgen raises AR protein levels, which likely contributes to the increase in AR transcriptional activity in the presence of MAGE-11. In contrast, binding of a strong agonist such as DHT decreases the association between AR and MAGE-11. This is consistent with competition by MAGE-11 for the androgen-induced interaction between the AR F*XX*LF motif and AF2.

We found that MAGE-11 competes for the androgen-induced AR N/C interaction by specifically binding the AR F*XX*LF motif and relieves inhibition at AF2. Binding of MAGE-11 to the AR F*XX*LF α helical region stabilizes the ligand-free AR, and in presence of an agonist, increases exposure of AF2 to the recruitment and activation by the SRC/p160 coactivators. Intracellular association between AR and MAGE-11 is supported by their coimmunoprecipitation and colocalization in the absence and presence of hormone and by competitive inhibition of the N/C interaction. AR transactivation increases in response to MAGE-11 and the SRC/p160 coactivators through mechanisms that include, but are not limited to the AF2 site. MAGE-11 is expressed in androgen dependent tissues, with highest levels in human testis, and in prostate cancer cell lines in parallel with AR expression levels. The results suggest that MAGE-11 is a unique AR coregulator that increases AR activity by modulating the AR interdomain interaction.

Bai S, He B, Wilson EM 2005 Melanoma antigen gene protein MAGE-11 regulates androgen receptor function by modulating the interdomain interaction. ***Mol Cell Biol*** 25:1238-1257

Structural characterization of F*XX*LF and L*XX*LL motif binding to the AR ligand binding domain–In contrast to other nuclear receptors that bind the L*XX*LL motifs of coactivators, the AR ligand binding domain is preferentially engaged in an interdomain interaction with the AR F*XX*LF motif known as the N/C interaction. Weak transactivation by AR AF2 results in part from evolving sequence changes that reduce L*XX*LL motif binding. Concurrently, the AR F*XX*LF motif evolved with the expanding NH_2-terminal AF1 and avidly binds AF2, further limiting coactivator recruitment by competitive binding at AF2.

In a collaborative study with Robert Gampe at GlaxoSmithKline, we determined the molecular basis for F*XX*LF and L*XX*LL motif binding to AF2 based on a comparison of F*XX*LF and L*XX*LL peptide-bound and peptide-free AR ligand binding domain crystal structures and site directed mutagenesis. We show that AR amino acid residues 20-30 containing the F*XX*LF motif and TIF2 residues 740-753 containing the third L*XX*LL motif, bind AR AF2. The F*XX*LF motif peptide binds with an intact primary charge clamp and better recognition conferring hydrophobic contacts than does the L*XX*LL motif. Key amino acid residues were identified that differentiate F*XX*LF motif binding. Differential binding affinity and specificity are established by distinct electrostatic and hydrophobic interactions revealed in the AR-R1881 crystal structures bound with AR F*XX*LF and TIF2-III L*XX*LL peptides. Through an induced fit

mechanism, AR 20-30 contacts E897 with classical charge clamp H-bonding that is absent in the bound TIF2 third L*XX*LL motif. Although new distant contacts form between the TIF2-III L*XX*LL motif and AR, the interactions apparently provide insufficient energy to recover what might arise from close NH_2-terminal backbone H-bonds with E897. More importantly, selective high affinity binding by AR AF2 of phenylalanines in F*XX*LF suggests that the hydrophobic character, size and complementarity contribute a substantial nonpolar binding energy. The crystal structures show that the AR AF2 solvent exposed hydrophobic cleft shelters hydrophobic residues of bound amphipathic peptides from the solvent shell. We also show that evolving sequence changes decrease L*XX*LL binding by PR and GR AF2, with increasing size and functional importance of AF1.

The data suggest a transition in dominant transactivation domains from AF2 to AF1 during nuclear receptor evolution. An activation function transition hypothesis is proposed that suggests an evolutionary decline in L*XX*LL motif binding that parallels expansion and functional dominance of the NH_2-terminal transactivation domain in the steroid receptor subfamily.

He B, Gampe RT, Kole AJ, Hnat AT, Stanley TB, An G, Stewart EL, Kalman RI, Minges JT, Wilson EM 2004 Structural basis for androgen receptor interdomain and coactivator interactions suggests a transition in nuclear receptor activation function dominance. ***Mol Cell*** 16:425-438

Probing the functional link between androgen receptor coactivator and ligand binding sites in prostate cancer and androgen insensitivity–The androgen receptor (AR) is a ligand activated transcription factor required for male sex development and virilization and contributes to prostate cancer initiation and progression. High affinity androgen binding triggers conformational changes required for AR transactivation. In this report we characterized naturally occurring AR gene mutations in the region of activation function 2 (AF2) that decrease or increase AR transcriptional activity by altering the region bounded by AF2 and the ligand binding pocket without affecting equilibrium androgen binding affinity. In the androgen insensitivity syndrome, germline AR mutations increase the androgen dissociation rate and reduce AR F*XX*LF motif binding and the recruitment of steroid receptor coactivator (SRC)/p160 coactivator L*XX*LL motifs. In prostate cancer, somatic AR mutations in AF2 or near the bound ligand slow androgen dissociation and increase AR stabilization and coactivator recruitment. Crystal structures of the AR ligand binding domain bound to R1881 and F*XX*LF or L*XX*LL motif peptide indicate the mutations are proximal to the AF2 bound peptide, adjacent to the ligand pocket, or in a putative ligand gateway. The results suggest a bidirectional structural relay between bound ligand and coactivator that establishes AR functional potency in vivo.

He B, Gampe RT, Hnat AT, Faggart JL, Minges JT, French FS, Wilson EM 2006 Probing the functional link between androgen receptor coactivator and ligand binding sites in prostate cancer and androgen insensitivity. ***J Biol Chem*** 281:6648-6663

Key research accomplishments

- EGF and heregulin increase AR transactivation in the presence of androgen by increasing TIF2 phosphorylation mediated through MAP kinase signaling pathways.
- Although tissue levels of DHT, DHEA, DHEA sulfate and androstenedione were lower in recurrent cancer in castrate men than in benign prostate, tissue levels of testosterone were similar in recurrent prostate cancer (3.25 nM) and benign prostate (3.27 nM).
- HER receptor tyrosine kinases 1 through 4 are expressed in CWR-R1 cell line derived from the CWR22 recurrent prostate cancer xenograft. Heregulin activates HER2 (ErbB2) and HER3 (ErbB3) and increases androgen dependent AR activation of reporter genes in CWR-R1 cells.
- Dominant negative mediators of AR transcriptional activity inhibit the proliferation of CWR-R1 prostate cancer cells.
- CHIP, the carboxyl-terminus of Hsp70-interacting protein, is an AR binding partner that functions as a negative regulator of AR transcriptional activity by promoting AR degradation.

- The melanoma antigen gene product, MAGE-11, was identified as a novel AR coregulator that specifically binds the AR NH_2-terminal F*XX*LF motif and regulates AR transcriptional activity by exposing the AF2 site in the ligand binding domain.
- AR20-30 containing the F*XX*LF motif binds with an intact primary charge clamp and better recognition conferring hydrophobic contacts than does TIF2-740-753 containing the third L*XX*LL motif as revealed in the AR-R1881 crystal structures. Through an induced fit mechanism, AR 20-30 contacts E897 with classical charge clamp H-bonding that is absent in the bound TIF2-III.
- The structural basis for several AR mutations in prostate cancer was determined based on the crystal structures of the wild-type AR. Several mutations slow the dissociation rate of the bound androgen leading to a more transcriptionally active AR in prostate cancer.
- By characterizing AR mutations in prostate cancer, a bidirectional structural relay was identified between the bound ligand and coactivator that establish AR functional potency in vivo.

Reportable outcomes: Publications

1. Gregory CW, Fei X, Ponguta LA, He B, Bill HM, French FS, Wilson EM 2004 Epidermal growth factor increases coactivation of the androgen receptor in recurrent prostate cancer. ***J Biol Chem*** 279:7119-7130
2. Mohler JL, Gregory CW, Ford OH, Kim D, Weaver CM, Petrusz P, Wilson EM, French FS 2004 The androgen axis in recurrent prostate cancer, ***Clin Can Res*** 10:440-448
3. Ponguta LA, Bill HM, Fei X, Chen Y, Gregory CW 2004 Repression of androgen receptor function and cellular proliferation in the CWR-R1 recurrent prostate cancer cell line with dominant negatives and RNA interference. ***FASEB J*** 18:A935 (Selected for the Chugai Award Lecture and Symposium for Young Investigators, American Society for Investigative Pathology Minisymposium, Experimental Biology Meeting 2004, Washington, DC.)
4. He B, Bai S, Hnat AT, Kalman RI, Minges JT, Patterson C, Wilson EM 2004 An androgen receptor NH_2-terminal signature motif interacts with carboxyl terminus of Hsp70-interacting protein CHIP. ***J Biol Chem*** 279:30643-30653
5. He B, Gampe RT, Kole AJ, Hnat AT, Stanley TB, An G, Stewart EL, Kalman RI, Minges JT, Wilson EM 2004 Structural basis for androgen receptor interdomain and coactivator interactions suggests a transition in nuclear receptor activation function dominance. ***Mol Cell*** 16:425-438
6. Gregory CW, Whang YE, McCall W, Fei X, Liu Y, Ponguta LA, French FS, Wilson EM, Earp HS 2005 Heregulin-induced activation of HER2 and HER3 increases androgen receptor transactivation and CWR-R1 human recurrent prostate cancer cell growth, ***Clin Cancer Res*** 11:1704-1712
7. Bai S, He B, Wilson EM 2005 Melanoma antigen gene protein MAGE-11 regulates androgen receptor function by modulating the interdomain interaction. ***Mol Cell Biol*** 25:1238-1257
8. Gregory CW, Whang YE, McCall W, Fei X, Liu Y, Ponguta LA, French FS, Wilson EM, Earp HS 2005 Heregulin-induced activation of HER2 and HER3 increases androgen receptor transactivation and CWR-R1 human recurrent prostate cancer cell growth, ***Clin Cancer Res*** 11:1704-1712
9. He B, Gampe RT, Hnat AT, Faggart JL, Minges JT, French FS, Wilson EM 2006 Probing the functional link between androgen receptor coactivator and ligand binding sites in prostate cancer and androgen insensitivity. ***J Biol Chem*** 281:6648-6663
10. The CWR-R1 cell line was established from the recurrent CWR22 human xenograft and characterized.

Conclusions

The goal of our studies has been to characterize the functional properties of AR that contribute to increased cell proliferation in recurrent prostate cancer. We have identified two key AR interacting proteins that modulate AR activity in prostate cancer: CHIP (carboxyl-terminus of Hsp70-interacting protein) and MAGE-11 (melanoma antigen gene product). We have clarified the interrelationship between EGF signaling pathways and AR activity in prostate cancer cells. We have established the structural basis for the AR NH_2-terminal F*XX*LF motif and SRC/p160 coactivator L*XX*LL motif interaction with the AF2 region of the AR ligand binding domain. Our studies continue to focus on the role of CHIP and MAGE-11 on AR activity in prostate cancer cells. In addition, we are directing our

efforts to neutralize AR activity in recurrent prostate cancer as a possible means for therapeutic intervention. We are pursuing direct interactions between SRC1 and TIF2 with MAGE-11 and their combined effects on AR transcriptional activity.

References (NA)

Appendices

1. Gregory CW, Fei X, Ponguta LA, He B, Bill HM, French FS, Wilson EM 2004 Epidermal growth factor increases coactivation of the androgen receptor in recurrent prostate cancer. ***J Biol Chem*** 279:7119-7130
2. He B, Bai S, Hnat AT, Kalman RI, Minges JT, Patterson C, Wilson EM 2004 An androgen receptor NH_2-terminal signature motif interacts with carboxyl terminus of Hsp70-interacting protein CHIP. ***J Biol Chem*** 279:30643-30653
3. He B, Gampe RT, Kole AJ, Hnat AT, Stanley TB, An G, Stewart EL, Kalman RI, Minges JT, Wilson EM 2004 Structural basis for androgen receptor interdomain and coactivator interactions suggests a transition in nuclear receptor activation function dominance. ***Mol Cell*** 16:425-438
4. Bai S, He B, Wilson EM 2005 Melanoma antigen gene protein MAGE-11 regulates androgen receptor function by modulating the interdomain interaction. ***Mol Cell Biol*** 25:1238-1257
5. He B, Gampe RT, Hnat AT, Faggart JL, Minges JT, French FS, Wilson EM 2006 Probing the functional link between androgen receptor coactivator and ligand binding sites in prostate cancer and androgen insensitivity. ***J Biol Chem*** 281:6648-6663

THE JOURNAL OF BIOLOGICAL CHEMISTRY
Vol. 279, No. 8, Issue of February 20, pp. 7119–7130, 2004

Printed in U.S.A.

Epidermal Growth Factor Increases Coactivation of the Androgen Receptor in Recurrent Prostate Cancer*

Received for publication, July 16, 2003, and in revised form, December 2, 2003
Published, JBC Papers in Press, December 8, 2003, DOI 10.1074/jbc.M307649200

Christopher W. Gregory‡§¶, Xiaoyin Fei‡‖, Liliana A. Ponguta¶, Bin He‡‖, Heather M. Bill¶, Frank S. French‡§‖, and Elizabeth M. Wilson‡§‖**‡‡**

*From the ‡Laboratories for Reproductive Biology, §Lineberger Comprehensive Cancer Center, and the Departments of ¶Pathology and Laboratory Medicine, ‖Pediatrics, and **Biochemistry and Biophysics, University of North Carolina, Chapel Hill, North Carolina 27599-7500*

Growth of normal and neoplastic prostate is mediated by the androgen receptor (AR), a ligand-dependent transcription factor activated by high affinity androgen binding. The AR is highly expressed in recurrent prostate cancer cells that proliferate despite reduced circulating androgen. In this report, we show that epidermal growth factor (EGF) increases androgen-dependent AR transactivation in the recurrent prostate cancer cell line CWR-R1 through a mechanism that involves a post-transcriptional increase in the p160 coactivator transcriptional intermediary factor 2/glucocorticoid receptor interacting protein 1 (TIF2/GRIP1). Site-specific mutagenesis and selective MAPK inhibitors linked the EGF-induced increase in AR transactivation to phosphorylation of TIF2/GRIP1. EGF signaling increased the coimmunoprecipitation of TIF2 and AR. AR transactivation and its stimulation by EGF were reduced by small interfering RNA inhibition of TIF2/GRIP1 expression. The data indicate that EGF signaling through MAPK increases TIF2/GRIP1 coactivation of AR transactivation in recurrent prostate cancer.

Prostate cancer is a common disease in men that initiates in an environment of abundant circulating androgen. Proliferation of androgen-dependent prostate cancer cells is mediated by the androgen receptor (AR),[1] a ligand-dependent transcription factor that is activated by binding testosterone or dihydrotestosterone (DHT) (1–4). Androgen-induced cell proliferation is associated with the expression of an array of androgen-regulated genes (5, 6). Most prostate cancers regress in response to androgen deprivation therapy or anti-androgen treatment, reflecting their dependence on androgens for growth. Androgen deprivation results initially in reduced AR levels and reduced expression of androgen-regulated genes (7). Nevertheless, prostate cancers recur after a period of remission (8, 9). It has been suggested that prostate cancer recurrence occurs under selective pressure of androgen withdrawal or anti-androgen treatment and results from the clonal expansion of a subpopulation of cells that is independent of androgen for growth (10). The recurrence of prostate cancer after androgen deprivation is a major clinical challenge for improving disease outcome.

An abundance of evidence suggests that the AR is critical to recurrent prostate cancer growth despite reduced circulating androgen levels. AR is expressed in most recurrent prostate cancers (11) and is implicated in cancer growth by a cadre of androgen-regulated genes that continue to be expressed in the absence of testicular androgen (11–15). Recent studies show that selective AR inactivation using a ribozyme inhibits proliferation of LNCaP cells in culture (16). LNCaP prostate tumor growth and PSA secretion were inhibited *in vivo* using antisense oligonucleotides to inhibit AR expression (17).

To account for the functional importance of AR in recurrent prostate cancer, a number of adaptive mechanisms have been proposed (18). Each involves alternative pathways for increased AR activation. One compelling observation is that the AR gene is amplified in ~30% of prostate cancers, and AR levels are increased (9, 19–21). Higher AR expression would be expected to increase the sensitivity of prostate cancer cells to low androgen levels, as reported recently (22).

Mutation of the AR coding sequence is another mechanism for increased AR activation in late stage prostate cancer growth. Unlike mutations that cause androgen insensitivity by inactivating AR (23), most AR mutations identified in prostate cancer retain responsiveness to DHT (24–27). Some of these mutations broaden the ligand binding specificity, allowing additional steroids including adrenal androgens to induce AR transactivation (27–32). For some mutants, such as AR-T877A, in the LNCaP prostate tumor and derived cell lines, antagonists such as hydroxyflutamide gain agonist activity. AR mutations identified in prostate cancer include shorter than average CAG repeat lengths (33) associated with increased AR levels (34). The overall frequency of AR mutations in early stage disease is <5% (35), indicating that AR mutations do not account for prostate cancer initiation in most patients. The frequency of AR mutations increases in late stage recurrent prostate cancer (4, 35, 36) and may reflect adaptive changes to low androgen levels or anti-androgen treatment (37) or is in-

* This work was supported by NICHD, National Institutes of Health (NIH), United States Public Health Service Grants HD16910 and HD04466, NCI, NIH, Grant P01 CA77739, United States Army Medical Research and Material Command Grants DAMD17-00-1-0094 and DAMD17-02-1-0110, the International Training and Research in Population and Health Program supported by the Fogarty International Center and NICHD, NIH, and by an unsolicited donation from the Yamanouchi USA Foundation (Washington, D. C.). The costs of publication of this article were defrayed in part by the payment of page charges. This article must therefore be hereby marked "*advertisement*" in accordance with 18 U.S.C. Section 1734 solely to indicate this fact.

‡‡ To whom correspondence should be addressed: Laboratories for Reproductive Biology, CB# 7500, Rm. 3340C, Medical Biomolecular Research Bldg., 103 Mason Farm Rd., University of North Carolina, Chapel Hill, NC 27599-7500. Tel.: 919-966-5168; Fax: 919-966-2203; E-mail: emw@med.unc.edu.

[1] The abbreviations used are: AR, androgen receptor; DHT, dihydrotestosterone; TIF2, transcriptional intermediary factor 2; GRIP1, glucocorticoid receptor interacting protein; EGF, epidermal growth factor; PSA, prostate-specific antigen; MMTV, mouse mammary tumor virus; Luc, luciferase; MAPK, mitogen-activated protein kinase; MEK, mitogen-activated protein kinase/extracellular signal-regulated kinase kinase; AF2, activation function 2; siRNA, small interfering RNA; TGF, transforming growth factor; ERK, extracellular signal-regulated kinase.

dicative of the inherent genetic instability that characterizes advanced cancer cells.

Another mechanism for recurrent prostate cancer growth is increased expression of nuclear receptor coactivators. The p160 coactivators include steroid receptor coactivator 1 (SRC1) (38), transcriptional intermediary factor 2 (TIF2) (39), also known as SRC2 or the mouse homologue, glucocorticoid receptor interacting protein (GRIP1) (40), and the related SRC3 variants TRAM1, AIB1, RAC3, ACTR, and p/CIP (41). When overexpressed in transient transfection assays, these coactivators increase AR transactivation in the presence of testosterone and DHT (42, 43) or lower affinity adrenal androgens (44). Some of the p160 coactivators have histone acetyltransferase activity that modifies histones to increase chromatin accessibility during gene activation (45). We found increased levels of TIF2 and SRC1 in the majority of a randomly selected set of clinical specimens of recurrent prostate cancer compared with coactivator levels detected in benign prostate (44). Increased coactivator expression is associated with estrogen receptor-mediated gene activation in breast (46, 47) and ovarian cancer (48), suggesting that p160 coactivator overexpression is linked to growth stimulation in cancer cells controlled by sex steroids.

Increased kinase signaling in response to growth factors is another adaptive change implicated in AR transactivation in prostate cancer (49–51). Signaling pathways that trigger increased cyclic AMP-dependent protein kinase A may be a mechanism for increased AR transactivation in recurrent prostate cancer (52, 53). Mitogen activation of AR is reported to occur in the absence and presence of androgen (52) and influences AR phosphorylation (54, 55) and dephosphorylation (56). Insulin-like growth factor-1, keratinocyte growth factor, and epidermal growth factor (EGF) are reported to increase AR transactivation in the absence of androgen (8, 9, 57). Mitogen-activated protein kinase (MAPK) signaling pathways and overexpression of the receptor ErbB2 induced ligand-independent AR transactivation (58). ErbB2 lacks a ligand partner but heterodimerizes with other members of the EGF receptor family to activate MAPK and phosphatidylinositol 3-kinase signaling pathways. Other reports suggest that EGF-induced increases in AR transactivation require the presence of androgen (59, 60). Heregulin-α and ErbB3 were overexpressed in prostate cancer in association with less favorable prognosis in advanced disease (61).

In this report, we investigated the mechanisms involved in an EGF-induced increase in AR transcriptional activity in recurrent prostate cancer cells. We present evidence that an EGF-induced increase in TIF2/GRIP1 phosphorylation is mediated through the MAPK signaling pathway and increases the functional activity of the androgen-activated AR.

EXPERIMENTAL PROCEDURES

CWR22 Tumor Propagation—Androgen-dependent and recurrent CWR22 tumors were originally provided by Thomas G. Pretlow (Case Western Reserve University) and were maintained as xenograft implants in nude mice (13, 62). CWR22 tumors of ~1 cm or less were resected and dispersed by protease digestion. Cell suspensions (10^6 cells/site) were injected subcutaneously with 100 μl of Matrigel™ (BD Biosciences) into nu/nu athymic mice (Harlan Sprague-Dawley, Inc., Indianapolis, IN) that were previously implanted with 12.5 mg of sustained release testosterone pellets to normalize circulating levels to ~4 ng/ml testosterone (Innovative Research of America, Sarasota, FL). For analysis of the androgen-dependent CWR22 tumor, tumors were grown to ~0.75 g over ~30 days until the mice were sacrificed by cervical dislocation, and tumors were resected. Testosterone propionate (25 mg/kg/day) in sesame oil (Schein Pharmaceutical, Inc., Port Washington, NY) was injected intraperitoneally, or 150 μg/kg/day EGF in sterile water (BD Biosciences) was injected subcutaneously. For recurrent CWR22 tumors, tumor cell-Matrigel suspensions were injected into castrated athymic mice and grown to ~0.75 g before resection after ~30 days. Tumors were frozen in liquid N_2 and used to prepare protein lysates for immunoblot analysis. Animals were maintained in accordance with National Institutes of Health and University of North Carolina at Chapel Hill animal use guidelines.

Plasmids—Expression vectors were described previously for full-length human AR pCMVhAR (63), AR NH_2-terminal and DNA binding and hinge region fragment pCMVhAR 1–660 (64, 65), the AR N/C interaction mutant pCMVhAR-F*XX*AA/A*XX*AA in which alanine substitutions were introduced into the ^{23}FQNLF^{27} and ^{433}WHTLF^{437} AR NH_2-terminal sequence (66–68), and GAL-AR 624–919 coding for the GAL4 DNA binding domain as a fusion protein with the AR ligand binding domain (69, 70). VPTIF2.1-S736A contained TIF2 residues 624–1287 and a serine to alanine mutation and was prepared by polymerase chain reaction mutagenesis, and the DNA sequence was verified. The following vectors were generously provided: prostate-specific antigen-luciferase reporter PSA-Luc (referred to previously as PSE-Luc) containing the −5220 PSA enhancer and promoter region with an internal deletion of −2876 to −540 (71) from Young E. Whang (University of North Carolina, Chapel Hill, NC) and Lily Wu (University of California Los Angeles), VPTIF2.1 coding for TIF2 residues 624–1287 as a fusion protein with the VP16 activation domain from Heinrich Gronemeyer (Institute of Genetics and Molecular and Cellular Biology) (39, 70), pSG5-GRIP1 and pSG5-GRIP1-S736A from Michael R. Stallcup and Peter J. Kushner (University of Southern California), mouse mammary tumor virus long terminal repeat-luciferase reporter vector (MMTV-Luc) from Stanley M. Hollenberg and Ronald M. Evans (Salk Institute), and the GAL4 luciferase reporter 5×GAL4Luc3 from Donald P. McDonnell (Duke University).

Transient Reporter Gene Assays—Cotransfection assays were performed in the CWR-R1 cell line derived from the CWR22 recurrent human prostate cancer xenograft (22). To study transcriptional activity of endogenous AR, CWR-R1 cells were transfected with 0.5 μg/6-cm dish MMTV-Luc reporter vector in the absence and presence of 0.1 μg of pSG5 empty vector, pSG5-GRIP1, or pSG5-GRIP1-S736A. To study transcriptional activity of transiently expressed wild-type pCMVhAR and pCMVAR 1–660 or pCMVAR-F*XX*AA/A*XX*AA, AR expression vector DNA (10 ng) was transfected with 0.5 μg of MMTV-Luc or 1 μg of PSA-Luc reporter vector as indicated. DNA was transfected into ~75% confluent CWR-R1 cells plated the day before at 10^6 cells/6-cm dish using prostate growth medium without exogenous EGF, containing Richter's improved minimal essential medium (Irvine Scientific, Santa Ana, CA) supplemented with 10 mM nicotinamide, 5 μg/ml insulin, 5 μg/ml transferrin, 5 ng/ml selenium, 100 units/ml penicillin, 100 μg/ml streptomycin, and 2% fetal bovine serum. The Effectene transfection reagent (Qiagen, Valencia, CA) was used according to the manufacturer. 1 ml of a DNA reaction mix containing 150 μl of EC buffer (Qiagen), 4 μl of enhancer, 4 μl of Effectene reagent (Qiagen), and 1 ml of 2% serum containing prostate growth medium lacking EGF was added to cell cultures containing 3 ml/dish fresh medium with 2% fetal calf serum without added EGF. The next day, the prostate growth medium was replaced with phenol red-free, serum-free medium (Improved MEM Zinc Option; Invitrogen) with or without the addition of EGF or DHT as indicated, and incubations were continued for 24 h. Cells were harvested in 0.5 ml of lysis buffer containing 25 mM Tris phosphate, pH 7.8, 2 mM EDTA, and 1% Triton X-100 (67). Luciferase activity was measured using an automated LumiStar Galaxy (BMG Labtechnologies, Durham, NC) multiwell plate reader luminometer.

For two-hybrid interaction assays, CWR-R1 cells (1×10^6 cells/6-cm dish) were transfected using Effectene as described above with 10 ng of VPTIF2.1 (VP16 activation residues 411–456 fused to TIF2 residues 624–1287) or the serine to alanine mutant VPTIF2.1-S736A, 100 ng of GAL-AR 624–919, and 0.1 μg of 5×GAL4Luc-3 containing five tandem GAL-4 binding sites and the luciferase coding sequence. Cells were treated with hormone as indicated and analyzed for luciferase activity as described above.

Immunoblot, Immunoprecipitation, and Stability Assays—Monkey kidney COS-1 cells were maintained in Dulbecco's modified Eagle's medium containing 2 mM L-glutamine, 20 mM Hepes, pH 7.2, 10% bovine calf serum, penicillin, and streptomycin. COS cells were plated at ~50% confluence (1.2×10^6 COS cells/10-cm dish) and transfected the next day using Effectene reagent. To each plate containing 8 ml of fresh serum-containing medium was added 1 ml of a reaction mix prepared according to the manufacturer to contain, per plate, 2 μg of pCMVhAR, pCMVhAR 1–660, pSG5-GRIP1, or pSG5-GRIP1-S736A as indicated, 300 μl of EC buffer (Qiagen), 16 μl of enhancer, 10 μl of Effectene reagent (Qiagen), and 1 ml of serum-containing medium. After an overnight incubation in 10% serum-containing medium, the medium was exchanged with serum-free, phenol red-free medium. CWR-R1 cells in log phase growth were plated in prostate growth

medium lacking EGF as described. For experiments without transfection, the CWR-R1 cell culture medium was replaced for 24 h with serum-free medium lacking phenol red and containing 0.2% lipid-rich bovine serum albumin (AlbuMax I; Invitrogen). Hormones and growth factors were added as indicated, and cells were incubated for ~20 h with DHT in the absence and presence of EGF. CWR-R1 and COS cells with or without transient DNA transfection were rinsed with phosphate-buffered saline and placed on ice. Cells were scraped into 1 ml of buffered saline on ice, transferred to 1.5-ml microcentrifuge tubes, and centrifuged at 12,000 × *g* for 2 min. The buffer was aspirated, and 50 or 100 μl of RIPA buffer with protease inhibitors was added (RIPA: 1% Nonidet P-40, 0.5% sodium deoxycholate, 0.1% SDS, and phosphate-buffered saline containing the protease inhibitors 0.02 mg/ml pancreas extract, 0.005 mg/ml Pronase, 0.0005 mg/ml thermolysin, 0.003 mg/ml chymotrypsin, and 0.33 mg/ml papain (Roche Applied Science)). Cell pellets were disrupted by vortexing for 15 s, and lysates were incubated on ice for 15 min. After centrifugation for 15 min at 12,000 × *g*, supernatants were collected, and protein concentrations were determined using the Bio-Rad protein assay. Lysates from CWR22 tumors were prepared as described (72). Proteins (25 or 50 μg/lane as indicated) were separated on 8% acrylamide gradient gels for TIF2/GRIP1 or 10% acrylamide gels for AR and electroblotted after SDS-PAGE to nitrocellulose membranes (NitroBind, 0.22 μm; Osmonics, Inc., Westborough, MA). Rabbit polyclonal AR NH_2-terminal anti-peptide antibody AR32 (73) was used at 0.7 μg/ml, anti-TIF2 mouse monoclonal (BD Biosciences) at 1:1,000 dilution, and anti-phospho-p42/44 antibody (Cell Signaling Technology, Beverly, MA) at 1:1,000 dilution. Incubations with primary antibody were for 1 h at room temperature (AR32 and TIF2) or overnight at 4 °C (pp42/44). Anti-rabbit and anti-mouse horseradish peroxidase-conjugated secondary IgG antibodies (Amersham Biosciences) were used at 1:10,000 dilution for 1 h at room temperature. Specific signals were detected using chemiluminescence (SuperSignal® West Dura Extended Duration Substrate; Pierce).

For TIF2 immunoprecipitation, cells were removed and washed in buffered saline containing 2.5 mM sodium vanadate and 10 mM sodium fluoride. Cell lysates were prepared in 1 ml of RIPA with protease inhibitor (Complete Mini; Roche Applied Science) and phosphatase inhibitor mixtures 1 and 2 (Sigma). 4 mg of protein was immunoprecipitated using anti-TIF2 antibody following a preclear step using normal mouse IgG and Protein G-Plus-agarose (Santa Cruz Biotechnology, Inc., Santa Cruz, CA). GRIP-1 antibody (8 μg; NeoMarkers, Inc., Fremont, CA) and 40 μl of Protein G-Plus-agarose was added to precleared lysates, and samples were incubated overnight at 4 °C with rocking. The agarose was pelleted at 1500 rpm for 30 s at 4 °C and washed three times with RIPA containing protease inhibitors and phosphatase inhibitors 2.5 mM sodium vanadate and 10 mM sodium fluoride. The final pellet was resuspended in 40 μl of electrophoresis sample buffer, and protein was fractionated on SDS-containing 8% acrylamide gels (Gradipore Ltd.). Proteins were electroblotted to Immobilon™-P membrane (Millipore Corp., Bedford, MA) overnight. Membranes were incubated with blocking solution (Zymed Laboratories Inc., South San Francisco, CA) containing 2.5 mM sodium vanadate and 10 mM sodium fluoride overnight at 4 °C followed by incubation overnight at 4 °C with a mixture of anti-phosphoserine antibody clone PSR-45 (Sigma) at 1:500 dilution and anti-phosphoserine antibodies 4A3, 4A9, and 16B4 (Calbiochem), each at a dilution of 1:250. Following four 30-min washes with 0.9% NaCl, 0.05% Tween 20, and 10 mM Tris, pH 7.5, membranes were incubated with anti-mouse IgG (Amersham Biosciences) at a 1:10,000 dilution for 30 min at room temperature, and the signal was detected by enhanced chemiluminescence (Supersignal; Pierce).

For AR stability assays, COS cells (1.2×10^6 COS cells/10-cm dish) were transfected with 1 μg of pCMVhAR or pCMVhAR 1–660 using Effectene reagent (Qiagen) as described above. After an overnight incubation in 10% serum-containing medium, cells were rinsed with phosphate-buffered saline and incubated in methionine-free modified Eagle's medium (Sigma) for 30 min. Tran^{35}S-label (100 μCi/dish) (PerkinElmer Life Sciences) was added to the cells with or without DHT or EGF treatment and incubated for 1.5 h. Cells were washed, fresh culture medium with or without hormone was added, and cells were incubated for 0, 8, and 24 h. Lysates were prepared from labeled cells using RIPA buffer containing protease inhibitors. ^{35}S-Labeled AR protein was immunoprecipitated using AR52 IgG (73) and Pansorbin cells (Calbiochem) and analyzed by SDS gel electrophoresis. Autoradiographic signals were quantitated by densitometric scanning using an AlphaImager™ 3400 densitometer and AlphaEaseFC software (AlphaInnotech, San Leandro, CA).

Northern Blot Analysis—CWR-R1 cells (5×10^6/10-cm dish) were plated in prostate growth medium lacking EGF. The next day, cells were washed with phosphate-buffered saline, and the medium was changed to phenol red-free improved MEM zinc option (Invitrogen) containing 0.2% albumin (AlbuMax I; Invitrogen). After an overnight incubation, cells were treated without or with 100 ng/ml EGF for 24 h in the same medium prior to RNA isolation using TRIzol Reagent (Invitrogen) according to the manufacturer's instructions. RNA (15 μg) aliquots were fractionated on 1% agarose gels, transferred to nylon membranes, and hybridized with ^{32}P-labeled pSG5TIF2 BamHI fragment containing nucleotides 629–869 and a pGEM-18S-4 (Promega) Sp6-generated fragment for control 18 S ribosomal RNA.

RNA Interference—PCR primers to amplify TIF2/GRIP1 target regions were synthesized to incorporate T7 polymerase promoters on the sense and antisense DNA strands. PCR primer sequences were based on the DNA sequence published by Voegel *et al.* (39) as follows with flanking T7 sequence in brackets: TIF2-A nucleotides 197–216, 5′-[TAATACGACTCACTATAGG]CCAGGGCAGAGACAAGAAAG-3′; TIF2-B nucleotides 356–376, 5′-[TAATACGACTCACTATAGG]TTGCACATTTGTCAGGTTTGA-3′. pSG5-TIF2 was used as template for *Taq* DNA polymerase (Invitrogen) to amplify target regions by polymerase chain reaction using the following conditions: 94 °C for 1 min, 55 °C for 30 s, 72 °C for 30 s (30 cycles), and 72 °C for 10 min. PCR products were gel-purified and used as template for *in vitro* transcription using T7 RNA polymerase and the *Silencer*™ siRNA mixture kit (Ambion Inc., Austin, TX). Following DNase and RNase A treatment for 1 h, double-stranded RNA was purified through spin columns and digested with RNase III according to the manufacturer to yield siRNA mixtures. The mixtures of 12–30-bp double-stranded RNAs contain 5′-PO_4, 3′-OH, and 2-nucleotide 3′ overhangs similar to siRNA produced *in vivo*. Recent studies demonstrated that siRNAs generated by RNase III cleavage are efficient for RNA interference in mammalian cells (74, 75). CWR-R1 cells were transiently cotransfected with pCMVhAR, PSA-Luc, and 10 nM siRNA mixtures for TIF2 or with glyceraldehyde-3-phosphate dehydrogenase as a control, using Effectene reagent (Qiagen) as described above. In some studies, cells were cotransfected with pSG5-TIF2 (50 ng/6-cm dish) to overcome inhibition by the siRNAs. Cells were treated with and without DHT and EGF overnight and lysed, and luciferase activity was measured.

RESULTS

Effect of EGF on AR Transactivation in CWR-R1 Cells—The effect of EGF on AR transactivation was determined in the CWR-R1 cell line derived from the CWR22 recurrent human prostate cancer xenograft. Like the CWR22 recurrent prostate tumor, CWR-R1 cells express AR-H874Y that retains wild-type sensitivity to androgens but has increased responsiveness to other steroids (31). In the absence of androgen, EGF at 10, 100, and 500 ng/ml induced a 2.0 ± 0.3-fold increase in transactivation of MMTV-Luc that was independent of the dose of EGF (Fig. 1*A*). Activation in response to EGF alone was negligible compared with the 43 ± 3.5-fold increase in response to 0.1 nM DHT, and the addition of EGF and 0.1 mM DHT increased this further by 3.3 ± 0.6-fold. An androgen-dependent EGF-induced increase in AR transcriptional activity of 1.8 ± 0.2-fold was seen also with transient expression of wild-type AR and a PSA-Luc reporter in CWR-R1 cells, and again the increase in activity was negligible with EGF alone in the absence of DHT (Fig. 1*B*). The PSA-Luc reporter is activated only weakly by endogenous AR in CWR-R1 cells in the presence of androgen (data not shown).

The requirement for an activated AR for a substantial EGF response was supported by transiently expressing the constitutively active AR NH_2-terminal and DNA binding domain fragment AR 1–660 that lacks the ligand binding domain. EGF increased AR 1–660 transactivation of MMTV-Luc and PSA-Luc reporters by 3–4-fold in CWR-R1 cells (Fig. 1*C*). The data suggest that the EGF-induced increase in AR-mediated gene activation depends on an AR that is rendered transcriptionally competent by androgen binding or artificially by deleting the ligand binding domain.

Effects of EGF on AR Levels—To investigate the mechanism whereby EGF increases AR transcriptional activity in the presence of androgen, we determined the effect of EGF on AR

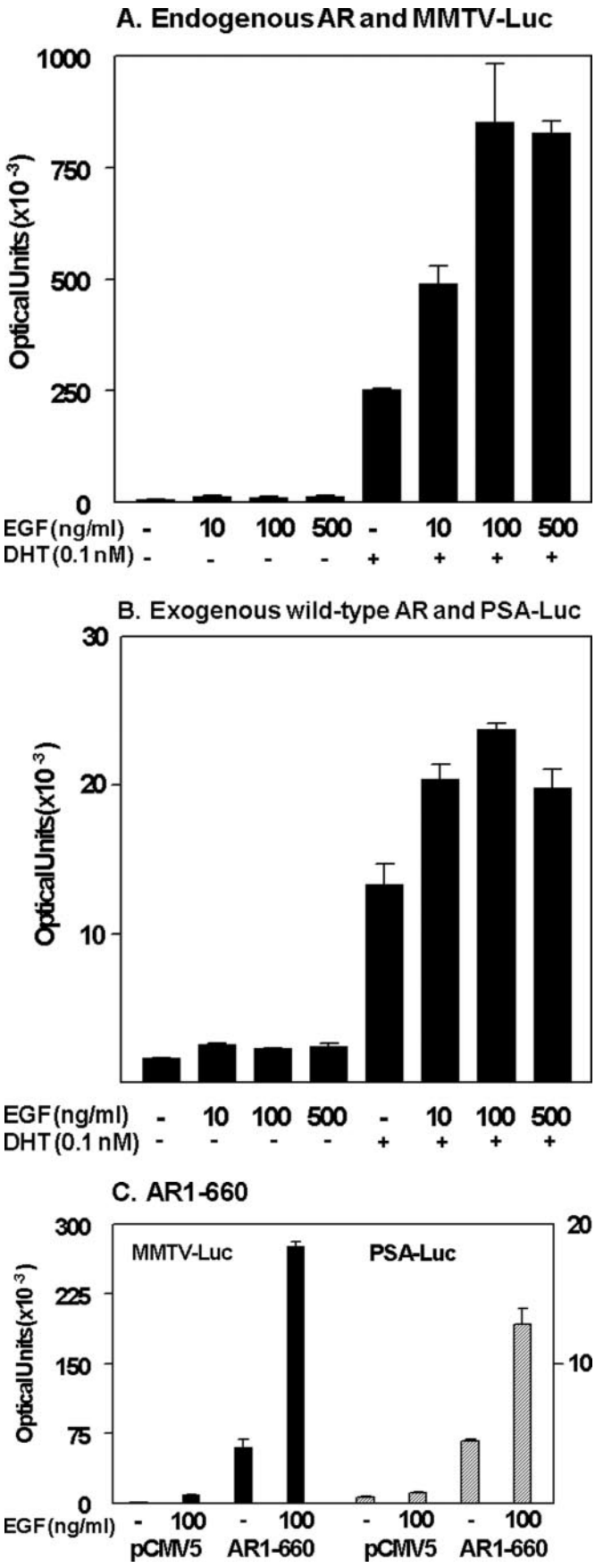

FIG. 1. **EGF stimulation of AR transcriptional activity in CWR-R1 cells.** CWR-R1 cells were assayed as described under "Experimental Procedures" for endogenous AR transactivation using MMTV-Luc (0.5 μg/6-cm dish) (*A*), exogenous wild-type AR activity determined by transfecting pCMVhAR (10 ng/dish) and PSA-Luc (1 μg/dish) (*B*), and constitutively active AR deletion mutant pCMVAR 1–660 (10 ng/dish) that lacks the ligand binding domain with MMTV-Luc and PSA-Luc (0.5 and 1 μg/dish) or 10 ng of empty parent vector pCMV5 (*C*). Cells were incubated for 24 h in the absence and presence of 10, 100, and 500 ng/ml EGF with and without 0.1 nM DHT as indicated. The mean luciferase activity values in optical units plus error of the mean are representative of at least three independent experiments.

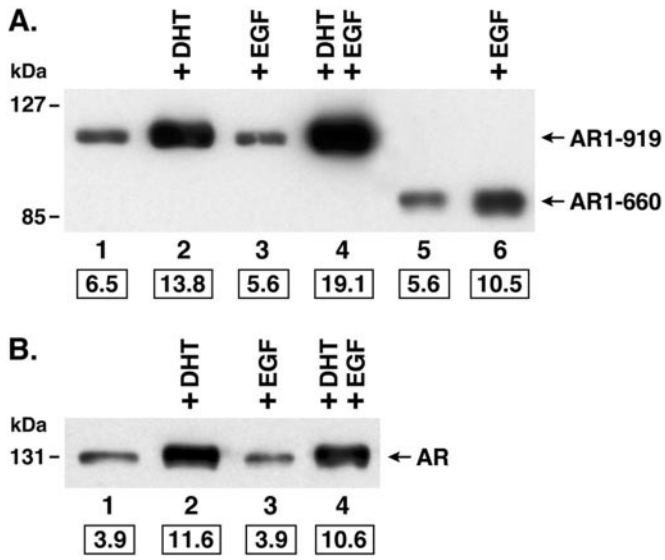

FIG. 2. **Effect of EGF on AR protein levels in COS and CWR-R1 cells.** In *A*, COS cells were transiently transfected as described under "Experimental Procedures" with 2 μg of pCMVhAR coding for full-length AR (*lanes 1–4*) and for the AR NH_2-terminal fragment pCMVhAR 1–660 (*lanes 5* and *6*). Cells were incubated in the absence and presence of 100 ng/ml EGF with or without 10 nM DHT for 24 h as indicated. Immunoblots are shown with 25 μg of protein/lane for COS cell lysates. In *B*, CWR-R1 cells were incubated with and without 100 ng/ml EGF in the absence and presence of 1 nM DHT for 24 h. Extracts were analyzed using 50 μg of protein/lane for CWR-R1 cells. Blots were incubated with AR32, an AR NH_2-terminal specific antibody. Densitometry values for specific bands are included *below* the *lanes* and are representative of more than three independent experiments.

protein levels. COS cells transiently expressing full-length wild-type AR were treated for 24 h in the absence and presence of 10 nM DHT with or without 100 ng/ml EGF. Cell lysates were analyzed on immunoblots using an AR-specific antibody (Fig. 2*A*). Full-length AR protein levels increased 2.1-fold in the presence of 10 nM DHT, reflecting androgen-induced AR stabilization (76), and 2.9-fold in the presence of DHT and EGF (Fig. 2*A*, *lane 4*), but there was no increase in the presence of EGF alone (*lane 3*). The latter result indicated that EGF did not increase transient expression of AR from the pCMVhAR plasmid. EGF also increased by 1.9-fold the level of AR 1–660, a constitutively active AR NH_2-terminal and DNA binding domain fragment (Fig. 2*A*, *lanes 5* and *6*). In CWR-R1 cells, endogenous AR protein levels increased 3.0-fold in the presence of DHT, but a further increase in the presence of EGF was not detectable, and there was no increase in the presence of EGF alone (Fig. 2*B*). Endogenous AR in CWR-R1 cells was shown previously to be relatively stable in the absence of added androgen (22).

A possible effect of EGF on AR stabilization was investigated by determining AR degradation half-times by [^{35}S]methionine pulse-chase labeling at 37 °C in COS cells. The half-time of AR degradation in the absence of DHT (t = 11.3 ± 2.7 h) increased 2-fold in the presence of DHT (t = 22.7 ± 3.8 h), but there was no further increase in the presence of DHT and EGF (t = 24.0 ± 3.0 h). The degradation half-time of AR 1–660, which lacks the ligand binding domain, was 20.0 ± 3.8 h in the absence of EGF and 24.8 ± 2.7 h in the presence of EGF (p = 0.16). The data

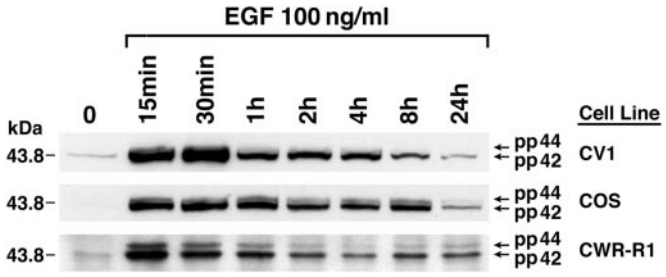

FIG. 3. **EGF-induced MAPK activity.** CV1, COS, and CWR-R1 cells were incubated with 100 ng/ml EGF for the times indicated from 15 min to 24 h. Immunoblots of cell lysates (50 μg of protein/lane) were incubated with phospho-p42/p44 antibody as described under "Experimental Procedures." The data are representative of at least three independent experiments.

suggest that an effect of EGF on AR stabilization could not be detected in COS cells.

Role of MAPK—We determined whether the EGF-induced increase in AR transcriptional activity was associated with an increase in MAPK activity. Growth factor activation of MAPK results in phosphorylation at threonine 202 and tyrosine 204 in ERK1 (pp42) and ERK2 (pp44) that can be detected on immunoblots using phosphorylation-specific antibodies (77). Within 15 min of treating CWR-R1, COS, and CV1 cells with 100 ng/ml EGF, specific phosphorylation of ERK1 (pp42) and ERK2 (pp44) was detected, followed by a decline in signal intensity over 24 h in the three cell lines (Fig. 3). The rapid increase in MAPK activity in CWR-R1 cells in response to EGF was inhibited by pretreatment with 10 μM U0126, a MEK1 and MEK2 inhibitor that prevents phosphorylation of ERK1/2 (data not shown).

The effects of the MEK inhibitor U0126 and the EGF receptor (ErbB1)-specific inhibitor ZD1839 were tested on endogenous AR transactivation in CWR-R1 cells in the absence and presence of EGF using the MMTV-Luc reporter (Fig. 4*A*). Increasing concentrations of U0126 from 0.1 to 2.5 μM inhibited AR transactivation in the absence and presence of added EGF. In contrast, ZD1839 blocked the EGF-induced increase in luciferase activity but had no effect on the transcriptional response in the absence of added EGF. Control experiments indicated that U0126 and ZD1839 did not inhibit general transcription, since the same concentrations of inhibitors in CWR-R1 cells did not reduce the activity of constitutively active reporter vectors pSG5-Luc, pSV2-Luc, or pA3RSV400Luc (78) (data not shown).

The data indicate that the transcriptional capacity of the androgen-activated endogenous AR in CWR-R1 cells is increased by EGF through the MAPK pathway. The kinase inhibitor results suggest that a possible autocrine regulatory loop involving ligands in the EGF family is present in CWR-R1 cells and may not depend solely on the ErbB1 receptor, since the EGF receptor-selective inhibitor ZD1839 did not diminish AR activity in the absence of added EGF. On the other hand, inhibition of transcription by U0126 in the absence of added EGF suggested that other members of the EGF receptor family, such as ErbB2 and ErbB3, mediate signals through the MAPK pathway to increase DHT-dependent AR transcriptional activity in the CWR-R1 recurrent prostate cancer cell line.

The MAPK pathway was also implicated in the EGF-induced increase in AR observed in COS cells in the presence of DHT. ZD1839 (2.5 μM) and U0126 (2.5 μM) blocked the EGF-induced increase in AR levels observed in the presence of DHT (Fig. 4*B*). In contrast, these inhibitors had no effect on DHT-induced AR stabilization (Fig. 4*B*) that was shown previously to require the androgen-induced NH_2-terminal and carboxyl-terminal (N/C) interaction in AR (79). The results support that MAPK signaling acts synergistically with DHT.

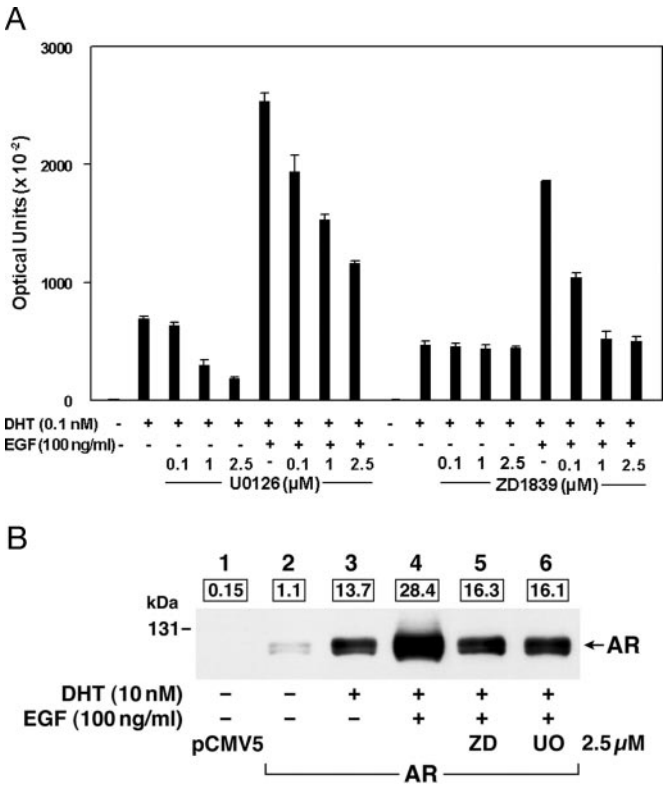

FIG. 4. **Inhibition of AR transactivation and EGF-induced AR stabilization by EGF receptor and MEK inhibitors.** In *A*, transactivation by endogenous AR was determined in CWR-R1 cells transfected with MMTV-Luc (0.5 μg/6-cm dish) as described under "Experimental Procedures." Cells were incubated for 24 h with and without 0.1 nM DHT in the absence and presence of 100 ng/ml EGF and increasing concentrations (0.1–2.5 μM) of the MEK inhibitor U0126 or the EGF receptor (ErbB1) inhibitor ZD1839. Luciferase activity is shown as the mean and error and is representative of at least three experiments. In *B*, pCMV5 empty parent vector (*lane 1*) and pCMVhAR (2 μg of DNA/10-cm dish; *lanes 2–6*) were transiently expressed in COS cells. Cells were treated in the absence and presence of 10 nM DHT with or without 100 ng/ml EGF as indicated. Some of the cells treated with DHT and EGF were also incubated with 2.5 μM ZD1839 (*lane 5*) or 2.5 μM U0126 (*lane 6*). Immunoblots of cell lysates (25 μg of protein/lane) were probed with the AR32 antibody. Densitometry values for specific bands are included *above* the *lanes*.

EGF Regulation of TIF2 Expression—We showed previously that progression to recurrent growth of prostate cancer is associated with increased levels of p160 coactivators (44) that can increase AR activity (68). We therefore investigated expression levels and effects of EGF on endogenous TIF2 levels in several cell lines including the CWR-R1 cell line and in the CWR22 human prostate cancer xenograft. Steady state levels of TIF2 were highest in the CWR-R1 cell line compared with prostate cancer cell lines PC3, LNCaP, and LNCaP-C4-2 and HeLa cells when equal amounts of protein were analyzed by immunoblot (Fig. 5*A*). Lower levels of TIF2 were detected in COS and CV1 cells, and TIF2 was undetectable in a nontransformed human foreskin fibroblast cell line. EGF increased TIF2 levels in CWR-R1 cells after 8 h compared with an earlier increase in COS cells and little change in CV1 cells (Fig. 5*B*). The higher steady state level of TIF2 in CWR-R1 cells and the increase after EGF treatment support the possibility that elevated levels of TIF2 contribute to the EGF-induced increase in androgen-dependent AR transactivation. We ruled out a direct effect of EGF on TIF2 transcription, since Northern blot analysis showed similar levels of TIF2 mRNA in CWR-R1 cells with and without EGF treatment (Fig. 5*C*).

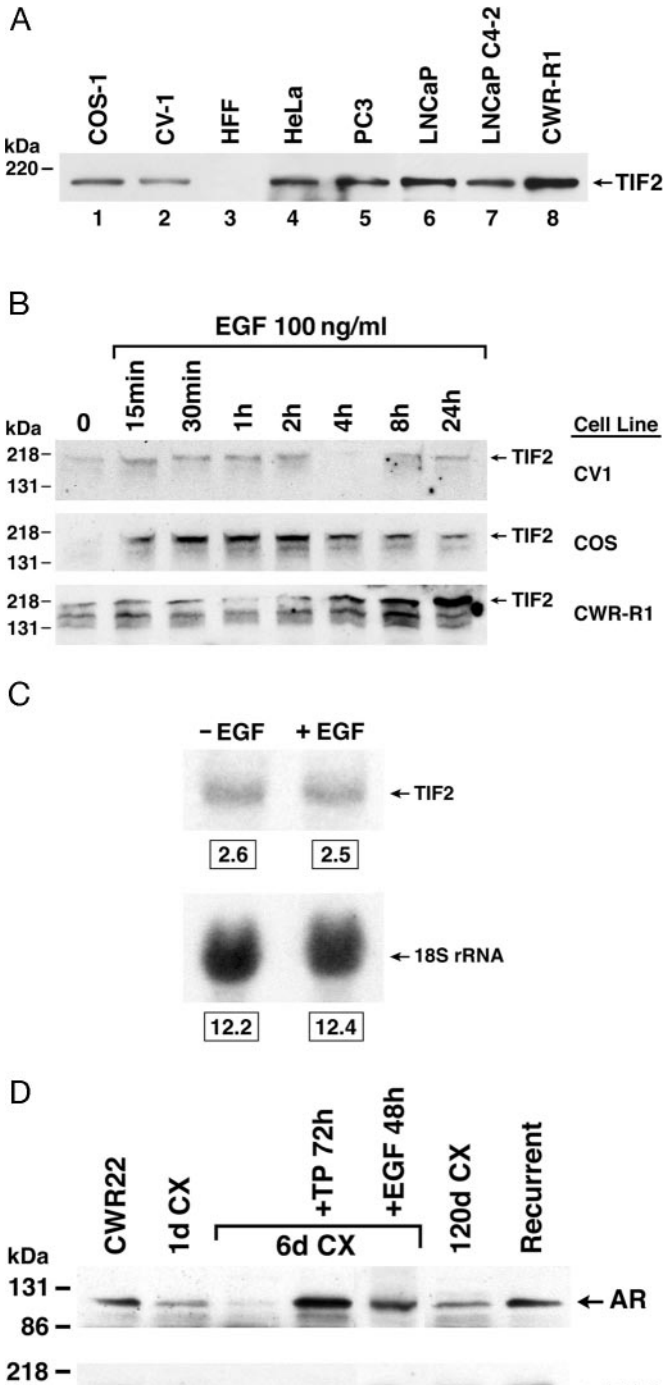

FIG. 5. **Endogenous TIF2 expression and regulation by EGF.** In *A*, endogenous TIF2 levels were assessed in whole cell lysates from the indicated cell lines harvested during logarithmic growth. The immunoblot was performed on cell extracts (50 μg of protein/lane) prepared in RIPA buffer in the presence of protease inhibitors. All cell lines were grown in the absence of supplemental EGF. Blots were probed with anti-TIF2 antibody (BD Biosciences). In *B*, CV1, COS, and CWR-R1 cells were untreated (0) or were incubated with 100 ng/ml EGF for increasing times from 15 min to 24 h as indicated. The blot was probed with the anti-TIF2 antibody. For the Northern blot in *C*, CWR-R1 cells were incubated without and with EGF (100 ng/ml) in the absence of serum for 24 h. RNA was isolated using TRIzol reagent as described under "Experimental Procedures." 15 μg of RNA was fractionated on 1% agarose gels, transferred to a nylon membrane, and hybridized with ^{32}P-labeled TIF2 and 18 S ribosomal RNA cDNAs. Densitometry values of the specific bands are included *below* the *lanes*. In *D*, the levels of AR (*upper panel*) and TIF2 (*lower panel*) were determined by immunoblot of cell lysates from the androgen-dependent CWR22 tumor (*lane 1*), and from CWR22 tumors harvested 1 day (*lane 2*), 6 days (*lanes 3–5*), and 120 days (*lane 6*) after castration and removal of the testosterone implants. The recurrent tumors were propagated in castrated mice and harvested ~45 days later (*lane 7*). Six days after castration, some mice received a single injection of 25 mg/kg testosterone propionate in sesame oil intraperitoneally, and cell lysates were prepared 72 h later (*lane 4*), or mice received a single injection of 150 μg/kg subcutaneous EGF in sterile water, and cell lysates were prepared 48 h later (*lane 5*). Immunoblots of cell lysates (100 μg of protein/lane) were incubated with AR32 or TIF2 antibody. Data in *A* represent two independent experiments, data in *B* represent three experiments, and data in *C* represent 2–6 tumors in each treatment group.

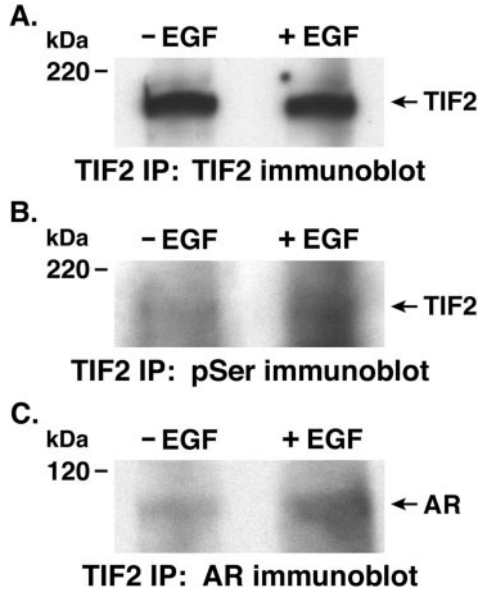

FIG. 6. **Effects of EGF on TIF2 phosphorylation and interaction with AR by TIF2 immunoprecipitation.** CWR-R1 cells were incubated with and without 100 ng/ml EGF in the absence of serum for 24 h. Equal amounts of protein (4 mg) from cell lysates were immunoprecipitated (*IP*) using anti-TIF2 monoclonal antibody as described under "Experimental Procedures." In *A*, immunoprecipitated TIF2 was subjected to immunoblot analysis using anti-TIF2 antibody. In *B*, CWR-R1 cells were incubated with 1 nM DHT in the absence and presence of 100 ng/ml EGF, and equal amounts of cell lysate protein were immunoprecipitated with anti-TIF2 antibody. Shown is an immunoblot using anti-phosphoserine antibodies (*pSer*) to detect phosphorylated TIF2. In *C*, CWR-R1 cells were incubated with 1 nM DHT with and without 100 ng/ml EGF, and equal amounts of cell lysate protein were immunoprecipitated using anti-TIF2 antibodies. The immunoblot was probed with AR polyclonal antibody AR32 to detect AR co-immunoprecipitated with TIF2. The data are representative of at least three independent experiments.

The EGF-induced increase in TIF2 levels was also observed in the androgen-dependent CWR22 tumor that was propagated in nu/nu athymic mice implanted with testosterone pellets (62, 72) (Fig. 5*D*). Six days after castration and removal of the testosterone source, TIF2 was barely detectable in the CWR22 androgen-dependent tumor (Fig. 5*D*, *lanes 1–3*) but increased 4–6-fold when mice were treated 6 days after castration with EGF and analyzed 48 h later (*lane 5*). TIF2 levels also increased 5–10-fold after mice were treated with a single injection of 25 mg/kg testosterone propionate 6 days after castration and analyzed 72 h later (*lane 4*). The increase in TIF2 levels in response to testosterone could be indirect through EGF, since testosterone has been shown to increase circulating EGF levels in castrated mice (80, 81). Testosterone may also increase EGF levels through a direct effect on xenograft tumor cells. In the recurrent CWR22 tumor that develops after prolonged androgen deprivation, TIF2 levels were elevated in the absence of androgen replacement (Fig. 5*D*), suggesting that additional

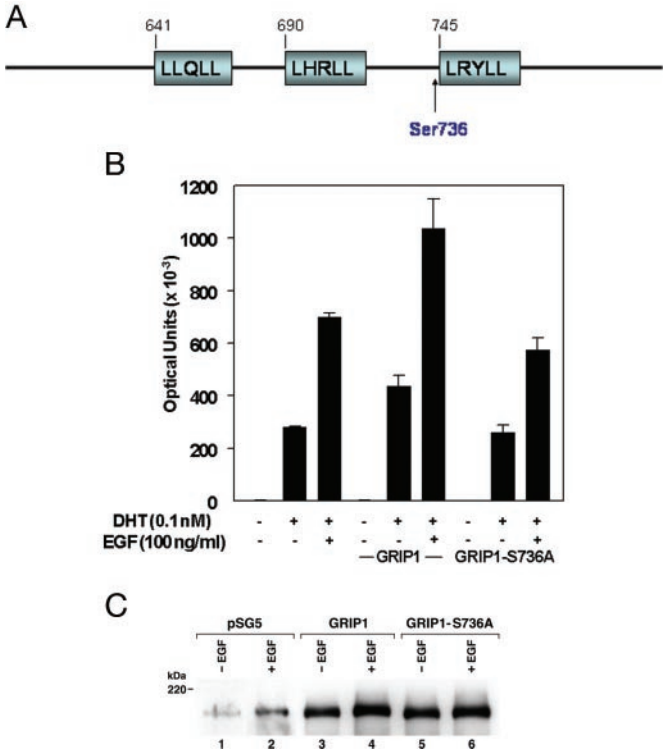

FIG. 7. **Effects of EGF on the AR-TIF2/GRIP1 interaction.** *A*, schematic diagram of the three L*XX*LL motifs of TIF2/GRIP1 and their position relative to the MAPK consensus site at Ser[736] that flanks the third L*XX*LL motif of TIF2/GRIP1, the predominant interaction site for the AR AF2 region (67, 70). Amino acid residues are numbered. *B*, CWR-R1 cells were transfected with MMTV-Luc (0.5 μg/6-cm dish) and 0.1 μg/dish of pSG5 empty vector, pSG5-GRIP1, or pSG5-GRIP1-S736A. Cells were incubated for 24 h in the absence and presence of 0.1 nM DHT with and without 100 ng/ml EGF as indicated. In *C*, immunoblot of endogenous TIF2 (*lanes 1* and *2*), transiently transfected pSG5-GRIP1 (*lanes 3* and *4*), and pSG5-GRIP1-S736A (*lanes 5* and *6*) before and after treatment with 100 ng/ml EGF for 24 h. 50 μg of protein extracts of COS cells were analyzed by immunoblot using the TIF2 antibody as described under "Experimental Procedures." Exposure times of the film were 5 min to detect endogenous TIF2 (*lanes 1* and *2*) and 30 s for transiently expressed TIF2/GRIP1 (*lanes 3–6*).

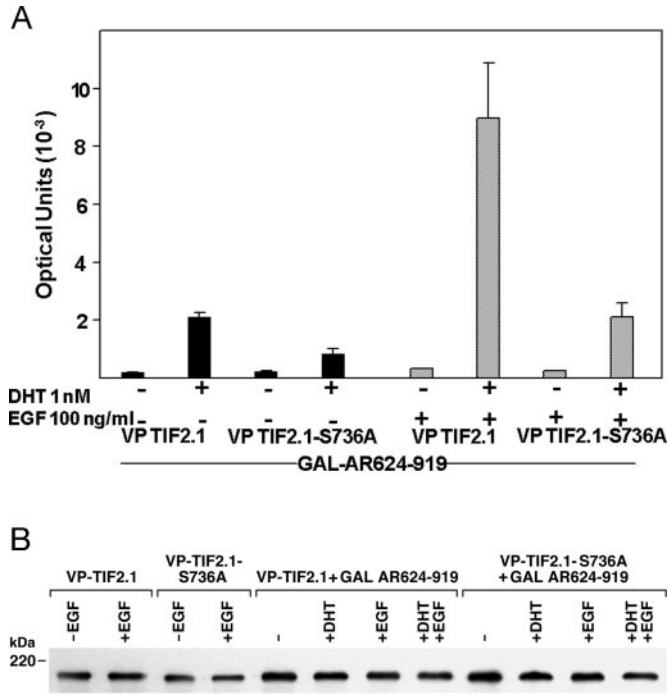

FIG. 8. **Effect of EGF on the interaction between AR and TIF2.** In *A*, two hybrid interaction assays were performed in CWR-R1 cells by cotransfecting 10 ng of VPTIF2.1 (TIF2 residues 624–1287) or VP-TIF2.1-S736A with 100 ng of GAL-AR 624–919 and 0.1 μg of 5×GAL4Luc3. CWR-R1 cells were incubated with or without 1 nM DHT in the absence and presence of 100 ng/ml EGF. The mean and S.E. of luciferase activity are representative of three independent experiments. In *B*, COS cells were transiently transfected as described under "Experimental Procedures" with 1 μg each of VP-TIF2.1 or VPTIF2.1-S736A with and without 1 μg of GAL-AR 624–919 using Effectene reagent. Cells were incubated overnight in the absence and presence of EGF (100 ng/ml) with and without 10 nM DHT. Cell lysates (10 μg of protein/lane) were immunoblotted, and membranes were incubated with anti-TIF2 antibody. The data are representative of three independent experiments.

mechanisms such as autocrine signaling contribute to increased TIF2 levels in prostate cancer tumor progression.

AR levels also increased after testosterone treatment 6 days after castration and to a lesser extent with EGF alone (Fig. 5*D*). In comparison with the tumor analyzed 6 days after castration, the recurring CWR22 tumor growing at 120 days after castration showed higher AR expression that approached the level observed in the recurrent tumor as reported previously (82). The results indicate that androgen and EGF increase TIF2 and AR levels in the androgen-sensitive CWR22 tumor to levels seen in the recurrent tumor.

Mechanism for the EGF-induced Increase in AR Transactivation—The EGF-induced increase in TIF2 levels and AR transactivation led us to investigate TIF2 phosphorylation, since previous studies on the estrogen and progesterone receptors suggested that EGF increases phosphorylation of p160 coactivators (83). Using an anti-TIF2-specific antibody, TIF2 was immunoprecipitated from lysates of CWR-R1 cells incubated in the absence and presence of EGF (Fig. 6*A*). Immunoblotting using phosphoserine antibodies suggested an increase in TIF2 phosphorylation in the presence of EGF (Fig. 6*B*). Moreover, in a separate experiment in the presence of DHT, we found that AR coimmunoprecipitated with TIF2, and the amount of AR in the coimmunoprecipitate increased in the presence of EGF (Fig. 6*C*). The data raised the possibility that EGF-induced phosphorylation of TIF2 increases its interaction with AR.

The proximity of the TIF2 MAPK site Ser[736] and the third L*XX*LL motif of TIF2 (Fig. 7*A*) suggested that EGF-induced phosphorylation of TIF2 might increase AR transactivation by enhancing its interaction with AR. The third L*XX*LL motif of TIF2 is the predominant interaction site among the three L*XX*LL motifs that bind activation function 2 (AF2) in the AR ligand binding domain (68, 78). Coexpression of GRIP1, the mouse homologue of human TIF2 that differs by only 2 amino acids (83), with an MMTV-Luc reporter increased DHT-dependent transcriptional activity of endogenous AR in CWR-R1 cells in the absence and presence of EGF (Fig. 7*B*). When the GRIP1-S736A phosphorylation mutant was expressed, the transcriptional response to DHT alone and to DHT and EGF was similar to that observed in the absence of GRIP1 transient expression. Transient expression levels of GRIP1 and the GRIP1-S736A mutant were similar, as shown in immunoblots of COS cell extracts (Fig. 7*C*, *lanes 3* and *6*), in agreement with a previous report (83), suggesting that expression levels were also similar in CWR-R1 cells. A direct comparison of expression levels of the wild-type and mutant GRIP1 plasmids in CWR-R1 cells was complicated by the relatively high TIF2 levels in CWR-R1 cells (see Fig. 5*A*) combined with low expression of plasmid DNA. As shown above (Fig. 5*B*), EGF increased endogenous TIF2/GRIP1 levels in COS cells (Fig. 7*C*, *lanes 1* and *2*) and the levels of transiently expressed GRIP1 but not the GRIP1-S736A mutant (Fig. 7*C*, *lanes 5* and *6*). The data sug-

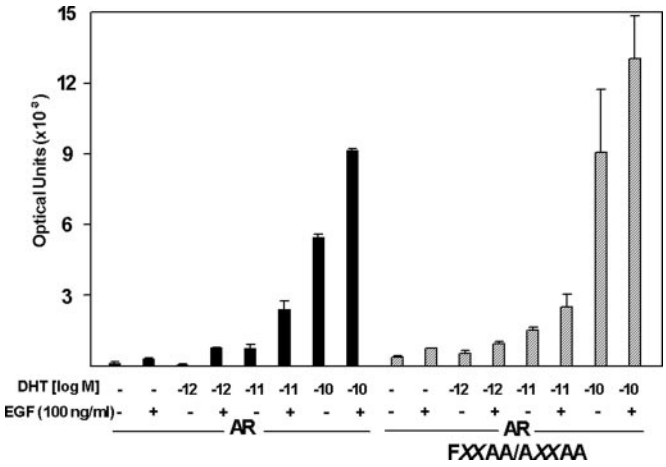

FIG. 9. **Transcriptional activation of PSA-Luc by an AR N/C interaction mutant in CWR-R1 cells.** CWR-R1 cells were transfected with 1 μg of PSA-Luc reporter and 10 ng of pCMVhAR or the AR N/C interaction mutant pCMVhAR-F*XX*AA/A*XX*AA in which ^{23}FQNLF^{27} and ^{433}WHTLF^{437} in the AR NH_2-terminal domain were mutated to FQNAA and AHTAA, respectively (66). Cells were transfected using Effectene as described under "Experimental Procedures" and incubated for 24 h with and without increasing concentrations of DHT as indicated in the absence and presence of 100 ng/ml EGF. The data are representative of three independent experiments.

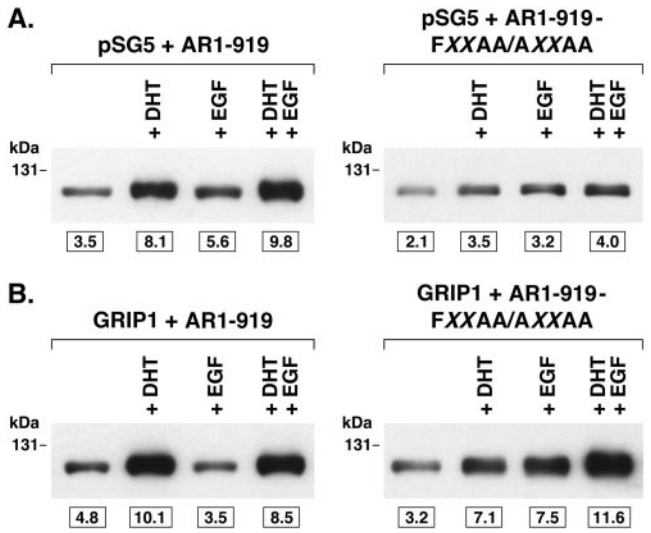

FIG. 10. **Effects of EGF and GRIP1 on expression levels of AR and the AR N/C interaction mutant.** Wild-type and N/C interaction mutant AR levels were determined in COS cells by transient expression of 1 μg of wild-type pCMVhAR or pCMVhAR-F*XX*AA/A*XX*AA in the absence and presence of 1 μg of pSG5 empty vector or pSG5-GRIP1 using Effectene as described under "Experimental Procedures." Cells were treated in the absence and presence of 10 nM DHT with and without 100 ng/ml EGF as indicated. Immunoblots were probed with AR antibody AR32 from cell lysates (25 μg of protein/lane) for wild-type AR and the N/C interaction mutant AR-F*XX*AA/A*XX*AA in the absence (*A*) or presence (*B*) of transiently expressed GRIP1. Densitometry values for specific bands are included *below* the *lanes*.

gest that the EGF-induced increase in AR transcriptional activity is mediated at least in part by phosphorylation of GRIP1 at Ser^{736} and by increased levels of TIF2/GRIP1.

The requirement for GRIP1 phosphorylation in its interaction with AR was evaluated further in the CWR-R1 cell line using a two-hybrid interaction assay. VPTIF2.1 coding for the VP16 activation domain and TIF2 residues 624–1287 (39, 70) was co-expressed with GAL-AR 624–919 coding for the AR ligand binding domain and GAL4 DNA binding domain. The androgen-dependent interaction between GAL-AR 624–919 and VPTIF2.1 was reduced with the phosphorylation site mutant VPTIF2.1-S736A (Fig. 8*A*). The addition of EGF increased the interaction between AR and VPTIF2.1 and between AR and VPTIF2.1-S736A but was greater for wild-type TIF2. The high levels of endogenous TIF2 in CWR-R1 cells probably contributed to some of the activity observed in the presence of the TIF2 mutant. Expression levels of the VPTIF2.1 and VPTIF2.1-S736A plasmid DNA were similar in the absence and presence of GAL-AR 624–919, as demonstrated in COS cells (Fig. 8*B*). The results suggest that EGF increases the interaction between AR and TIF2 through phosphorylation at serine 736 adjacent to the third L*XX*LL motif and probably through additional phosphorylation sites in TIF2.

Role of the AR N/C Interaction—We showed previously that the androgen-dependent AR NH_2- and carboxyl-terminal N/C interaction is mediated by the NH_2-terminal F*XX*LF and W*XX*LF motifs (66) and is required for DHT-induced AR stabilization (67, 84) and slows the dissociation rate of bound androgen (66, 67, 79). The AR-F*XX*AA/A*XX*AA mutant that lacks the N/C interaction activates the MMTV-Luc reporter in CV1 cells to essentially the same extent as wild-type AR, but in CV1 cells this mutant only weakly activates the PSA-Luc reporter compared with wild-type AR (68). We now show that transiently expressed AR-F*XX*AA/A*XX*AA in CWR-R1 cells is equipotent to wild-type AR in activating PSA-Luc (Fig. 9), and EGF increases the androgen-dependent activity.

Previous studies demonstrated that increased expression of TIF2 in CV1 cells could overcome the requirement for the AR N/C interaction in activating the PSA-Luc reporter (68). Since an important functional consequence of the N/C interaction is stabilization of the AR that may be necessary for AR activity *in vivo* (67, 79, 84), we investigated whether increased coactivator levels could replace this function by stabilizing the AR-F*XX*AA/A*XX*AA mutant. Under conditions of low endogenous TIF2/GRIP1 levels in COS cells, DHT had little effect on AR-F*XX*AA/A*XX*AA levels compared with the increase seen with wild-type AR (Fig. 10), as previously reported (67). The addition of EGF only slightly increased AR-F*XX*AA/A*XX*AA levels in the presence or absence of DHT. In contrast, when GRIP1 was overexpressed, there was a striking increase in AR-F*XX*AA/A*XX*AA levels with DHT, which was further increased in the presence of EGF (Fig. 10). It is noteworthy that EGF in the presence of GRIP1 but in the absence of androgen also increased AR-F*XX*AA/AXXAA levels. The results suggest that increased TIF2/GRIP1 expression that can occur in response to EGF and that is frequently observed in recurrent prostate cancer (44) contributes to increased AR-mediated transactivation. Increased levels of TIF2 may compete more effectively for the N/C interaction, resulting in increased coactivator recruitment and AR transactivation.

Effect of TIF2/GRIP1 siRNA on AR Transactivation—To determine whether TIF2/GRIP1 is required for AR transactivation by DHT and EGF in CWR-R1 cells, we used RNA interference to inhibit endogenous TIF2/GRIP1 expression. An siRNA mixture consisting of 12–30 bp of double-stranded RNA coding for TIF2/GRIP1 was transiently transfected into CWR-R1 cells together with pCMVhAR and PSA-Luc. TIF2 siRNA directed at nucleotides 197–376 inhibited AR transactivation of PSA-Luc by 5-fold, whereas a glyceraldehyde-3-phosphate dehydrogenase siRNA mixture had no effect (Fig. 11). Specificity for the TIF2 siRNA inhibition was established by cotransfecting pSG5TIF2 with 10 nM TIF2 siRNA. Partial recovery of AR transactivation of PSA-Luc activity in the presence of overexpressed TIF2 provided evidence that inhibition by TIF2 siRNA was specific.

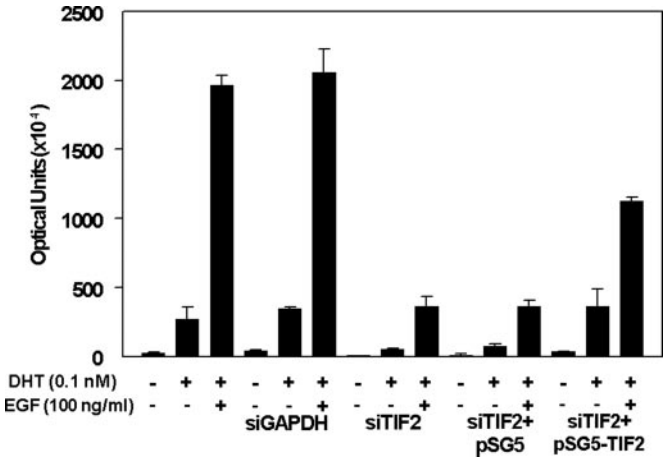

FIG. 11. **Interference of AR transcriptional activity by TIF2 siRNA.** CWR-R1 cells were transfected with the PSA-Luc reporter and pCMVhAR with and without 10 nM glyceraldehyde-3-phosphate dehydrogenase (*GAPDH*) siRNA or TIF2 siRNA in the absence and presence of 0.05 μg of pSG5 or pSG5-TIF2 using Effectene as described under "Experimental Procedures." Cells were incubated for 24 h with and without 0.1 nM DHT in the absence and presence of 100 ng/ml EGF. The data are representative of four independent experiments.

DISCUSSION

The recurrent growth of prostate cancer after prolonged androgen deprivation is recapitulated by human xenograft models such as CWR22 (22, 62, 85) and LAPC-4 and LAPC-9 (86) prostate tumors. Like human prostate cancers that are androgen-dependent for growth, these human tumors propagated in nude mice regress following androgen withdrawal by castration but after several months regrow in an environment of low circulating androgen. Most reports implicate a critical role for the AR in recurrent prostate cancer growth and progression despite reduced circulating androgen levels, and some studies suggest that mitogen signaling bypasses the requirement for androgen. In the present report, we provide evidence that EGF signaling through MAPK increases androgen-dependent AR transcriptional activity in the CWR-R1 recurrent human prostate cancer cell line. EGF increased androgen-dependent AR transactivation in association with increased levels of TIF2 in the CWR-R1 cell line. EGF and testosterone each increased AR and TIF2 levels in the androgen-dependent CWR22 xenograft tumor, supporting their complementary relationship. EGF increased TIF2 phosphorylation and the interaction between phosphorylated forms of TIF2 and AR. The effects of EGF were mediated in part through phosphorylation of TIF2/GRIP1 at Ser^{736}. TIF2/GRIP1 in CWR-R1 cells also probably contributed to increased transactivation by the NH_2-terminal activation function 1 of the AR NH_2-terminal DNA binding domain fragment AR 1–660. Reducing TIF2/GRIP1 levels in CWR-R1 cells using inhibitory RNAs resulted in a decreased AR transcriptional response to DHT and EGF. The data provide evidence for a direct link between AR transcriptional activity in recurrent prostate cancer, EGF signaling, and increased p160 coactivator levels. In addition, the studies provide a mechanism to explain the recent finding that a majority of recurrent prostate cancers have elevated levels of TIF2 (44).

Mechanisms described thus far to account for increased AR transactivation in recurrent prostate cancer include ligand-independent activation by mitogen signaling, AR overexpression, and AR mutations. Of these, increased signaling by EGF and TGFα was reported to occur in association with the transition from androgen-dependent to recurrent prostate cancer (87), and prostate cancer cell lines have been shown to synthesize and secrete EGF and related peptides (88). In addition, the EGF family of receptors is expressed in most recurrent prostate cancers (89), with ErbB2 protein expression most frequently reported (90–93). The CWR22 xenograft (62, 94–97) expresses ErbB1, -2, and -3 as shown by reverse transcription PCR (62, 94, 95), and the CWR-R1 cell line expresses ErbB1, -2, -3, and -4.[2] This agrees with reports that the ErbB1 inhibitor ZD1839 reduces the growth of androgen-dependent and recurrent CWR22 cells in culture (98) and that growth in primary cultures of androgen-dependent and recurrent CWR22 cells was inhibited by a monoclonal antibody to ErbB2 that blocked heregulin-induced activation of MAPK and Akt (94).

The link between EGF signaling and AR is supported by a number of previous studies, most of which relied on the overexpression of key signaling molecules. In the LNCaP prostate cancer cell line, increased growth and PSA expression were observed after stable overexpression of ErbB2 through the MAPK pathway (99). Overexpression of ErbB2 was associated with ligand-independent activation of AR in recurrent prostate cancer growth (99). Cell signaling by interleukin-6 in LNCaP cells was mediated by tyrosine phosphorylation of ErbB2 and ErbB3 (100). Stable overexpression of a constitutively active mitogen-activated protein kinase kinase kinase 1-induced apoptosis in LNCaP cells expressing AR, but there was no change in PC3 or DU145 cells that lack AR expression (101). ErbB2 was reported to activate Akt-directed phosphorylation at AR serine residues 213 and 791 in association with growth of recurrent prostate cancer in the absence of androgen (102). MAPK-directed AR phosphorylation was also implicated in hormone-independent AR activation in prostate cancer (99, 101). Overall, the results support the link between the MAPK pathway and AR transcriptional activity.

The data presented in this report indicate that increased AR transcriptional activity occurs in response to EGF in part from an increase in the androgen-dependent association between AR and TIF2/GRIP1. The interaction between p160 coactivator TIF2/GRIP1 and AR is mediated primarily by binding of the third L*XX*LL motif of TIF2 to the AF2 hydrophobic surface in the AR ligand binding domain (103–105). Under normal conditions of low coactivator expression as shown here for a human foreskin fibroblast cell line, AR interaction with p160 coactivators might be limited by the lower binding affinity of the coactivator L*XX*LL motifs to the AR AF2 binding site compared with binding of the AR NH_2-terminal F*XX*LF motif that mediates the androgen-dependent N/C interaction (66, 106). An optimal transcriptional response of AR to TIF2/GRIP1 depends on the interaction between the L*XX*LL motifs and the AR AF2 region (68). We have shown previously that increased levels of p160 coactivators compete for the androgen-induced N/C interaction to gain access to the AF2 region in the ligand binding domain (67). Mutating Ser^{736} adjacent to the third and predominant interacting L*XX*LL motif of TIF2/GRIP1 reduced the interaction between TIF2/GRIP1 and AR, supporting a key role for L*XX*LL motif binding. The importance of phosphorylation at TIF2/GRIP1 serine 736 was shown previously for coactivation of the estrogen and progesterone receptors (83). In the present report, we provide further evidence that this MAPK signaling pathway contributes to increased AR transactivation in recurrent prostate cancer.

We found that transient expression of TIF2/GRIP1 in the presence of DHT and EGF had a stabilizing effect on AR-F*XX*AA/A*XX*AA, an AR with mutations in the NH_2-terminal ^{23}FQNLF^{27} and ^{433}WHTLF^{437} sequences that are required for the androgen-induced AR N/C interaction (66–68). Mutations

[2] C. W. Gregory, W. McCall, X. Fei, Y. E. Whang, F. S. French, E. M. Wilson, and H. S. Earys, unpublished results.

that cause loss of the N/C interaction allow greater accessibility of AF2 in the ligand binding domain to activation by p160 coactivators such as TIF2/GRIP1 (67). Surprisingly, whereas loss of the N/C interaction reduced AR transactivation of the PSA promoter in other cell lines (68), this mutant was as effective as wild-type AR when assayed in the CWR-R1 cell line, supporting the notion that higher levels of TIF2 compensate for loss of the AR N/C interaction.

EGF also increased transactivation by the AR NH_2-terminal and DNA binding domain fragment AR 1–660 that lacks the ligand binding domain. This agrees with previous reports that p160 coactivators interact with multiple regions of steroid receptors, including an interaction between the glutamine-rich region of p160 coactivators and the NH_2-terminal domains of steroid receptors (70, 107, 108). The EGF-induced increased in TIF2/GRIP1 activity in CWR-R1 cells therefore also probably contributes to AR transactivation through interactions with the AR NH_2-terminal region. Previous studies on the effects of EGF on the progesterone and estrogen receptors support increased p160 coactivator activity as a mechanism for growth factor regulation of nuclear receptors (83).

Evidence presented here and previously suggests that recurrent prostate cancer is influenced by autocrine loops involving EGF signaling. Recurrent growth of the androgen-dependent CWR22 xenograft in the absence of testis-derived androgen occurred in the presence of increased expression of TGFα, which could establish an autocrine regulatory loop through the EGF receptor (87). Recurrent CWR22 tumors express high levels of EGF-related ligands compared with the androgen-dependent tumor (94), and increased immunostaining of TGFα was found in recurrent CWR22 xenografts (87). Further support for an autocrine regulatory loop comes from observations that CWR-R1 cells express EGF, heparin-binding EGF, TGFα, and heregulin messenger RNAs.[2] In the present report, we show that ZD1839, an EGF receptor (ErbB1)-specific inhibitor, did not diminish the transcriptional activity of endogenous AR in CWR-R1 cells, whereas the downstream MEK inhibitor U0126 decreased DHT-induced AR transactivation in CWR-R1 cells in the absence of added EGF. These data suggest that an endogenous EGF or TGFα-like ligand induces MAPK signaling independent of the EGF receptor, ErbB1. The ErbB2 and ErbB3 receptors may therefore be key modulators of AR activation in CWR-R1 cells, as reported for heregulin and ErbB3 in advanced prostate cancer (61). EGF-related peptides produced by CWR-R1 cells could interact with other members of the EGF receptor family (50). Our studies did not provide evidence that autocrine signaling through the EGF receptor family can override a requirement for androgen. Rather, autocrine regulation of recurrent prostate cancer cells appears to contribute to androgen-activated AR-mediated gene transcription. Earlier evidence suggested that prostate cancer cells establish an autocrine loop through EGF or TGFα and their receptors (109), and studies cited above indicate that this autocrine loop is present in the recurrent CWR22 xenograft and CWR-R1 cell line.

The apparent requirement for androgen by recurrent prostate cancer cells for AR transactivation raises the question of the source of ligand. In prostate cancer patients that are castrated or treated with luteinizing hormone-releasing hormone agonists to suppress testicular androgen production in response to pituitary luteinizing hormone, adrenal androgens circulate at levels sufficient to serve as precursors for the biosynthesis of testosterone and DHT. Remarkably, testosterone levels in recurrent prostate cancer tissue specimens during androgen withdrawal therapy were found to be similar to levels in benign prostate hyperplasia tissue from untreated patients (110). DHT levels in recurrent prostate cancer tissue were reduced to 10% compared with benign prostate. These results suggest that tissue androgen production may be sufficient in recurrent prostate cancer to activate AR after the withdrawal of circulating androgen. Furthermore, the range of steroids that activate AR in some prostate cancers is increased by certain AR mutations in the ligand binding domain, such as the LNCaP AR mutant T877A and AR-H874Y mutant in the CWR22 tumor and derived cell lines (31). Human prostate cancer xenografts expressing wild-type AR (10, 86) have a pattern of recurrent growth in nu/nu mice like that for recurrent prostate cancer in patients after androgen deprivation by castration, suggesting that tissue androgen or other AR-activating ligands are sufficient in the xenografts to trigger AR transactivation.

Therapeutic strategies for prostate cancer have been aimed recently at inhibiting the EGF signaling pathway. Inhibitors such as GW572016 gained attention in attempts to block tumor progression (111). This approach was effective in targeting ErbB2 for the treatment of breast cancer. But unlike breast cancer, where ErbB2 receptors are frequently overexpressed (112), these receptors are present but not highly expressed in most recurrent prostate cancer specimens (90, 99). Clinical targeting of ErbB2 with antitumor agents such as Herceptin (trastuzumab), a humanized monoclonal antibody to the extracellular domain of ErbB2, was ineffective in advanced prostate cancer patients that were negative for ErbB2 expression (113) but more effective when receptors were overexpressed (114). The anti-ErbB2 antibody Herceptin inhibited growth of androgen-dependent CWR22 and LNCaP xenografts but did not inhibit growth of the recurrent CWR22 tumor (115). A monoclonal antibody that binds a different region from the Herceptin binding site inhibited association of ErbB2 receptor with other EGF receptor family members, blocking heregulin-mediated signaling in androgen-dependent and -independent prostate cancer cell lines (94). Other approaches have been taken to inhibit prostate tumor growth by indirectly targeting the AR. Proliferation of prostate cancer cells and xenografts was reduced by an hsp90 inhibitor and decreased AR, ErbB2, and Akt expression levels, supporting the role of these pathways in androgen-dependent and recurrent tumor growth (116).

Acknowledgments—We thank Lori W. Lee, John T. Minges, Rebecca I. Kalman, K. Michelle Cobb, Yianrong Chen and De-Ying Zang for excellent technical assistance; Jiann-an Tan for advice on immunostaining with anti-phosphoserine antibodies; and Tona Gilmer and David Rusnak (GlaxoSmithKline, Research Triangle Park, NC) for providing the inhibitor ZD1839.

REFERENCES

1. Lubahn, D. B., Joseph, D. R., Sullivan, P. M., Willard, H. F., French, F. S., and Wilson, E. M. (1988) *Science* **240,** 327–330
2. Chang, C. S., Kokontis, J., and Liao, S. T. (1988) *Science* **240,** 324–326
3. Roy, A. K., Lavrovsky, Y., Song, C. S., Chen, S., Jung, M. H., Velu, N. K., Bi, B. Y., and Chatterjee, B. (1999) *Vitam. Horm.* **55,** 309–352
4. Gelmann, E. P. (2002) *J. Clin. Oncol.* **20,** 3001–3015
5. Nelson, P. S., Clegg, N., Arnold, H., Ferguson, C., Bonham, M., White, J., Hood, L., and Lin, B. (2002) *Proc. Natl. Acad. Sci. U. S. A.* **99,** 11890–11895
6. Jiang, F., and Wang, Z. (2003) *Endocrinology* **144,** 1257–1265
7. Isaacs, J. T. (1994) *Vitam. Horm.* **49,** 433–502
8. Feldman, B. J., and Feldman, D. (2001) *Nat. Rev. Cancer* **1,** 34–45
9. Grossmann, M. E., Huang, H., and Tindall, D. J. (2001) *J. Natl. Cancer Inst.* **93,** 1687–1697
10. Craft, N., Chhor, C., Tran, C., Belldegrun, A., DeKernion, J., Witte, O. N., Said, J., Reiter, R. E., and Sawyers, C. L. (1999) *Cancer Res.* **59,** 5030–5036
11. van der Kwast, T. H., Schalken, J., Ruizeveld de Winter, J. A., van Vroonhover, C. C., Mulder, E., Boersma, W., and Trapman, J. (1991) *Int. J. Cancer* **48,** 189–193
12. de vere White, R., Meyers, F., Chi, S. G., Chamberlain, S., Siders, D., Lee, F., Stewart, S., and Gumerlock, P. H. (1997) *Eur. Urol.* **31,** 1–6
13. Gregory, C. W., Hamil, K. G., Kim, D., Hall, S. H., Pretlow, T. G., Mohler, J. L., and French, F. S. (1998) *Cancer Res.* **58,** 5718–5724
14. Sadi, M. V., Walsh, P. C., and Barrack, E. R. (1991) *Cancer* **67,** 3057–3064
15. Chodak, G. W., Kranc, D. M., Puy, L. A., Takeda, H., Johnson, K., and Chang, C. (1992) *J. Urol.* **147,** 798–803

16. Zegarra-Moro, O. L., Schmidt, L. J., Huang, H., and Tindall, D. J. (2002) *Cancer Res.* **62,** 1008–1013
17. Eder, I. E., Hoffmann, J., Rogatsh, H., Schafer, G., Zopf, D., Bartsch, G., and Klocker, H. (2002) *Cancer Gene Ther.* **9,** 117–125
18. Lara, P. N., Jr., Kung, H. J., Gumerlock, P. H., and Meyers, F. J. (1999) *Crit. Rev. Oncol. Hematol.* **32,** 197–208
19. Koivisto, P., Kononen, J., Palmberg, C., Tammela, T., Hyytinen, E., Isola, J., Trapman, J., Cleutjens, K., Noordzij, A., Visakorpi, T., and Kallioniemi, O. P. (1997) *Cancer Res.* **57,** 314–319
20. Palmberg, C., Koivisto, P., Kakkola, L., Tammela, T. L., Kallioniemi, O. P., and Visakorpi, T. (2000) *J. Urol.* **64,** 1992–1995
21. Linja, M. J., Savinainen, K. J., Saramaki, O. R., Tammela, T. L., Vessella, R. L., and Visakorpi, T. (2001) *Cancer Res.* **61,** 3550–3555
22. Gregory, C. W., Johnson, R. T., Mohler, J. L., French, F. S., and Wilson, E. M. (2001) *Cancer Res.* **61,** 2892–2898
23. Quigley, C. A., De Bellis, A., Marschke, K. B., el-Awady, M. K., Wilson, E. M., and French, F. S. (1995) *Endocr. Rev.* **16,** 271–321
24. Koivisto, P., Kolmer, M., Visakorpi, T., and Kallioniemi, O. P. (1998) *Am. J. Pathol.* **152,** 1–9
25. Marcelli, M., Ittmann, M., Mariani, S., Sutherland, R., Nigam, R., Murthy, L., Zhao, Y., DiConcini, D., Puxeddu, E., Esen, A., Eastham, J., Weigel, N. L., and Lamb, D. J. (2000) *Cancer Res.* **60,** 944–949
26. Buchanan, G., Greenberg, N. M., Scher, H. I., Harris, J. M., Marshall, V. R., and Tilley, W. D. (2001) *Clin. Cancer Res.* **7,** 1273–1281
27. Shi, X. B., Ma, A. H., Xia, L., Kung, H. J., and de Vere White, R. W. (2002) *Cancer Res.* **62,** 1496–1502
28. Culig, Z., Hobisch, A., Cronauer, M. V., Cato, A. C., Hittmair, A., Radmayr, C., Eberle, J., Bartsch, G., and Klocker, H. (1993) *Mol. Endocrinol.* **7,** 1541–1550
29. Peterziel, H., Culig, Z., Stober, J., Hobisch, A., Radmayr, C., Bartsch, G., Klocker, H., and Cato, A. C. (1995) *Int. J. Cancer* **63,** 544–550
30. Elo, J. P., Kvist, L., Leinonen, K., Isomaa, V., Henttu, P., Lukkarinen, O., and Vihko, P. (1995) *J. Clin. Endocrinol. Metabol.* **80,** 3494–3500
31. Tan, J., Sharief, Y., Hamil, K. G., Gregory, C. W., Zang, D. Y., Sar, M., Gumerlock, P. H., de Vere White, R. W., Pretlow, T. G., Harris, S. E., Wilson, E. M., Mohler, J. L., and French, F. S. (1997) *Mol. Endocrinol.* **11,** 450–459
32. Chang, C. Y., Walther, P. J., and McDonnell, D. P. (2001) *Cancer Res.* **61,** 8712–8717
33. Hakimi, J. M., Schoenberg, M. P., Rondinelli, R. H., Piantadosi, S., and Barrack, E. R. (1997) *Clin. Cancer Res.* **3,** 1599–1608
34. Choong, C. S., Kemppainen, J. A., Zhou, Z. X., and Wilson, E. M. (1996) *Mol. Endocrinol.* **10,** 1527–1535
35. Newmark, J. R., Hardy, D. O., Tonb, D. C., Carter, B. S., Epstein, J. I., Isaacs, W. B., Brown, T. R., and Barrack, E. R. (1992) *Proc. Natl. Acad. Sci. U. S. A.* **89,** 6319–6323
36. Taplin, M. E., and Ho, S. M. (2001) *J. Clin. Endocrinol. Metabol.* **86,** 3467–3477
37. Balk, S. P. (2002) *Urology* **60,** Suppl. 3A, 132–139
38. Onate, S. A., Tsai, S. Y., Tsai, M. J., and O'Malley, B. W. (1995) *Science* **270,** 1354–1357
39. Voegel, J. J., Heine, M. J., Tini, M., Vivat, V., Chambon, P., and Gronemeyer, H. (1998) *EMBO J.* **17,** 507–519
40. Hong, H., Kohli, K., Garabedian, M. J., and Stallcup, M. R. (1997) *Mol. Cell Biol.* **17,** 2735–2744
41. McKenna, N. J., Lanz, R. B., and O'Malley, B. W. (1999) *Endocr. Rev.* **20,** 321–344
42. Tan, J., Hall, S. H., Petrusz, P., and French, F. S. (2000) *Endocrinology* **141,** 3440–3450
43. Heinlein, C. A., and Chang, C. (2002) *Endocr. Rev.* **23,** 175–200
44. Gregory, C. W., He, B., Johnson, R. T., Ford, O. H., Mohler, J. L., French, F. S., and Wilson, E. M. (2001) *Cancer Res.* **61,** 4315–4319
45. Ogryzko, V. V., Kotani, T., Zhang, X., Schlitz, R. L., Howard, T., Yang, X. J., Howard, B. H., Qin, J., and Nakatani, Y. (1998) *Cell* **94,** 35–44
46. Murphy, L. C., Simon, S. L., Parkes, A., Leygue, E., Dotzlaw, H., Snell, L., Troup, S., Adeyinka, A., and Watson, P. H. (2000) *Cancer Res.* **60,** 6266–6271
47. Graham, J. D., Bain, D. L., Richer, J. K., Jackson, T. A., Tung, L., and Horwitz, K. B. (2000) *J. Steroid Biochem. Mol. Biol.* **74,** 255–259
48. Anzick, S. L., Kononen, J., Walker, R. L., Azorsa, D. O., Tanner, M. M., Guan, X. Y., Sauter, G., Kallioniemi, O. P., Trent, J. M., and Meltzer, P. S. (1997) *Science* **277,** 965–968
49. Darne, C., Veyssiere, G., and Jean, C. (1998) *Eur. J. Biochem.* **256,** 541–549
50. Kung, H. J., Tepper, C. G., and de Vere White, R. W. (2001) in *Prostate Cancer: Biology, Genetics and the New Therapeutics* (Chung, L. W., Isaacs, W. B., and Simons, J. W., eds) pp. 241–266, Humana Press, Inc., Totowa, NJ
51. Sadar, M. D., Hussain, M., and Bruchovsky, N. (1999) *Endocrine-related Cancer* **6,** 487–502
52. Nazareth, L. V., and Weigel, N. L. (1996) *J. Biol. Chem.* **271,** 19900–19907
53. Jia, L., Kim, J., Shen, H., Clark, P. E., Tilley, W. D., and Coetzee, G. A. (2003) *Mol. Cancer Res.* **1,** 385–392
54. Weigel, N. L. (1996) *Biochem. J.* **319,** 657–667
55. Culig, Z., Hobisch, A., Hittmair, A., Peterziel, H., Cato, A. C., Bartsch, G., and Klocker, H. (1998) *Prostate* **35,** 63–70
56. Blok, L. J., de Ruiter, P. E., and Brinkmann, A. O. (1998) *Biochemistry* **37,** 3850–3857
57. Culig, Z., Hobisch, A., Cronauer, M. V., Radmayr, C., Hittmair, A., Zhang, J., Thurnher, M., Bartsch, G., and Klocker, H. (1996) *Prostate* **28,** 392–405
58. Craft, N., Shostak, Y., Carey, M., and Sawyers, C. L. (1999) *Nat. Med.* **5,** 280–285
59. Reinikainen, P., Palvimo, J. J., and Janne, O. A. (1996) *Endocrinology* **137,** 4351–4357
60. Orio, F., Terouanne, B., Georget, V., Lumbroso, S., Avances, C., Siatka, C., and Sultan, C. (2002) *Mol. Cell Endocrinol.* **198,** 105–114
61. Leung, H. Y., Weston, J., Gullick, W. J., and Williams, G. (1997) *Br. J. Urol.* **79,** 212–216
62. Wainstein, M. A., He, F., Robinson, D., Kung, H. J., Schwartz, S., Giaconia, J. M., Edgehouse, N. L., Pretlow, T. P., Bodner, D. R., Kursh, E. D., Resnick, M. I., Seftel, A., and Pretlow, T. G. (1994) *Cancer Res.* **54,** 6049–6052
63. Lubahn, D. B., Joseph, D. R., Sar, M., Tan, J., Higgs, H. N., Larson, R. E., French, F. S., and Wilson, E. M. (1988) *Mol. Endocrinol.* **2,** 1265–1275
64. Simental, J. A., Sar, M., Lane, M. V., French, F. S., and Wilson, E. M. (1991) *J. Biol. Chem.* **266,** 510–518
65. Zhou, Z. X., Sar, M., Simental, J. A., Lane, M. V., and Wilson, E. M. (1994) *J. Biol. Chem.* **269,** 13115–13123
66. He, B., Kemppainen, J. A., and Wilson, E. M. (2000) *J. Biol. Chem.* **275,** 22986–22994
67. He, B., Bowen, N. T., Minges, J. T., and Wilson, E. M. (2001) *J. Biol. Chem.* **276,** 42293–42301
68. He, B., Lee, L. W., Minges, J. T., and Wilson, E. M. (2002) *J. Biol. Chem.* **277,** 25631–25639
69. Langley, E., Zhou, Z. X., and Wilson, E. M. (1995) *J. Biol. Chem.* **270,** 29983–29990
70. He, B., Kemppainen, J. A., Voegel, J. J., Gronemeyer, H., and Wilson, E. M. (1999) *J. Biol. Chem.* **274,** 37219–37225
71. Pang, S., Dannull, J., Kaboo, R., Xie, Y., Tso, C. L., Michel, K., de Kernion, J. B., and Belldegrun, A. S. (1997) *Cancer Res.* **57,** 495–499
72. Gregory, C. W., Johnson, R. T., Presnell, S. C., Mohler, J. L., and French, F. S. (2001) *J. Androl.* **22,** 537–548
73. Quarmby, V. E., Kemppainen, J. A., Sar, M., Lubahn, D. B., French, F. S., and Wilson, E. M. (1990) *Mol. Endocrinol.* **4,** 1399–1407
74. Yang, D., Buchholz, F., Huang, Z., Goga, A., Chen, C. Y., Brodsky, F. M., and Bishop, J. M. (2002) *Proc. Natl. Acad. Sci. U. S. A.* **99,** 9942–9947
75. Calegari, F., Haubensak, W., Yang, D., Huttner, W. B., and Buchholz, F. (2002) *Proc. Natl. Acad. Sci. U. S. A.* **99,** 14236–14240
76. Kemppainen, J. A., Lane, M. V., Sar, M., and Wilson, E. M. (1992) *J. Biol. Chem.* **267,** 968–974
77. Payne, D. M., Rossomando, A. J., Martino, P., Erickson, A. K., Her, J. H., Shabanowitz, J., Hunt, D. F., Weber, M. J., and Sturgill, T. W. (1991) *EMBO J.* **10,** 885–892
78. He, B., Minges, J. T., Lee, L. W., and Wilson, E. M. (2002) *J. Biol. Chem.* **277,** 10226–10235
79. Langley, E., Kemppainen, J. A., and Wilson, E. M. (1998) *J. Biol. Chem.* **273,** 92–101
80. Perheentupa, J., Lakshmanan, J., Hoath, S. B., and Fisher, D. A. (1984) *Acta Endocrinol.* **107,** 571–576
81. Perheentupa, J., Lakshmanan, J., Hoath, S. B., Beri, U., Kim, H., Macaso, T., and Fisher, D. A. (1985) *Am. J. Physiol.* **248,** E391–E396
82. Kim, D., Gregory, C. W., French, F. S., Smith, G. J., and Mohler, J. L. (2002) *Am. J. Pathol.* **160,** 219–226
83. Lopez, G. N., Turck, C. W., Schaufele, F., Stallcup, M. R., and Kushner, P. J. (2001) *J. Biol. Chem.* **276,** 22177–22182
84. He, B., and Wilson, E. M. (2002) *Mol. Genet. Metabol.* **75,** 293–298
85. Nagabhushan, M., Miller, C. M., Pretlow, T. P., Giaconia, J. M., Edgehouse, N. L., Schwartz, S., Kung, H. J., de Vere White, R. W., Gumerlock, P. H., Resnick, M. I., Amini, S. B., and Pretlow, T. G. (1996) *Cancer Res.* **56,** 3042–3046
86. Klein, K. A., Reiter, R. E., Redula, J., Moradi, H., Zhu, X. L., Brothman, A. R., Lamb, D. J., Marcelli, M., Belldegrun, A., Witte, O. N., and Sawyers, C. L. (1997) *Nat. Med.* **3,** 402–408
87. Myers, R. B., Oelschlager, D., Manne, U., Coan, P. N., Weiss, H., and Grizzle, W. E. (1999) *Int. J. Cancer* **82,** 424–429
88. Connolly, J. M., and Rose, D. P. (1990) *Prostate* **16,** 209–218
89. Scher, H. I., Sarkis, A., Reuter, V. E., Cohen, D., Netto, G., Petrylak, D., Lianes, P., Fuks, Z., Mendelsohn, J., and Cordon-Cardo, C. (1995) *Clin. Cancer Res.* **1,** 545–550
90. Calvo, B. F., Levine, A. M., Marcos, M., Collins, Q. F., Iacocca, M. V., Caskey, L. S., Gregory, C. W., Lin, Y., Whang, Y. E., Earp, H. S., and Mohler, J. L. (2003) *Clin. Cancer Res.* **9,** 1087–1097
91. Reese, D. M., Small, E. J., Magrane, G., Waldman, F. M., Chew, K., and Sudilovsky, D. (2001) *Am. J. Clin. Pathol.* **116,** 234–239
92. Shi, Y., Brands, F. H., Chatterjee, S., Fendg, A. C., Groshen, S., Schewe, J., Lieskovsky, G., and Cote, R. J. (2001) *J. Urol.* **166,** 1514–1519
93. Osman, I., Scher, H. I., Drobnjak, M., Verbel, D., Morris, M. J., Agus, D. B., Ross, J. S., and Cordon-Cardo, C. (2001) *Clin. Cancer Res.* **7,** 2643–2647
94. Agus, D. B., Akita, R. W., Fox, W. D., Lewis, G. D., Higgins, B., Pisacane, P. I., Lofgren, J. A., Tindell, C., Evans, D. P., Maisese, K., Scher, H. I., and Sliwkowski, M. X. (2002) *Cancer Cell* **2,** 127–137
95. Robinson, D., He, F., Pretlow, T. G., and Kung, H.-J. (1996) *Proc. Natl. Acad. Sci. U. S. A.* **93,** 5958–5962
96. Rusnak, D. W., Lackey, K., Affleck, K., Wood, E. R., Alligood, K. J., Rhodes, N., Keith, B. R., Murray, D. M., Glennon, K., Knight, W. B., Mullin, R. J., and Gilmer, T. M. (2001) *Mol. Cancer Ther.* **1,** 85–94
97. Manin, M., Baron, S., Goossens, K., Beaudoin, C., Jean, C., Veyssiere, G., Verhoeven, G., and Morel, L. (2002) *Biochem. J.* **366,** 729–736
98. Sirotnak, F. M., She, Y., Lee, F., Chen, J., and Scher, H. I. (2002) *Clin. Cancer Res.* **8,** 3870–3876
99. Yeh, S. Y., Lin, H. K., Kang, H. Y., Thin, T. H., Lin, M. F., and Chang, C. (1999) *Proc. Natl. Acad. Sci. U. S. A.* **96,** 5458–5463
100. Qiu, Y., Ravi, L., and Kung, H. J. (1998) *Nature* **393,** 83–85
101. Abreu-Martin, M. T., Chari, A., Pallidino, A. A., Craft, N. A., and Sawyers, C. L. (1999) *Mol. Cell Biol.* **19,** 5143–5154
102. Wen, Y., Hu, M. C., Makino, K., Spohn, B., Bartholomeusz, G., Yan, D. H., and Hung, M. C. (2000) *Cancer Res.* **60,** 6841–6845

103. Heery, D. M., Kalkhoven, E., Hoare, S., and Parker, M. G. (1997) *Nature* **387,** 733–736
104. Nolte, R. T., Wisely, G. B., Westin, S., Cobb, J. E., Lambert, M. H., Kurokawa, R., Rosenfeld, M. G., Willson, T. M., Glass, C. K., and Milburn, M. V. (1998) *Nature* **395,** 137–143
105. Darimont, B. D., Wagner, R. L., Apriletti, J. W., Stallcup, M. R., Kushner, P. J., Baxter, J. D., Fletterick, R. J., and Yamamoto, K. R. (1998) *Genes Dev.* **12,** 3343–3356
106. He, B., and Wilson, E. M. (2003) *Mol. Cell Biol.* **23,** 2135–2150
107. Onate, S. A., Boonyaratanakornkit, V., Spencer, T. E., Tsai, S. Y., Tsai, M. J., Edwards, D. P., and O'Malley, B. W. (1998) *J. Biol. Chem.* **273,** 12101–12108
108. Bevan, C. L., Hoare, S., Claessens, F., Heery, D. M., and Parker, M. G. (1999) *Mol. Cell Biol.* **19,** 8383–8392
109. Steiner, M. S. (1997) in *Prostate: Basic and Clinical Aspects* (Naz, R. K., ed) pp. 151–180, CRC Press, Inc., Boca Raton, FL
110. Mohler, J. L., Gregory, C. W., Ford, O. H., Kim, D., Weaver, C. M., Petrusz, P., Wilson, E. M., and French, F. S. (2004) *Clin. Cancer Res.*, **10,** in press
111. Xia, W., Mullin, R. J., Keith, B. R., Liu, L. H., Ma, H., Rusnak, D. W., Owens, G., Alligood, K. J., and Spector, N. L. (2002) *Oncogene* **21,** 6255–6263
112. Menard, S., Tagliabue, E., Campiglio, M., and Pupa, S. M. (2000) *J. Cell Physiol.* **182,** 150–162
113. Morris, M. J., Reuter, V. E., Kelly, W. K., Slovin, S. F., Kenneson, K., Verbel, D., Osman, I., and Scher, H. I. (2002) *Cancer* **94,** 980–986
114. Baselga, J. (2002) *Cancer Cell* **2,** 93–95
115. Agus, D. B., Scher, H. I., Higgins, B., Fox, W. D., Heller, G., Fazzari, M., Cordon-Cardo, C., and Golde, D. W. (1999) *Cancer Res.* **59,** 4761–4764
116. Solit, D. B., Zheng, F. F., Drobnjak, M., Munster, P. N., Higgins, B., Verbel, D., Heller, G., Tong, W., Cordon-Cardo, C., Agus, D. B., Scher, H. I., and Rosen, N. (2002) *Clin. Cancer Res.* **8,** 986–993

THE JOURNAL OF BIOLOGICAL CHEMISTRY
Vol. 279, No. 29, Issue of July 16, pp. 30643–30653, 2004

Printed in U.S.A.

An Androgen Receptor NH_2-terminal Conserved Motif Interacts with the COOH Terminus of the Hsp70-interacting Protein (CHIP)*

Received for publication, March 19, 2004, and in revised form, April 21, 2004
Published, JBC Papers in Press, April 23, 2004, DOI 10.1074/jbc.M403117200

Bin He‡§¶, Suxia Bai‡§, Andrew T. Hnat‡§, Rebecca I. Kalman‡§, John T. Minges‡§, Cam Patterson‖, and Elizabeth M. Wilson‡§‡‡**

*From the ‡Laboratories for Reproductive Biology and the Departments of §Pediatrics, ‖Medicine, and **Biochemistry and Biophysics, University of North Carolina, Chapel Hill, North Carolina 27599*

The NH_2-terminal sequence of steroid receptors is highly variable between different receptors and in the same receptor from different species. In this study, a primary sequence homology comparison identified a 14-amino acid NH_2-terminal motif of the human androgen receptor (AR) that is common to AR from all species reported, including the lower vertebrates. The evolutionarily conserved motif is unique to AR, with the exception of a partial sequence in the glucocorticoid receptor of higher species. The presence of the conserved motif in AR and the glucocorticoid receptor and its absence in other steroid receptors suggests convergent evolution. The function of the AR NH_2-terminal conserved motif was suggested from a yeast two-hybrid screen that identified the COOH terminus of the Hsp70-interacting protein (CHIP) as a binding partner. We found that CHIP functions as a negative regulator of AR transcriptional activity by promoting AR degradation. In support of this, two mutations in the AR NH_2-terminal conserved motif previously identified in the transgenic adenocarcinoma of mouse prostate model reduced the interaction between CHIP and AR. Our results suggest that the AR NH_2-terminal domain contains an evolutionarily conserved motif that functions to limit AR transcriptional activity. Moreover, we demonstrate that the combination of comparative sequence alignment and yeast two-hybrid screening using short conserved peptides as bait provides an effective strategy to probe the structure-function relationships of steroid receptor NH_2-terminal domains and other intrinsically unstructured transcriptional regulatory proteins.

Steroid receptors depend on multiple domains for their function as ligand-dependent transcriptional activators. The DNA- and ligand-binding domains have been studied extensively and have a high degree of structural and functional conservation. In contrast, the largely unstructured NH_2-terminal domains (1–3) are highly variable in size and sequence, and the molecular mechanisms that contribute to transactivation are not well understood. The size of the NH_2-terminal region of steroid receptors increases with evolutionary expansion (4, 5), from estrogen receptor-α (185 amino acid residues) to the glucocorticoid receptor (GR[1]; 420 residues), androgen receptor (AR; 558 residues), progesterone receptor (B form; 566 residues), and mineralocorticoid receptor (602 residues). In contrast, transcription factors such as p53, NF-κB, and VP16 typically have transcriptional activation domains of $<$100 residues.

The importance of the NH_2-terminal domain for AR functional activity is attributed largely to activation function-1 (AF1) between amino acid residues 142 and 337 (6). This region was further resolved into two noncontiguous activation segments, AF1a and AF1b (7). The functional importance of the AR NH_2-terminal region is supported by the extensive post-translational modification that occurs in the region, including phosphorylation (8–10), sumoylation (11), and ubiquitylation (12, 13). In addition, a conserved region between AR residues 225 and 259 in the region of AF1 was predicted to form an α-helix and to contribute to AR transactivation and was shown to be a binding site for the general transcription factor TFIIF (14). Earlier evidence also suggested that the AR NH_2-terminal region contains functional domains involved in transcriptional repression (15). In contrast, activation function-2 (AF2) in the AR ligand-binding domain, although highly conserved, has little inherent transcriptional activity when assayed in mammalian cells (16).

In this study, we identify sequence ^{234}AKELCKAVSVSMGL^{247} in the human AR NH_2-terminal domain, which is highly conserved in all AR sequences characterized thus far through multiple fish species. Based on the premise that strict amino acid sequence conservation indicates a site of critical function, we investigated the functional importance of human AR residues 234–247 using a yeast two-hybrid screen. The COOH terminus of the Hsp70-interacting protein (CHIP) was identified as a binding partner and was found to contribute to AR down-regulation.

MATERIALS AND METHODS

Plasmids—The yeast vector pGBT8 was kindly provided by Yue Xiong (University of North Carolina, Chapel Hill). pCMV-hAR-L237A/

* This work was supported by United States Public Health Service Grant HD16910 from NICHD, National Institutes of Health; by Grant PO1-CA77739 from NCI, National Institutes of Health; by Cooperative Agreement U54-HD35041 as part of the Specialized Cooperative Centers Program in Reproductive Research of the National Institutes of Health; and by Fogarty International Center Grant R03TW001234 from the National Institutes of Health (to Frank S. French). The costs of publication of this article were defrayed in part by the payment of page charges. This article must therefore be hereby marked "*advertisement*" in accordance with 18 U.S.C. Section 1734 solely to indicate this fact.

¶ Present address: Dept. of Molecular and Cellular Biology, Baylor College of Medicine, Houston, TX 77030.

‡‡ To whom correspondence should be addressed: Labs. for Reproductive Biology, CB 7500, Medical Biomolecular Research Bldg., Rm. 3340, 103 Mason Farm Rd., University of North Carolina, Chapel Hill, NC 27599. Tel.: 919-966-5168; Fax: 919-966-2203; E-mail: emw@med.unc.edu.

[1] The abbreviations used are: GR, glucocorticoid receptor; AR, androgen receptor; AF, activation function; CHIP, COOH terminus of the Hsp70-interacting protein; GST, glutathione *S*-transferase; TPR, tetratricopeptide repeat; MMTV, mouse mammary tumor virus; Luc, luciferase; DHT, dihydrotestosterone; TRITC, tetramethylrhodamine isothiocyanate; E3, ubiquitin-protein isopeptide ligase; TRAMP, transgenic adenocarcinoma of mouse prostate; PSA-Enh-Luc, prostate-specific antigen enhancer luciferase.

K239M/V241A/V243A, pCMV-hAR-A234T, and pCMV-hAR-E236G (17) were created using a double PCR strategy by cloning the fragment into the AflII and BstEII sites of pCMV-hAR. The yeast bait vector pGBT8-AR-(220–270) contains the conserved sequence ^{234}AKELCKAVSVSMGL^{247} and was constructed by PCR amplifying the corresponding region of human AR and inserting the fragment into the EcoRI and BamHI sites in the pGBT8 vector and was confirmed by DNA sequencing. GST-AR-(220–270) and GST-AR-(220–270m4), which contains mutations L237A/K239M/V241A/V243A, were created by digesting pGBT8-AR-(220–270) with and without the mutations with EcoRI and SalI and cloning the fragment into the EcoRI and SalI sites of pGEX-5X-1. GST-AR-(220–270)-A234T and GST-AR-(220–270)-E236G were made by PCR amplifying the corresponding regions of pCMV-hAR-A234T and pCMV-hAR-E236G, and the fragment was inserted into the EcoRI and SalI sites of pGEX-5X-1. Gal-AR-(234–247) and Gal-AR-(229–254), coding for the Gal4 DNA-binding domain fusion protein with the indicated AR NH_2-terminal residues, were created by cloning two annealed oligonucleotides into the EcoRI and BamHI sites of pGal0. Gal-AR-(220–270) and Gal-AR-(220–270m4) were created by PCR amplifying the corresponding regions of AR and ARm4 (AR with mutations L237A/K239M/V241A/V243A) and cloning into the EcoRI and BamHI sites of pGal0. pCMV5-CHIP and pCMV5-CHIPΔTPR, expressing CHIP with a deletion of the tetratricopeptide repeat (TPR) domain at residues 27–147 (see Fig. 3*A*), were created by digesting pcDNA3-CHIP and pcDNA3-CHIPΔTPR with EcoRI and XbaI and ligating the inserts to the EcoRI and XbaI sites of pCMV5. All PCR-amplified sequences were verified for the absence of random errors.

Yeast Two-hybrid Screen—A two-hybrid screen of a human testis library was performed by sequential transformation of bait and library plasmids as recommended by the manufacturer (Clontech, YEASTMAKER Transformation System 2 user's manual, catalog number K1606-1). Yeast strain HF7c was transformed with the bait vector pGBT8-AR-(220–270) and plated onto synthetic medium lacking Trp with the addition of 0.8 mM 3-amino-1,2,4-triazole to inhibit intrinsic activity. The yeast clone containing the bait vector was transformed using 100 μg of an amplified human testis MATCHMAKER cDNA library (BD Biosciences) and plated onto synthetic medium lacking Leu, Trp, and His with the addition of 0.8 mM 3-amino-1,2,4-triazole. Yeast colonies grown on synthetic medium lacking Leu, Trp, and His were further tested for activity using a two-hybrid interaction β-galactosidase filter assay performed following the instructions of the manufacturer (Clontech, yeast protocols handbook, catalog number PT3024-1, PR13103). Large fresh colonies were transferred to Whatman No. 5 filter paper, and the filters were immersed in liquid nitrogen for 10 s and allowed to thaw at room temperature. Freshly prepared Z buffer containing 60 mM NA_2HPO_4, 40 mM NaH_2PO_4, 10 mM KCl, 1 mM $MgSO_4$, 50 mM 2-mercaptoethanol, pH 7.0, and 0.33 mg/ml 5-bromo-4-chloro-3-indolyl-β-D-galactopyranoside (X-gal) was added to the filter and incubated at room temperature to score blue colonies after 30 min to overnight. Plasmids from the positive yeast colonies in the β-galactosidase filter assay were rescued. Colonies that grew on synthetic medium lacking Leu gradually lost the bait vector, but not the library plasmids. The library vector was purified using the Clontech YEASTMAKER yeast plasmid isolation kit (catalog number K1611-1).

In Vitro Protein Interaction Assay—GST-AR-(220–270), GST-AR-(220–270m4), GST-AR-(220–270)-A234T, and GST-AR-(220–270)-E236G were expressed from pGEX-5X-1 as GST fusion proteins. The GST fusion proteins were expressed in *Escherichia coli* XL1-Blue cells treated with 0.5 mM isopropyl-β-D-thiogalactopyranoside; extracted in 0.15 M NaCl, 5 mM EDTA, 10% glycerol, 100 μM phenylmethylsulfonyl fluoride, 10 mM dithiothreitol, and 50 mM Tris-HCl (pH 8.0); and incubated with glutathione-agarose beads (Amersham Biosciences) as described (18). Full-length CHIP and mutants CHIPΔTPR, CHIPΔU, and CHIP-K30A were expressed from pcDNA3 and *in vitro* translated in the presence of 25 μCi of [^{35}S]methionine (PerkinElmer Life Sciences) using the TnT T7 quick coupled transcription/translation system (Promega). Washed beads were boiled in SDS-containing buffer. Input lanes contained 30% of the binding reactions.

Transient Transfection Assays—Human hepatocellular carcinoma HepG2 cells (American Type Culture Collection) were maintained in 5% CO_2 at 37 °C in Eagle's minimal essential medium (Invitrogen) containing 10% fetal bovine serum (Gemini Laboratories), 0.1 mM nonessential amino acids, 1 mM sodium pyruvate, 2 mM L-glutamine, and penicillin and streptomycin. Cells were plated at 2×10^5 cells/well on 12-well tissue culture plates and transfected with the indicated concentrations of expression vector DNA and 0.1 μg of 5xGal4-Luc3 reporter vector using (per well) 50 μl of EC buffer (QIAGEN Inc.), 1 μg of enhancer, and 1 μl of Effectene. 24 h after transfection, the medium was changed to serum-free medium, and when appropriate, the indicated hormones were added. Luciferase activity was determined 24 h later by harvesting cells in 0.22 ml of lysis buffer containing 1% Triton X-100, 2 mM EDTA, and 25 mM Tris phosphate (pH 7.8) (19). After a 30-min incubation at room temperature, 0.1-ml aliquots were assayed for luciferase light units using a LumiStar Galaxy multiplate reader luminometer (BMG Labtechnologies).

To measure inherent transcriptional activation by the AR NH_2-terminal conserved motif, Gal4 DNA-binding domain fusion proteins were expressed in HepG2 cells with the indicated regions of the AR NH_2-terminal domain and the 5xGal4-Luc3 reporter vector. The effect of the NH_2-terminal conserved motif on AR transactivation was determined in HepG2 cells using full-length AR vectors with the indicated deletions or mutations and the mouse mammary tumor virus-luciferase (MMTV-Luc) reporter or the PSA-Enh-Luc reporter (provided by Michael Carey, University of California, Los Angeles). The influence of CHIP on AR transcriptional activity was determined in HepG2 cells using (per well) 50 ng of pCMV5 AR expression vector, 25 ng of pCMV5-CHIP and pCMV5-CHIPΔTPR vectors, and 0.25 μg of MMTV-Luc reporter. Cells were incubated for 24 h in the absence and presence of the indicated hormones and assayed for luciferase activity as described above.

In mammalian two-hybrid experiments, human epithelioid cervical carcinoma HeLa cells were maintained in Eagle's minimal essential medium supplemented with 10% fetal bovine serum, 2 mM L-glutamine, and penicillin and streptomycin. HeLa cells (1.5×10^5/well of 12-well plates) were transfected with 0.1 μg of 5xGal4-Luc3 reporter and the indicated AR and CHIP vectors using Effectene as described above.

Immunoblot Analysis—Monkey kidney COS cells were cultured in Dulbecco's modified Eagle's medium containing 10% bovine calf serum (Hyclone Laboratories), 2 mM L-glutamine, 20 mM HEPES (pH 7.2), and penicillin and streptomycin in a 5% CO_2 incubator at 37 °C. Cells (1.5×10^6/10-cm dish) were transfected using DEAE-dextran or the Effectene reagent kit (QIAGEN Inc.), which included (per 10-cm dish) 0.3 ml of EC buffer, 16 μl of enhancer, 10 μl of Effectene, and 1 ml of medium added to 7 ml of fresh medium. After transfection, the medium was replaced with serum-free medium with and without 50 nM dihydrotestosterone (DHT). The next day, cells were washed with cold phosphate-buffered saline and harvested in 1 ml of phosphate-buffered saline. After centrifugation at 5000 rpm at 4 °C, cells were suspended in 0.1 ml of lysis buffer containing 0.15 M NaCl, 0.5% Nonidet P-40, 50 mM NaF, 1 mM dithiothreitol, 50 mM Tris-HCl (pH 7.5), 1 mM phenylmethylsulfonyl fluoride, and protease inhibitor mixture (Sigma) and incubated for 1 h at 0 °C. After centrifugation at 12,000 rpm for 15 min at 4 °C, the supernatant protein concentration was determined using the Bio-Rad assay. Samples (10 μg of protein/lane) were separated on 10 or 8–16% acrylamide gels containing SDS. After electrophoresis, gel proteins were electrophoretically transferred to nitrocellulose membranes. The blots were incubated with 1 μg/ml rabbit antibody AR32, raised against an AR NH_2-terminal peptide, or with a 1:500 dilution of mouse anti-Gal4 DNA-binding domain IgG2a (sc-510, Santa Cruz Biotechnology). Immunoreactive bands were visualized using chemiluminescence (SuperSignal Western Dura extended duration substrate, Pierce).

Immunocytochemistry—COS cells (1.25×10^6/well) were transfected in 12-well tissue culture plates, with each well containing a 0.15-mm thick cover glass (Fisher). Cells were transfected using Effectene as described above with 0.2 μg of pCMV-hAR and pCMV5-FLAG-CHIP and treated with and without 100 nM DHT 24 and 48 h after transfection. Cells were fixed with freshly prepared 3% paraformaldehyde, permeabilized with 0.2% Triton X-100, blocked with 0.5% bovine serum albumin as described (20), and incubated for 1 h with primary antibodies: mouse anti-FLAG monoclonal antibody M2 (1:250 dilution; Sigma) and rabbit anti-AR polyclonal antibody 3510 (1:250 dilution; Abcam, Inc.). After several washes with phosphate-buffered saline, cells were incubated for 30 min with secondary antibodies: TRITC-conjugated AffiniPure donkey anti-mouse IgG (1:50 dilution; Jackson ImmunoResearch Laboratories, Inc.) and fluorescein isothiocyanate-conjugated AffiniPure donkey anti-rabbit IgG (1:50 dilution; Jackson ImmunoResearch Laboratories, Inc.). The cover glasses were mounted on slides using DakoCytomation fluorescent mounting medium (Fisher) and viewed using a Zeiss LSM 210 confocal microscope.

RESULTS

Identification of an AR NH_2-terminal Conserved Motif—Comparison of AR NH_2-terminal sequences from human to lower vertebrates shows that much of the region is not conserved (Fig. 1*A*). This is despite the important functional role of the AR NH_2-terminal domain in transactivation (6). Among the

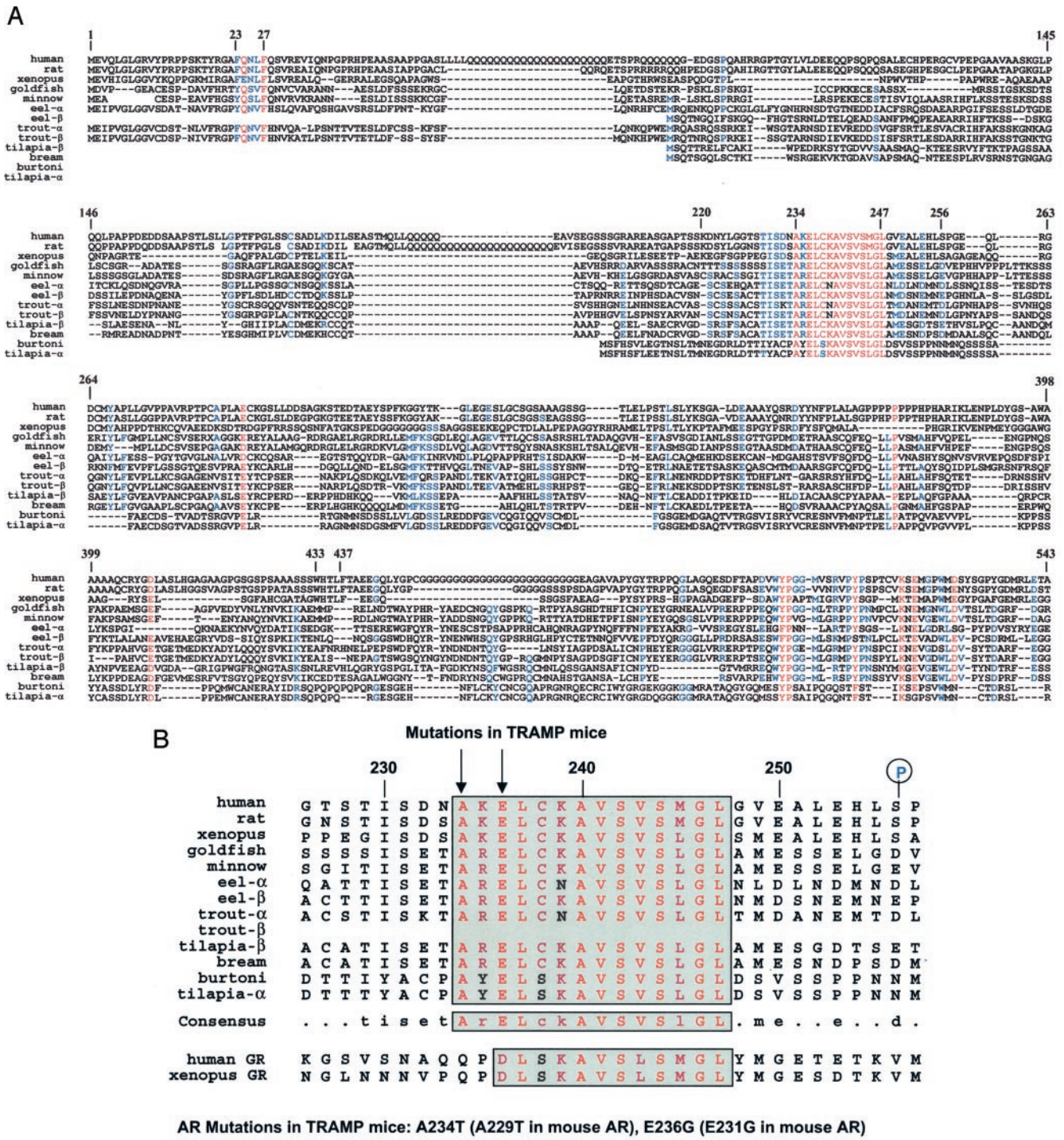

FIG. 1. **Alignment of the AR NH_2-terminal amino acid sequence from different species.** *A*, AR sequences were obtained from the GenBank™/EBI Data Bank with the following accession numbers: human AR, M20132 and J03180; Norway rat AR, J05454; *Xenopus laevis* African clawed frog AR, U67129; goldfish AR, AY090897; fathead minnow, AY004868; Japanese eel AR-α, AB023960; Japanese eel AR-β, AB025361; rainbow trout AR-α, AB012095; rainbow trout AR-β, AB012096; Nile tilapia AR-β, AB045212; red sea bream AR, AB017158; *Haplochromis burtoni* cichlid fish AR, AF121257 and AY082342; and Nile tilapia AR-α, AB045211. Amino acid residues conserved by amino acid, charge, or structure are shown in *red*, and partially conserved residues are shown in *blue*. The AR FXXLF motif is at residues 23–27, and the NH_2-terminal conserved motif is at residues 234–247. Amino acid positions are based on the human AR sequence (22). The region shown is human AR NH_2-terminal residues 1–543. *B*, shown is an amino acid sequence alignment of the AR NH_2-terminal conserved motif and flanking sequence, the AR consensus sequence, and the corresponding homologous sequence in GR. Sequences shown were extracted from the sites listed above and include human GR (X03225 and M10901) and *X. laevis* African clawed frog GR (X72211). Conserved residues are shown in *orange-red*, and partially conserved residues are shown in *maroon*. The human AR phosphorylation site Ser^{256} (10) and AR mutations from TRAMP prostate cancer tumors (A234T and E236G) are indicated. Shown are amino acid sequences corresponding to human AR residues 226–257 with numbering as previously reported (22) and human GR residues 67–98 (72).

poorly conserved regions are the previously reported AR transactivation subdomains AF1a (rat AR residues 154–167 and human AR residues 173–186) and AF1b (rat AR residues 295–359 and human AR residues 297–361), which are critical for transcriptional activity (7). Lack of sequence conservation in these regions is surprising and suggests that the NH_2-terminal

domain evolved with its interacting partners. In contrast, several short regions of the AR NH_2-terminal region show a high degree of sequence conservation. The previously described F*XX*LF motif at human AR NH_2-terminal residues 23–27 (18, 21) is conserved as (F/Y)Q(N/S)(L/V)F from lower vertebrates through primates, although some species of fish seem to lack the NH_2-terminal 5′-coding region of the AR gene that includes the F*XX*LF motif (Fig. 1*A*). Absence of the extreme NH_2-terminal region could reflect incomplete sequence analysis or that certain species of fish have yet to evolve the AR F*XX*LF motif. An evolving F*XX*LF motif during vertebrate expansion is conceivable since the W*XX*LF motif at human AR residues 433–437, which contributes to the F*XX*LF motif-mediated AR NH_2- and COOH-terminal interaction (18), is conserved from primates to *Xenopus*, but not in fish and other lower vertebrates (Fig. 1*A*).

Another AR NH_2-terminal region that shows striking sequence conservation across species is positioned at human AR residues 234–247 (Fig. 1*A*) with the consensus sequence ^{234}A(K/R/Y)EL(C/S)KAVSVS(M/L)GL^{247} (Fig. 1*B*), numbered according to the human AR sequence of Lubahn *et al.* (22) and the AR mutation data base.[2] Sequence conservation of hydrophobic residues in the region was noted previously (14). Also notable is Ser^{256}-Pro^{257} since Ser^{256} was shown previously to be phosphorylated in human AR (10). Ser^{256} and Pro^{257} are not conserved; but remarkably, the negatively charge residues Asp and Glu most often replace Ser^{256} in lower species (Fig. 1, *A* and *B*), suggesting that a negative charge at this position is important for AR function.

Sequence conservation of AR NH_2-terminal residues 234–247 suggests a conserved motif for the AR gene family. A search of the protein sequence data base supports this, with one exception. GR from human and *Xenopus*, but not GR from fish, contains sequence ^{77}DLSKAVSLSMGL^{88} at human GR residues 77–88, which is homologous to 12 of the 14 residues in the AR NH_2-terminal conserved motif (Fig. 1*B*). The closer evolutionary distance between AR and the progesterone receptor compared with AR and GR (4) and the absence of the conserved motif in the progesterone receptor suggest that AR and GR acquired the sequence independently for a common function by convergent evolution.

Analysis of the predicted order and disorder composition of the AR NH_2-terminal domain using the PONDR Protein Disorder Predictor[3] indicates that the F*XX*LF motif and the AR NH_2-terminal conserved motif form short structurally ordered regions as indicated by PONDR scores of <0.1. Each motif is predicted to form an amphipathic α-helix, indicating the presence of short structured segments in an NH_2-terminal region that is otherwise predicted to be largely unstructured.

Intrinsic Activity of the AR NH_2-terminal Conserved Motif—We tested for the presence of transcriptional activity inherent to the AR NH_2-terminal conserved motif by expressing Gal4 DNA-binding domain-AR fusion proteins in mammalian cells (Fig. 2*A*). The NH_2-terminal conserved motif residues 234–247 lacked activity, but a low level of activity was detectable when the sequence was extended in Gal-AR-(229–254). A larger fragment, Gal-AR-(220–270), elicited 20% the activity of the AR NH_2-terminal domain in Gal-AR-(1–503). When mutations at four residues (L237A/K239M/V241A/V243A) were introduced into the NH_2-terminal conserved motif in Gal-AR-(220–270) (Gal-AR-(220–270m4)) (Fig. 2*A*), the transcriptional response was reduced to background levels. Expression levels of the Gal-AR fusion proteins were similar as determined by immunoblotting (Fig. 2*C*, *left panel*).

The results suggest that although the NH_2-terminal conserved motif itself lacks intrinsic transcriptional activity, a larger region that includes flanking sequence of the conserved motif induces a transcriptional response that depends on residues within the AR NH_2-terminal conserved motif. The flanking region may therefore be necessary for proper folding or presentation of the NH_2-terminal conserved motif.

Contribution of the core conserved motif to AR transcriptional activity was investigated further by testing several mutants of full-length AR. Deletion of region 220–270 (ARΔ220–270) caused a ~50% decrease in AR transcriptional activity using the MMTV-Luc and PSA-Enh-Luc reporter vectors (Fig. 2*B*), confirming the importance of the region for AR activity. The decrease in transcriptional activity by ARΔ220–270 and additional mutants was independent of AR expression levels (Fig. 2*C*, *right panel*). Deleting only the NH_2-terminal conserved motif (ARΔ234–247) caused less of a decrease in activity, and the decrease was similar to that seen with ARm4. Mutating the flanking Ser^{256} (Fig. 1*B*) to alanine to inhibit phosphorylation at this previously reported AR phosphorylation site (10) or to aspartic acid to mimic the negative charge of a phosphate group had no effect on the AR transcriptional response. The results suggest that the AR NH_2-terminal conserved motif and closely flanking sequence contribute to AR transactivation.

AR NH_2-terminal Conserved Motif Interaction with CHIP—The high sequence conservation of the AR NH_2-terminal motif in AR gene evolution, its predicted structure, and evidence for a role in AR transcriptional activation led us to perform a yeast two-hybrid screen using a 51-amino acid residue fusion peptide as bait to probe a human testis cDNA library. Yeast strain HF7c was initially transformed with pGBT8-AR-(220–270), coding for the Gal4 DNA-binding domain and human AR residues 220–270. In agreement with the transcriptional response seen with Gal-AR-(220–270) in mammalian cells, the addition of 0.8 mM 3-amino-1,2,4-triazole was required to reduce intrinsic activity of pGBT8-AR-(220–270). Screening 10^6 clones of an amplified library revealed 138 positive clones that grew on synthetic medium lacking Leu, Trp, and His. Of these, 48 clones were positive in a β-galactosidase filter assay performed in yeast. Sequence analysis revealed five identical clones coding for CHIP. The clones coded for CHIP residues 20–303, representing full-length CHIP lacking the first 19 NH_2-terminal amino acids. That the interaction was specific was suggested by a parallel screen of the same library using a similarly sized AR fragment from a different region of the AR NH_2-terminal domain. In this case, none of the positive clones that grew on synthetic medium lacking Leu, Trp, and His coded for CHIP.[4]

CHIP is a U-box-containing ubiquitin-protein isopeptide ligase (E3) (23–26) that interacts with heat shock proteins Hsp70 and Hsp90 through its NH_2-terminal TPR domain (Fig. 3*A*) and has been reported to cause ubiquitylation of AR (13). To further investigate the role of the AR NH_2-terminal conserved motif in the AR and CHIP interaction, we tested several AR mutants in a mammalian two-hybrid assay using a Gal-CHIP-(20–303) fusion protein. Deletion of AR residues 220–270 (ARΔ220–270) strongly reduced the interaction with CHIP (Fig. 3*B*), supporting the role of the NH_2-terminal conserved motif region in the AR interaction with CHIP. A small portion of this reduction was attributed to the slight decrease in background AR activity that resulted from the deletion of residues 220–270, in agreement with the results of Fig. 2 (*A* and *B*) showing that residues 220–270 harbor a transcriptional activation function. The background AR activity evident upon co-

[2] Available at ww2.mcgill.ca/androgendb/data.htm.
[3] Available at www.pondr.com/PONDR/pondr.cgi.
[4] S. Bai, B. He, and E. M. Wilson, unpublished data.

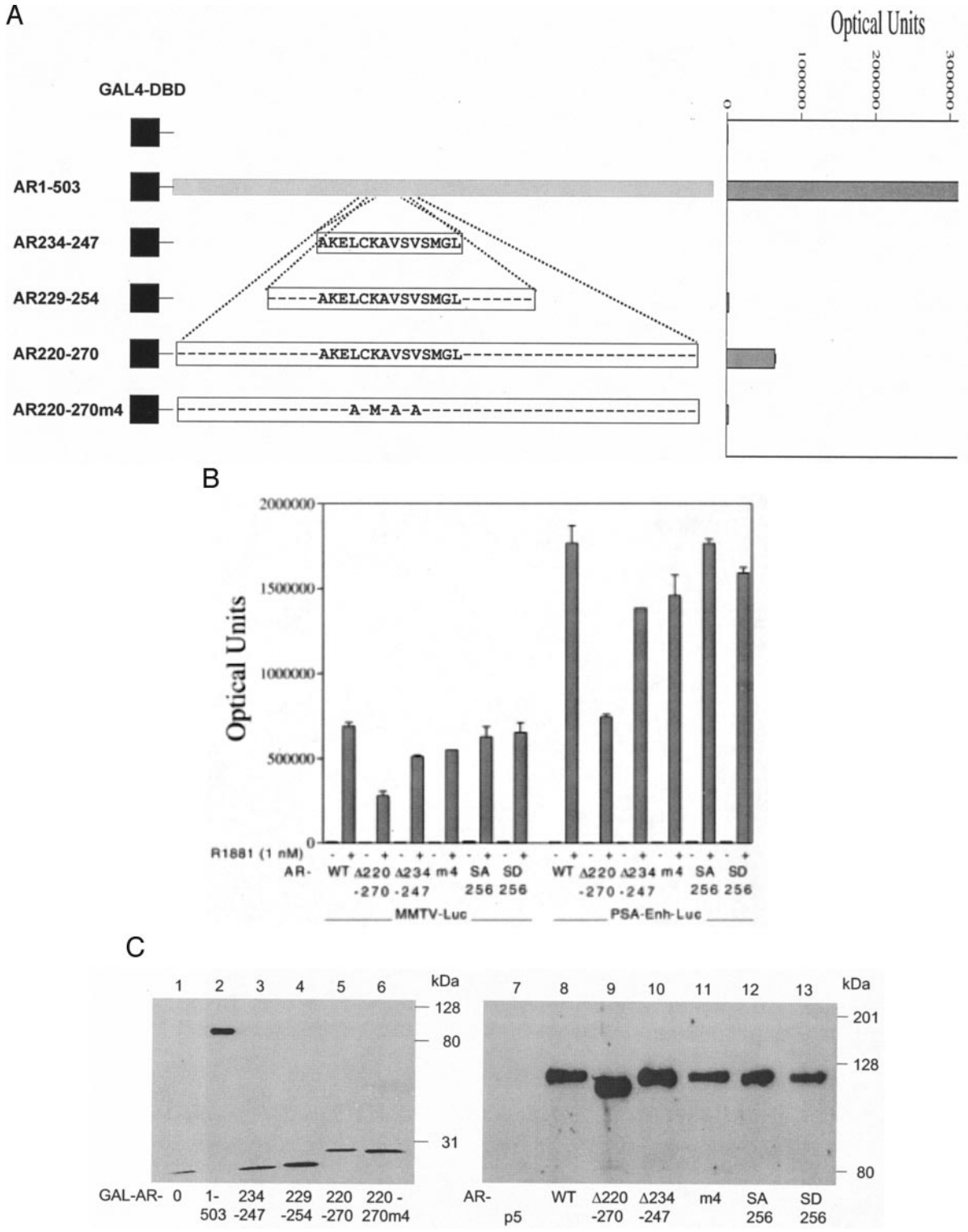

FIG. 2. **Transcriptional activity of the AR NH_2-terminal conserved motif.** *A*, the transcriptional activity of the AR NH_2-terminal conserved motif and flanking sequence was determined by expressing Gal4 DNA-binding domain fusion proteins with no insert (*GAL4-DBD*) or with AR fragments in Gal-AR-(1–503), Gal-AR-(234–247), Gal-AR-(229–254), Gal-AR-(220–270), and Gal-AR-(220–270m4). Activity was determined in HepG2 cells using 50 ng of pGal vector and 0.1 μg of 5xGal4-Luc3 reporter vector. Cells were transfected using Effectene as described under "Materials and Methods." The transcriptional response is indicated in optical light units and error and are representative of three independent experiments. *B*, shown is the effect of the NH_2-terminal conserved motif region on AR transactivation. HepG2 cells were transiently transfected as described under "Materials and Methods" with 0.25 μg of MMTV-Luc or 0.25 μg of PSA-Enh-Luc together with 50 ng of pCMV-hAR with wild-type sequence (*WT*), with deletion of the conserved region (ARΔ220–270 and ARΔ234–247), with the four-residue mutation in the NH_2-terminal conserved motif (ARm4 (*m4*)), and with mutations S256A (*SA*) and S256D (*SD*) at an AR phosphorylation site. *C*, shown are immunoblots of AR mutants. Wild-type and mutant Gal-AR (10 μg/10-cm dish) and pCMV5-AR plasmids (2 μg/dish) were transiently expressed in COS cells (1.8×10^6/10 dish) using DEAE-dextran in the absence of added androgen. For the Gal-AR vectors, cells were incubated in serum-containing medium with 1 μM MG132 proteasome inhibitor for 1 h at 37 °C prior to harvest. Protein extracts (10 μg/lane) were analyzed using anti-Gal4 DNA-binding domain antibody (*left panel*) for the Gal-AR fusion proteins tested for transcriptional activity in *A* or antibody AR32 (*right panel*) for the AR mutants tested for transcriptional activity in *B*.

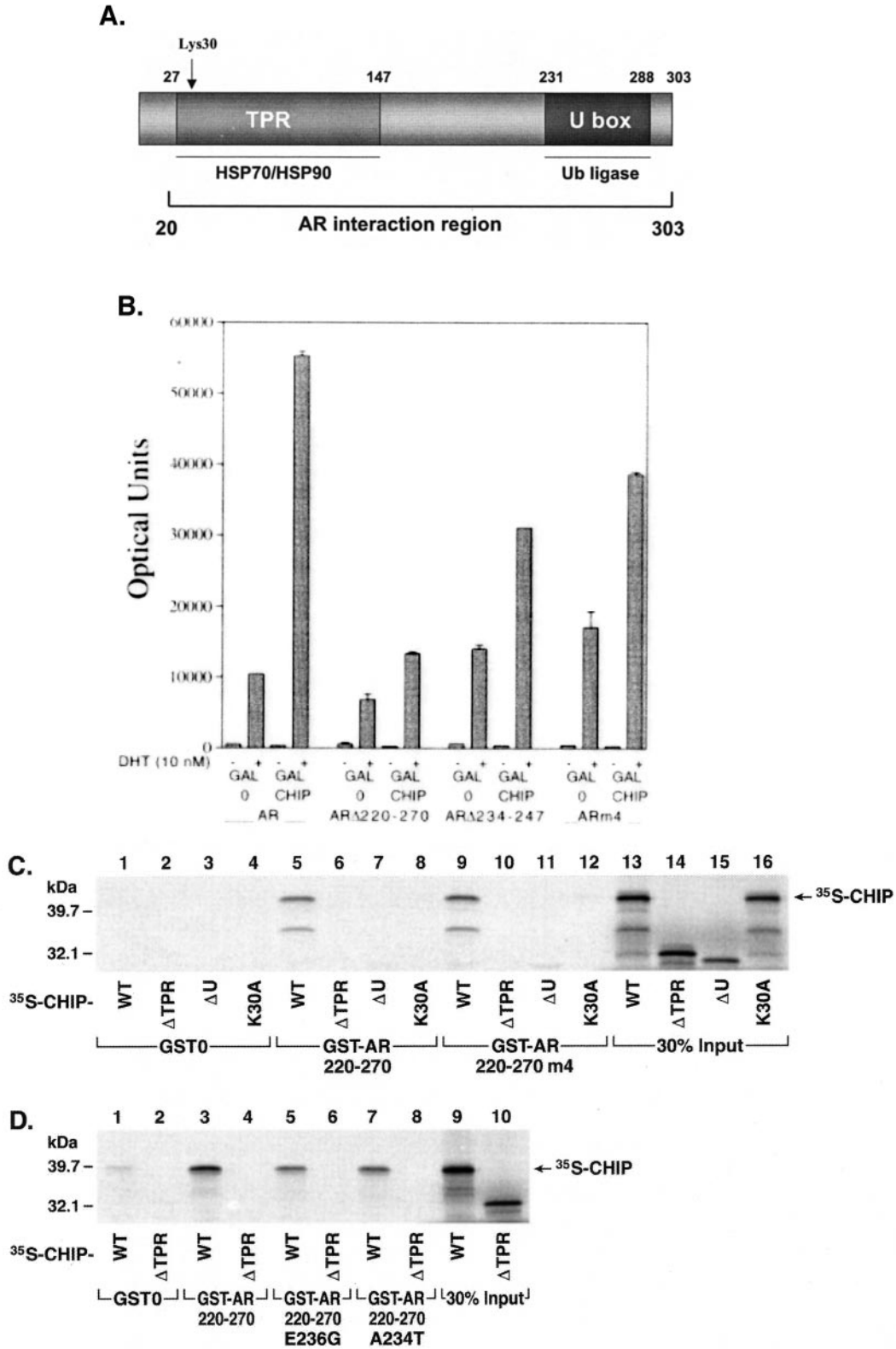

FIG. 3. **Interaction of CHIP with the AR NH_2-terminal conserved motif.** *A*, schematic diagram of full-length CHIP (303 amino acids) containing the NH_2-terminal TPR domain at residues 27–147, which interacts with Hsp70 and Hsp90, and the COOH-terminal U-box domain at residues 231–288, which imparts E3 (ubiquitin-protein isopeptide ligase (*Ub ligase*)) activity (23, 24). Lys^{30} is required for the interaction between the TPR domain and Hsp70·Hsp90 (C. Patterson, unpublished data). The results from GST affinity binding studies shown in *C* indicate that the TPR and U-box domains of CHIP are required for interaction with AR (shown by the *bracket*). *B*, interaction of CHIP with full-length AR in a mammalian two-hybrid assay. The assay was performed in HeLa cells using full-length wild-type AR, ARΔ220–270, ARΔ234–247, and ARm4 and cotransfected with the parent pGal0 empty plasmid (*GAL 0*) or Gal-CHIP-(20–303) (*GAL CHIP*). HeLa cells were transfected using 10 ng of AR, 50 ng of Gal expression plasmid, and 0.1 μg of 5xGal4-Luc3 in 12-well plates using Effectene as described. Optical light units reflect luciferase activity and error and are representative of three independent experiments. *C*, *in vitro* interaction between CHIP and the AR NH_2-terminal conserved motif. ^{35}S-Labeled full-length wild-type CHIP (*WT*; *lanes 1*, *5*, and *9*), CHIPΔTPR (lacking the TPR domain; *lanes 2*, *6*, and *10*), CHIPΔU (lacking the U-box domain; *lanes 3*, *7*, and *11*), and CHIP-K30A (*lanes 4*, *8*, and *12*) were incubated with GST (*GST0*; lacking AR sequence; *lanes 1–4*), GST-AR-(220–270) (containing

expression of the pGal0 empty vector results from a cryptic androgen response element in the 5xGal4-Luc3 reporter (19). Deleting the NH_2-terminal conserved motif in ARΔ234–247 or introducing the multiple mutations L237A/K239M/V241A/V243A into AR (ARm4) did not decrease background AR transcriptional activity and reduced (but did not eliminate) the AR and CHIP interaction.

The results support a role for the NH_2-terminal conserved motif in the AR and CHIP interaction, but also suggest that additional direct or indirect interactions occur between AR and CHIP. One possible interaction site is the AR ligand-binding domain, which was shown to bind the Hsp70·Hsp90 heterocomplex (27, 28), and Hsp70·Hsp90 interacts with CHIP (23). A recent study demonstrating that CHIP functions as a dimer provides a basis for this type of interaction (29).

GST in Vitro Adsorption Assay—To confirm a direct interaction between the AR NH_2-terminal conserved motif and CHIP, GST affinity matrix binding assays were performed. Wild-type GST-AR-(220–270) and GST-AR-(220–270m4) were expressed in *E. coli*, purified, and incubated with ^{35}S-labeled *in vitro* translated full-length CHIP and several CHIP mutants. A strong interaction was evident between GST-AR-(220–270) and ^{35}S-labeled CHIP that was not detected using the pGST0 empty vector control (Fig. 3*C*, *lanes 1* and *5*). The AR interaction with CHIP was eliminated by deleting the CHIP TPR domain (*lane 6*), by deleting the CHIP U-box domain (*lane 7*), or by introducing a K30A mutation into the CHIP TPR domain (*lane 8*). Lys^{30} is highly conserved in the TPR domain (30) and was shown to be required for the interaction between the CHIP TPR domain and Hsp70 or Hsp90.[5]

Two AR mutations identified in the transgenic adenocarcinoma of mouse prostate (TRAMP) model for prostate cancer, E236G and A234T (17), also reduced the AR and CHIP interaction by 43 and 16%, respectively (Fig. 3*D*). In contrast, no decrease in the AR and CHIP interaction was seen using GST-AR-(220–270m4), in which four mutations (L237A/K239M/V241A/V243A) were introduced into the NH_2-terminal conserved motif (Fig. 3*C*).

The data indicate a direct interaction between AR and CHIP mediated by the short AR NH_2-terminal fragment that contains the conserved motif. A reduced AR and CHIP interaction by AR mutations derived from the TRAMP model suggests that the AR NH_2-terminal conserved motif functions to limit AR activity and that mutations in this region confer increased AR activity, which contributes to prostate cancer growth. However, unlike the transcriptional activity detected in this region that depended on four conserved residues of the NH_2-terminal conserved motif, the AR and CHIP interaction was not diminished by the L237A/K239M/V241A/V243A mutations.

CHIP-induced Inhibition of AR Transcriptional Activity and AR Steady-state Levels—Coexpression of full-length CHIP decreased both AR and GR transcriptional activity (Fig. 4*A*). This is in contrast to the activity observed without any further DNA addition, with coexpression of the pCMV5 empty vector control, or with coexpression of the CHIP mutant lacking the TPR domain (CHIPΔTPR) (Fig. 4*A*, Δ*TP*). Surprisingly, deletion of the conserved sequence in ARΔ234–247 or ARΔ220–270 did not eliminate the inhibitory effect of CHIP on AR transactivation (data not shown). Furthermore, the constitutive transcriptional activities of AR truncation mutant AR-(1–660), which

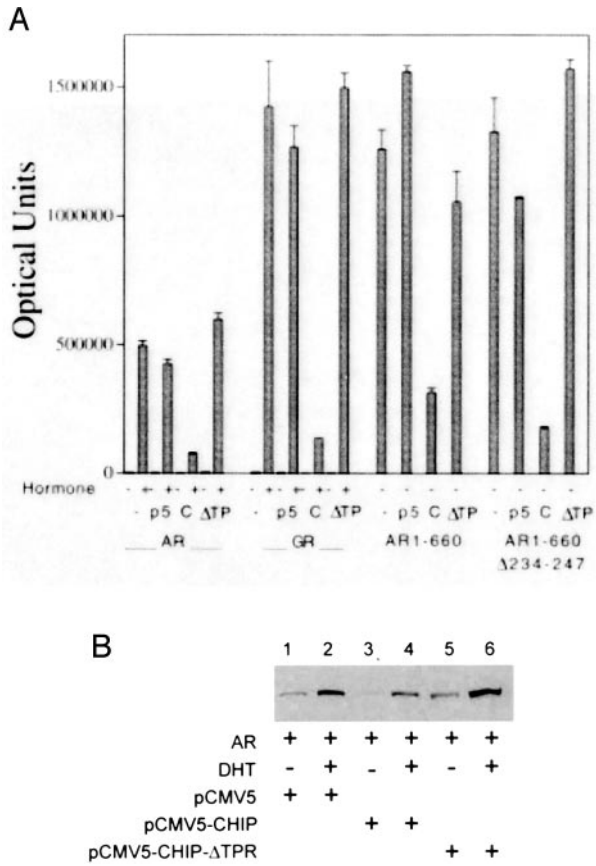

FIG. 4. **Effect of CHIP on transcriptional activity and AR steady-state levels.** *A*, HepG2 cells (0.2×10^5/well of a 12-well plate) were transiently transfected as described under "Materials and Methods" with 0.25 μg of MMTV-Luc/well using Effectene in the presence of (per well) 50 ng of pCMV-hAR (*AR*), 50 ng of pCMV-hGR (*GR*), 10 ng of pCMV-AR-(1–660), or 10 ng pCMV-AR-(1–660)Δ234–247, together with no further addition (−), the pCMV5 empty vector (*p5*), pCMV5-CHIP (*C*), or pCMV5-CHIPΔTPR (Δ*TP*). Cells were incubated for 24 h in the absence of hormone, with 0.1 nM R1881 for AR, or with 10 nM dexamethasone for GR. *B*, shown is an immunoblot of AR coexpressed with CHIP and the CHIP mutant lacking the TPR domain. COS cells were transiently transfected using Effectene as described under "Materials and Methods" with 1 μg of pCMV-hAR in the presence of 1 μg of pCMV5 empty vector (*lanes 1* and *2*), 1 μg of pCMV5-CHIP (*lanes 2* and *3*), and pCMV5-CHIPΔTPR (*lanes 5* and *6*). Cells were incubated 24 h after transfection in the absence and presence of 50 nM DHT as indicated, harvested, and analyzed by immunoblotting using antibody AR32 as described under "Materials and Methods." Immunoblots of parallel experiments using mouse anti-β-actin monoclonal antibody (1:2500 dilution; Abcam, Inc.) confirmed similar protein loading between the lanes (data not shown). The data are representative of three independent experiments.

[5] C. Patterson, unpublished data.

the AR NH_2-terminal conserved motif; *lanes 5–9*), and GST-AR-(220–270m4) (with the L237A/K239M/V241A/V243A mutations; *lanes 9–12*). *30% Input* (*lanes 13–16*) represents 30% of total ^{35}S-labeled CHIP or CHIP mutant used in the reactions and had the following band intensities, indicating similar protein loading: 166 integrated optical units (*lane 13*), 180 (*lane 14*), 162 (*lane 15*), and 173 (*lane 16*). Radiolabeled bands detected by exposure to x-ray film indicate ^{35}S-labeled CHIP interaction with GST-AR-(220–270) and GST-AR-(220–270m4). *D*, reduction in the *in vitro* interaction between CHIP and the AR NH_2-terminal conserved motif by AR mutations from the TRAMP model for prostate cancer. ^{35}S-Labeled full-length wild-type CHIP and CHIPΔTPR were incubated with GST (*GST0*), GST-AR-(220–270), GST-AR-(220–270)-E236G, or GST-AR-(220–270)-A234T as indicated. *30% Input* (*lanes 9* and *10*) represent 30% of total ^{35}S-labeled CHIP used in the reactions and had band intensities of 106 (*lane 9*) and 112 (*lane 10*). Radiolabeled band intensities detected by exposure to x-ray film for the ^{35}S-labeled CHIP interaction were 58 for wild-type GST-AR-(220–270) (*lane 3*), 33 for GST-AR-(220–270)-E236G (*lane 5*), and 49 for GST-AR-(220–270)-A234T (*lane 7*). The data are representative of three independent experiments.

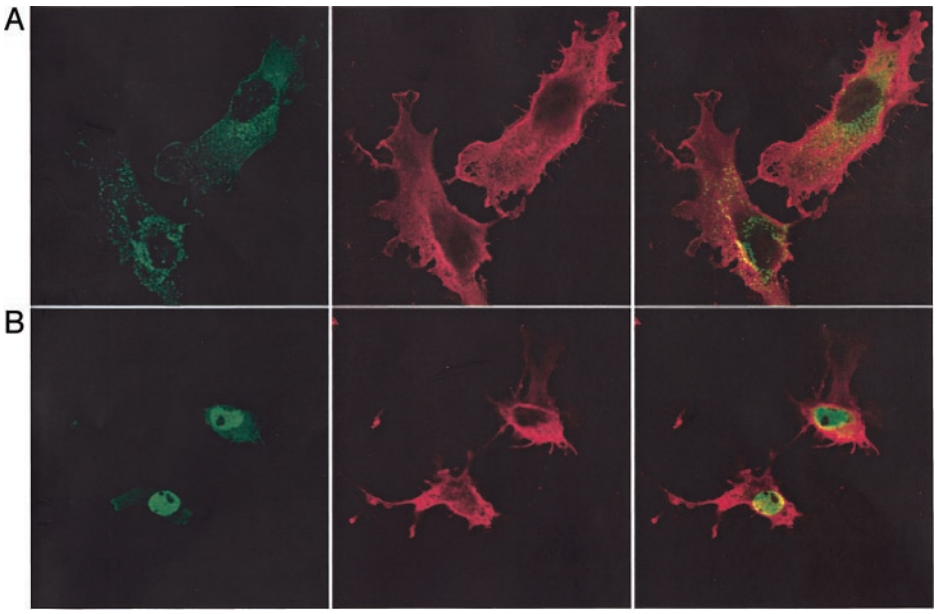

FIG. 5. **Immunocytochemistry of CHIP and AR.** COS cells were transiently transfected with pCMV-FLAG-CHIP and pCMV-hAR. Immunostaining was detected after incubation in the absence (*A*) and presence (*B*) of 100 nM DHT as described under "Materials and Methods." Shown is *green* fluorescence for AR (*left panels*), *red* fluorescence for FLAG-CHIP (*middle panels*), and the merged images (*right panels*).

lacks the ligand-binding domain, and AR-(1–660)Δ234–247, which lacks, in addition, the NH_2-terminal conserved motif, were both strongly inhibited by CHIP (Fig. 4*A*). That this inhibitory effect of CHIP was mediated by sequences outside of the NH_2-terminal conserved motif was also supported by our observations that CHIP inhibited, to a similar extent, transactivation by the progesterone receptor, a receptor that lacks the conserved motif (data not shown). When the activity of a pCMV-Luc constitutive reporter was tested in the presence of CHIP expression, there was no significant decrease in transcriptional activity above that observed with the empty vector control or with pCMV5-CHIPΔTPR (data now shown), suggesting that the inhibitory effect of CHIP is not due to inhibition of general transcription mechanisms.

The results indicate that CHIP strongly represses AR and GR transcriptional activity independent of the NH_2-terminal conserved motif and independent of the ligand-binding domain. This is despite the interaction mediated by the AR NH_2-terminal conserved motif and CHIP. The requirement for the TPR domain of CHIP for transcriptional repression of AR, AR-(1–660), and GR suggests that the heat shock protein heterocomplex is involved since the CHIP TPR domain binds heat shock proteins Hsp70 and Hsp90 (31). CHIP may modulate AR and GR transcriptional activity through mechanisms independent of the NH_2-terminal conserved motif.

The influence of CHIP on AR steady-state levels was also tested. The low level of AR detected in the absence of androgen was further reduced by coexpression of CHIP (Fig. 4*B*, *lanes 1* and *3*). CHIP also decreased the stabilizing influence of androgen on AR levels (*lanes 2* and *4*). In contrast, deletion of the CHIP TPR region eliminated the reduction in AR levels induced by coexpression of CHIP. The results indicate that the TPR region of CHIP is required for the inhibitory effects of CHIP on AR steady-state levels and AR transcriptional activity.

Colocalization of CHIP and AR—The subcellular localization of CHIP and AR was determined in the absence and presence of DHT by immunocytochemistry. In the absence of DHT, transiently expressed AR (*green*) and FLAG-tagged CHIP (*red*) localized in the cytoplasm, with no evidence of nuclear staining (Fig. 5*A*). This is in agreement with a previous report that CHIP is a cytoplasmic protein (23). The partial colocalization of CHIP and AR in the cytoplasm supports their interaction in the absence of hormone. In the presence of DHT, AR was nuclear, whereas CHIP remained primarily in the cytoplasm (Fig. 5*B*). The data suggest that CHIP regulates AR degradation prior to androgen binding and that androgen-induced nuclear targeting sequesters AR from the inhibitory effects of CHIP.

DISCUSSION

The NH_2-terminal regions of steroid receptors lack strict structural requirements like those of the DNA- and ligand-binding domains. To address structure-function relationships of the AR NH_2-terminal domain, we searched for evolutionarily conserved sequences that predict a critical role in AR function. Our approach was based in part on studies of the AR NH_2-terminal F*XX*LF motif, which is one of few highly conserved regions in the AR NH_2-terminal domain (32). The F*XX*LF motif has a dominant role in the androgen-dependent interdomain NH_2- and COOH-terminal interaction required for AR function, whereas the less well conserved AR NH_2-terminal W*XX*LF motif contributes only weakly to the AR NH_2- and COOH-terminal interaction (18, 32). Considering its essential role in transcriptional activation, it is surprising that more of the AR NH_2-terminal domain is not conserved (6). In particular, the two major activation regions of AF1 lack significant sequence conservation across species. This suggests that the NH_2-terminal activation domain has evolved in parallel with its interacting partners, with one interacting partner being the AR COOH-terminal ligand-binding domain. In contrast to the NH_2-terminal region, the COOH-terminal region including AF2 is structurally conserved. AF2 interacts with the L*XX*LL motifs of p160 coactivators (33–36) and, for AR, interacts in addition with the F*XX*LF motif that is present in the AR NH_2-terminal region (16, 18) and in some AR coregulators (19, 37, 38).

In this study, we have identified an extraordinarily conserved 14-amino acid NH_2-terminal sequence at human AR amino acid residues 234–247 that is common to all published sequences of AR, including the lower vertebrate fish species. The conserved motif lacks intrinsic transcriptional activity *per se*, but contributes to the transcriptional response of a larger region between residues 220 and 270. The AR NH_2-terminal conserved motif lies within a previously described α-helical region (2) and is NH_2-terminal to a recently reported hydrophobic motif identified among cellular and viral transcription factors that act as binding sites for transcription factor TFIIF (14), a general transcription factor reported to interact with AR (39, 40). To study the function of the AR NH_2-terminal conserved motif, we performed a yeast two-hybrid screen and

identified CHIP as the interacting partner for the conserved AR NH_2-terminal conserved motif. CHIP is highly conserved across species and interacts with the NH_2-terminal motif that is conserved throughout the entire AR gene family. Coexpression studies have shown that CHIP limits AR function by promoting AR degradation most likely through the previously described role of CHIP in ubiquitylation (13).

CHIP, named for its interaction with Hsp70, was originally identified from a screen for TPR domains. The TPR, first described in yeast proteins (41, 42), is a tandem 34-amino acid repeat composed of antiparallel α-helices (30). The TPR domains of CHIP mediate its interaction with Hsp90 and Hsp70 to redirect incompletely folded proteins for degradation (31). TPR protein interaction surfaces on the chaperone cofactors Hip (Hsp70-interacting protein) (43) and Hop (Hsp90/Hsp70-organizing protein) (44) interact with the COOH-terminal EEVD motif of Hsp70 and Hsp90 during the chaperone heterocomplex formation that mediates protein folding (30, 45, 46). CHIP inhibits Hsp70 ATPase and protein refolding activities, although paradoxically, its overexpression increases chaperone activity (47). CHIP contains a U-box domain at its COOH terminus (25). Structurally similar to a RING finger domain, U-box-containing proteins are a third group of ubiquitin ligases with E3 activity that direct ubiquitylation of chaperone protein complex substrates, leading to increased degradation by the proteasome (24, 26, 48). CHIP was shown to promote ubiquitylation and degradation through the proteasome of GR (31), AR (13), and other proteins (26, 49), including ErbB2/Neu (50, 51). However, it was previously suggested that the predominant effect of CHIP on AR is inhibition of protein folding and reduced degradation (13). CHIP may act as a molecular link between the protein folding chaperone functions and proteasome-mediated protein degradation processes of the Hsp70·Hsp90 heterocomplex (52). CHIP also directly modulates the stress response by activating heat shock factor-1 (53) and influences protein trafficking (54).

A direct interaction between CHIP and the AR NH_2-terminal conserved motif was confirmed in mammalian two-hybrid and GST affinity matrix binding assays, supporting the initial identification of CHIP in a yeast two-hybrid screen as a *bona fide* AR-interacting protein. A BLAST search of the protein data base showed that besides AR, GR from *Xenopus* and higher species is the only other protein that contains a homologous sequence. However, in the yeast two-hybrid interaction assay, CHIP did not interact with a GR fragment containing the partial sequence (data not shown), even though CHIP decreased GR transcriptional activity to an extent similar to the decrease in AR activity. It is conceivable that CHIP also associates with AR and GR indirectly via the ligand-binding domain through an association with Hsp70 and Hsp90. The requirement of the TPR region of CHIP for inhibition of AR and GR transcriptional activity suggests a mechanism involving CHIP interaction with the heat shock protein complex. The AR·CHIP·Hsp complex may be further stabilized by the NH_2-terminal conserved motif. On the other hand, CHIP also decreased the transcriptional activity of an AR deletion mutant lacking the ligand-binding domain, and deletion of the conserved sequence did not eliminate the inhibitory effect. The lack of a requirement for the AR NH_2-terminal conserved motif and the ligand-binding domain for the inhibitory effect of CHIP on AR transactivation suggests that other factors are involved.

Our immunostaining results show that, in the absence of androgen, AR and CHIP partially colocalized in the cytoplasm. The addition of DHT translocated AR to the nucleus, but CHIP remained predominantly cytoplasmic. The data suggest the model shown in Fig. 6, whereby CHIP, in association with the heat shock protein complex, targets AR for degradation in the cytoplasm prior to hormone binding, thereby contributing to the rapid turnover of AR in the absence of ligand (55). Ligand-induced targeting of AR to the nucleus would favor its stabilization not only by sequestering it in the nuclear compartment away from CHIP, but also by the androgen-induced interdomain AR NH_2- and COOH-terminal interaction that increases AR stabilization (56, 57). The subcellular segregation of CHIP and androgen-bound AR provides an additional mechanism for AR stabilization subsequent to hormone binding.

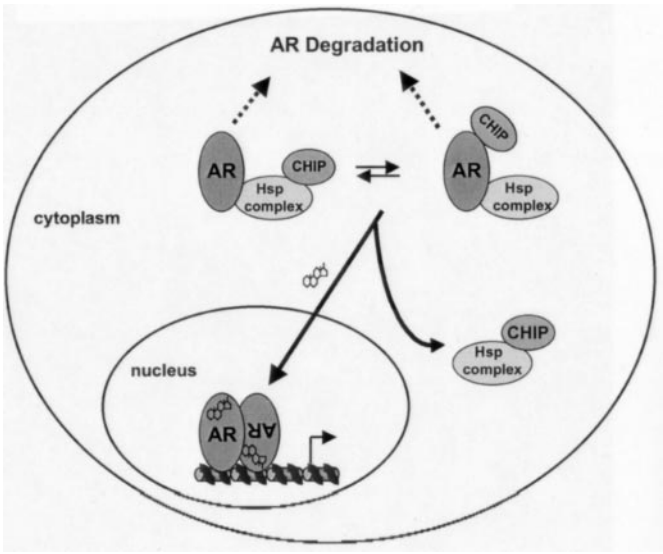

FIG. 6. **Model of the functional relationship between AR and CHIP.** The data suggest that AR and CHIP interact in the cytoplasm prior to androgen binding. This interaction contributes to AR degradation, resulting in reduced AR-mediated transcriptional activity. The requirement for the TPR and U-box domains of CHIP in its interaction with AR suggests a role for the heat shock protein complex that includes Hsp70 and Hsp90. Hormone binding induces AR translocation to the nucleus and results in subcellular segregation of CHIP and androgen-bound AR. This provides an additional mechanism for AR stabilization. Binding of AR to response element DNA present in androgen-responsive genes is thought to occur as an antiparallel dimer.

A requirement for Hsp90 in androgen binding to AR was reported previously (27). Geldanamycin, an inhibitor of the Hsp90 chaperone function (58), inhibits androgen binding, increases AR degradation, and inhibits AR functional activity (27, 59). CHIP was reported to decrease AR synthesis, to inhibit folding of AR by actions not involving its E3 activity, and to reduce AR degradation (13). The studies reported here support that CHIP increases AR degradation in the absence and presence of androgen. This is consistent with a previous study showing that CHIP promotes ubiquitylation of AR, but conflicts with observations that CHIP does not increase AR degradation (13). A region at human AR residues 11–172, which is NH_2-terminal to the conserved AR motif, was also reported to interact with a different ubiquitin ligase, a RING domain-containing protein called AR-NIP (AR NH_2 terminus-interacting protein) (12).

Several spontaneous somatic AR mutations were reported in the TRAMP model of prostate cancer during tumor progression, two of which (E236G and A234T) are within the AR NH_2-terminal conserved motif. TRAMP tumors were derived in transgenic mice in response to overexpression of the SV40 large and small tumor antigens under the control of the minimal -426 to $+28$ regulatory sequence of the prostate-specific rat probasin promoter (60). The interaction between AR and CHIP was reduced as a result of these AR mutations. This is in support of the AR NH_2-terminal conserved motif functioning to limit AR activity. Interference with the AR and CHIP interac-

tion would be expected to increase AR activity, which could lead to increased prostate cancer growth. In agreement with this, recent studies have shown that the E236G mutation, which we found inhibited the AR and CHIP interaction to the greatest extent, is associated with an increased incidence of tumor formation when the AR mutant is overexpressed.[6] Furthermore, it was reported that the E236G mutant increases AR transactivation in the presence of AR coactivators (17). The results support the inhibitory role of the AR NH_2-terminal conserved motif mediated by CHIP. With the recent report of increased AR levels as a common feature of hormone refractory recurrent prostate cancer (61), down-regulation of or mutations in CHIP may contribute to increased AR steady-state levels during prostate cancer progression.

However, increased degradation of AR cannot necessarily be construed as a decrease in AR functional activity. In many instances, ligand-activated transcription factors are rapidly degraded. Among the steroid receptors, AR (55) and the vitamin D receptor (62) are exceptions. AR is distinguished by its rapid degradation in the absence of ligand (55) and androgen-induced stabilization (56). Part of the mechanism for androgen-induced AR stabilization involves the androgen-dependent NH_2- and COOH-terminal interaction (57, 63) mediated by the F*XX*LF and W*XX*LF motifs mentioned above (18, 21). It is plausible that through the interaction of CHIP and the AR NH_2-terminal conserved motif, CHIP helps to maintain low levels of AR in normal cells. We have shown that CHIP is mainly in the cytoplasm, and CHIP has been reported to be highly expressed in non-proliferating cells (23). In contrast to the low level of AR in non-proliferating cells, AR levels in prostate cancer are elevated (61), and AR has increased stability, which results in a greater sensitivity to low levels of circulating androgen (64) or to androgens present in prostate cancer tissue (65). It is possible that nuclear localization of AR that is detected in prostate cancer cells in the absence of androgen (66) contributes to increased AR levels by sequestering AR in the nucleus away from the degrading influence of CHIP in the cytoplasm. Alterations in CHIP levels, mutations in CHIP, or, as shown here, mutations in AR could decrease AR degradation, resulting in increased AR-dependent proliferation of recurrent prostate cancer cells.

Sequence homology comparisons in the AR gene family show that Ser^{256} in human and rat AR replaces the negatively charged residue aspartic or glutamic acid in AR from lower species. Phosphorylation at Ser^{256} was reported for human AR (10) and effectively reintroduces the constitutive negative charge present in lower species. The proximity of Ser^{256} to the NH_2-terminal conserved motif suggests that a negative charge at this position modulates protein interactions at the NH_2-terminal conserved motif and that phosphorylation at this site is a regulatory switch. Although the interaction between CHIP and AR was not significantly influenced by the S256A and S256D mutations in mammalian two-hybrid assays, the transition from the constitutive negative charge of lower species to the conditional charge regulated by phosphorylation may influence other interacting partners at this site. Higher vertebrates gain the ability to regulate the negative charge by phosphorylation. This is also suggested by the human AR phosphorylation site Ser^{650} (8, 10), which is Asp in lower species. Similarly, the human estrogen receptor-α phosphorylation site Ser^{118} (67, 68) is Asp in the lamprey estrogen receptor (4). Increased regulation introduced by phosphorylation likely helps to modulate protein interactions to increase the overall level of homeostatic control.

[6] N. M. Greenberg, personal communication.

NH_2-terminal domains of steroid receptors are largely unstructured, and amino acid sequence is poorly conserved; yet computational programs that predict protein structure can identify short ~20-amino acid residue segments with ordered secondary structure, some of which are conserved across species. The PONDR Protein Disorder Predictor indicates that the F*XX*LF and W*XX*LF motifs are structured, and similarly, an ordered amphipathic α-helical structure is predicted for the AR NH_2-terminal conserved motif described in this work. We designed a yeast two-hybrid screening approach based on sequence conservation and structure predictions that short ordered regions, especially amphipathic α-helices, are surfaces for protein-protein interactions. In support of this, the highly conserved AR F*XX*LF motif and flanking sequence mediate the androgen-dependent interaction with AF2 in the ligand-binding domain (18, 21) and the interaction of coregulatory proteins (19, 38). The predicted amphipathic α-helices of the p160 coactivator L*XX*LL motifs were also confirmed by structural studies (69, 70). Thus, although transcriptional activation domains of regulatory proteins are largely unstructured and not conserved, short segments within these regions are predicted to form amphipathic α-helices whose structure is likely stabilized by binding coregulatory proteins (2, 71). We previously proposed a reversal of the acidic transcriptional activation domain-coactivator interaction model, implicating charge interactions that precede nonpolar contacts of hydrophobic residues in protein-protein interactions mediated by amphipathic α-helices (21). In the present study, we used comparative sequence alignment and structure predictions to identify a 14-amino acid AR NH_2-terminal conserved motif conserved in all AR sequences throughout the lower vertebrates. We have demonstrated the usefulness of yeast two-hybrid library screening using short ~50-amino acid fusion peptides containing conserved sequence and predicted structure in the identification of interacting partners. The results demonstrate a novel strategy to identify interacting partners and to probe the functional significance of short conserved sequences present in steroid receptor NH_2-terminal domains.

Acknowledgments—We are grateful for the excellent technical assistance of K. Michelle Cobb and De-Ying Zang. We thank Frank S. French, who kindly reviewed the manuscript.

REFERENCES

1. Bain, D. L., Franden, M. A., McManaman, J. L., Takimoto, G. S., and Horwitz, K. B. (2000) *J. Biol. Chem.* **275,** 7313–7320
2. Reid, J., Kelly, S. M., Watt, K., Price, N. C., and McEwan, I. J. (2002) *J. Biol. Chem.* **277,** 20079–20086
3. Baskakov, I. V., Kumar, R., Srinivasan, G., Ji, Y., Bolen, D. W., and Thompson, E. B. (1999) *J. Biol. Chem.* **274,** 10693–10696
4. Thornton, J. W. (2001) *Proc. Natl. Acad. Sci. U. S. A.* **98,** 5671–5676
5. Thornton, J. W., Need, E., and Crews, D. (2003) *Science* **301,** 1714–1717
6. Simental, J. A., Sar, M., Lane, M. V., French, F. S., and Wilson, E. M. (1991) *J. Biol. Chem.* **266,** 510–518
7. Chamberlain, N. L., Whitacre, D. C., and Miesfeld, R. L. (1996) *J. Biol. Chem.* **271,** 26772–26778
8. Zhou, Z. X., Kemppainen, J. A., and Wilson, E. M. (1995) *Mol. Endocrinol.* **9,** 605–615
9. Nazareth, L. V., and Weigel, N. L. (1996) *J. Biol. Chem.* **271,** 19900–19907
10. Gioeli, D., Ficarro, S. B., Kwiek, J. J., Aaronson, D., Hancock, M., Catling, A. D., White, F. M., Christian, R. E., Settlage, R. E., Shabanowitz, J., Hunt, D. F., and Weber, M. J. (2002) *J. Biol. Chem.* **277,** 29304–29314
11. Poukka, H., Karvonen, U., Jänne, O. A., and Palvimo, J. J. (2000) *Proc. Natl. Acad. Sci. U. S. A.* **97,** 14145–14150
12. Beitel, L. K., Elhaji, Y. A., Lumbroso, R., Wing, S. S., Panet-Raymond, V., Gottlieb, B., Pinsky, L., and Trifiro, M. A. (2002) *J. Mol. Endocrinol.* **29,** 41–60
13. Cardozo, C. P., Michaud, C., Ost, M. C., Fliss, A. E., Yang, E., Patterson, C., Hall, S. J., and Caplan, A. J. (2003) *Arch. Biochem. Biophys.* **410,** 134–140
14. Betney, R., and McEwan, I. J. (2003) *J. Mol. Endocrinol.* **31,** 427–439
15. Zhou, Z. X., Sar, M., French, F. S., and Wilson, E. M. (1993) in *Steroid Hormone Receptors: Basic and Clinical Aspects* (Moudgil, V. K., ed) pp. 407–426, Birkhauser, Boston
16. He, B., Kemppainen, J. A., Voegel, J. J., Gronemeyer, H., and Wilson, E. M. (1999) *J. Biol. Chem.* **274,** 37219–37225
17. Han, G., Foster, B. A., Mistry, S., Buchanan, G., Harris, J. M., Tilley, W. D., and Greenberg, N. M. (2001) *J. Biol. Chem.* **276,** 11204–11213

18. He, B., Kemppainen, J. A., and Wilson, E. M. (2000) *J. Biol. Chem.* **275,** 22986–22994
19. He, B., Minges, J. T., Lee, L. W., and Wilson, E. M. (2002) *J. Biol. Chem.* **277,** 10226–10235
20. Feng, Q., Cao, R., Xia, L., Erdjument-Bromage, H., Tempst, P., and Zhang, Y. (2002) *Mol. Cell. Biol.* **22,** 536–546
21. He, B., and Wilson, E. M. (2003) *Mol. Cell. Biol.* **23,** 2135–2150
22. Lubahn, D. B., Joseph, D. R., Sar, M., Tan, J., Higgs, H. N., Larson, R. E., French, F. S., and Wilson, E. M. (1988) *Mol. Endocrinol.* **2,** 1265–1275
23. Ballinger, C. A., Connell, P., Wu, Y., Hu, Z., Thompson, L. J., Yin, L. Y., and Patterson, C. (1999) *Mol. Cell. Biol.* **19,** 4535–4545
24. Jiang, J., Ballinger, C. A., Wu, Y., Dai, Q., Cyr, D. M., Hohfeld, J., and Patterson, C. (2001) *J. Biol. Chem.* **276,** 42938–42944
25. Cyr, D. M., Hohfeld, J., and Patterson, C. (2002) *Trends Biochem. Sci.* **27,** 368–375
26. Demand, J., Alberti, S., Patterson, C., and Hohfeld, J. (2001) *Curr. Biol.* **11,** 1569–1577
27. Fang, Y., Fliss, A. E., Robins, D. M., and Caplan, A. J. (1996) *J. Biol. Chem.* **271,** 28697–28702
28. Vanaja, D. K., Mitchell, S. H., Toft, D. O., and Young, C. Y. (2002) *Cell Stress Chaperones* **7,** 55–64
29. Nikolay, R., Wiederkehr, T., Rist, W., Kramer, G., Mayer, M. P., and Bukau, B. (2004) *J. Biol. Chem.* **279,** 2673–2678
30. Scheufler, C., Brinker, A., Bourenkov, G., Pegoraro, S., Moroder, L., Bartunik, H., Hartl, F. U., and Moarefi, I. (2000) *Cell* **101,** 199–210
31. Connell, P., Ballinger, C. A., Jiang, J., Wu, Y., Thompson, L. J., Hohfeld, J., and Patterson, C. (2001) *Nat. Cell Biol.* **3,** 93–96
32. He, B., Lee, L. W., Minges, J. T., and Wilson, E. M. (2002) *J. Biol. Chem.* **277,** 25631–25639
33. Heery, D. M., Kalkhoven, E., Hoare, S., and Parker, M. G. (1997) *Nature* **387,** 733–736
34. McInerney, E. M., Rose, D. W., Flynn, S. E., Westin, S., Mullen, T. M., Krones, A., Inostroza, J., Torchia, J., Nolte, R. T., Assa-Munt, N., Milburn, M. V., Glass, C. K., and Rosenfeld, M. G. (1998) *Genes Dev.* **12,** 3357–3368
35. Voegel, J. J., Heine, M. J., Tini, M., Vivat, V., Chambon, P., and Gronemeyer, H. (1998) *EMBO J.* **17,** 507–519
36. Torchia, J., Rose, D. W., Inostroza, J., Kamei, Y., Westin, S., Glass, C. K., and Rosenfeld, M. G. (1997) *Nature* **387,** 677–684
37. Hsu, C. L., Chen, Y. L., Yeh, S., Ting, H. J., Hu, Y. C., Lin, H., Wang, X., and Chang, C. (2003) *J. Biol. Chem.* **278,** 23691–23698
38. Zhou, Z. X., He, B., Hall, S. H., Wilson, E. M., and French, F. S. (2002) *Mol. Endocrinol.* **16,** 287–300
39. McEwan, I. J., and Gustafsson, J. (1997) *Proc. Natl. Acad. Sci. U. S. A.* **94,** 8485–8490
40. Reid, J., Murray, I., Watt, K., Betney, R., and McEwan, I. J. (2002) *J. Biol. Chem.* **277,** 41247–41253
41. Sikorski, R. S., Boguski, M. S., Goebl, M., and Hieter, P. (1990) *Cell* **60,** 307–317
42. Hirano, T., Kinoshita, N., Morikawa, K., and Yanagida, M. (1990) *Cell* **60,** 319–328
43. Hohfeld, J., Minami, Y., and Hartl, F. U. (1995) *Cell* **83,** 589–598
44. Chen, S., Prapapanich, V., Rimerman, R. A., Honore, B., and Smith, D. F. (1996) *Mol. Endocrinol.* **10,** 682–693
45. Brinker, A., Scheufler, C., Von Der Mulbe, F., Fleckenstein, B., Herrmann, C., Jung, G., Moarefi, I., and Hartl, F. U. (2002) *J. Biol. Chem.* **277,** 19265–19275
46. Prapapanich, V., Chen, S., Toran, E. J., Rimerman, R. A., and Smith, D. F. (1996) *Mol. Cell. Biol.* **16,** 6200–6207
47. Kampinga, H. H., Kanon, B., Salomons, F. A., Kabakov, A. E., and Patterson, C. (2003) *Mol. Cell. Biol.* **23,** 4948–4958
48. Murata, S., Minami, Y., Minami, M., Chiba, T., and Tanaka, K. (2001) *EMBO Rep.* **2,** 1133–1138
49. Meacham, G. C., Patterson, C., Zhang, W., Younger, J. M., and Cyr, D. M. (2001) *Nat. Cell Biol.* **3,** 100–105
50. Xu, W., Marcu, M., Yuan, X., Mimnaugh, E., Patterson, C., and Neckers, L. (2002) *Proc. Natl. Acad. Sci. U. S. A.* **99,** 12847–12852
51. Citri, A., Alroy, I., Lavi, S., Rubin, C., Xu, W., Grammatikakis, N., Patterson, C., Neckers, L., Fry, D. W., and Yarden, Y. (2002) *EMBO J.* **21,** 2407–2417
52. McClellan, A. J., and Frydman, J. (2001) *Nat. Cell Biol.* **3,** E51–E53
53. Dai, Q., Zhang, C., Wu, Y., McDonough, H., Whaley, R. A., Godfrey, V., Li, H. H., Madamanchi, N., Xu, W., Neckers, L., Cyr, D., and Patterson, C. (2003) *EMBO J.* **22,** 5446–5458
54. Jiang, J., Cyr, D., Babbitt, R. W., Sessa, W. C., and Patterson, C. (2003) *J. Biol. Chem.* **278,** 49332–49341
55. Kemppainen, J. A., Lane, M. V., Sar, M., and Wilson, E. M. (1992) *J. Biol. Chem.* **267,** 968–974
56. Zhou, Z. X., Lane, M. V., Kemppainen, J. A., French, F. S., and Wilson, E. M. (1995) *Mol. Endocrinol.* **9,** 208–218
57. He, B., Bowen, N. T., Minges, J. T., and Wilson, E. M. (2001) *J. Biol. Chem.* **276,** 42293–42301
58. Grenert, J. P., Sullivan, W. P., Fadden, P., Haystead, T. A., Clark, J., Mimnaugh, E., Krutzsch, H., Ochel, H. J., Schulte, T. W., Sausville, E., Neckers, L. M., and Toft, D. O. (1997) *J. Biol. Chem.* **272,** 23843–23850
59. Segnitz, B., and Gehring, U. (1997) *J. Biol. Chem.* **272,** 18694–18701
60. Greenberg, N. M., DeMayo, F., Finegold, M. J., Medina, D., Tilley, W. D., Aspinall, J. O., Cunha, G. R., Donjacour, A. A., Matusik, R. J., and Rosen, J. M. (1995) *Proc. Natl. Acad. Sci. U. S. A.* **92,** 3439–3443
61. Chen, C. D., Welsbie, D. S., Tran, C., Baek, S. H., Chen, R., Vessella, R., Rosenfeld, M. G., and Sawyers, C. L. (2004) *Nat. Med.* **10,** 33–39
62. Arbour, N. C., Prahlm, J. M., and DeLuca, H. F. (1993) *Mol. Endocrinol.* **7,** 1307–1312
63. Langley, E., Kemppainen, J. A., and Wilson, E. M. (1998) *J. Biol. Chem.* **273,** 92–101
64. Gregory, C. W., Johnson, R. T., Mohler, J. L., French, F. S., and Wilson, E. M. (2001) *Cancer Res.* **61,** 2892–2898
65. Mohler, J. L., Gregory, C. W., Ford, O. H., Kim, D., Weaver, C. M., Petrusz, P., Wilson, E. M., and French, F. S. (2004) *Clin. Cancer Res.* **10,** 440–448
66. Gregory, C. W., Hamil, K. G., Kim, D., Hall, S. H., Pretlow, T. G., Mohler, J. L., and French, F. S. (1998) *Cancer Res.* **58,** 5718–5724
67. Ali, S., Metzger, D., Bornert, J. M., and Chambon, P. (1993) *EMBO J.* **12,** 1153–1160
68. Le Goff, P., Montano, M. M., Schodin, D. J., and Katzenellenbogen, B. S. (1994) *J. Biol. Chem.* **269,** 4458–446661
69. Darimont, B. D., Wagner, R. L., Apriletti, J. W., Stallcup, M. R., Kushner, P. J., Baxter, J. D., Fletterick, R. J., and Yamamoto, K. R. (1998) *Genes Dev.* **12,** 3343–3356
70. Shiau, A. K., Barstad, D., Loria, P. M., Cheng, L., Kushner, P. J., Agard, D. A., and Greene, G. L. (1998) *Cell* **95,** 927–937
71. Uesugi, M., Nyanguile, O., Lu, H., Levine, A. J., and Verdine, G. L. (1997) *Science* **277,** 1310–1313
72. Hollenberg, S. M., Weinberger, C., Ong, E. S., Cerelli, G, Oro, A., Lebo, R., Thompson, E. B., Rosenfeld, M. G., and Evans, R. M. (1985) *Nature* **318,** 635–641

Molecular Cell, Vol. 16, 425–438, November 5, 2004, Copyright ©2004 by Cell Press

Structural Basis for Androgen Receptor Interdomain and Coactivator Interactions Suggests a Transition in Nuclear Receptor Activation Function Dominance

Bin He,[1,2,3,9] Robert T. Gampe, Jr.,[7] Adam J. Kole,[7,8] Andrew T. Hnat,[1,3] Thomas B. Stanley,[5] Gang An,[5] Eugene L. Stewart,[6] Rebecca I. Kalman,[1,3] John T. Minges,[1,3] and Elizabeth M. Wilson[1,2,3,4,*]

[1]Laboratories for Reproductive Biology
[2]Lineberger Comprehensive Cancer Center
[3]Department of Pediatrics
[4]Department of Biochemistry and Biophysics
University of North Carolina at Chapel Hill
Chapel Hill, North Carolina 27599
[5]Gene Expression and Protein Biochemistry
[6]Computational Chemistry
[7]Structural Sciences
Discovery Research
GlaxoSmithKline
Research Triangle Park, North Carolina 27709
[8]Department of Chemistry
Duke University
Durham, North Carolina 27710

Summary

The androgen receptor (AR) is required for male sex development and contributes to prostate cancer cell survival. In contrast to other nuclear receptors that bind the L*XX*LL motifs of coactivators, the AR ligand binding domain is preferentially engaged in an interdomain interaction with the AR F*XX*LF motif. Reported here are crystal structures of the ligand-activated AR ligand binding domain with and without bound F*XX*LF and L*XX*LL peptides. Key residues that establish motif binding specificity are identified through comparative structure-function and mutagenesis studies. A mechanism in prostate cancer is suggested by a functional AR mutation at a specificity-determining residue that recovers coactivator L*XX*LL motif binding. An activation function transition hypothesis is proposed in which an evolutionary decline in L*XX*LL motif binding parallels expansion and functional dominance of the NH_2-terminal transactivation domain in the steroid receptor subfamily.

Introduction

Nuclear hormone receptors (NRs) are transcriptional activators that regulate hormone-dependent differentiation (Tsai and O'Malley, 1994; Chawla et al., 2001) and increase gene activity by recruiting coactivators that assist in chromatin remodeling (Glass and Rosenfeld, 2000). Steroid receptors, a subgroup of the NR superfamily, have two predominant activation regions. Activation function 1 (AF1) in the NH_2-terminal region is variable in sequence and its activity is receptor and cell-type dependent (Metzger et al., 1992; Tremblay et al., 1999). Activation function 2 (AF2) in the ligand binding domain (LBD) is a highly conserved hydrophobic cleft flanked by opposing charge residues (Webster et al., 1989; Nolte et al., 1998; He and Wilson, 2003) that binds the L*XX*LL motifs of the steroid receptor coactivator (SRC) family of coactivators (Onate et al., 1995; Hong et al., 1996; Voegel et al., 1998). Some coactivators and associated complexes such as p300/CBP have potent histone acetyl transferase activity (Ogryzko et al., 1996). Hormone binding regulates these activities by repositioning helix 12 to complete the AF2 binding surface (Moras and Gronemeyer, 1998).

Sequence conservation of NR AF2 reflects a common function of coactivator binding. The androgen receptor (AR) AF2 has weak activity in mammalian cells but recruits SRC coactivators when highly expressed as in recurrent prostate cancer (Gregory et al., 2001). AR AF2 preferentially binds the F*XX*LF motif in the AR NH_2-terminal region (He et al., 2000) and AR coregulatory proteins (He et al., 2002b; Hsu et al., 2003). Interaction of the AR F*XX*LF motif ^{23}FQNLF^{27} with AF2 is androgen dependent and mediates the NH_2- and carboxy (C)-terminal (N/C) interaction (Langley et al., 1998). An additional NH_2-terminal W*XX*LF binding motif ^{433}WHTLF^{437} contributes to the N/C interaction by binding AF2 (He et al., 2002a). These interdomain interactions are important in regulating some but not all androgen-dependent genes in transient reporter assays.

Here we report the molecular basis for F*XX*LF and L*XX*LL motif binding to AF2 based on a comparison of peptide bound and peptide-free AR LBD crystal structures and site-directed mutagenesis. We demonstrate that AR 20-30 F*XX*LF and TIF2-III 740-753 L*XX*LL motifs bind AR AF2, but only the F*XX*LF motif peptide binds with an intact primary charge clamp and better recognition conferring hydrophobic contacts than does the L*XX*LL motif. Shown are key residues that differentiate F*XX*LF motif binding and a functional AR mutation in prostate cancer that recovers L*XX*LL motif binding. The data suggest a transition in dominant transactivation domains from AF2 to AF1 during NR evolution.

Results

AR F*XX*LF Peptide-AR LBD-R1881 Structure

Human AR LBD bound to R1881 was cocrystallized with human AR F*XX*LF peptide 20-30, TIF2 coactivator L*XX*LL peptide 740-753, and without peptide. The resulting monomeric structures contain 12 α helices and 4 small β strands assembled into the familiar 3-layer α-helical structure (Figures 1A and 1B). The arrangement resembles structures of the progesterone receptor (PR) (Williams and Sigler, 1998), glucocorticoid receptor (GR) (Bledsoe et al., 2002), AR (Matias et al., 2000; Sack et al., 2001), and other NRs (Gampe et al., 2000). R1881 is bound in the ligand binding pocket in a mode consistent with that of Matias et al. (2000). The characteristic A- and D ring hydrogen (H) bonding network and other key interactions are maintained.

*Correspondence: emw@med.unc.edu
[9]Present address: M533 DeBakey Building, Department of Molecular and Cellular Biology, Baylor College of Medicine, One Baylor Plaza, Houston, Texas 77030.

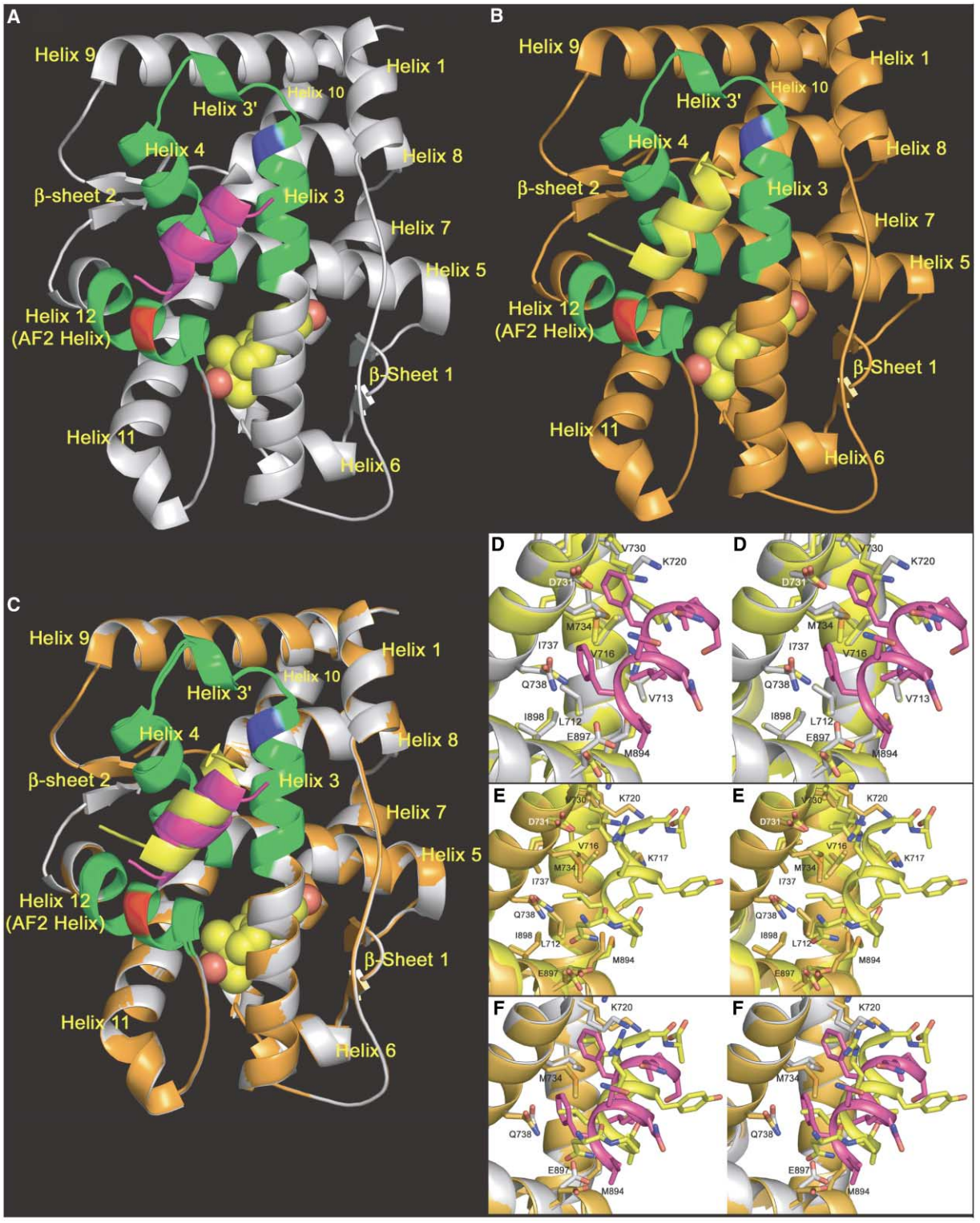

Figure 1. Structures of the AR F*XX*LF and TIF2-III L*XX*LL Peptides Bound to AR-R1881

(A) Global architecture of AR 20-30 F*XX*LF (magenta ribbon) and R1881 (space filled atoms yellow carbon and red oxygen) bound to AR LBD (gray ribbon) with helices 3, 3′, 4, and 12 (green ribbon) in AF2. Conserved charge-clamp residues are K720 (blue) in helix 3 and E897 (red) in helix 12.

(B) Global architecture of TIF2-III 740-753 L*XX*LL (yellow ribbon) and R1881 (as in [A]) bound to AR LBD (orange ribbon) with helices 3, 3′, 4, and 12 (green ribbon) in AF2.

(C) A ~2.0 Å C-terminal shift of bound TIF2-III (yellow ribbon) relative to bound AR F*XX*LF (magenta ribbon) by superimposition of (A) and (B) (backbone root-mean-square distance [rmsd] 0.21 Å).

Table 1. Crystallographic Data and Refinement Statistics

Crystals	AR R1881 AR20-30	AR R1881 TIF2-III	AR R1881 None
X-ray source	Rigaku-RU-H2R-200	APS-32ID	APS-17ID
Space group	$P2_12_12_1$	$P2_12_12_1$	$P2_12_12_1$
Unit cell	a = 54.9, b = 66.1, c = 70.4	a = 54.6, b = 66.7, c = 69.4	a = 56.9, b = 65.8, c = 72.6
Resolution (Å)	50.0–1.8	50.0–1.9	50.0–2.3
Unique reflections	22,123	20,036	13,364
Completeness (%)	90.4	93.0	99.4
I/σ (last shell)	37.8 (2.1)	30.0 (4.7)	32.0 (2.7)
R_{sym}[a] (%)	4.1	7.3	5.7
Refinement			
Resolution range	50.0–1.8	50.0–1.9	50.0–2.3
R factor[b] (%)	21.0	22.1	21.5
R_{free} (%)	21.3	24.1	24.2
Rmsd bond lengths (Å)	0.007	0.006	0.007
Rmsd bond angles (°)	1.1	1.1	1.1
Total nonhydrogen atoms	2,267	2,185	2,086
Accession numbers	1XOW	1XQ2	1XQ3

Rmsd is the root-mean-square deviation from ideal geometry.
[a] $R_{sym} = \Sigma|Iavg - Ii|/\Sigma Ii$
[b] R factor = $\Sigma|F_P - F_{Pcalc}|/\Sigma F_p$, where F_p and F_{pcalc} are observed and calculated structure factors; R_{free} was calculated from a random set of reflections that were excluded from refinement and R factor calculations.

Excellent quality electron density accounts for AR F*XX*LF residues 21–30 (Figure 2A and Table 1) and is clearly visible as a two-turn amphipathic α helix where F23, L26, and F27 are directed toward the LBD surface and Q24, N25, and Q28 are exposed to the solvent (Figure 2C). FQNLF is H bonded NH_2- to C-terminal by the conserved oxy-steroid E897 (helix 12) and K720 (helix 3), respectively, which reside in clusters of opposite charge (He and Wilson, 2003). This result is reminiscent of the charge clamp originally revealed in the SRC-1-PPARγ (Nolte et al., 1998) and other coactivator bound NR structures (Darimont et al., 1998; Shiau et al., 1998; Gampe et al., 2000). Two H bonds are observed between the E897 carboxylate and A22 and F23 amides. Backbone carbonyl oxygens from F27 and V30 H bond with the side chain of K720 (Figure 2A). No interactions are observed from other residues that reside in either charge cluster. Between the charge clusters, ten mostly hydrophobic residues from helices 3, 4, and 12 form the AF2 cleft floor (I898, L712, I737, and V716, Figure 2F), which is bounded on one side by a low rise from M894, V713, and K717, and on the other by a helix 4 ridge from Q738, M734, V730, and Q733. Binding F*XX*LF increases the distance between M734 and M894 by ~1.5 Å, allowing extensive hydrophobic exposure through face on interactions from the F23 and F27 phenyl rings with the helix 4 ridge of the AF2 cleft (Figures 2C and 2F). Both F23 and F27 adopt similar conformers and lie in a staggered, almost parallel orientation near M734 that allows the planar aromatic ring of F23 to contact the Q738 side chain (carbons Cγ and Cδ) and be enclosed by L712, V716, M734, I737, M894, I898, and L26. All F23 aromatic side chain atoms lie between 3.5 and 3.9 Å of the Q738 Cδ and Cγ carbons. The planar aromatic ring of F27 contacts the Cγ carbon and Sδ sulfur of M734 and the K720 Cδ and Cε carbons and is enclosed by V716, V730, Q733, and I737. All F27 aromatic side chain atoms lie between 3.4 and 4.0 Å of the M734 side chain, with additional hydrophobic contact between the L26 side chain and V713, V716, and M894 from helix 12.

Superimposition of backbone heavy atoms indicates no major rearrangement of the protein backbone or ligand binding pocket with F*XX*LF binding. However, consistent with an induced fit mechanism, F*XX*LF causes conformational changes in AR side chains contacting the peptide (Figure 1D). Charge-clamp residues K720 and E897 move and form H bonds with the peptide. Side chain interactions between Q738 and F23 induce conformational changes in V716 and in the flexible M734. An increased distance from 3.0 to 3.9 Å between Q738 Oε1 and Q902 Nε2 suggests Q738 and F23 interactions disrupt a H bond network from Q738 to Q902 and K905 in helix 12 that was observed in the peptide-free structure. At the start of helix 4, V730 is drawn closer to F27. Combined interactions of F27 and the F*XX*LF C-terminal backbone force K720 toward R726, whose guanadinium group moves 4 Å away from its location in the peptide-free structure (Figures 2C and 2F). A change of this magnitude may be driven in part by contact between R726 and an adjacent molecule in the crystal. In helix 12, M894 moves to contact L26 of ^{23}FQNLF^{27}. We conclude that M734, M894, E897, and

(D) Stereoview of AR AF2 showing conformational differences in AR 20-30 bound and unbound states. Amino acid residues of AR (gray)-R1881-F*XX*LF (magenta) and AR (yellow)-R1881 without peptide are superimposed (backbone rmsd 0.21 Å).
(E) Stereoview of AR AF2 showing conformational differences in TIF2-III 740-753 bound and unbound states. Amino acid residues for AR (orange)-R1881-L*XX*LL (yellow) and AR (yellow)-R1881 without peptide structures are superimposed (backbone rmsd 0.20 Å).
(F) Superimposed stereoview of AR AF2 from AR F*XX*LF (magenta)-AR (gray)-R1881 and TIF2-III (yellow)-AR (orange)-R1881 structures (backbone rmsd 0.21 Å). The C-terminal shifted TIF2-III fails to H bond with E897 and forces a conformational change on K720. TIF2-III L745 and L749 Cδ2 carbons occupy similar space to AR 20-30 F23 and F27 but fail to establish extensive hydrophobic contact afforded by F23 and F27.

K720 play a prominent role in AR F*XX*LF binding and undergo notable conformational change along with R726 that does not contact the peptide (Figure 1A, 2C, and 2F).

TIF2 L*XX*LL Peptide-AR LBD-R1881 Structure

Good quality electron density defines the bound TIF2-III 740–753 peptide as a two-turn amphipathic α helix with L745, L748, and L749 turned toward the LBD surface and R746 and Y747 exposed to the solvent (Figures 1B and 2D, and Table 1). Backbone amides of TIF2-III ^{745}LRYLL^{749} are too distant to H bond with the disordered carboxylate oxygen atoms of AR E897 in helix 12 or other residues in the negative charge cluster (Figures 2B and 2D). Lack of an NH_2-terminal backbone H bond to the charge-clamp residue distinguishes L*XX*LL binding to AR from previously described coactivator bound NR structures. Disorder in the E897 carboxylate oxygens also prevents defining a stable electrostatic interaction to the proximal TIF2-III N742 Nδ2, which further H bonds to Nϵ2 of AR Q738 and participates in the H bond network to helix 12 Q902 and K905 described above. On the C-terminal end of L*XX*LL, the backbone carbonyls of L748, L749, and K751(A) accept a H bond from AR K720 Nζ. The side chain of AR R726 moves to strongly H bond (2.6 Å) with the AR Q733 side chain and weakly (3.5 Å) with the TIF2-III L749 carbonyl. Ten residues in helices 3, 4, and 12 interact with the branched leucine side chains in TIF2-III. Both TIF2-III L745 and L749 adopt similar conformers and lie in a staggered almost parallel orientation near AR M734. Since fewer side chain atoms from the branched TIF2-III L745 and L749 are directed toward the helix 4 ridge, fewer hydrophobic contacts are made. The single Cδ2 methyl of L745 makes only two contacts with the AR Q738 side chain at Cγ (3.3 Å) and Cδ (3.5 Å) and is enclosed by AR V716, M734, and M894. Likewise, TIF2-III L749 Cδ2 makes two contacts (3.9 Å) with AR M734 Cγ and Sδ and is enclosed by AR K720, V730, and I737. Additional hydrophobic contact occurs between the TIF2-III L748 side chain and AR M894 in helix 12 and is enclosed by AR V716 and V713.

Like F*XX*LF, L*XX*LL peptide binding does not impose large changes in the global structure, but induces conformational changes in AR side chains that contact or lie near the peptide (Figures 1B, 1E, and 2D). Slight movement in AR E897 may arise from the adjacent TIF2-III N742 side chain since it is too distant to H bond to the peptide backbone. On the other end, AR K720 rearranges to H bond with TIF2-III L748, L749, and the C terminus. A movement of $\sim$2.0 Å is observed for AR R726 as it forms interactions with TIF2-III L749 and AR Q733 (Figure 2) similar to the secondary charge clamp described for GR (Bledsoe et al., 2002). However, 3.5 Å between the AR R726 side chain and TIF2-III L749 backbone oxygen indicates a weak H bond, and 4.4 Å between TIF2-III R746 and AR D731 is too distant for a second direct H bond. Thus, these interactions do not qualify as a fully intact secondary charge clamp. A moderate change in the flexible AR M734 side chain is seen as the Cδ2 methyls from L745 and L749 make contact with M734. TIF2-III L745 induces a slight change in AR Q738 and M894 side chains. M734, Q738, M894, K720, and in particular R726, contribute to binding the TIF2-III peptide and undergo notable conformational change (Figures 1E, 2D, and 2F).

Superimposition of the AR structures illustrates similarities and differences between the AR 20-30 and TIF2-III binding modes (Figures 1C, 1F, and 2E). Both amphipathic peptides align along a similar helical axis and shelter hydrophobic residues within the AF2 cleft. However, a $\sim$2.0 Å C-terminal shift along the helical axis for TIF2-III relative to AR20-30 is observed, separating TIF2-III from charge-clamp residue AR E897 and preventing H bonding. The sizeable shift and resulting absence of H bonding distinguishes TIF2-III from AR 20-30 motif binding to the AR LBD. TIF2-III induces conformational changes where AR K720 is pushed away relative to the F*XX*LF and peptide-free structures and R726 contributes a new distant H bond to the TIF2-III L749 backbone oxygen and a closer one to the AR Q733 side chain. Despite the sizeable shift of L*XX*LL, the respective i+1, i+4, and i+5 leucine residues appear in register and respectively contact many of the same residues as F*XX*LF. However, these contacts are fewer and less optimized due to the geometry and conformation of the branched leucine side chains in relation to the AF2 surface.

Determinants of AF2 Binding Specificity

Consistent with previous cell-based and in vitro binding studies (He et al., 2001; He and Wilson, 2003), the AR LBD binds AR 20-30 F*XX*LF (9.2 $\pm$ 0.4 μM) with higher affinity than the L*XX*LL peptide TIF2-III 740-751 (78 $\pm$ 28 μM) determined by fluorescence polarization (Figures 3A and 3B). In contrast, ERα LBD preferentially binds the L*XX*LL peptide (2.1 $\pm$ 0.2 μM) over the F*XX*LF peptide (>100 μM).

Crystal structures and comparative sequence alignment (Figure 3C) suggest V730 and M734 discriminate F*XX*LF and L*XX*LL binding. AR-V730I-M734I that mimics PR AF2 and AR-V730L-M734V that mimics ERα AF2 decrease binding of the AR F*XX*LF peptide (Figure 3D). The ERα-like mutant also decreases binding of F*XX*LF sequences from coregulatory proteins ARA54 and ARA70 (Figure 3E). In contrast, both mutants increase AR binding of the TIF2-III and SRC1-IV L*XX*LL peptides (Figure 3D).

An effect of V730 and M734 on AR F*XX*LF binding was also evident in transcription assays using PSA-Enh-Luc (Huang et al., 1999) and p21-Luc (Lu et al., 1999) that require the AR N/C interaction for maximal gene activation, with $\sim$90% loss of activity by the AR-^{23}F*XX*AA^{27} mutant (Figures 4A and 4B). The PR-like and ERα-like AR mutants reduce androgen-dependent transactivation of these reporters but cause little change in MMTV-Luc, a reporter less dependent on the AR N/C interaction (He et al., 2002a). The results support AR AF2 residues V730 and M734 are critical for F*XX*LF motif binding.

Ligand Dissociation Rates Support the Role of M734 in F*XX*LF Motif Binding

Mutations that disrupt the AR N/C interaction exhibit reduced half-times ($t_{1/2}$) of androgen dissociation (He et al., 2000, 2001). [^{3}H]R1881 dissociation from the PR-like mutant AR-V730I/M734I ($t_{1/2}$ = 72 $\pm$ 11 min; K_d = 0.71 $\pm$ 0.28 nM) and ERα-like mutant AR-V730L/M734V ($t_{1/2}$ =

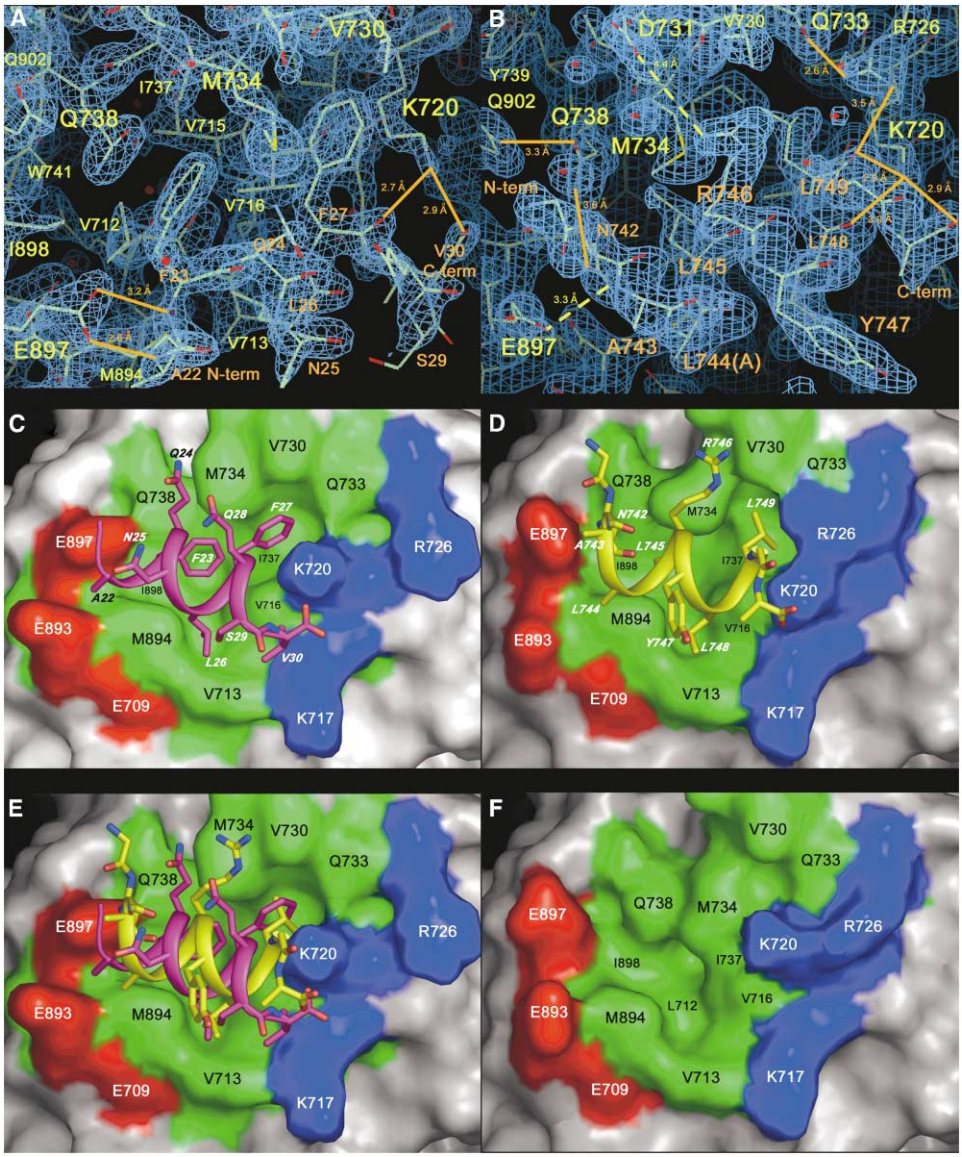

Figure 2. Structural Details for AR FXXLF and TIF2-III LXXLL Peptide-AR LBD-R1881 Complexes

(A) $2F_o - F_c$ electron density map (blue) contoured at 1.8σ from 1.8 Å data for bound AR 20-30. Except for NH_2-terminal arginine, clearly ordered electron density is observed for all peptide residues. Carbon atoms are green, oxygen red, and nitrogen blue; annotations for AR LBD are in yellow, AR 20-30 in orange with intact charge-clamp H bonds in solid orange lines with distances.

(B) $2F_o - F_c$ electron density map (blue) contoured at 1.4σ from 1.9 Å data for bound TIF2-III 740-753. Electron density is devoid for K740, D752, and D753 and poor for L744 and K751 that were built as alanine. H bond interactions are shown with solid orange lines. Excess distance and/or the disordered E897 carboxylate oxygens prevent description of electrostatic interactions to the TIF2-III backbone amides and the proximal N742 side chain. Also the D731 to TIF2-III R746 distance is too long to support direct H bonding (dashed yellow lines with distances and colors as in [A]).

(C) Surface representation of AR AF2 with bound AR 20-30. AR E897, E893, and E709 with K720, K717, and R726 (Roman font) create charge clusters (positive in blue, negative in red) that flank FQNLF (italicized font). F*XX*LF is charge clamped by E897 and K720.

(D) Surface representation of AR AF2 bound to TIF2-III. AR E897, E893, and E709 and K720, K717, and R726 (Roman font) create charge clusters (positive blue, negative red) that flank LRYLL (italicized font). TIF2-III lacks backbone H bonds to AR E897 but H bonds with K720 and AR R726 that moves left to weakly H bond with L749. TIF2-III L745 and L749 make fewer less optimal hydrophobic contacts with Q738, M734, and V730 located in AF2 (green) helix 4 ridge and K720 as does L748 to AR V713.

(E) Superimposed surface representation of the C-terminal shift of TIF2-III (yellow) to the AR F*XX*LF (magenta)-AR-R1881 structure (backbone rmsd 0.21 Å). TIF2-III LRYLL i+1 (not visible) and i+5 leucines are shifted but in register with corresponding phenylalanines in AR 20-30. Binding TIF2-III requires AR K720 to move (Figure 2D) allowing AR R726 to move and participate in L*XX*LL binding.

(F) Surface representation of peptide-free AR AF2. AR E897, E893, E709 and K720, K717, R726 present negative (red) and positive (blue) charge clusters that flank AF2 (green).

71 ± 7 min; K_d = 1.4 ± 0.63 nM) was faster than from wild-type AR ($t_{1/2}$ = 109 ± 11 min; K_d = 0.52 ± 0.08 nM) (Figure 4C) even though equilibrium binding affinities were not altered. A similarly fast dissociation rate from AR-M734I ($t_{1/2}$ = 75 ± 7 min; K_d = 0.75 ± 0.09 nM) indicates M734 is critical for F*XX*LF motif binding.

A Functional AR Mutation in Prostate Cancer at Specificity-Determining Residue V730

V730M is a functional somatic mutation that increases AR transactivation by adrenal androgens (Culig et al., 1993; Peterziel et al., 1995). Because mutations at V730 to longer side chain residues increase L*XX*LL motif binding (Figure 3D, data not shown), we tested whether a functional mutation at this site alters binding specificity and coactivator recruitment. We found the interaction between AR-V730M and GAL-SRC1-IV increases compared to wild-type AR in the presence of R1881, dihydrotestosterone (DHT), androstenedione, and androstanediol, but not progesterone (Figures 4D and 4E). The small decrease in F*XX*LF binding agrees with ligand dissociation studies that show AR-V730M ($t_{1/2}$ = 112 ± 22 min; K_d = 0.42 ± 0.15 nM) similar to wild-type AR.

In vitro binding of GST-TIF2 and GST-SRC1 L*XX*LL fragments to ^{35}S-AR-LBD-V730M also increases in the presence of DHT or androstenedione compared to wild-type AR (Figure 4F). But there is no increase in AR-V730M binding of AR F*XX*LF in the presence of DHT. Specificity for F*XX*LF motif binding in the presence of high-affinity androgens is also evident. The results suggest somatic prostate cancer AF2 mutant AR-V730M recovers L*XX*LL binding with minimal effect on F*XX*LF binding.

Declining AF2 Activity in PR, GR, and AR

AR AF2 residue V713 is present in ERα, ERβ, and steroid receptor progenitors in sea lamprey and mollusk, but is replaced by L727 in PR and I572 in GR (Figure 3C). In agreement with the structures, we found that V713 is important for AR binding of the F*XX*LF and L*XX*LL motifs. AR-V713L and AR-V713I mimic PR and GR at this site and reduce binding of AR F*XX*LF and coactivator L*XX*LL motifs (Figure 5A), suggesting selective pressure maintained ancestral V713 for F*XX*LF binding.

Transition of valine to longer chain residues in PR and GR raised the possibility that L*XX*LL binding and AF2 activity decreases during evolution. Based on sequence alignment and crystal structures (Williams and Sigler, 1998), AR AF2 V713, V730, and M734 correspond to PR L727, I744, and I748 and GR I572, L589, and M593 (Figure 3C). Transactivation by GAL-PR-LBD-L727V is greater than wild-type (Figure 5B) and increases with the L727V-I748V mutations that restore both ancestral valines. GAL-GR-LBD-I572V strongly increases transactivation relative to wild-type, as did the corresponding mutant GAL-GR-LBD-I572V-M593V, suggesting that evolving sequence changes in PR and GR decrease inherent activity of AF2. Inserting a set of AR AF2 residues in GAL-PR-LBDm4 and GAL-GR-LBDm6 reduced AF2 activity.

We found that evolving sequence changes in PR and GR that reduce AF2 activity correlate with decreased binding of the SRC coactivators. GAL-PR-LBD-L727V increases SRC/p160 coactivator binding (Figure 5C). The m4 mutant in which four PR AF2 residues are replaced by corresponding residues of AR, increases coactivator binding, but to a lower extent than the single mutant relative to wild-type. Similarly, GAL-GR-LBD-I572V increases coactivator interaction (Figure 5D) as does GAL-GR-LBDm6, but to a lower extent than the single mutant. Evolving AF2 sequence in PR and GR limits inherent transcriptional activity of AF2 by decreasing coactivator recruitment. The decrease is less than that for AR where evolutionary changes favor F*XX*LF binding.

F*XX*LF Motif Binding by PR and GR Mutants

Structural determinants of AF2 binding specificity were tested by attempting to convert PR and GR AF2 into an F*XX*LF binding site. GAL-PR-LBD and VP-AR1-660 do not interact, but GAL-PR-LBD-L727V interacts with this AR NH_2-terminal fragment (Figure 5E) and increases further when AR V713, V730, M734, and I898 replace corresponding PR residues. A similar set of mutations in GAL-GR-LBD-m6 increases binding of VP-AR1-660 compared to wild-type GAL-GR-LBD, and binding is eliminated by the AR F*XX*AA mutation (Figure 5F). The results support M734, V730, and V713 as key residues in AR F*XX*LF motif binding. It is noteworthy that PR-LBDm4 and GR-LBD-m6 retain L*XX*LL binding (Figures 5C and 5D), suggesting additional determinants contribute to binding specificity.

Transition to AF1

Dependence of NR AF1 activity on length of the NH_2-terminal domain was measured using human NR-GAL4 DNA binding domain fusion proteins expressed in HepG2 (Figure 6A). We found an exponential increase in transcriptional activity with NH_2-terminal domain length ($R = 0.99$, $n = 9$), with a similar trend seen in HeLa, CV1, and COS cells (data not shown). The data support that AF1 transcriptional strength increases with NH_2-terminal length as it evolves in the NR family.

Discussion

Molecular Determinants of F*XX*LF and L*XX*LL Motif Binding

Our data indicate that differential binding affinity and specificity are established by distinct electrostatic and hydrophobic interactions revealed in our AR-R1881 crystal structures bound with AR F*XX*LF and TIF2-III L*XX*LL peptides. Through an induced fit mechanism, AR 20-30 contacts E897 with classical charge-clamp H bonding that is absent in the bound TIF2-III. Although new distant contacts form between the TIF2-III and AR, the interactions apparently provide insufficient energy to recover what might arise from close NH_2-terminal backbone H bonds with E897. More importantly, selective high-affinity binding by AR AF2 of phenylalanines at i+1 and i+5 suggests that the hydrophobic character, size, and complementarity contribute a substantial nonpolar binding energy.

The crystal structures show that the AR AF2 solvent-exposed hydrophobic cleft shelters hydrophobic residues of bound amphipathic peptides from the solvent

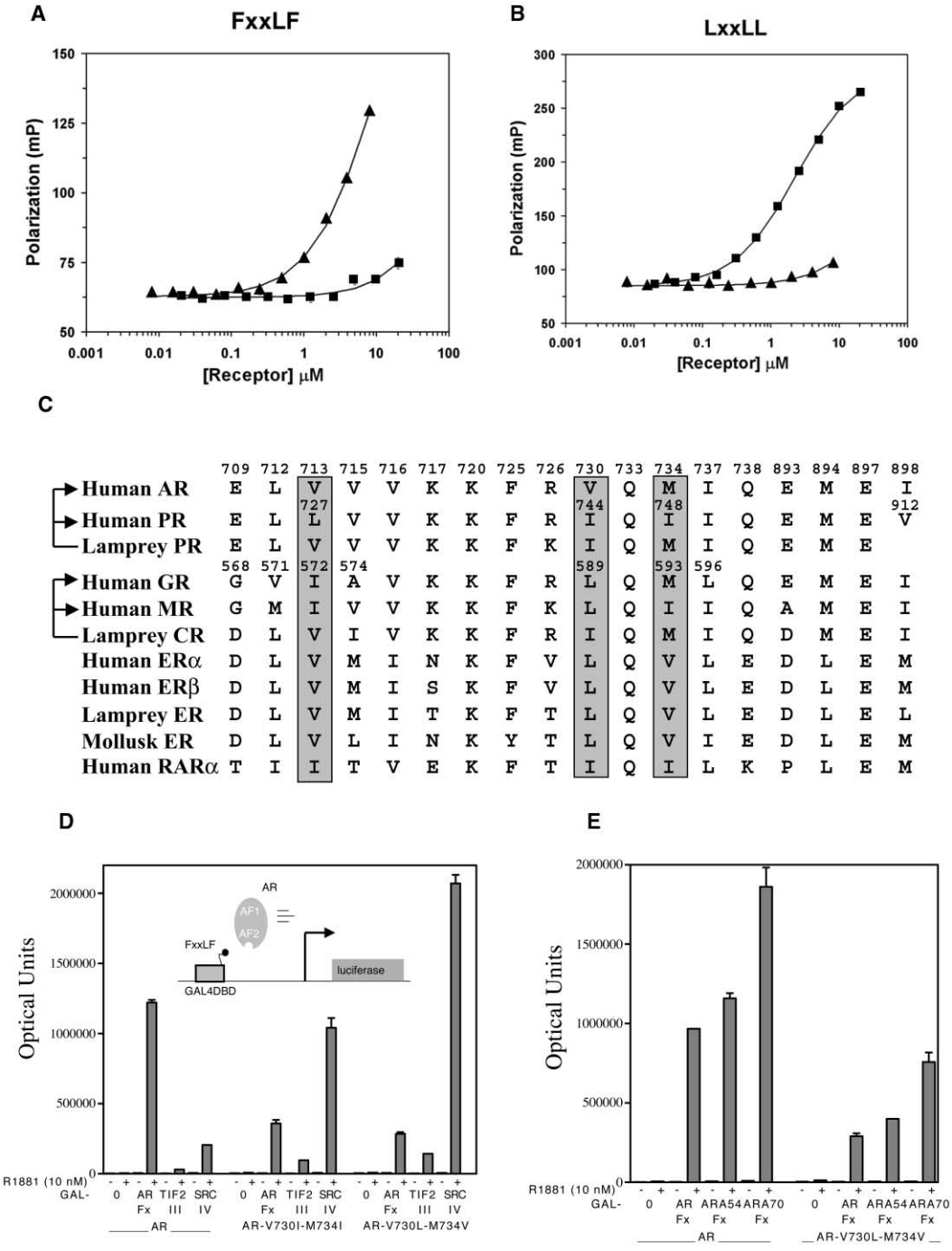

Figure 3. AF2 Determinants of F*XX*LF and L*XX*LL Motif Binding Specificity

(A and B) Affinities of F*XX*LF and L*XX*LL peptides for AR and ERα LBDs. Binding of ERα (■) and AR (▲) LBDs to AR 20-30 ([A], F*XX*LF) and TIF2-III 740-751 ([B], L*XX*LL) and fluoroscein-labeled peptides were measured by fluorescence polarization.

(C) Sequence alignment of AF2 surface residues for human AR GenBank M20132, human PR QRHUP, sea lamprey progestin receptor AY028458, human GR P04150, human mineralocorticoid receptor NP000892, sea lamprey corticoid receptor AY028457, human ERα P03372, human ERβ NP001428, sea lamprey ER AY028456, California sea hare *Aplysia californica* mollusk ER AY327135, and human retinoic acid receptor α P10276. AR AF2 residues involved in F*XX*LF motif binding are shaded.

(D) Substitution of PR and ER residues in AR AF2. Two-hybrid assays in HepG2 cells with and without 10 nM R1881 used 5×GAL4Luc 3 and 10 ng/well pCMVhAR, AR-V730I-M734I, or AR-V730L-M734V, with 50 ng/well of GAL0, GAL-AR20-30 (ARFx), GAL-TIF2-738-756 (TIF2-III, 3rd L*XX*LL), or GAL-SRC1-1428-1441 (SRC-IV, 4th and C-terminal L*XX*LL). Inset: schematic of two-hybrid assay for F*XX*LF motif binding by AR.

(E) Reduction in coregulator F*XX*LF motif binding by ER-like AR mutant. Two-hybrid assays in HepG2 cells with and without 10 nM R1881 used 10 ng/well pCMVhAR or AR-V730L-M734V with 50 ng/well GAL0, GAL-ARFx, GAL-ARA54-447-465 (ARA54Fx), or GAL-ARA70-321-340 (ARA70Fx).

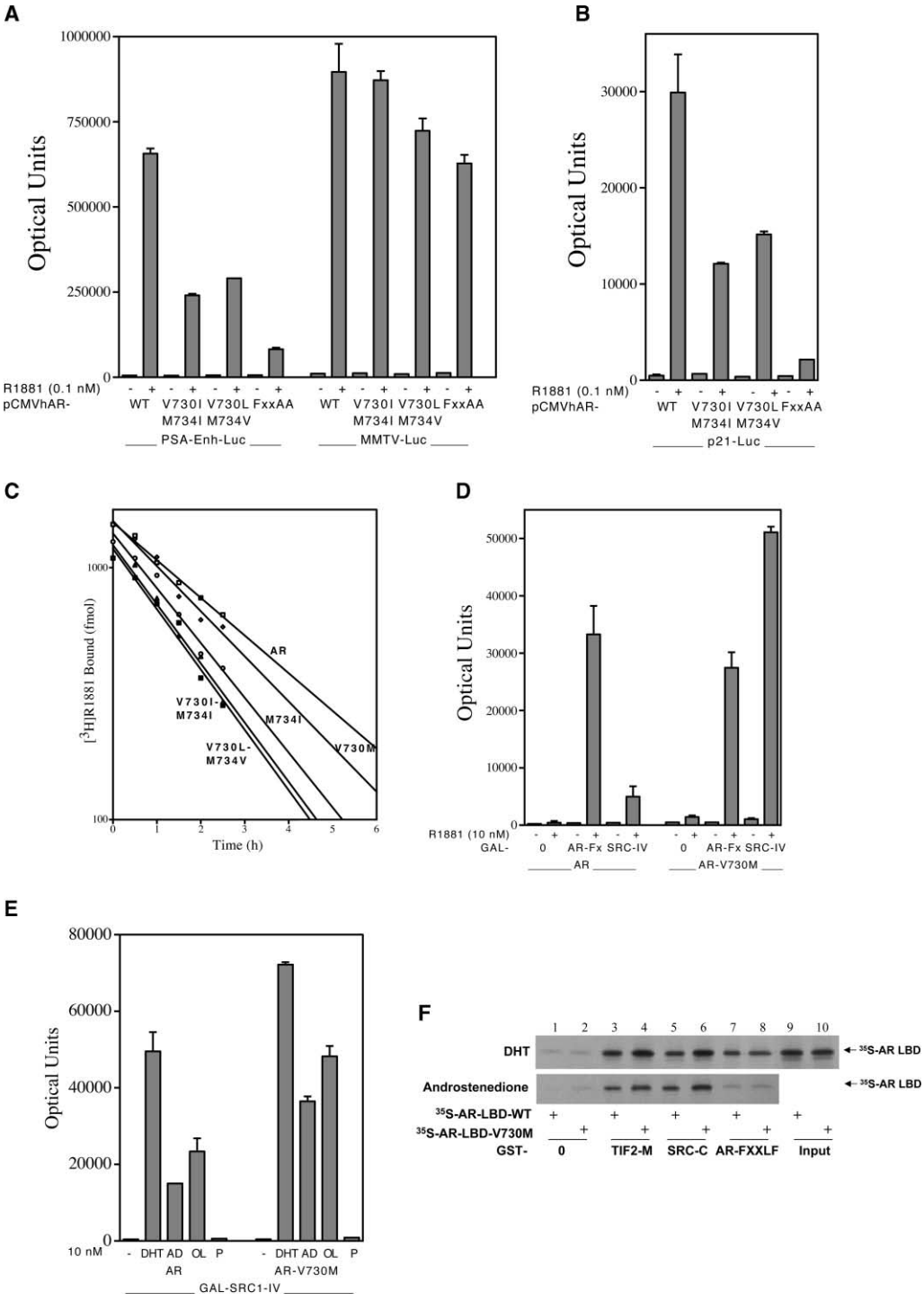

Figure 4. Promoter Dependence and Prostate Cancer Functional Mutant AR-V730M

(A and B) Dependence on the AR NC interaction. Transcriptional activity of AR and mutants was determined in HepG2 cells with and without 0.1 nM R1881 using 50 ng/well pCMVhAR (WT), AR-V730I/M734I, V730L/M734V or L26A/F27A (F*XX*AA) with PSA-Enh-Luc, MMTV-Luc, and p21-Luc.

(C) Reduced AR N/C interaction and increased androgen dissociation. COS cells transfected with pCMVhAR or AR-V730M, M734I, V730I-M734I, or V730L-M734V were incubated with 10 nM [^{3}H]R1881 and dissociation rates measured.

(D) Increase in L*XX*LL binding by prostate cancer AR mutant. Two-hybrid assays in HepG2 cells with and without 10 nM R1881 used 5×GAL4Luc and 10 ng/well pCMVhAR or AR-V730M with 50 ng/well GAL0, GAL-AR20-30 (GAL-ARFx), or GAL-SRC1-1428-1441 (GAL-SRC-IV).

(E) Effects of steroids on L*XX*LL binding. Two-hybrid assays in HeLa cells were performed with and without 10 nM DHT, androstenedione (AD), androstanediol (OL), or progesterone (P) using 50 ng/well GAL-SRC1-IV and 10 ng/well of pCMVhAR or AR-V730M.

(F) Increase in L*XX*LL binding in vitro. Partially purified GST-0, GST-TIF2-624-1141 (TIF2-M), GST-SRC1-1139-1441 (SRC-C), and GST-AR4-52 (AR-F*XX*LF) were incubated with ^{35}S-AR624-919 (WT) and AR-LBD-V730M with and without 1 μM DHT or androstenedione. Input lanes have 30% of the reaction.

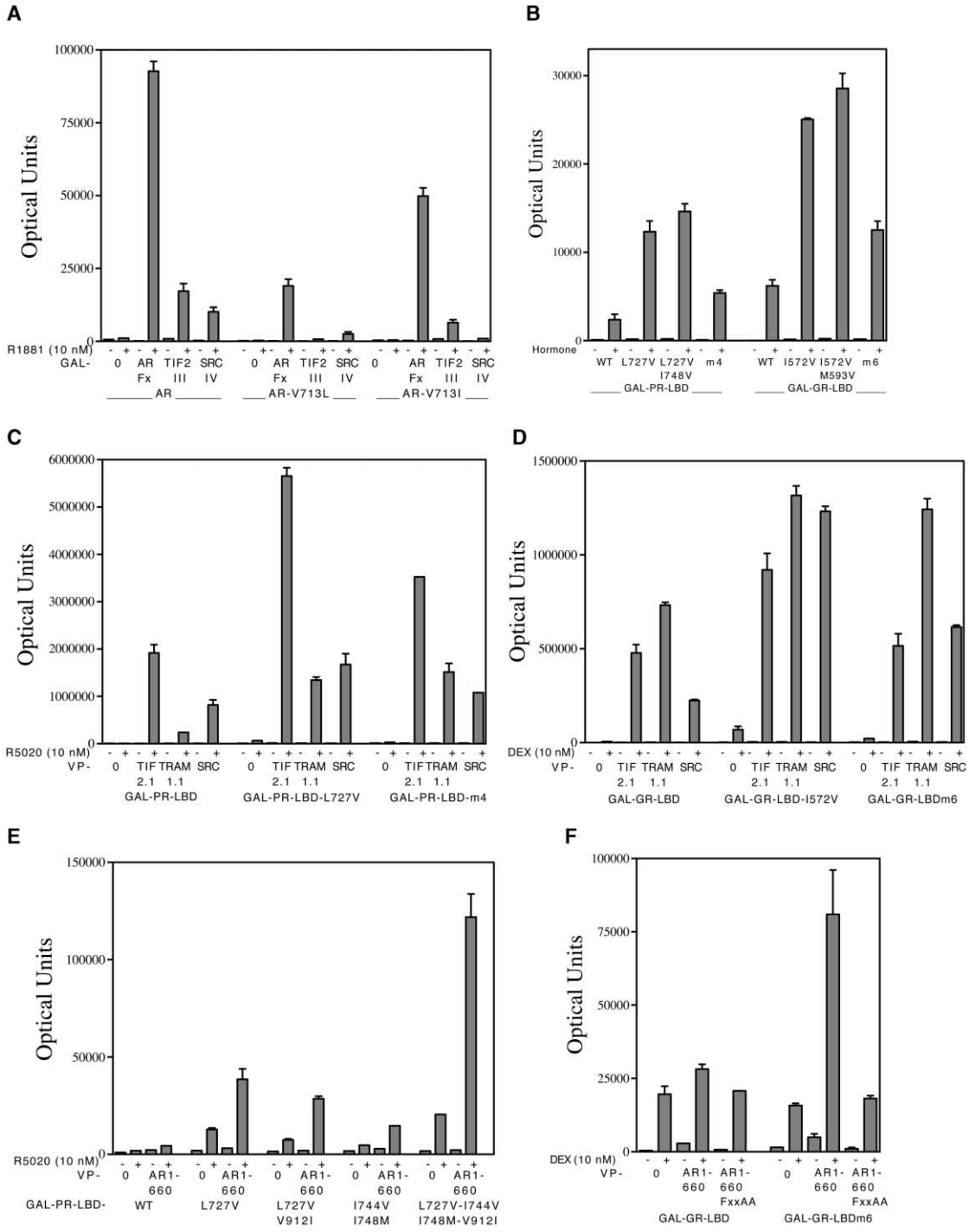

Figure 5. Evolutionary Decline in AF2 Activity and FXXLF Motif Binding by PR and GR Mutants

(A) Role of AR V713. Two-hybrid assays in HepG2 cells with and without 10 nM R1881 used 5×GAL4Luc3 and 5 ng/well pCMVhAR, AR-V713L, or V713I with 50 ng/well GAL0, GAL-AR20-30 (ARFx), GAL-TIF2-738-756 (TIF2-III), or GAL-SRC1-1428-1441 (SRC-IV).

(B) Inherent transcriptional activity of PR and GR AF2 mutants. HeLa cells were assayed using 50 ng/well GAL-PR-LBD (residues 636–933) or mutants L727V, L727V-I748V, or L727V-I744V-I748M-V912I (m4) with and without 1 nM R5020 or with 50 ng/well GAL-GR-LBD (residues 486–777) or mutants I572V, I572V-M593V, or G568E-V571L-I572V-A574V-L589V-L596I (m6) with and without 10 nM dexamethasone (DEX).

(C) Increase in LXXLL binding by PR AF2 mutants. Two-hybrid assays in HepG2 cells with or without 10 nM R5020 used 50 ng/well GAL-PR-LBD or mutants L727V or L727V-I744V-I748M-V912I (m4) with 50 ng/well pNLVP16 (0), VP-TIF2-624-1287 (TIF2.1), VP-TRAM1-604-1297 (TRAM1.1), or VP-SRC1-568-1441 (SRC).

(D) Increase in LXXLL binding by GR AF2 mutants. Two-hybrid assays in HepG2 cells with and without 10 nM DEX used 50 ng/well GAL-GR-LBD (residues 486–777) or mutants I572V or G568E-V571L-I572V-A574V-L589V-L596I (GR-LBDm6) with 50 ng/well VP-0, VP-TIF2.1, VP-TRAM1.1, or VP-SRC.

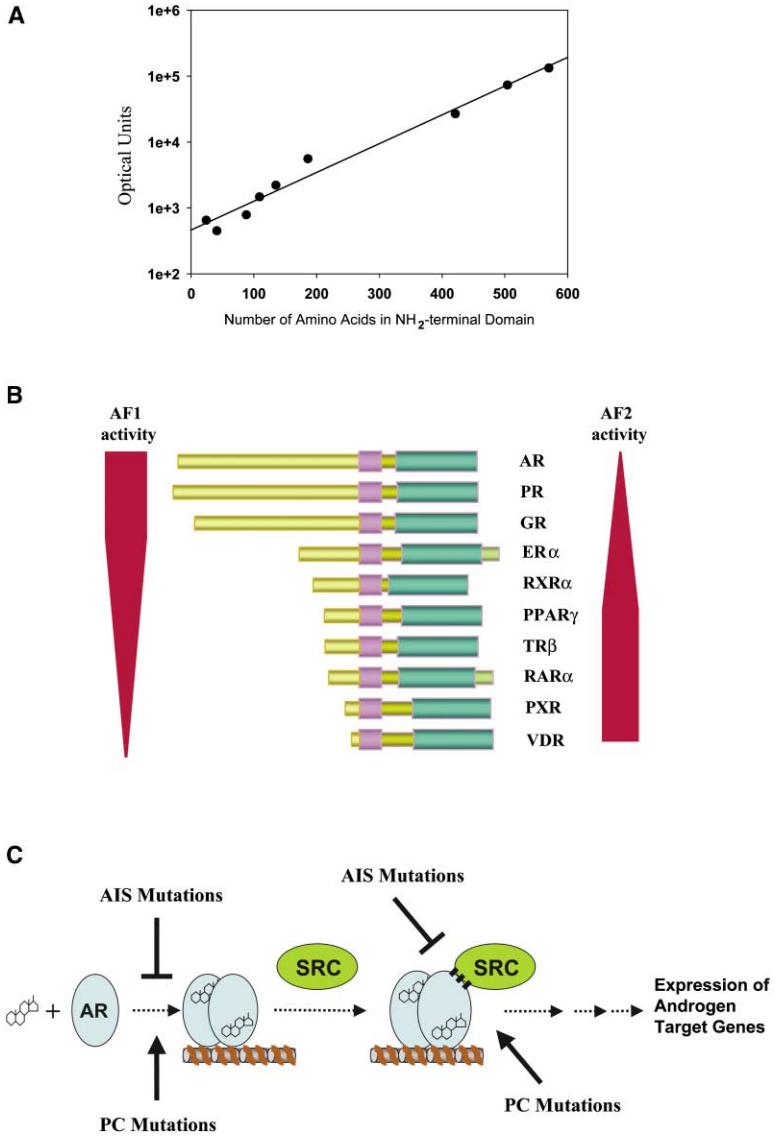

Figure 6. Direct Correlation between AF1 Activity and Length, and Models of NR Transactivation

(A) AF1 activity of NR NH_2-terminal regions. Human PRB1-569, AR1-503, GR1-420, ERα1-185, RXRα1-134, PPARγ1-108, RARα1-87, PXR1-40, and VDR1-23 expressed as GAL4 DNA binding domain fusion proteins (150 ng/well) were assayed in HepG2 cells using 5×GAL4Luc3.

(B) NR AF2 to AF1 transition. The data support an evolutionary transition from AF2 to AF1 as the dominant activation function from nonsteroid NRs to steroid receptors. Transition to AF1 parallels expansion and sequence diversity of the NH_2-terminal region. We speculate that the requirements for high-affinity hormone binding impose structural constraints on AF2 that limit evolutionary diversity in gene regulation. The NH_2-terminal region expands in length and functional significance during steroid receptor evolution. ER is intermediate between nonsteroid NRs and steroid receptors.

(C) Schematic of AR gene regulation. AR transactivation is inhibited by loss-of-function mutations that cause the androgen insensitivity syndrome (AIS). AR transactivation increases from gain-of-function mutations in prostate cancer (PC). An AR mutant in prostate cancer reverts to increased binding of SRC/p160 coactivators L*XX*LL motif.

shell. The 12 aromatic phenyl carbons in FQNLF present a larger hydrophobic contact surface than does L745 and L749 of TIF2-III. Conformational changes to AR M734 from F23 and F27 and M894 from L26 widens AF2 with F*XX*LF compared to L*XX*LL. The gap distance between M734 and M894 sulfur atoms is 10.4 Å for F*XX*LF, 8.4 Å for L*XX*LL, and 8.9 Å without peptide (Figure 2F). The narrower gap may reflect a poorer hydrophobic match between TIF2-III LRYLL and AR AF2 and may also contribute to the C-terminal shift and lost backbone H bonds to E897. Steric hindrance from a motif flanking residue such as L744(A) could also not be inferred due to the absence of electron density beyond the Cβ carbon. For the bound ^{23}FQNLF^{27}, specific enhancement of hydrophobic interactions may favorably position AR20-30 to H bond with E897 in helix 12. The F23 Cζ carbon lies ~1 Å closer to I737 in the AF2 floor than the TIF2-III L745 Cδ2 methyl in the bound ^{745}LRYLL^{749} structure. This orientation provides extensive and improved nonpolar contacts from F23 to Q738, L26 to M894 and V713, and from F27 to M734 and V730 in the helix 4 ridge.

Prominent roles of AR M734, V730, and V713 in F*XX*LF binding and recognition are supported by ligand dissociation studies. In the PR-like mutant AR-M734I, the smaller more rigid isoleucine increases ligand dissociation, suggesting important nonpolar interactions between M734 and F27 are altered. Faster ligand dissociation from the ER-like AR mutant V730L-M734V implies that the larger rigid leucine and smaller rigid valine at

(E) PR AF2 mutants bind AR F*XX*LF. Two-hybrid assays in HepG2 cells with and without 10 nM R5020 used 50 ng/well GAL-PR-636-933 (PR-LBD) or mutants L727V, L727V-V912I, I744V-I748M, or L727V-I744V-I748M-V912I with 50 ng/well pNLVP16 (VP-0) or VP-AR1-660.

(F) GR AF2 mutants bind AR F*XX*LF. Two-hybrid assays in HepG2 cells with and without 10 nM DEX used 50 ng/well GAL-GR486-777 (GR-LBD) or mutant G568E-V571L-I572V-A574V-L589V-L596I (GR-LBDm6) with 50 ng/well VP-0, VP-AR1-660, or VP-AR1-660-F*XX*AA.

F27 destabilize FQNLF interactions with AF2. Slightly faster ligand dissociation rates also occur for PR-like mutant AR-V730I-M734I. Increased binding of L*XX*LL by these AR mutants indicates M734 and V730 contribute to peptide recognition.

The contribution of V730 to F*XX*LF recognition is further explained by the small valine side chain that accommodates the bulky F27, establishing good complementary shape and distance separation. In contrast, ER, PR, and GR have the larger isoleucine or leucine relative to AR V730, preferentially binding L*XX*LL with its smaller i+5 leucine. The even larger methionine in the AR prostate cancer mutant V730M improves L*XX*LL binding but does not greatly affect F*XX*LF binding. The flexible methionine side chain may improve hydrophobic interactions when presented with an i+5 leucine from L*XX*LL or adapt to an i+5 phenylalanine from F*XX*LF. From the crystal structures, sufficient space accommodates the various conformations of a methionine side chain that could account for this exception. Mismatching F*XX*LF to a receptor with larger, rigid isoleucine or leucine could also lead to unfavorable contacts between side chains. Reduced interaction between F*XX*LF and AR V713L or V713I that mimic PR and GR likely result from unfavorable interactions between the i+4 L26 and the larger mutated side chain. The data indicate AR M734, V730, and V713 contribute to F*XX*LF recognition and preference through optimized residue matching and complementary hydrophobic shape.

Other regions of the LBD impose allosteric effects on coactivator binding depending on the bound ligand (Shulman et al., 2004; Nettles et al., 2004). AR favors F*XX*LF binding when bound to DHT and L*XX*LL with the partial agonist androstenedione (Gregory et al., 2001). When AR V730 and M734 are changed to corresponding residues in PR and ER, AR binding of SRC1 and TIF2 increases in the presence of high-affinity agonists. However, transcriptional activities of the AR mutants remain weak compared to PR or GR. Activities of PR and GR LBDs are greater than the AR LBD when mutated at multiple sites to mimic the AR AF2 surface, suggesting additional determinants of NR AF2 activity.

AR AF2 preferentially binds F*XX*LF and other steroid receptors bind L*XX*LL (Heery et al., 1997), but AF2 binding is not exclusive to a single motif. We show that AR binds coactivator L*XX*LL motifs with weaker affinity than F*XX*LF but can bind artificial L*XX*LL peptides with higher affinity (Chang et al., 1999). Mutated PR and GR AF2 bind both F*XX*LF and L*XX*LL motifs. Adaptability of AF2 is supported by variant sequences F*XX*LL (Huang et al., 1998) and L*XX*IL (Li et al., 1999) that mediate coregulators interactions.

Evolutionary Decline in AF2 Activity

Weak transactivation by AR AF2 (He et al., 1999) results from evolving sequence changes that reduce L*XX*LL binding. Concurrently, AR F*XX*LF evolved with the expanding NH_2-terminal AF1 and avidly binds AF2, further limiting coactivator recruitment by competitive binding at AF2 (He et al., 2001) (Figure 6B). We show that evolving sequence changes also decrease L*XX*LL binding by PR and GR AF2, with increasing size and functional importance of AF1 (Sartorius et al., 1994). Evolutionarily older nonsteroid NRs such as RXR and RAR also tend toward NH_2-terminal expansion and increased AF1 activity, although AF2 typically predominates (Nagpal et al., 1993). ERα is evolutionarily intermediate between nonsteroid and steroid receptors (Thornton, 2001) with intermediate NH_2-terminal length and cell-type-dependent AF1 and AF2 activities (Metzger et al., 1992; Tremblay et al., 1999). Orphan NRs can also have extensive NH_2-terminal regions with potent AF1 activity. AF1 of Nurr1 mediates strong autonomous transactivation in various cells (Nordzell et al., 2004), whereas transactivation by its LBD is cell-type dependent (Castro et al., 1999). Thus, evolving NH_2-terminal domains occur among liganded and orphan NRs.

Sequence diversity in the NH_2-terminal region contrasts the conserved LBDs, where the structural constraints of high-affinity hormone binding limit the binding surfaces to L*XX*LL and F*XX*LF-like motifs. Evolution of AF1 as the dominant activation domain can provide unique interaction sites for tissue and species-specific coregulators. Such diversification can increase specificity in gene regulation by AR, PR, GR, and the mineralocorticoid receptor, which bind similar DNA response elements. Our hypothesis for an AF2 to AF1 switch in dominant activation domain also allows for increased diversity in gene regulation between receptor isoforms. In contrast to PR-B, PR-A is less active and can function as a repressor through progesterone and estrogen signaling pathways, allowing progesterone to activate and repress gene transcription through separate isoforms of the same receptor. In this case, the PR LBD functions more like a regulatory domain than a transactivation domain.

The hormone requirement for AR and GR DNA binding may minimize inappropriate gene activity by the evolving AF1. This contrasts nonsteroid NRs for vitamin D, thyroid hormone, and retinoic acid that have weaker AF1 activity, and in the absence of hormone, bind DNA and recruit corepressors to actively repress transcription. Sequestering steroid receptors by heat shock proteins further minimizes inadvertent gene activation by AF1 in the absence of hormone. For ERα in the absence of hormone, an NH_2-terminal A domain LL*XX*I helix competes with the corepressor for a hydrophobic cleft in the LBD to maintain ERα in an inactive state (Metivier et al., 2002).

Selective Advantage in Prostate Cancer

Increased AR activity in prostate cancer is associated with increased levels of AR (Visakorpi et al., 1995) and SRC/p160 coactivators, and autocrine signaling (Gregory et al., 2004). Functional AR mutations tend to appear after antiandrogen or androgen withdrawal therapy (Gelmann, 2002) and contrast loss-of-function mutations that cause androgen insensitivity (Quigley et al., 1995) (Figure 6C). AR transactivation is typically retained in prostate cancer and for some mutants, transactivation increases with different steroids (Culig et al., 1993; Peterziel et al., 1995; Tan et al., 1997).

Here we link an AR somatic prostate cancer mutation to increased L*XX*LL motif binding and SRC coactivator recruitment. AR-V730M retains high-affinity binding of DHT and increased transcriptional activity by adrenal androgens (Newmark et al., 1992; Culig et al., 1993;

Peterziel et al., 1995) (data not shown). V730M increases L*XX*LL binding without reducing F*XX*LF binding and could impact early and late stage cancer. Increased coactivator recruitment by a somatic mutation is a mechanism for aberrant gene regulation that could provide a selective growth advantage to prostate cancer cell survival.

Experimental Procedures

Protein Preparation

NH_2-terminal 6×His-tagged human AR LBD residues 663–919 with a thrombin protease site was expressed from pET15b in *E. coli* Bl21DE3. Cells were grown overnight at 17°C in nutrient-rich media amended with 5 μM R1881 and 1 mM isopropyl-thiogalactopyranoside. Overnight thrombin digestion (5 NIH units/mg protein) at 4°C was performed on pooled, immobilized metal affinity chromatography-purified fractions prior to cation exchange and gel filtration chromatography. The dilute binary complex in 25 mM HEPES (pH 7.5), 0.5 M NaCl, 5 mM DTT, 0.5 mM EDTA, 0.05% β-n-octoglucoside, 10% glycerol, and 10 μM R1881 was used or amended with 2- to 3-fold molar excess of AR 20-30 peptide RGAFQNLFQSV (He et al., 2002b). The dilute binary complex dissolved in 25 mM HEPES (pH 7.5), 0.15 M Li_2SO_4, 10 mM DTT, 0.5 mM EDTA, 0.05% β-n-octoglucoside, 10% glycerol, and 10 μM R1881 was amended with 2- to 3-fold molar excess of TIF2-740-753 L*XX*LL-III peptide KENALLRYLLDKDD (Voegel et al., 1998). Samples were filtered and concentrated to 2–3 mg/ml prior to crystallization.

Crystallization and Data Collection

All crystals grew at 20°C to ~150 μM in 2 weeks by vapor diffusion using a 1:1 (v/v) ratio of complex to well solution. Well solution for AR LBD-R1881 with and without AR 20-30 contained 100 mM Bis-Tris propane (pH 7.5 or 8.5), with a 0.6–1.2 M gradient of lithium sulfate. For TIF2-III 740-753 complexes, a solution containing 100 mM Bis-Tris propane (pH 7.9) and 0.6 M Na/K tartrate was used. Well solutions with 20% glycerol were used to transiently mix the crystals prior to flash freezing in liquid N_2. X-ray diffraction data were collected at −180°C with a MAR-345 detector on a Rigaku RU-H-2R-200 generator, an ADSC 210 detector at the IMCA-CAT, sector 17ID or MARCCD at sector 32ID at the Advanced Photon Source. The observed reflections were processed with the HKL2000 package (Otwinowski and Minor, 1997).

Structure Determination and Refinement

The AR-DHT structure (Sack et al., 2001) (access code 1I37) yielded a convincing AMoRe (Navaza, 2001) molecular replacement solution with one AR LBD complex in the asymmetric unit. Multiple cycles of manual model building were completed with QUANTA (Accelrys, Inc.) and refined with CNX (Accelrys, Inc.) (Brunger, et al., 1998). Initial AR-R1881 and AR-R1881-TIF2 structures were determined from the final AR-R1881-AR 20-30 LBD structure, followed by iterative building and refinement with CNX. Table 1 summarizes the crystallographic and structure refinement statistics. Superimpositions were performed using the homology modeling package in Insight (Accelrys, Inc.). Figures 1 and 2C–2F were generated with PyMol from Delano Scientific (www.pymol.org).

Cell Transfections and Biochemical Measurements

Peptide binding affinities were determined by fluorescence polarization (Stanley et al., 2003) using 40 μM R1881 and 17β-estradiol and 10 nM AR 20-30 (fluorescein-RGAFQNLFQSV) and TIF2-III 740-751 (fluoroscein-KENALLRYLLDK). GAL4-DNA binding domain and VP16 activation domain fusion peptides were prepared (He et al., 2002b). AR transcriptional activity and two-hybrid interaction assays were by transfection of HepG2 and HeLa cells in 12 well tissue culture plates using Effectene (Qiagen). MMTV-Luc, PSA-Enh-Luc (Huang et al., 1999), and p21-Luc (Lu et al., 1999) were used at 0.25 μg/well and 5×GAL4Luc3 at 0.1 μg/well (He and Wilson, 2003). Cells were incubated with and without hormones for 24 hr at 37°C and luciferase activity measured (He et al., 2001). GST fusion proteins and ^{35}S-methionine in vitro translated AR LBD (pcDNA3-HA-AR624-919) were analyzed (He et al., 2002a). Apparent equilibrium binding and dissociation rate studies of [^{3}H]R1881 were determined after transient expression in COS cells (He et al., 2001).

Acknowledgments

The work was supported by Public Health Service Grant HD16910 and cooperative agreement U54-HD35014 of the Specialized Cooperative Center Program in Reproductive Research from NICHD, P01-CA77739 from NCI, and NIH Fogarty International Center grant R03TW001234 to Frank S. French. X-ray diffraction data collected at the Industrial Macromolecular Crystallography Association-Collaborative Access Team (IMCA-CAT) of the Advanced Photon Source are supported by companies of the IMCA-CAT under contract with the Illinois Institute of Technology (IIT), executed through the IIT Center for Synchrotron Radiation Research and Instrumentation. Use of the Advanced Photon Source is supported by the US Department of Energy, Basic Energy Sciences, Office of Science, under Contract No. W-31-109-Eng-38.

Received: April 22, 2004
Revised: July 26, 2004
Accepted: August 26, 2004
Published: November 4, 2004

References

Bledsoe, R.K., Montana, V.G., Stanley, T.B., Delves, C.J., Apolito, C.J., McKee, D.D., Consler, T.G., Parks, D.J., Stewart, E.L., Willson, T.M., et al. (2002). Crystal structure of the glucocorticoid receptor ligand binding domain reveals a novel mode of receptor dimerization and coactivator recognition. Cell *110*, 93–105.

Brunger, A.T., Adams, P.D., Clore, G.M., DeLano, W.L., Gros, P., Grosse-Kunstleve, R.W., Jiang, J.S., Kuszewski, J., Nilges, M., Pannu, N.S., et al. (1998). Crystallography and NMR system: a new software suite for macromolecular structure determination. Acta Crystallogr. D Biol. Crystallogr. *54*, 905–921.

Castro, D.S., Arvidsson, M., Bondesson Bolin, M., and Perlmann, T. (1999). Activity of the Nurr1 carboxyl-terminal domain depends on cell type and integrity of the activation function 2. J. Biol. Chem. *274*, 37483–37490.

Chang, C., Norris, J.D., Gron, H., Paige, L.A., Hamilton, P.T., Kenan, D.J., Fowlkes, D., and McDonnell, D.P. (1999). Dissection of the L*XX*LL nuclear receptor-coactivator interaction motif using combinatorial peptide libraries: discovery of peptide antagonists of estrogen receptors alpha an beta. Mol. Cell. Biol. *19*, 8226–8239.

Chawla, A., Repa, J.J., Evans, R.M., and Mangelsdorf, D.J. (2001). Nuclear receptors and lipid physiology: opening the X-files. Science *294*, 1866–1870.

Culig, Z., Hobisch, A., Cronauer, M.V., Cato, A.C., Hittmair, A., Radmayr, C., Eberle, J., Bartsch, G., and Klocker, H. (1993). Mutant androgen receptor detected in an advanced-stage prostatic carcinoma is activated by adrenal androgens and progesterone. Mol. Endocrinol. *7*, 1541–1550.

Darimont, B.D., Wagner, R.L., Apriletti, J.W., Stallcup, M.R., Kushner, P.J., Baxter, J.D., Fletterick, R.J., and Yamamoto, K.R. (1998). Structure and specificity of nuclear receptor-coactivator interactions. Genes Dev. *12*, 3343–3356.

Gampe, R.T., Jr., Montana, V.G., Lambert, M.H., Miller, A.B., Bledsoe, R.K., Milburn, M.V., Kliewer, S.A., Willson, T.M., and Xu, E.X. (2000). Asymmetry in the PPARγ/RXRα crystal structure reveals the molecular basis of heterodimerization among nuclear receptors. Mol. Cell *5*, 545–555.

Gelmann, E.P. (2002). Molecular biology of the androgen receptor. J. Clin. Oncol. *20*, 3001–3015.

Glass, C.K., and Rosenfeld, M.G. (2000). The coregulator exchange in transcriptional functions of nuclear receptors. Genes Dev. *14*, 121–141.

Gregory, C.W., He, B., Johnson, R.T., Ford, O.H., Mohler, J.L., French, F.S., and Wilson, E.M. (2001). A mechanism for androgen receptor mediated prostate cancer recurrence after androgen deprivation therapy. Cancer Res. *61*, 4315–4319.

Gregory, C.W., Fei, X., Ponguta, L.A., He, B., Bill, H.M., French, F.S., and Wilson, E.M. (2004). Epidermal growth factor increases coactivation of the androgen receptor in recurrent prostate cancer. J. Biol. Chem. *279*, 7119–7130.

He, B., and Wilson, E.M. (2003). Electrostatic modulation of steroid receptor recruitment of the L*XX*LL and F*XX*LF motifs. Mol. Cell. Biol. *23*, 2135–2150.

He, B., Kemppainen, J.A., Voegel, J.J., Gronemeyer, H., and Wilson, E.M. (1999). Activation function 2 in the human androgen receptor ligand binding domain mediates interdomain communication with the NH_2-terminal domain. J. Biol. Chem. *274*, 37219–37225.

He, B., Kemppainen, J.A., and Wilson, E.M. (2000). F*XX*LF and W*XX*LF sequences mediate the NH_2-terminal interaction with the ligand binding domain of the androgen receptor. J. Biol. Chem. *275*, 22986–22994.

He, B., Bowen, N.T., Minges, J.T., and Wilson, E.M. (2001). Androgen-induced NH_2- and COOH-terminal interaction inhibits p160 coactivator recruitment by activation function 2. J. Biol. Chem. *276*, 42293–42301.

He, B., Lee, L.W., Minges, J.T., and Wilson, E.M. (2002a). Dependence of selective gene activation on the androgen receptor NH_2- and carboxyl-terminal interaction. J. Biol. Chem. *277*, 25631–25639.

He, B., Minges, J.T., Lee, L.W., and Wilson, E.M. (2002b). The F*XX*LF motif mediates androgen receptor-specific interactions with coregulators. J. Biol. Chem. *277*, 10226–10235.

Heery, D.M., Kalkhoven, E., Hoare, S., and Parker, M.G. (1997). A signature motif in transcriptional co-activators mediates binding to nuclear receptors. Nature *387*, 733–736.

Hong, H., Kohli, K., Trivedi, A., Johnson, D.L., and Stallcup, M.R. (1996). GRIP1, a novel mouse protein that serves as a transcriptional coactivator in yeast for the hormone binding domains of steroid receptors. Proc. Natl. Acad. Sci. USA *93*, 4948–4952.

Hsu, C.L., Chen, Y.L., Yeh, S., Ting, H.J., Hu, Y.C., Lin, H., Wang, X., and Chang, C. (2003). The use of phage display technique for the isolation of androgen receptor interacting peptides with (F/W)*XX*L(F/W) and F*XX*LY new signature motifs. J. Biol. Chem. *278*, 23691–23698.

Huang, N., vom Baur, E., Garnier, J.M., Lerouge, T., Vonesch, J.L., Lutz, Y., Chambon, P., and Losson, R. (1998). Two distinct nuclear receptor interaction domains in NSD1, a novel SET protein that exhibits characteristics of both corepressors and coactivators. EMBO J. *17*, 3398–3412.

Huang, W., Shostak, Y., Tarr, P., Sawyers, C., and Carey, M. (1999). Cooperative assembly of androgen receptor into a nucleoprotein complex that regulates the prostate-specific antigen enhancer. J. Biol. Chem. *274*, 25756–25768.

Langley, E., Kemppainen, J.A., and Wilson, E.M. (1998). Intermolecular NH_2-/carboxyl-terminal interactions in androgen receptor dimerization revealed by mutations that cause androgen insensitivity. J. Biol. Chem. *273*, 92–101.

Li, D., Desai-Yajnik, V., Lo, E., Schapira, M., Abagyan, R., and Samuels, H.H. (1999). NRIF3 is a novel coactivator mediating functional specificity of nuclear hormone receptors. Mol. Cell. Biol. *19*, 7191–7202.

Lu, S., Liu, M., Epner, D.E., Tsai, S.Y., and Tsai, M.J. (1999). Androgen regulation of the cyclin-dependent kinase inhibitor p21 gene through an androgen response element in the proximal promoter. Mol. Endocrinol. *13*, 376–384.

Matias, P.M., Donner, P., Coelho, R., Thomaz, M., Peixoto, C., Macedo, S., Otto, N., Joschko, S., Scholz, P., Wegg, A., et al. (2000). Structural evidence for ligand specificity in the binding domain of the human androgen receptor. Implications for pathogenic gene mutations. J. Biol. Chem. *275*, 26164–26171.

Metivier, R., Stark, A., Flouriot, G., Hubner, M.R., Brand, H., Penot, G., Manu, D., Denger, S., Reid, G., Kos, M., et al. (2002). A dynamic structural model for estrogen receptor-alpha activation by ligands, emphasizing the role of interactions between distant A and E domains. Mol. Cell *10*, 1019–1032.

Metzger, D., Losson, R., Bornert, J.M., Lemoine, Y., and Chambon, P. (1992). Promoter specificity of the two transcriptional activation functions of the human oestrogen receptor in yeast. Nucleic Acids Res. *20*, 2813–2817.

Moras, D., and Gronemeyer, H. (1998). The nuclear receptor ligand-binding domain: structure and function. Curr. Opin. Cell Biol. *10*, 384–391.

Nagpal, S., Friant, S., Nakshatri, H., and Chambon, P. (1993). RARs and RXRs: evidence for two autonomous transactivation functions (AF-1 and AF-2) and heterodimerization *in vivo*. EMBO J. *12*, 2349–2360.

Navaza, J. (2001). AMoRe: implementation of molecular replacement in AMoRe. Acta Crystallogr. D. Biol. Crystallogr. *57*, 1367–1372.

Nettles, K.W., Sun, J., Radek, J.T., Sheng, S., Rodriguez, A.L., Katzenellenbogen, J.A., Katzenellenbogen, B.S., and Greene, G.L. (2004). Allosteric control of ligand selectivity between estrogen receptors α and β: implications for other nuclear receptors. Mol. Cell *13*, 317–327.

Newmark, J.R., Hardy, D.O., Tonb, D.C., Carter, B.S., Epstein, J.I., Isaacs, W.B., Brown, T.R., and Barrack, E.R. (1992). Androgen receptor gene mutations in human prostate cancer. Proc. Natl. Acad. Sci. USA *89*, 6319–6323.

Nolte, R.T., Wisely, G.B., Westin, S., Cobb, J.E., Lambert, M.H., Kurokawa, R., Rosenfeld, M.G., Willson, T.M., Glass, C.K., and Milburn, M.V. (1998). Ligand binding and co-activator assembly of the peroxisome proliferator-activated receptor-gamma. Nature *395*, 137–143.

Nordzell, M., Aarnisalo, P., Benoit, G., Castro, D.S., and Perlmann, T. (2004). Defining an N-terminal activation domain of the orphan nuclear receptor Nurr1. Biochem. Biophys. Res. Commun. *313*, 205–211.

Ogryzko, V.V., Schiltz, R.L., Russanova, V., Howard, B.H., and Nakatani, Y. (1996). The transcriptional coactivators p300 and CBP are histone acetyltransferases. Cell *87*, 953–959.

Onate, S.A., Tsai, S.Y., Tsai, M.J., and O'Malley, B.W. (1995). Sequence and characterization of a coactivator for the steroid hormone receptor superfamily. Science *270*, 1354–1357.

Otwinowski, Z., and Minor, W. (1997). Processing of x-ray diffraction data collected in oscillation mode. Methods Enzymol. *276*, 307–326.

Peterziel, H., Culig, Z., Stober, J., Hobisch, A., Radmayr, C., Bartsch, G., Klocker, H., and Cato, A.C. (1995). Mutant androgen receptors in prostatic tumors distinguish between amino-acid-sequence requirements for transactivation and ligand binding. Int. J. Cancer *63*, 544–550.

Quigley, C.A., De Bellis, A., Marschke, K.B., El-Awady, M.K., Wilson, E.M., and French, F.S. (1995). Androgen receptor defects: historical, clinical and molecular perspectives. Endocr. Rev. *16*, 271–321.

Sack, J.S., Kish, K.F., Wang, C., Attar, R.M., Kiefer, S.E., An, Y., Wu, G.Y., Scheffler, J.E., Salvati, M.E., Krystek, S.R., Jr., et al. (2001). Crystallographic structures of the ligand-binding domains of the androgen receptor and its T877A mutant complexed with the natural agonist dihydrotestosterone. Proc. Natl. Acad. Sci. USA *98*, 4904–4909.

Sartorius, C.A., Melville, M.Y., Hovland, A.R., Tung, L., Takimoto, G.S., and Horwitz, K.B. (1994). A third transactivation function (AF3) of human progesterone receptors located in the unique N-terminal segment of the B-isoform. Mol. Endocrinol. *8*, 1347–1360.

Shiau, A.K., Barstad, D., Loria, P.M., Cheng, L., Kushner, P.J., Agard, D.A., and Greene, G.L. (1998). The structural basis of estrogen receptor/coactivator recognition and the antagonism of this interaction by tamoxifen. Cell *95*, 927–937.

Shulman, A.I., Larson, C., Mangelsdorf, D.J., and Rama, R. (2004). Structural determinants of allosteric ligand activation in RXR heterodimers. Cell *116*, 417–429.

Stanley, T.B., Leesnitzer, L.M., Montana, V.G., Galardi, C.M., Lambert, M.H., Holt, J.A., Xu, H.E., Moore, L.B., Blanchard, S.G., and Stimmel, J.B. (2003). Subtype specific effects of peroxisome proliferator-activated receptor ligands on corepressor affinity. Biochemistry *42*, 9278–9287.

Tan, J., Sharief, Y., Hamil, K.G., Gregory, C.W., Zang, D.Y., Sar, M.,

Gumerlock, P.H., deVere White, R.W., Pretlow, T.G., Harris, S.E., et al. (1997). Dehydroepiandrosterone activates mutant androgen receptors expressed in the androgen-dependent human prostate cancer xenograft CWR22 and LNCaP cells. Mol. Endocrinol. *11*, 450–459.

Thornton, J.W. (2001). Evolution of vertebrate steroid receptors from an ancestral estrogen receptor by ligand exploitation and serial genome expansions. Proc. Natl. Acad. Sci. USA *98*, 5671–5676.

Tremblay, G.B., Tremblay, A., Labrie, F., and Giguere, V. (1999). Dominant activity of activation function 1 (AF-1) and differential stoichiometric requirements for AF-1 and -2 in the estrogen receptor alpha-beta heterodimeric complex. Mol. Cell. Biol. *19*, 1919–1927.

Tsai, M.J., and O'Malley, B.W. (1994). Molecular mechanisms of action of steroid/thyroid receptor superfamily members. Annu. Rev. Biochem. *63*, 451–486.

Visakorpi, T., Hyytinen, E., Koivisto, P., Tanner, M., Keinanen, R., Palmberg, C., Palotie, A., Tammela, T., Isola, J., and Kallioniemi, O.P. (1995). In vivo amplification of the androgen receptor gene and progression of human prostate cancer. Nat. Genet. *9*, 401–406.

Voegel, J.J., Heine, M.J., Tini, M., Vivat, V., Chambon, P., and Gronemeyer, H. (1998). The coactivator TIF2 contains three nuclear receptor-binding motifs and mediates transactivation through CBP binding-dependent and -independent pathways. EMBO J. *17*, 507–519.

Webster, N.J., Green, S., Tasset, D., Ponglikitmongkol, M., and Chambon, P. (1989). The transcriptional activation function located in the hormone-binding domain of the human oestrogen receptor is not encoded in a single exon. EMBO J. *8*, 1441–1446.

Williams, S.P., and Sigler, P.B. (1998). Atomic structure of progesterone complexed with its receptor. Nature *378*, 392–396.

Accession Numbers

The Protein Data Bank (http://www.rcsb.org/pdb) accession numbers for the crystal structures presented here are 1XOW (FXXLF), 1XQ2 (LXXLL), and 1XQ3 (no peptide).

MOLECULAR AND CELLULAR BIOLOGY, Feb. 2005, p. 1238–1257 Vol. 25, No. 4
0270-7306/05/$08.00+0 doi:10.1128/MCB.25.4.1238–1257.2005

Melanoma Antigen Gene Protein MAGE-11 Regulates Androgen Receptor Function by Modulating the Interdomain Interaction

Suxia Bai, Bin He,† and Elizabeth M. Wilson*

Laboratories for Reproductive Biology, Lineberger Comprehensive Cancer Center, and Departments of Pediatrics and Biochemistry and Biophysics, University of North Carolina, Chapel Hill, North Carolina

Received 13 August 2004/Returned for modification 15 September 2004/Accepted 15 November 2004

Gene activation by steroid hormone receptors involves the recruitment of the steroid receptor coactivator (SRC)/p160 coactivator LXXLL motifs to activation function 2 (AF2) in the ligand binding domain. For the androgen receptor (AR), AF2 also serves as the interaction site for the AR NH_2-terminal FXXLF motif in the androgen-dependent NH_2-terminal and carboxyl-terminal (N/C) interaction. The relative importance of the AR AF2 site has been unclear, since the AR FXXLF motif interferes with coactivator recruitment by competitive inhibition of LXXLL motif binding. In this report, we identified the X chromosome-linked melanoma antigen gene product MAGE-11 as an AR coregulator that specifically binds the AR NH_2-terminal FXXLF motif. Binding of MAGE-11 to the AR FXXLF α-helical region stabilizes the ligand-free AR and, in the presence of an agonist, increases exposure of AF2 to the recruitment and activation by the SRC/p160 coactivators. Intracellular association between AR and MAGE-11 is supported by their coimmunoprecipitation and colocalization in the absence and presence of hormone and by competitive inhibition of the N/C interaction. AR transactivation increases in response to MAGE-11 and the SRC/p160 coactivators through mechanisms that include but are not limited to the AF2 site. MAGE-11 is expressed in androgen-dependent tissues and in prostate cancer cell lines. The results suggest MAGE-11 is a unique AR coregulator that increases AR activity by modulating the AR interdomain interaction.

The androgen receptor (AR) is a member of the steroid receptor subfamily of nuclear receptors. Like other steroid receptors, AR has multiple domains involved in ligand and DNA binding and transcriptional activation. Recently, several unique properties of AR that distinguish it from other steroid receptors have gained attention. High-affinity androgen binding stabilizes AR (26), which is in contrast to most steroid receptors that are down regulated by agonist binding. Agonist-induced AR stabilization results in part from the NH_2-terminal and carboxyl-terminal (N/C) interdomain interaction mediated by the androgen-dependent interaction between the AR NH_2-terminal FXXLF motif and activation function 2 (AF2) in the ligand binding domain (16, 17). The FXXLF motif ^{23}FQNLF^{27} is part of an amphipathic α-helical region that is similar in structure to the LXXLL motifs of the steroid receptor coactivator (SRC)/p160 family of coactivators. The AR FXXLF motif is highly conserved among vertebrates, supporting its functional importance across species (13, 18). Recent cocrystal structures and binding studies have confirmed preferential binding of the FXXLF motif to the AR AF2 site and adaptability of AF2 to coactivator LXXLL motif binding through an induced-fit mechanism (15, 22). FXXLF motif binding to AF2 requires binding of ligands that display agonist activity in vivo (27). In transient transfection reporter gene assays, the N/C interaction is required for the activation of some, but not all, androgen-regulated genes (2, 18). One consequence of the AR interdomain interaction is inhibition of recruitment of the SRC/p160 family of coactivators by competitive binding of FXXLF at the coactivator LXXLL motif binding site in AF2 (14). AR activation by the SRC/p160 family of coactivators is reduced by the interdomain interaction and by sequence changes in AF2 during evolution that favor FXXLF over LXXLL motif binding (15, 20).

Preference for FXXLF binding by AF2 but adaptability to coactivator LXXLL motif binding brings into question the role of the SRC/p160 family of coactivators in AR functional activity. The level of transcriptional intermediary factor 2 (TIF2) (also known as SRC2 or glucocorticoid receptor [GR] interacting protein 1 [GRIP1]) is low in normal prostate epithelial cells (9). In contrast, a majority of advanced prostate cancers that recur after androgen deprivation therapy can have increased levels of SRC1 and TIF2 (SRC2 or GRIP1) (10), suggesting that these coactivators have an important role in AR action that contributes to prostate tumor development and progression (1, 8). Increased expression of the SRC1 and TIF2 coactivators increases AR transactivation at gene promoters in transient transfection assays, even when the promoter depends on the AR N/C interaction for maximal activation (18). This is attributed to overall conservation of the AR AF2 binding site that allows coactivator LXXLL motif binding, albeit with lower affinity than for the FXXLF motif (15, 20).

These observations led us to postulate the existence of an AR coregulator that binds the AR FXXLF motif that would expose the AF2 site for coactivator binding. In this report, we made use of the AR NH_2-terminal FXXLF peptide as bait in a *Saccharomyces cerevisiae* two-hybrid screen of a human testis library to identify the melanoma antigen gene product

* Corresponding author. Mailing address: Laboratories for Reproductive Biology, CB# 7500, Rm. 3340, Medical Biomolecular Research Building, University of North Carolina, Chapel Hill, NC 27599. Phone: (919) 966-5168. Fax: (919) 966-2203. E-mail: emw@med.unc.edu.

† Present address: Baylor College of Medicine, Houston, TX 77030.

MAGE-11 as a novel AR coregulator. MAGE-11 competes for the androgen-induced AR N/C interaction by specifically binding the AR FXXLF motif and relieves inhibition at AF2.

MATERIALS AND METHODS

Plasmids. Expression vectors previously described include pCMVhAR (31); pCMVhAR1-660 (42); pCMVhAR-FXXAA (14); GAL-AR1-503 (30); VP-AR1-660; VP-AR1-660FXXAA (17); GAL-AR20-30, GAL-AR20-36, GAL-AR16-30 and GAL-AR16-36 (20); pcDNA3HA-AR624-919 (17, 18); pCMVhAR-C576A; pCMVhAR-R617M-K618M-K632M-R633M (ARm4) (52); pSG5-TIF2 (47); and the thyroid hormone receptor activator molecule expression vector pSG5-TRAM1 (44). pCMVhAR1-660FXXAA was prepared by digestion of pCMVhAR-FXXAA with TthIII and XbaI and blunt ending and religating the plasmid. GAL-AR16-36 mutants were described previously (20) or were prepared by cloning annealed complementary oligonucleotides into pGAL0, which expresses *S. cerevisiae* GAL4 DNA binding domain residues 1 to 147. pCMV5-Flag-hAR was constructed by cloning a PCR-amplified BglII- and AflII-digested AR NH_2-terminal fragment containing the Flag tag sequence DYKDDDDK, following the first methionine into pCMVhAR digested with the same enzymes. GR-FXXLF and GR-FXXAA contain human AR residues 1 to 132 with the wild-type and mutant FXXLF motif expressed as a fusion protein with human GR residues 132 to 777 in pCMV5. They were constructed by cloning the PCR-amplified AR NH_2-terminal region into the KpnI and SalI sites of pCMV5hGR. pCMVhGR1-550 was prepared by inserting a KpnI- and BamHI-digested human GR fragment into the same sites of pCMV5. p5mPRB-1-688 was prepared by digestion of p5mPRB with BclI and BglII, religation of the vector, and expansion of the isolated clone in SCS110 cells to avoid methylation that interferes with the BclI restriction site. GAL-AR4-52 and GAL-AR4-52FXXAA were constructed by digestion of pGBT8-AR4-52 with EcoRI and BamHI and ligating the fragment into pGAL0 digested with the same enzymes. GST-AR4-52 and GST-AR4-52FXXAA were constructed by PCR amplification of pGBT8-AR4-52 with primers with EcoRI and XhoI ends and cloning of the fragment into these sites in pGEX-4T-1.

The parent yeast bait vector pGBT8 was kindly provided by Yue Xiong, University of North Carolina at Chapel Hill. Wild-type bait vector pGBT8-AR4-52 and the FXXAA mutant containing the AR NH_2-terminal sequences ^{23}FQNLF^{27} and ^{23}FQNAA^{27} were constructed by PCR amplification of the region spanning amino acids 4 to 52 of pCMVhAR and pCMVhAR-FXXAA and cloning the fragments into the EcoRI and BamHI sites of pGBT8. pACT2-MAGE-11 was rescued from a positive yeast clone identified by two-hybrid screening of an amplified human testis library. Sequencing revealed a TGA stop codon between the GAL4 activation domain and the MAGE-11 coding regions. Translation read-through can occur in yeast (45) to produce the GAL–AD–MAGE-11 fusion protein. For expression in mammalian assays, MAGE-11 clones were constructed to begin at the first ATG of the coding region for the 429-amino-acid full-length protein or at the second codon for the fusion proteins.

GAL-MAGE-11 containing full-length MAGE-11 residues 2 to 429 and partial form GAL–MAGE-11-112-429 (GAL-MAGE-11-112-429) were constructed by PCR amplification of pACT2-MAGE-11 with primers with EcoRI and XhoI ends. The fragment was cloned into the EcoRI and SalI sites of pGAL0. VP-MAGE-11 containing full-length MAGE-11 residues 2 to 429 and VP–MAGE-11-112-429 (VP-MAGE-11-112-429) were constructed by the same strategy. GAL-MAGE-11 fragments were constructed by PCR amplification of GAL-MAGE-11 and cloning the fragments into pGAL0. MAGE-11 fragments were amplified with EcoRI- and SalI-ended primers (for GAL-MAGE-11-2-252, -2-362, -112-252, -112-362, and -222-362) or EcoRI- and XhoI-ended primers (for GAL-MAGE-11-222-429) and cloned into pGAL0 digested with EcoRI and SalI. For GAL-MAGE-11-332-429, primer ends and cloning sites were EcoRI and SacI. For GAL-MAGE-11-2-121, GAL-MAGE-11 was digested with Bsu36I and ClaI, blunt ended with the Klenow fragment of DNA polymerase I, and self ligated.

pSG5-MAGE-11 encoding full-length MAGE-11 amino acid residues 1 to 429 was constructed by digestion of pACT2-MAGE-11 with EcoRI and BglII. The fragment was cloned into pSG5 digested with the same enzymes. pSG5-MAGE-11-111-429 was constructed by digestion of pSG5-MAGE-11 with EcoRI and PshAI. The vector was blunt ended with the Klenow fragment of DNA polymerase I and self ligated. pCMV-Flag-MAGE-11 encoding full-length MAGE-11 was constructed by digestion of GAL-MAGE-11 with EcoRI and ClaI and ligation of the fragment into pCMV-Flagb (provided by Yi Zhang and Qin Feng, University of North Carolina at Chapel Hill) digested with the same enzymes. DNA sequences were verified for all PCR-amplified regions.

Yeast two-hybrid screen. A two-hybrid screen of an amplified human testis library was performed with YEASTMAKER Transformation System 2 (Clontech) as previously described (13). Yeast strain HF7c was transformed with pGBT8-AR4-52 and plated on synthetic medium lacking Trp. The yeast clone expressing the pGBT8-AR4-52 bait vector was transformed with 50 μg of amplified human testis MATCHMAKER cDNA library (BD Clontech) and plated on 25 15-cm dishes containing synthetic medium minus Leu, Trp, and His. Over a period of 9 days, colonies were scored according to their time of appearance and were transferred to plates containing synthetic medium lacking Leu, Trp, and His. Clones were retested by a two-hybrid interaction β-galactosidase filter assay (Clontech) by transference to a Whatman no. 5 filter, followed by immersion in liquid N_2 and thawing at room temperature for 5 min. Freshly prepared Z buffer containing 60 mM Na_2HPO_4, 40 mM NaH_2PO_4, 10 mM KCl, 1 mM $MgSO_4$ (pH 7.0), 50 mM 2-mercaptoethanol and 33 mg of 5-bromo-4-chloro-3-indolyl-β-D-galactoside (X-Gal) per ml was added to the filters and incubated at room temperature to score blue colonies after 2 h to overnight. Plasmids from the positive yeast colonies in the β-galactosidase filter assay were rescued. Colonies that grew in synthetic medium lacking Leu gradually lost the bait vector but not the library plasmids. The library vector was purified with a YEASTMAKER yeast plasmid isolation kit (catalogue number K1611-1).

Cell transfections. Human hepatocellular carcinoma HepG2 cells (American Type Culture Collection) were cultured and transfected with Effectene reagent (QIAGEN) as previously described (13). Typically, transfections were performed in 12-well tissue culture plates containing 2×10^5 HepG2 cells/well, 0.1 μg of 5XGAL4Luc3 reporter vector, and 50 ng of the GAL4 and VP16 expression vectors or 5 ng of pCMVhAR. To determine the effect of MAGE-11 on AR transactivation, monkey kidney CV1 cells (4.2×10^5 cells/6-cm dish) were transfected with calcium phosphate (14). The (prostate-specific antigen) PSA-Enh-Luc (PSA-Luc) reporter, provided by Michael Carey (University of California at Los Angeles), contains the PSA upstream enhancer region (21). Probasin $(-244$ to $-96)_3$-Luc was provided by Robert Matusik (Vanderbilt University) and contains three copies of the rat probasin promoter region. Luciferase activity was determined 48 h after the addition of hormone by harvesting cells in lysis buffer containing 1% Triton X-100, 2 mM EDTA, and 25 mM Tris phosphate (pH 7.8) (14). Luciferase light units were assayed with a LumiStar Galaxy multiplate reader luminometer (BMG Labtechnologies). Transfection data shown are representative of at least three independent experiments.

Ligand dissociation assays. Ligand dissociation rate studies were performed with COS cells (4×10^5 cells/well of 6-well culture plates) transfected with DEAE-dextran (19) with 1 μg of pCMVhAR/well with or without 1 μg of pSG5-MAGE-11 or pSG5-MAGE-11-111-429/well. At 48 h after transfection, cells were incubated with 5 or 10 nM ^{3}H-labeled R1881 (82 Ci/mmol; PerkinElmer Life Sciences) for 2.5 h at 37°C, followed by the addition of 50 μM unlabeled R1881. At increasing time intervals at 37°C, cells were washed and harvested in sodium dodecyl sulfate (SDS)-containing buffer, and radioactivity remaining with the cells was determined by scintillation counting. At least three independent experiments were performed to determine the mean and standard deviation of the half-time of dissociation.

GST affinity matrix binding assays. In vitro protein interaction assays were performed by expressing glutathione *S*-transferase (GST)-AR4-52 and GST-AR4-52-FXXAA in BL21 *Escherichia coli* cells treated with 1 mM isopropyl-1-thio-β-D-galactoside as previously described (13, 17). GST-AR fusion proteins were extracted in 0.1 M NaCl, 1 mM EDTA, 0.5% NP-40, 1 mM phenylmethylsulfonyl floride, 1 mM dithiothrietol, and 20 mM Tris-HCl (pH 8.0) and incubated with glutathione agarose beads (Amersham Biosciences). In vitro translation was performed in the presence of 4 μCi of [^{35}S]methionine (PerkinElmer Life Sciences) for pcDNA3HA-AR624-919 and 8 μCi of [^{35}S]methionine for pSG5-MAGE-11 with the TNT T7 Quick Coupled transcription-translation system (Promega). Washed beads were extracted with SDS buffer. Input lanes contained 5 or 10% of the binding reaction mixtures as indicated. The data shown are representative of three independent experiments.

Immunochemical methods. For coimmunoprecipitation and immunoblot experiments, COS cells (2×10^6 cells/10-cm dish) were transfected with DEAE-dextran (14) with the indicated amounts of wild-type and mutant pCMVhAR, pCMV-Flag-AR, pCMV-Flag-MAGE-11, pSG5-MAGE-11, pSG5-TIF2, or GAL-AR peptide vectors. Cells were incubated with and without hormone for 24 h in medium containing 10% charcoal-stripped fetal calf serum (Gemini or HyClone). Cells were harvested in phosphate-buffered saline. For immunoprecipitations, cells were incubated for 30 min at 4°C in, per 10-cm dish, 0.5 to 1 ml of lysis buffer containing 0.15 M NaCl, 0.5% NP-40, 50 mM NaF, and 50 mM Tris-HCl (pH 7.5) plus 1 mM phenylmethylsulfonyl fluoride and protease inhibitor cocktail (Roche) in the absence and presence of hormone. For immunoblot analysis, the radioimmunoprecipitation assay extraction buffer contained 1%

Triton X-100, 1% deoxycholate, 0.1% SDS, 0.15 M NaCl, 0.5 mM EDTA, 50 mM Tris-HCl (pH 7.4), and 1 mM phenylmethylsulfonyl fluoride and protease inhibitor cocktail (Roche). After centrifugation for 30 min at 14,000 × *g*, protein concentration was determined (Bio-Rad). For coimmunoprecipitation, samples were precleared with 100 μl of agarose (Sigma) and incubated for 1 h at 4°C. Supernatants of a 15-min 13,000 rpm centrifugation were incubated with 15 μl of anti-Flag M2 affinity gel (catalogue number A2220; Sigma) for 1 h at 4°C. Agarose pellets were washed four times with 1 ml of lysis buffer in the absence and presence of hormone. Adsorbed proteins were released in 50 μl of 4% SDS, 20% glycerol, 0.2% 2-mercaptoethanol, and 20 mM Tris-HCl (pH 6.8) and analyzed by immunoblotting. For immunoblots of cell extracts, samples (10 μg of protein/lane) were separated on 10% acrylamide gels containing SDS. After electrophoresis, gel proteins were electrophoretically transferred to nitrocellulose membranes, and the blots were incubated with anti-Flag M2 monoclonal antibody (1:2,000 dilution, catalogue number F-3165; Sigma), anti-TIF2 antibody (1:1,000 dilution; Transduction Laboratories), rabbit AR32 immunoglobulin G (IgG) polyclonal antibody (0.42 μg/ml), an anti-MAGE-11 peptide antibody described below (2.9 μg/ml), β-actin antibody AC-15 (1:5,000 dilution; Abcam, Inc.), or anti-GAL4 DNA binding domain antibody (1:500 dilution; Santa Cruz). Immunoreactive bands were visualized by chemiluminescence (SuperSignal Western Dura Extended Duration substrate; Pierce Biotechnology, Inc., Rockford, Ill.).

Immunocytochemistry was performed in COS cells (1.25×10^6 cells/well of 12 plates with cover glass) or the indicated human foreskin fibroblast or prostate cancer cell lines (13). Cells were transfected with Effectene with 0.2 μg of wild-type and mutant pCMVhAR with and without 0.2 μg of pCMVFlag-MAGE-11 and treated for 24 h at 37°C with or without 10 nM dihydrotestosterone (DHT). Prostate cancer cell lines were transfected with 0.2 μg of pCMVFlag-MAGE-11 with Effectene and treated with 10 nM DHT. Cells were fixed with paraformaldehyde, permeabilized with Triton X-100, blocked with bovine serum albumin (13), and incubated for 1 h with primary antibodies anti-Flag M2 monoclonal antibody (1:1,000 dilution; Sigma) and anti-AR polyclonal antibody ab3510 (1:250 dilution; Abcam, Inc.). Cells were incubated with secondary antibodies Rhodamine (tetramethyl rhodamine isocyanate)-conjugated AffiniPure donkey anti-mouse IgG (1:75 dilution; Jackson ImmunoResearch Laboratories, Inc.) and fluorescein isothiocyanate-conjugated AffiniPure donkey anti-rabbit IgG (1:50 dilution; Jackson ImmunoResearch Laboratories, Inc.). Slides were viewed with a Zeiss LSM 210 confocal microscope at an original magnification of ×63.

MAGE-11 NH_2-terminal 13 to 26 amino acid residue peptide C^{13}SPA SIKRKKKREDS^{26}, where C was added to the NH_2 terminus, was predicted to be antigenic (Princeton Biomolecules) and was used to raise a rabbit polyclonal antibody (Pocono Rabbit Farm & Laboratory, Inc., Canadensis, Pa.). Immunoreactivity for MAGE-11 was verified on immunoblots of extracts from COS cells transfected with pSG5-MAGE-11 and pCMV-Flag-MAGE-11. The antibody was purified by antigen affinity chromatography with activated immunoaffinity Affi-Gel 10 gel (Bio-Rad). The peptide antigen was coupled to the column in 0.2 M ethanolamine (pH 8.0). Antiserum was incubated for 2 h at 4°C and the antibody was eluted with 0.1 M glycine (pH 3.0) in 0.1 volume of 1 M Tris-HCl (pH 8.0) and used for immunoblotting at a concentration of 2.9 μg/ml.

RNA amplification. In vitro reverse transcription was performed according to the manufacturer of SuperScript II reverse transcriptase (Invitrogen Life Technologies) in 20-μl reaction mixtures with 2 μg of total RNA as a template, extracted from cells and tissues with Trizol reagent (Invitrogen Life Technologies). The first PCR amplification of the template was performed with 1 μl of the 20-μl reverse transcription product in reaction buffer containing 1.5 mM $MgCl_2$ and 0.1 μM forward (5′-GGAGACTCAGTTCCGCAGAG-3′) and reverse (5′-TGGGACCACTGTAGTTGTGG-3′) primers that amplify the coding region spanning amino acids 2 to 57 of MAGE-11. PCRs were performed for 5 min at 95°C, followed by 35 cycles (each cycle consisting of 50 s at 95°C, 50 s at 55°C, and 50 s at 72°C), followed by 10 min at 72°C. A second PCR was performed using 2 μl of the initial PCR product as a template with the same primers and the amplification conditions. Due to a genomic intron, the resulting 168-zbp fragment cannot be obtained from genomic DNA.

Nucleotide sequence accession number. DNA and the protein sequence for full-length MAGE-11 were deposited under accession number AY747607 in GenBank.

RESULTS

Identification of MAGE-11 as an AR NH_2-terminal FXXLF motif interacting protein. We showed previously that the androgen-dependent AR N/C interaction between the AR NH_2-terminal ^{23}FQNLF^{27} sequence and AF2 in the ligand binding domain is required for optimal activation of androgen-responsive promoter-enhancer regions (18). The AR N/C interaction appears to promote selective gene activation through AF1 in the AR NH_2-terminal domain. On the other hand, the androgen-induced AR N/C interaction competitively inhibits SRC/p160 coactivator binding to AF2 (14). We therefore proposed that a putative coregulator may exist that could bind the AR NH_2-terminal FXXLF motif, relieve inhibition at AF2, and increase AR transactivation by the SRC/p160 coactivators.

We performed a yeast two-hybrid screen of a human testis library using the AR NH_2-terminal FXXLF motif region as bait. The strategy was based on our previous observations that screening with short α-helical regions from the intrinsically unstructured AR NH_2-terminal transcriptional activation domain is a useful approach to identify interacting proteins (13). Approximately 5×10^5 yeast library clones were screened with pGBT8-AR4-52 as bait, which contains the AR NH_2-terminal FXXLF motif sequence. We identified 119 positive clones that grew on synthetic medium lacking Leu, Trp, and His. Two of the clones were positive by β-galactosidase filter assays. One clone encoded RanBPM, a previously reported AR-interacting protein (36). However, interaction between RanBPM and AR was not diminished by mutation of the FXXLF motif, indicating that binding to AR was not FXXLF motif specific (data not shown). The second positive clone encoded the melanoma antigen gene family protein, MAGE-11. Binding of MAGE-11 to AR4-52 was abolished by an AR4-52-FXXAA mutant in a yeast two-hybrid assay (data not shown), suggesting a specific interaction between MAGE-11 and the AR FXXLF motif.

A BLAST search of the human genome database confirmed that the isolated clone was coded from the Xq28 gene locus of the MAGE gene family (23, 39) (Fig. 1A). The five exons predict a 1,837-nucleotide MAGE-11 mRNA. Four of the exons encode the 429-amino-acid full-length MAGE-11 protein. MAGE-11 has a calculated molecular mass of 48 kDa but, as we will show, an apparent molecular mass of 70 kDa on SDS gels. The cloning results confirm a previous report of the additional upstream coding regions for the 110 NH_2-terminal amino acids unique to MAGE-11 (23).

Specific interaction between MAGE-11 and the AR NH_2-terminal FXXLF motif. We made use of mammalian two-hybrid assays to demonstrate a dependence of MAGE-11 binding to AR on the AR FXXLF motif. The GAL DNA binding domain and VP16 transactivation domain fusion proteins were expressed that contained full-length MAGE-11 or a previously reported short form (24, 39) that corresponds to MAGE-11-112-429. GAL and VP fusion proteins were created to contain the ^{23}FQNLF^{27} amphipathic α-helical region within increasing lengths of the AR NH_2-terminal region (Fig. 1B). A GAL-responsive luciferase reporter vector was cotransfected into HepG2 cells, and assays were performed in the absence and presence of 10 nM R1881, a synthetic androgen.

In the absence of androgen, GAL-MAGE-11 and GAL-MAGE-11-112-429 interacted with VP-AR1-660 (Fig. 2A). The interaction depended on the AR FXXLF motif, since no interaction was observed with VP-AR1-660-FXXAA containing the ^{23}FQNAA^{27} mutation. We also observed strong inter-

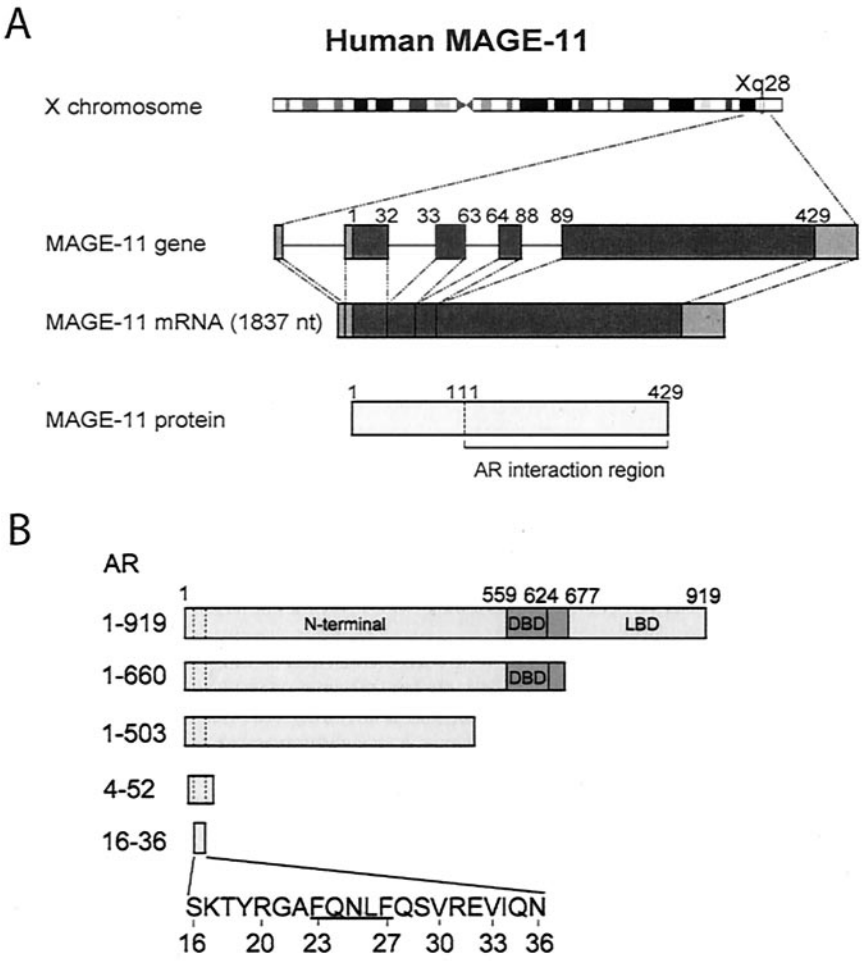

FIG. 1. Human MAGE-11 gene, mRNA, and protein, and AR NH_2-terminal fragments. (A) The MAGE-11 gene is carried on the long arm of the X chromosome at Xq28 and includes five exons that transcribe into a 1,837-nucleotide residue mRNA. The four-exon open reading frame (shown in black) translates to a 429-amino-acid-residue MAGE-11 protein (shown in white). The AR interaction region is based on data shown in Fig. 9. (B) AR NH_2-terminal fragments of full-length human AR1-919 were expressed as GAL and VP16 fusion proteins in two-hybrid assays. Each fragment contains the region spanning amino acids 16 to 36 with the FXXLF interaction motif sequence ^{23}FQNLF^{27} (underlined).

action between VP-MAGE-11 or VP-MAGE-11-112-429 with GAL-AR16-36, GAL-AR4-52, and GAL-AR1-503.

In the presence of androgen, we observed an FXXLF motif-dependent interaction between full-length AR and the same GAL-AR FXXLF motif peptides and GAL-MAGE-11 (Fig. 2B). The interaction of GAL-AR16-36 or GAL-AR4-52 with AR in the presence of androgen (Fig. 2B) reflects the androgen-dependent N/C interaction between the AR NH_2-terminal FXXLF motif in the GAL-AR fragment and AF2 in the ligand binding domain of full-length AR (17). Note that in this experimental design, luciferase activity in the two-hybrid assay requires androgen for the nuclear transport of full-length AR (20). This is in contrast to the androgen-independent interactions shown in Fig. 2A that made use of GAL4 and VP16 fusion proteins of AR NH_2-terminal fragments that lack the ligand binding domain and are in the nucleus independent of androgen (52). Expression of the fusion proteins was confirmed by immunoblot analysis (Fig. 3B and data not shown).

The results demonstrate that the same AR NH_2-terminal FXXLF motif region that mediates the androgen-dependent AR N/C interaction also interacted with MAGE-11. The data confirm the yeast two-hybrid results that MAGE-11 binding to AR depended on the AR FXXLF motif contained within a 21-amino-acid residue region of the AR NH_2-terminal domain.

Sequence requirements for FXXLF motif binding to MAGE-11. The flanking sequence requirements for the AR FXXLF motif to bind MAGE-11 and AF2 in AR were found to have similarities but also striking differences. Wild-type and mutant GAL-AR peptides were coexpressed in two-hybrid assays in HepG2 cells with full-length AR (Fig. 3A, left) and with VP-MAGE-11 (Fig. 3A, right) in the presence of a GAL-responsive luciferase reporter. In agreement with the data in Fig. 2A, interaction of GAL-AR16-36 with AR or VP-MAGE-11 was eliminated by the FXXAA mutation in GAL-AR16-36.

We tested several shorter fragments of the FXXLF motif region, since we showed previously that AR20-30 binds AF2 in AR more effectively than AR16-36. At that time, we speculated that R31 flanking FXXLF, which is deleted in AR20-30, undergoes electrostatic repulsion at the positive-charge cluster-containing charge clamp residue K720 (20). We found that

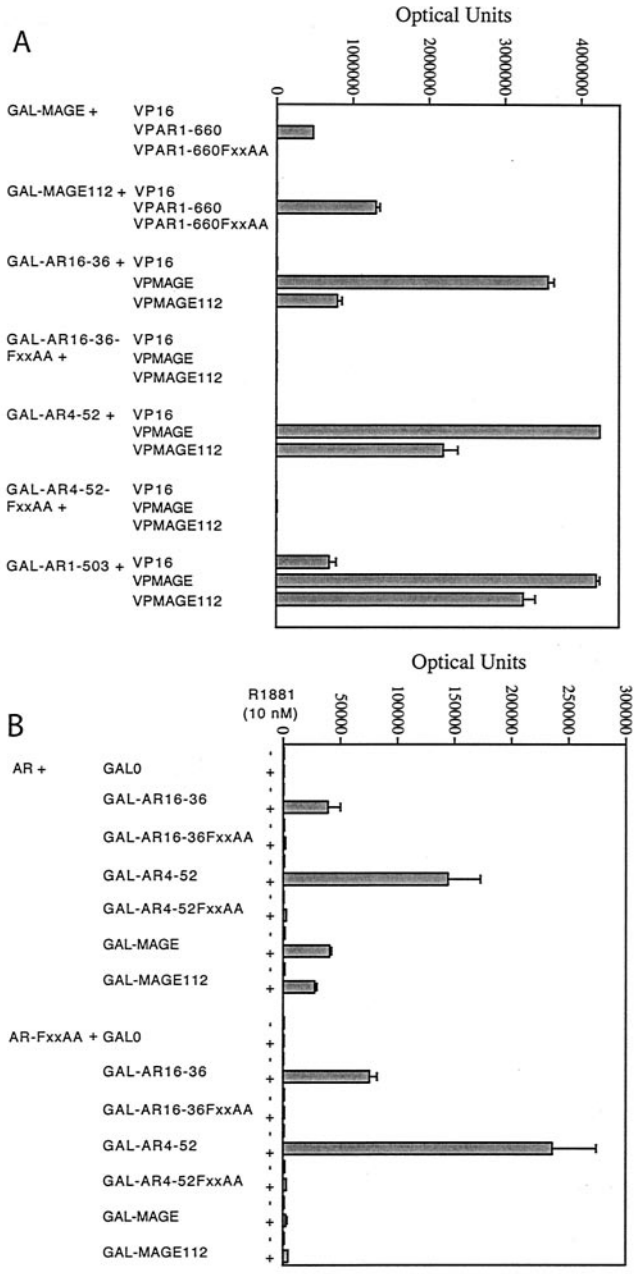

FIG. 2. FXXLF motif dependence of the AR and MAGE-11 interaction. Two-hybrid interaction assays were performed with HepG2 cells transfected with Effectene with 0.1 μg of 5XGAL4Luc3/well in 12-well plates with (A) 50-ng/well GAL-MAGE-11, GAL-MAGE-11-112-429 (GAL-MAGE112), or the indicated GAL-AR fusion proteins, with the VP16 empty vector control, wild-type or mutant VP-AR1-660, VP-MAGE-11, or VP-MAGE-11-112-429 (VP-MAGE112), and (B) 5 ng of pCMVhAR or pCMVhAR-FXXAA/well with 50 ng of the indicated GAL vectors/well. Cells were incubated for 24 h in the absence (A) or absence and presence (B) of 10 nM R1881. The FXXAA mutation is AR sequence ^{23}FQNLF^{27} changed to ^{23}FQNAA^{27}.

MAGE-11 did not bind GAL-AR20-30, GAL-AR20-36, or GAL-AR16-30, even though GAL-AR20-30 and GAL-AR16-30 (Fig. 3A, top) interacted to a greater extent with AR than does GAL-AR16-36, as previously reported (20).

We also noted a number of differences in the FXXLF motif-flanking sequence in GAL-AR16-36 required to bind AR and MAGE-11 (Fig. 3A, bottom). Mutations S29D, V30E, R31A, R31D, V33E, and I34A in GAL-AR16-36 each increased binding to AR AF2, whereas these mutations eliminated binding to MAGE-11. T18A and E32A increased binding of GAL-AR16-36 to both MAGE-11 and AR. S29A increased MAGE-11 binding but decreased AR binding; S16D, K17A, T18D, and V30A each increased MAGE-11 binding, with little effect on AR binding. S16A increased binding to AR but not MAGE-11, and R20A and R20D were detrimental to both interactions. Expression levels of the GAL-AR fusion proteins varied somewhat, but the differences did not correlate with the observed interactions (Fig. 3).

The data show that the flanking sequence of the AR FXXLF motif has different requirements for binding MAGE-11 and the AR AF2 site. Optimal binding to MAGE-11 required the extended 21-amino-acid FXXLF α-helical region, which is nearly twice the length of the minimal 11-amino-acid FXXLF region that optimally bound AF2 in the AR N/C interaction (Fig. 3C). The data also suggest that the MAGE-11 binding site differs substantially from AF2 in the AR ligand binding domain (15, 22).

Specificity of MAGE-11 binding to the AR FXXLF motif. We found that MAGE-11 binding to the AR NH_2-terminal FXXLF motif is highly specific. FXXLF motif sequences previously reported in several putative AR coregulators and LXXLL motif regions from the SRC/p160 coactivators did not interact with MAGE-11 in two-hybrid assays performed with HepG2 cells. Included in the comparison were ARA70/RFG (49, 50), ARA54 (25), and ARA55/Hic5 (7, 48), whose FXXLF motifs are required for the androgen-dependent interaction between these coregulators and the AR AF2 site (19). No interaction was found between VP-MAGE-11 and GAL-FXXLF fusion proteins containing ARA70-321-340, ARA70-321-499, ARA54-447-465, ARA54-361-474, ARA55-314-333, ARA55-427-444, or ARA55-251-444 (data not shown). Little or no interaction was detected between GAL-MAGE-11 and the LXXLL motif regions from the SRC/p160 coactivator family. These included VP-LXXLL motif fusion proteins containing SRC1-1139-1441, SRC1-568-1441, TIF2-624-1287, TRAM1-604-1297, and p300-1-133 (data not shown).

The results indicate a specific interaction between MAGE-11 and the AR FXXLF motif. The lack of an interaction between MAGE-11 and other FXXLF motifs from several potentially relevant AR coregulators supports our findings that residues within the extended α-helical region flanking FXXLF establish specificity for MAGE-11binding.

In vitro interaction between AR and MAGE-11. A direct interaction between AR and MAGE-11 was supported by in vitro GST affinity matrix binding assays. An interaction between GST-AR4-52 and ^{35}S-labeled MAGE-11 was observed in the absence of androgen, which was eliminated with GST-AR4-52FXXAA (Fig. 4). Similarly, an FXXLF motif-dependent interaction was observed in the presence of DHT between GST-AR4-52 and ^{35}S-labeled AR624-919 containing the AR ligand binding domain. ^{35}S-labeled MAGE-11 migrates a 70 kDa, and ^{35}S-labeled AR ligand binding domain migrates a 41 kDa.

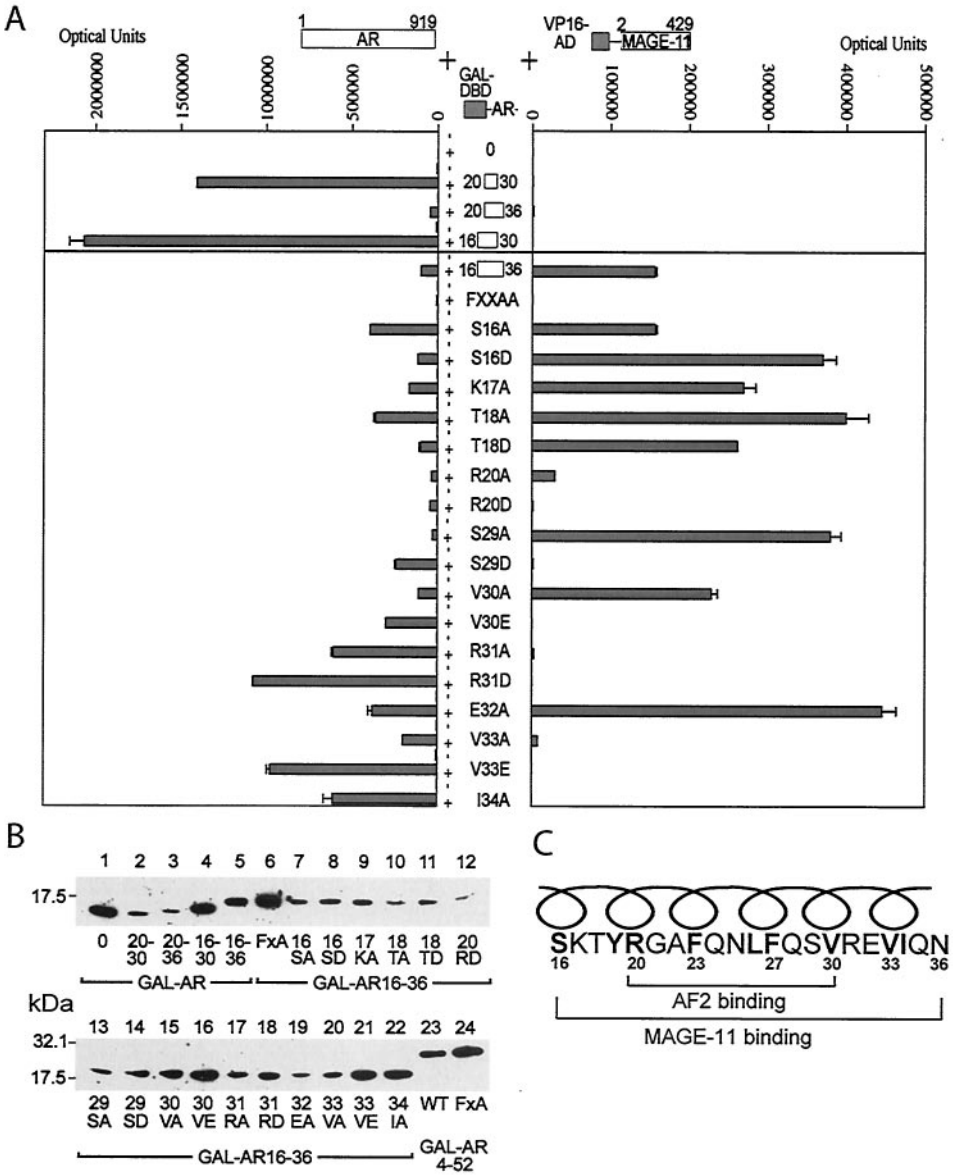

FIG. 3. Differences in flanking sequence requirements for FXXLF motif binding to AR and MAGE-11. (A) Two-hybrid interaction assays were performed with HepG2 cells as described in the legend to Fig. 2, except that 10 ng of pCMVhAR (AR1-919)/well (left) or 50 ng of VP-MAGE-11/well (right) with 50 ng of the indicated GAL-AR vectors/well was used. GAL-AR16-36FXXAA indicates the ^{23}FQNAA^{27} mutation. Each of the indicated amino acid changes was introduced into the GAL-DNA binding domain fusion vector GAL-AR16-36. (B) Immunoblots of GAL-AR peptides were performed using extracts from COS cells (2×10^6/10-cm dish) transfected with 10 μg of GAL-AR peptide DNA with DEAE-dextran. Cells were treated with 1 μM MG132 (Sigma), a proteasome inhibitor, 24 and 1 h prior to harvest. The GAL4 DNA binding domain antibody (1:500 dilution; Santa Cruz) was used to probe 25 μg of total protein in each lane. (C) Diagram of the predicted amphipathic α-helical AR NH_2-terminal FXXLF motif regions required to interact with AF2 in the AR ligand binding domain and MAGE-11. The predicted ideal α-helix may be disrupted to the left at G21. Hydrophobic residues F23, L26, and F27 contact the hydrophobic surface at AR AF2 in the N/C interaction (15). These residues plus V30, V33, and I34 in the extended helix are predicted to contact the binding surface of MAGE-11.

Coimmunoprecipitation of AR, MAGE-11 and TIF2. We found that coimmunoprecipitation of AR and MAGE-11 is selectively modulated by ligand binding and AR subcellular localization (Fig. 5A and B, top). AR transiently expressed in COS cells coimmunoprecipitates with Flag-MAGE-11 with a Flag antibody when assayed in the absence of DHT (Fig. 5A, lane 4). However, the interaction between AR and MAGE-11 was barely detectable in the presence of 10 nM DHT (Fig. 5A, lane 5, and Fig. 5B, lane 9). In the absence of DHT, the interaction between AR and MAGE-11 was greatly diminished by the AR-FXXAA mutant (Fig. 5A, lane 8). AR was coimmunoprecipitated with the Flag antibody only when Flag-MAGE-11 was expressed, suggesting the absence of nonspecific binding (Fig. 5A, top, lanes 2, 3, 6, and 7).

We tested a previously described AR nuclear transport mutant, ARm4, that contains mutations in the AR bipartite nu-

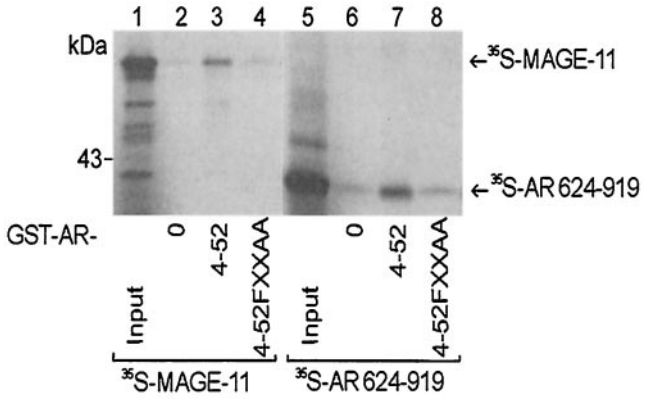

FIG. 4. In vitro binding of AR and MAGE-11. GST affinity matrix assays were performed with GST-AR NH_2-terminal fusion peptides and ^{35}S-labeled MAGE-11 expressed from pSG5-MAGE-11 (left) and ^{35}S-labeled AR624-919 expressed from pcDNA3HA-AR624-919 containing the AR ligand binding domain (right). GST empty vector pGEX-4T-1 (GST-AR-0), GST-AR4-52, and GST-AR4-52FXXAA were expressed in *E. coli* and incubated in the presence of ^{35}S-labeled MAGE-11 (lanes 2 to 4), and ^{35}S-labeled AR624-919 in the presence of 0.2 μM DHT (lanes 6 to 8). Input lanes contained 5% of the total reaction mixture for MAGE-11 (lane 1) and 10% of the reaction mixture for AR624-919 (lane 5). ^{35}S-labeled MAGE-11 (70 kDa) and AR ligand binding domain fragment 624–919 (41 kDa) are indicated by arrows.

clear transport signal. ARm4 retains high-affinity androgen binding but does not translocate to the nucleus in the presence of androgen (52). In contrast to wild-type AR which is nuclear in the presence of DHT, this constitutively cytoplasmic mutant coimmunoprecipitated with MAGE-11 in the absence and presence of DHT (Fig. 5A, lanes 12 and 13).

We also found that the stable association between AR and MAGE-11 persists in the presence of ligands that promote AR nuclear localization but are AR antagonists or poor agonists (26). These included 50 nM estradiol, 50 nM progesterone, and 1 μM hydroxyflutamide (Fig. 5B, lanes 10, 11, and 14). However, like DHT (10 nM), the stable association between AR and MAGE-11 was reduced in the presence of 50 nM androstenedione and 50 nM medroxyprogesterone acetate (MPA) (Fig. 5B, lanes 12 and 13). Coimmunoprecipitation of AR with Flag-MAGE-11 was indicative of a specific interaction, since AR was not detected when MAGE-11 was not expressed (Fig. 5B, lanes 1 to 7).

The coimmunoprecipitation results suggest that MAGE-11 stably interacts in the cytoplasm with the ligand-free AR and in the nucleus when AR is bound to an antagonist or poor agonist. In the presence of stronger agonists, the AR and MAGE-11 interaction becomes more transient. The effectiveness of androstenedione and MPA in disrupting the interaction with MAGE-11 was attributed in part to the high ligand concentrations. The persistent interaction of MAGE-11 with the constitutively cytoplasmic AR raised the possibility that both agonist binding and AR nuclear transport are required to destabilize the AR and MAGE-11 interaction.

To investigate whether MAGE-11 influences the interaction between AR and the p160 coactivator TIF2 and whether MAGE-11, AR, and TIF2 form an intracellular complex, we performed coimmunoprecipitation studies using Flag-AR (Fig. 5C). The 70-kDa MAGE-11 protein was detected with an antibody raised against the MAGE-11 NH_2-terminal peptide C^{13}SPASIKRKKKREDS^{26}, a sequence specific to MAGE-11. We noted an increase in TIF2 levels in cell extracts with the coexpression of AR in the presence of 10 nM DHT. In the Flag antibody immunoprecipitates, an association between AR and TIF2 was evident in the presence of DHT (Fig. 5C, lanes 3 and 4). We found that the AR and TIF2 interaction increased with coexpression of MAGE-11 in the absence and presence of androgen (Fig. 5C, lanes 7 and 8). Neither MAGE-11 nor TIF2 was detected in the immunoprecipitates in the absence of coexpressed Flag-AR (Fig. 5C, lanes 9 and 10). The results suggest that binding of MAGE-11 to AR increases the interaction between AR and TIF2.

MAGE-11 influences AR steady-state levels. Immunoblots of cell lysates from the immunoprecipitation studies shown in Fig. 5 show the expected androgen-induced increase in AR in the presence of 10 nM DHT. AR stabilization by DHT results from the AR N/C interaction (14), as evidenced by the lack of an increase with AR-FXXAA (Fig. 5A, lanes 6 and 7). We found that coexpression of MAGE-11 interferes with DHT-induced AR stabilization, since AR levels declined (Fig. 5B, lanes 8 and 9). MAGE-11 levels also decreased in the presence of 10 nM DHT, in association with the reduced interaction between AR and MAGE-11 (Fig. 5A, lanes 4 and 5). However, no decrease in MAGE-11 was observed in the presence of DHT and the nuclear transport mutant, ARm4 (Fig. 5A, lanes 12 and 13). A decrease in MAGE-11 was also observed with AR-FXXAA, suggesting an effect of MAGE-11 independent of the AR FXXLF motif.

The effect of MAGE-11 on steady-state levels of AR transiently expressed in COS cells was further investigated at increasing concentrations of androgen. DHT concentrations of 2 and 10 nM are below and near saturating levels, respectively, based on ^{3}H-labeled R1881 binding and AR nuclear transport studies in COS cells transiently expressing AR, and 50 nM DHT is saturating (references 17 and 52 and unpublished results). Coexpression of MAGE-11 in the presence of 2 and 10 nM DHT reduced AR levels in association with decreased levels of MAGE-11 (Fig. 6A, lanes 1 to 7). The level of AR-FXXAA also decreased with MAGE-11 expression but to a lesser extent. This result again raised the possibility that MAGE-11 has effects on AR that are FXXLF motif independent. In contrast, addition of 50 nM DHT apparently overcame the destabilizing effect of MAGE-11 on AR but not AR-FXXAA, and androgen-induced AR stabilization was restored (Fig. 6A, lanes 8 and 16). The AR-FXXAA mutant lacks an N/C interaction and was not stabilized by androgen (14). In [^{35}S]methionine-labeled AR pulse-chase experiments performed with COS cells in the presence of 10 nM DHT, the destabilizing effect of MAGE-11 on AR degradation could not be detected over the stabilizing influence of DHT on AR ($t_{1/2}$ = 4.7 ± 0.5 h) and the AR-FXXAA mutant ($t_{1/2}$ = 3.3 ± 0.4 h).

Paradoxically, we found that in the absence of androgen, MAGE-11 increases AR levels (Fig. 6A, lanes 1 and 5). Pulse-chase studies with [^{35}S]methionine-labeled AR in COS cells in the absence of DHT confirmed the half-time of AR degradation ($t_{1/2}$ = 1.3 ± 0.1 h) increased twofold with MAGE-11 expression ($t_{1/2}$ = 2.4 ± 0.3 h). Although we observed some

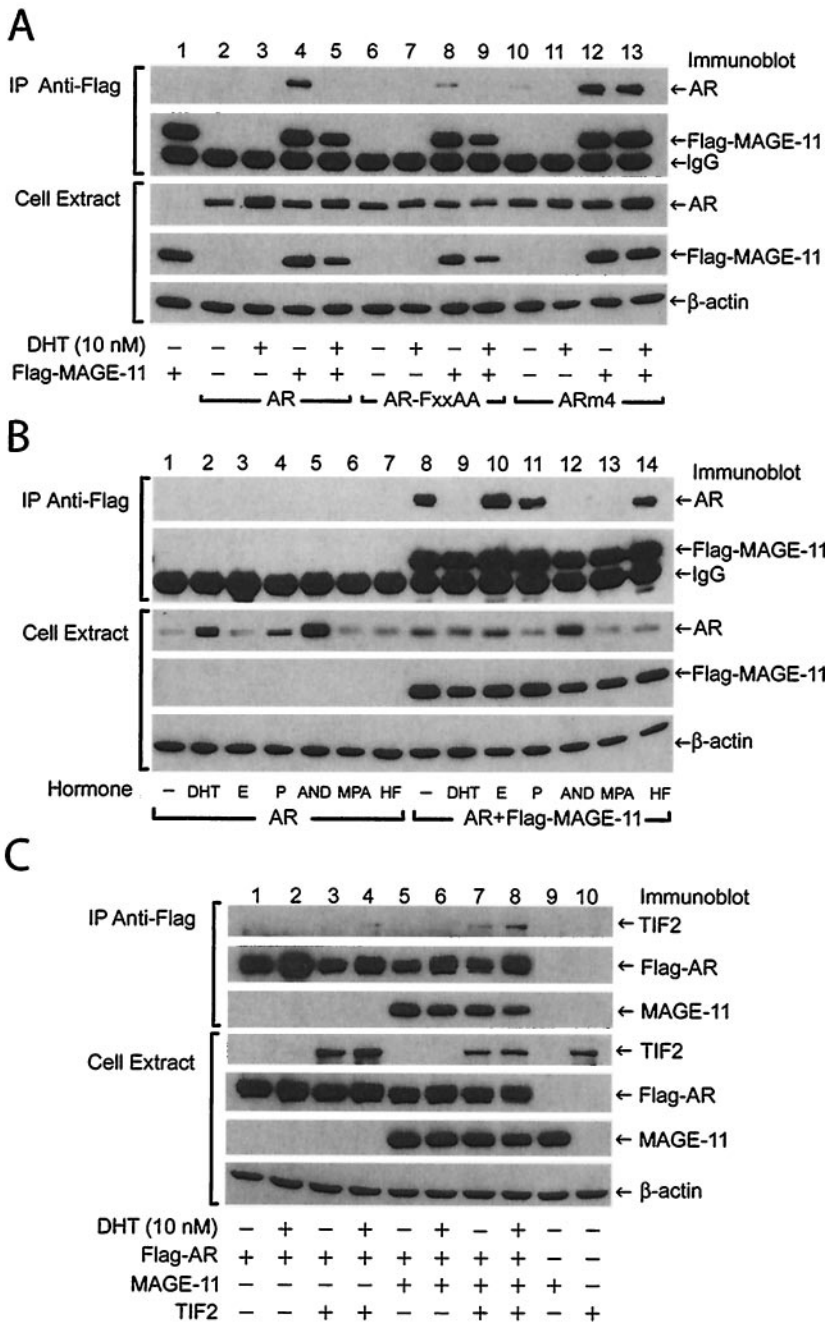

FIG. 5. Coimmunoprecipitation of AR, MAGE-11, and TIF2. (A and B) COS cells were transfected with 2 μg of pCMVhAR, pCMVhAR-FXXAA, and pCMVhARm4/10-cm dish in the absence and presence of 5 μg of pCMV-Flag-MAGE-11 with DEAE-dextran. Cells were incubated for 24 h in media containing 10% charcoal-stripped serum (Gemini) in the absence and presence of 10 nM DHT, 50 nM estradiol (E), 50 nM progesterone (P), 50 nM androstenedione (AND), 50 nM MPA, or 1 μM hydroxyflutamide (HF) as indicated. Cells were extracted in 0.5% NP-40 lysis buffer and immunoprecipitated with anti-Flag antibody as described in Materials and Methods. Immunoprecipitated proteins (A and B, top two panels) and a portion of the whole cell protein lysates (A and B, lower three panels) (10 μg/lane) were separated by electrophoresis on 10% acrylamide gels containing SDS. Immunoblots of immunoprecipitated proteins and cell extracts (10 μg) were exposed to X-ray film for 10 s. (C) COS cells were transfected with 2 μg of pCMV-Flag-hAR, 4 μg of pSG5-TIF2, and 2 μg of pSG5-MAGE-11; treated with and without 10 nM DHT; and extracted as above. Anti-Flag antibody immunoprecipitates of Flag-AR (top three panels) and whole cell extracts (bottom four panels; 20 μg protein/lane) were separated by electrophoresis on 10% acrylamide gels containing SDS. Immunoblots of the immunoprecipitates were exposed to X-ray film for 2 s for Flag-AR and MAGE-11 protein and 4 h for TIF2, and the cell lysates were exposed for 5 s for TIF2, 2 s for Flag-AR, and 1 s for MAGE-11 and β-actin. Immunoblots were probed as indicated with AR32 rabbit polyclonal antibody for AR (A and B) and Flag-AR (C), anti-Flag mouse monoclonal antibody for Flag-MAGE-11 (A and B), anti-TIF2 antibody (BD Bioscience) (C), peptide affinity-purified rabbit polyclonal anti-MAGE-11 antibody for MAGE-11 (C), and anti-β-actin antibody (A to C). The immunoblots are representative of more than three independent experiments.

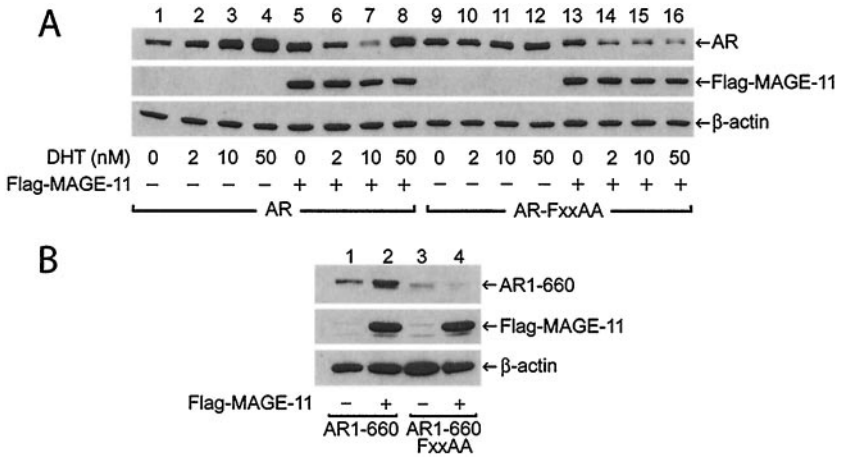

FIG. 6. Effect of MAGE-11 on AR steady-state levels. (A) Immunoblots are shown of whole-cell protein lysates of COS cells transfected with 2 μg of pCMVhAR or pCMVhAR-FXXAA without and with 5 μg of pCMV-Flag-MAGE-11 in the absence and presence of 2, 10, and 50 nM DHT. Whole-cell extracts (10 μg) were analyzed with the antibodies indicated on the right. The blot was exposed to X-ray film for 50 s. (B) Immunoblots of pCMVhAR1-660 and pCMVhAR1-660-FXXAA (2 μg) expressed in COS cells (2×10^6 cells/10-cm dish) using DEAE-dextran in the absence and presence of 5 μg of pCMV-Flag-MAGE-11 are shown. Each lane contains 15 μg of total protein, and the blots were exposed to X-ray film for 3 s.

increase in AR-FXXAA in the absence of androgen compared to wild-type AR as previously reported (14), the level of AR-FXXAA did not increase with MAGE-11 expression (Fig. 6A, lanes 9 and 13). In agreement with these results, the half-time of AR-FXXAA degradation ($t_{1/2} = 1.5 \pm 0.1$ h) in the absence of androgen was less affected by MAGE-11 ($t_{1/2} = 1.8 \pm 0.1$ h). MAGE-11 also increased the level of AR1-660, a constitutively active AR NH_2-terminal fragment that lacks the ligand binding domain, but not the level of AR1-660-FXXAA (Fig. 6B).

The results support a stable and specific interaction between MAGE-11 and AR in the absence of androgen that increases AR steady-state levels. The stabilizing effect of MAGE-11 in the absence of DHT is mediated at least in part through its interaction at the AR FXXLF site. In the presence of androgen, the interaction between AR and MAGE-11 is more transient and AR steady-state levels decline. The decrease in AR-FXXAA levels with MAGE-11 expression in the presence of androgen suggests that FXXLF motif-independent mechanisms contribute to the effects of MAGE-11 on AR.

AR and MAGE-11 colocalize in the cytoplasm and nucleus. Immunocytochemical staining of AR and MAGE-11 was determined to further establish their intracellular association. Immunostaining of transiently expressed AR in COS cells resulted in a typical cytoplasmic staining pattern in the absence of androgen and nuclear staining in the presence of DHT (Fig. 7A and B) (52). Flag-tagged MAGE-11 localized predominantly in nuclei with some cytoplasmic staining (Fig. 7C). We found that Flag-MAGE-11 and AR colocalize in the cytoplasm in the absence of androgen with persistent nuclear staining of MAGE-11 (Fig. 7D to F). With the addition of androgen, AR and MAGE-11 colocalized to the nucleus (Fig. 7G to I). Cytoplasmic colocalization of MAGE-11 and AR was also seen in the presence of 10 or 50 nM estradiol, and we observed both cytoplasmic and nuclear AR with 10 and 50 progesterone or 50 nM and 1 μM hydroxyflutamide. AR was nuclear with 10 and 50 nM androstenedione or MPA (data not shown).

Transient expression of Flag-MAGE-11 in human foreskin fibroblasts showed colocalization of MAGE-11 with endogenous AR in nuclei in the presence of androgen (Fig. 7J to L). Similarly, MAGE-11 colocalized with endogenous AR in human prostate cancer cell lines, LNCaP (Fig. 7M), CWR22-RV1 (Fig. 7N), and LAPC4 (Fig. 7O) assayed in the presence of androgen. Persistent cytoplasmic MAGE-11 was also evident in both fibroblasts and prostate cancer cells.

In contrast, the addition of androgen changed the immunostaining pattern of Flag-MAGE-11 and the nuclear transport mutant ARm4 from typical cytoplasmic staining (Fig. 8A to C) to colocalization in prominent cytoplasmic spots (Fig. 8D to F). For DNA binding mutant AR-C576A, addition of DHT changed cytoplasmic staining (Fig. 8G to I) to striking colocalization in subnuclear bodies (Fig. 8J to L). The results support an intracellular interaction between AR and MAGE-11 in the

FIG. 7. Immunocytochemistry of AR and MAGE-11. Cells were transiently transfected with pCMV-Flag-MAGE-11 or pCMVhAR alone or together with Effectene. Transiently expressed AR (A, B, and D to I) and endogenous AR (J to O) are represented by green fluorescence and were detected with rabbit anti-AR polyclonal antibody ab3510 (Abcam, Inc.). Transiently expressed Flag-MAGE-11 (C to O), represented by red fluorescence, was detected with anti-Flag M2 mouse monoclonal antibody. Yellow is indicative of AR and MAGE-11 colocalization. Representative illustrations are shown for pCMVhAR in COS cells without DHT (A), pCMVhAR in COS cells without DHT (B), pCMV-Flag-MAGE-11 in COS cells without DHT (C), pCMVhAR and pCMV-Flag-MAGE-11 in COS cells without DHT (D to F), and pCMVhAR and pCMV-Flag-MAGE-11 in COS cells with 50 nM DHT (G to I). pCMV-Flag-MAGE-11 was transfected alone into human foreskin fibroblasts (J to L), and human prostate cancer cell lines LNCaP (M), CWR22-RV1 (N), and LAPC4 (O), each incubated with 10 nM DHT. Original magnification, ×63.

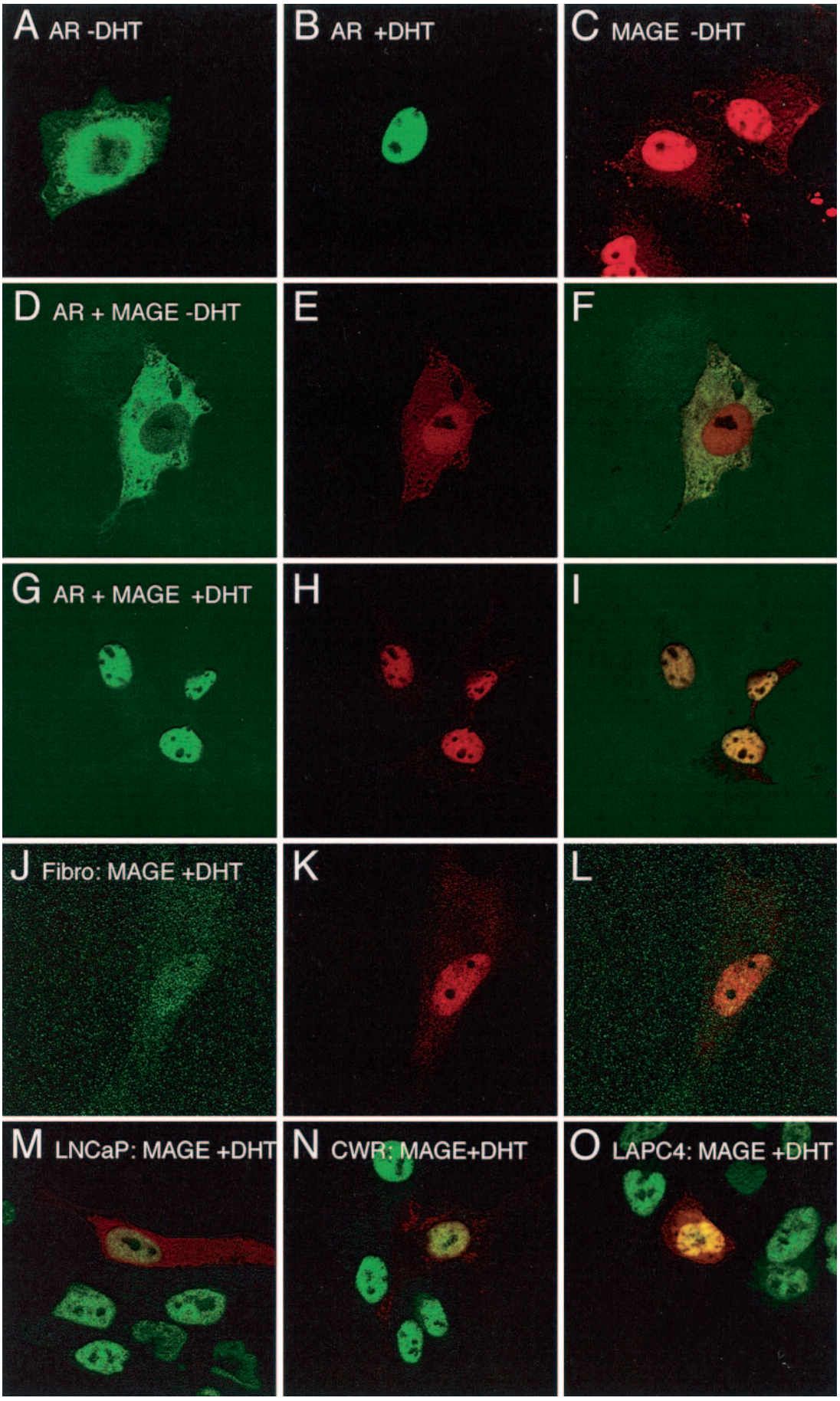
A AR -DHT
B AR +DHT
C MAGE -DHT
D AR + MAGE -DHT
E
F
G AR + MAGE +DHT
H
I
J Fibro: MAGE +DHT
K
L
M LNCaP: MAGE +DHT
N CWR: MAGE+DHT
O LAPC4: MAGE +DHT

cytoplasm in the absence of androgen and in the nucleus in the presence of androgen.

Inherent transcriptional activity and FXXLF-interacting domain of MAGE-11. Expression of GAL-MAGE-11 fusion proteins in mammalian two-hybrid assays demonstrated that MAGE-11 lacks a major intrinsic transactivation domain. Of the fusion proteins created to span the MAGE-11 sequence, only GAL-MAGE-11-2-252 had a low level of transcriptional activity (Fig. 9, top).

We also found that like AR, MAGE-11 binds the AR NH_2-terminal FXXLF motif through its carboxyl-terminal region (Fig. 9, bottom). GAL-MAGE-11-2-429 and GAL-MAGE-11-112-429 interacted to a similar extent with VP-AR1-660, which contains the AR FXXLF motif. Both of these larger MAGE-11 fragments interacted to a greater extent than GAL-MAGE-11-222-429. Shorter carboxyl-terminal fragments of MAGE-11 did not interact with AR. We also found that a MAGE-11 LXXLL motif sequence ^{229}LVHLL^{233} interacted only weakly with AR (data not shown). Thus, the carboxyl-terminal 112 to 429 residues of MAGE-11 represent the AR-interacting domain (Fig. 1A).

Competition for the N/C interaction. We performed two-hybrid assays and ligand dissociation rate studies to demonstrate that binding of MAGE-11 to the AR NH_2-terminal FXXLF motif competes for the androgen-induced N/C interaction. Using the assay that first demonstrated the AR N/C interaction (30), we found that coexpression of MAGE-11 inhibited the interaction between VP-AR1-660 and GAL-AR624-919 in the presence of androgen (Fig. 10A).

In a recent study, we showed that GAL-AR4-52 and GAL-AR20-30 compete for the AR N/C interaction by binding AF2 in AR (20). In this assay, the N/C interaction of full-length AR itself is not directly measured. Luciferase activity results from the interaction between the GAL-FXXLF peptide and AR that contains the strong AF1 NH_2-terminal transactivation domain. MAGE-11, on the other hand, lacks a major activation domain (Fig. 9). We found that coexpression of MAGE-11 inhibited the interaction between AR and GAL-AR4-52. We observed similar but slightly less inhibition of AR-FXXAA by MAGE-11. The decrease in luciferase activity appeared to be attributable largely to MAGE-11 binding to GAL-AR4-52. Increased exposure of AF2 resulting from the AR-FXXAA mutation would be expected to increase binding of GAL-AR4-52 to AF2 (14), which could account for the reduced inhibition of AR-FXXAA by MAGE-11.

To investigate this further, we tested GAL-AR20-30, since this short FXXLF motif peptide strongly engages the AR AF2 site indicative of the N/C interaction but does not bind MAGE-11 (Fig. 3). In this assay, the effect of MAGE-11 was mediated only by binding the NH_2-terminal FXXLF motif of full-length AR. We found that MAGE-11 increased the interaction between GAL-AR20-30 and AR (Fig. 10A). When AR-FXXAA was tested, binding of GAL-AR20-30 increased and was less dependent on MAGE-11. The results suggest that binding of MAGE-11 to the AR NH_2-terminal FXXLF motif competes for the AR N/C interaction and exposes AF2 to increased binding, in this case, of GAL-AR20-30.

Competition by MAGE-11 for the agonist-induced AR N/C interaction was also evident from the dissociation rate of bound androgen. These studies were based on previous observations that the N/C interaction slows the dissociation rate of bound androgen (14, 17, 51). COS cells expressing AR in the absence and presence of MAGE-11 were incubated with 5 nM [^{3}H]R1881. The half-time ($t_{1/2}$) of [^{3}H]R1881 dissociation from AR ($t_{1/2}$ = 109 ± 11 min) decreased with coexpression of MAGE-11 ($t_{1/2}$ = 71 ± 6 min) or MAGE-11-111-429 ($t_{1/2}$ = 71 ± 7 min). In contrast, dissociation of [^{3}H]R1881 from AR-FXXAA ($t_{1/2}$ = 40 ± 5 min) was unaffected by coexpression of MAGE-11 ($t_{1/2}$ = 40 ± 4 min) or MAGE-11-111-429 ($t_{1/2}$ = 44 ± 3 min).

The data provide evidence that MAGE-11 binding to the AR NH_2-terminal FXXLF motif competes for the AR N/C interaction and exposes the AF2 site in the ligand binding domain. Increased dissociation of androgen from the ligand binding pocket is indicative of this competitive interaction (14, 17, 51).

Effect of MAGE-11 on AR functional activity. To further address the possibility that binding of MAGE-11 to the AR NH_2-terminal FXXLF increases the accessibility of AF2, we determined the effect of MAGE-11 on AR transactivation in the absence and presence of increased SRC/p160 coactivator expression. We found that MAGE-11 increased AR transactivation of a PSA-Luc reporter to an extent similar to that seen with the coexpression of TIF2 and TRAM1 (Fig. 10B). Furthermore, the effects of MAGE-11 and the SRC/p160 coactivators on AR transactivation appeared to be synergistic. We also observed a small, biphasic increase in ligand-independent AR transactivation with increasing MAGE-11 expression that contributed to a persistent effect of MAGE-11 on the transcriptional activity of AR-FXXAA (Fig. 11A). Transactivation by AR-FXXAA in the absence of MAGE-11 was almost undetectable (Fig. 11A) due to the dependence of the PSA-Luc reporter activation on the AR N/C interaction, a dependence that is overcome by increased expression of the SRC/p160 coactivators (18). The small but noticeable increase in AR transactivation with MAGE-11 expression in the absence of androgen raised the possibility that MAGE-11 can influence transcriptional activity of the ligand free AR. The dose dependent increase in AR-FXXAA activity with MAGE-11 expression suggested that the transcriptional effects of MAGE-11 are not entirely FXXLF motif dependent.

To explore this further, the specificity of the stimulatory effects of MAGE-11 was tested with GR and AR-GR chimeras and the PSA-Luc reporter (Fig. 11B). The transcriptional activity of wild-type GR was only moderately increased with the coexpression of MAGE-11. In contrast, the AR-GR chimera AR1-132-GR132-777 (GR-FXXLF), which contains the AR NH_2-terminal FXXLF motif region, showed a striking increase in activity with the coexpression of MAGE-11. The increase in activity depended on the FXXLF motif, since it was not observed with a GR-FXXAA mutant.

The data suggest that the AR NH_2-terminal FXXLF motif region is sufficient to mediate the strong stimulatory effect of MAGE-11. However, the effect of MAGE-11 was not entirely specific to the AR FXXLF motif, since we also observed moderate increases in GR and PR-B activity on the PSA and mouse mammary tumor virus (MMTV)-Luc reporter vectors with higher expression levels of MAGE-11 (Fig. 11B and data not shown). MAGE-11 also increased AR transactivation of the MMTV-Luc and probasin promoters (Fig. 11C). However,

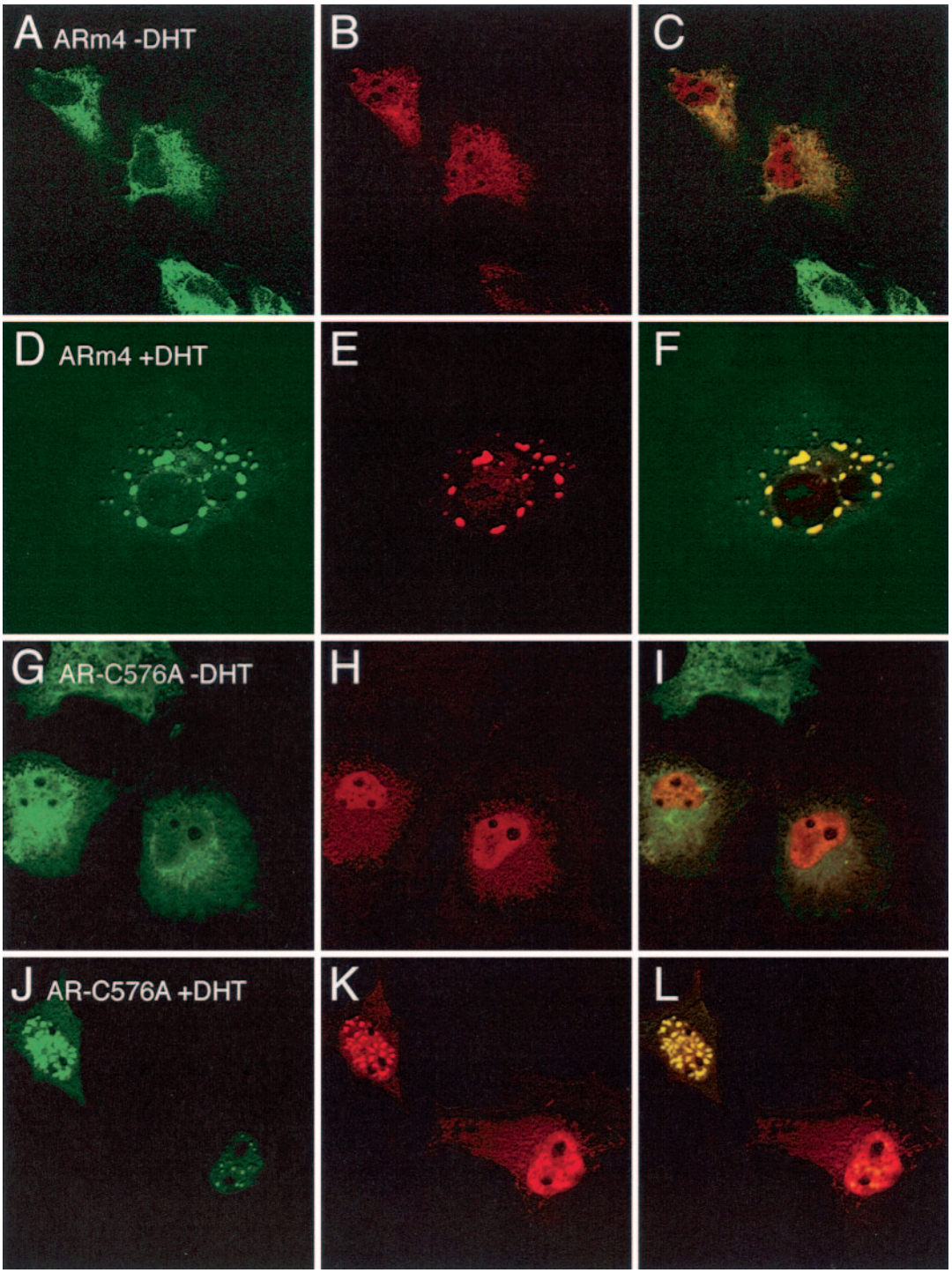

FIG. 8. Immunocytochemistry of AR mutants and MAGE-11. COS cells were transiently transfected with pCMV-Flag-MAGE-11 together with nuclear transport mutant pCMVhAR-R617M-K618M-K632M-R633M (ARm4) in the absence (A to C) and presence (D to F) of 50 nM DHT or with DNA binding domain mutant pCMVhAR-C576A in the absence (G to I) or presence (J to L) of 50 nM DHT. AR (green fluorescence), Flag-MAGE-11 (red fluorescence), and the merge (yellow fluorescence) are shown. Original magnification, ×63.

MAGE-11 did not increase the activity of the constitutive viral reporters, pSV2-Luc, pSG5-Luc, and CMV-Luc (data not shown), suggesting that the effects of MAGE-11 on transcriptional activation are receptor mediated.

MAGE-11 also strongly increased the constitutive transcriptional activity of AR1-660, an AR NH_2-terminal and DNA binding domain fragment that has only weak activity on the PSA-Luc reporter in the absence of MAGE-11 (Fig. 11D). The striking increase in AR1-660 transcriptional activity in response to MAGE-11 was FXXLF motif dependent, since the

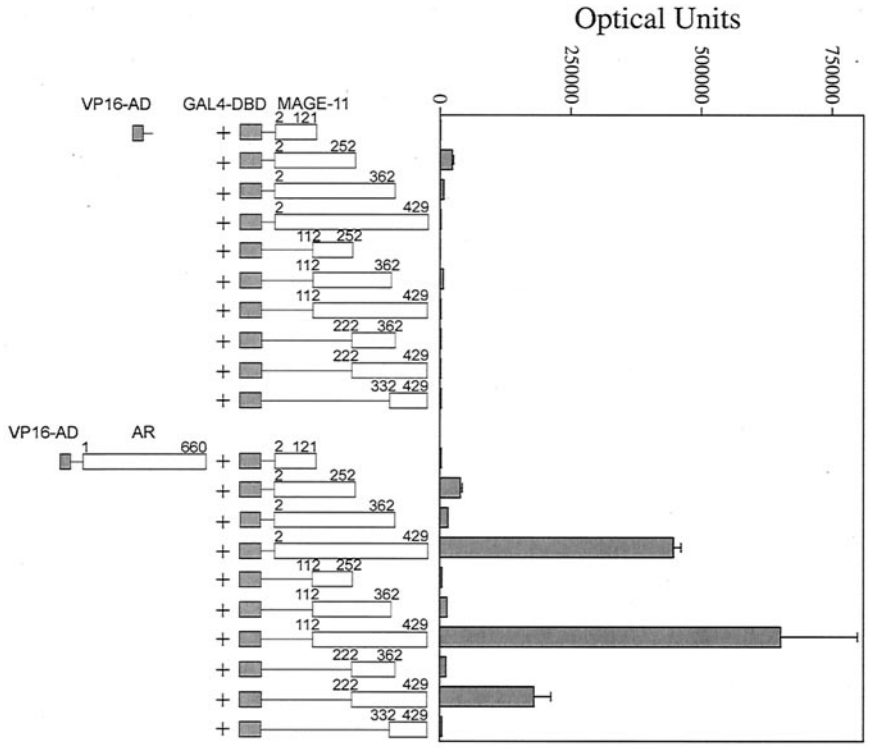

FIG. 9. Inherent transcriptional activity of MAGE-11 and the interaction domain for the AR FXXLF motif. Two-hybrid interaction assays were performed in HepG2 cells by transient transfection in 12-well plates with Effectene with 0.1 μg of 5XGAL4Luc3 reporter and 50 ng of the indicated GAL-MAGE-11 fusion protein vectors with either VP16 activation domain empty vector control (50 ng/well) (VP16-AD, top) or VP-AR1-660 (50 ng/well) (bottom). Luciferase activity and error were determined in the absence of hormone.

activity of the AR1-660-FXXAA mutant only marginally increased with MAGE-11 expression. Similar small increases were seen with GR1-550 and PRB-1-688, which are corresponding NH_2-terminal and DNA binding domain fragments but lack an FXXLF motif. However, higher amounts of MAGE-11 expression vector DNA (2 μg) increased the activity of AR-FXXAA and the other receptor NH_2-terminal fragments (data not shown). The data suggest that the presence of the AR FXXLF motif increases the sensitivity of AR to the stimulatory effects of MAGE-11.

Taken together, MAGE-11 appears to increase AR transactivation through mechanisms that include, but may not be limited to, its interaction with the FXXLF motif. The data support that MAGE-11 binding to the AR NH_2-terminal FXXLF motif exposes AF2 in the ligand binding domain to activation by the SRC/p160 family of coactivators. The data also show a striking stimulatory effect of MAGE-11 on the AR NH_2-terminal region that is independent of AF2.

In vivo expression of MAGE-11. Northern blot analysis of RNA from several prostate cancer cell lines and human testis failed to reveal MAGE-11 mRNA (data not shown), suggesting that MAGE-11 expression is low. RT-PCR amplification of total RNA revealed the 168-bp fragment indicative of MAGE-11 mRNA in LNCaP, LNCaP-C4-2, CWR-R1, CWR22-RV1, and LAPC4 prostate cancer cell lines (Fig. 12A, top). However, detection of MAGE-11 mRNA in PC-3 and DU-145, two prostate cancer cell lines that do not express AR, required a second amplification using the initial PCR product as template (Fig. 12A, bottom). MAGE-11 mRNA was also detected in HeLa cells, a HeLaAR1C cell line stably expressing Flag-AR, was weakly detected in a human foreskin fibroblast cell line, HepG2, and COS cells, but was not detected in CV1 cells. MAGE-11 mRNA was also expressed in samples from testis, ovary, prostate, cancerous prostate, breast, and adrenal tissue, but was weak to undetectable in liver and lung tissue (Fig. 12B).

Endogenous MAGE-11 protein was evident on immunoblots of extracts from several cancer cell lines cultured in the absence of androgen and probed with the MAGE-11 antibody raised against the MAGE-11 NH_2-terminal peptide. Endogenous MAGE-11 in HeLa cells and in the CWR-R1, LNCaP, PC-3, and DU-145 prostate cancer cell lines comigrated with 70-kDa recombinant MAGE-11 expressed in COS cells (Fig. 12C). Only faint comigrating bands persisted after preincubating the MAGE-11 antibody with the MAGE-11 peptide immunogen (Fig. 12C, right), and there was no evidence for an NH_2-terminally truncated form of MAGE-11. It was interesting that HeLaAR1C cells stably expressing Flag-tagged full-length human AR had higher MAGE-11 protein levels than HeLa cells lacking AR (Fig. 12C, lanes 2 and 3). The similar MAGE-11 mRNA levels evident in HeLa and HeLaAR1C cells (Fig. 12A) raise the possibility that the stabilizing effect of MAGE-11 on AR observed above in the absence of androgen contributes to the stabilization of MAGE-11.

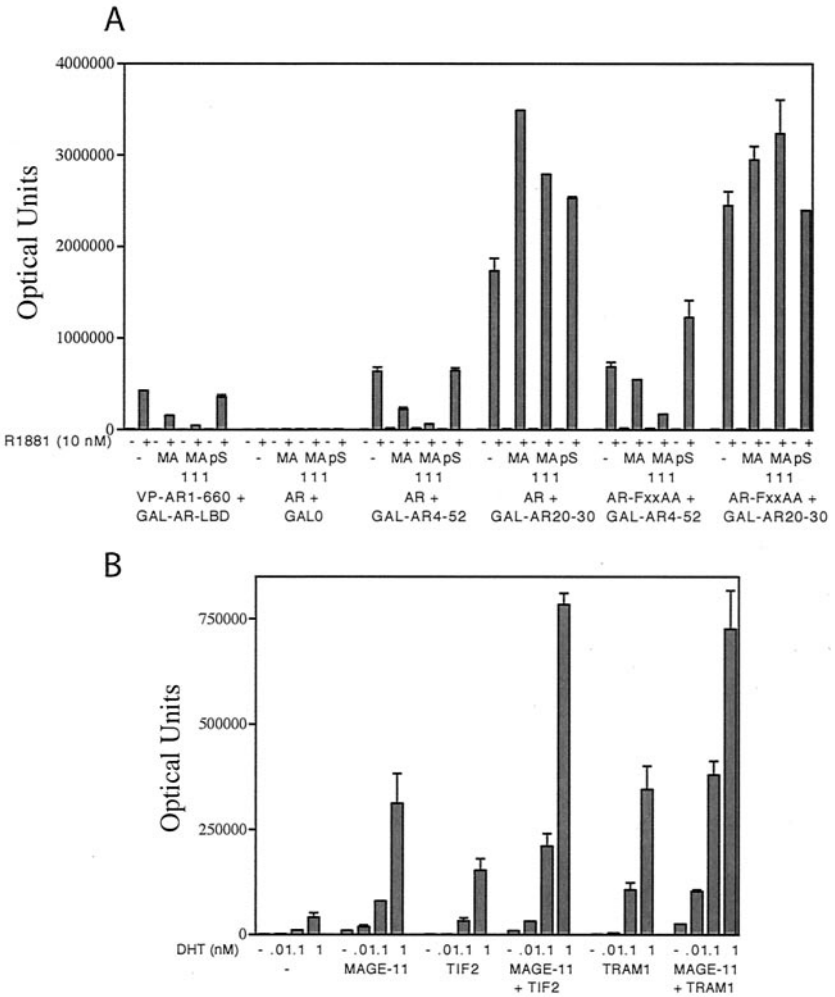

FIG. 10. Competition for the AR N/C interaction by MAGE-11 and a synergistic increase in AR transactivation. (A) Two-hybrid interaction assays were performed with HepG2 cells in 12-well plates with VP-AR1-660 and GAL-AR624-919 (GAL-AR-LBD) (50 ng/well) or 5 ng of pCMVhAR and pCMVhAR-FXXAA expressed together with 50 ng of pGAL0 empty vector control (GAL0), GAL-AR4-52, or GAL-AR20-30, without further vector addition (−), or with 50 ng pSG5-MAGE-11 (MA), pSG5-MAGE-11-111-429 (MA 111), or the pSG5 empty vector (pS). Assays were performed in the absence and presence of 10 nM R1881. (B) A total of 100 ng of pCMVhAR was expressed in CV1 cells in 6-cm dishes with calcium phosphate precipitation of DNA in the absence and presence of 2 μg of pSG5-MAGE-11, pSG5-TIF2, or pSG5-TRAM1 or in combination as indicated, together with 5 μg of PSA-Luc. Transfected cells were incubated for 40 h in the absence and presence of 0.01, 0.1, and 1 nM DHT as indicated. Parallel transfections of pCMVhAR and the pSG5 empty vector control showed no increase in activity (data not shown).

DISCUSSION

Identification of MAGE-11 as an AR coregulator. We have identified the X-linked protein MAGE-11 as a novel AR coregulator. MAGE-11 specifically binds the AR NH_2-terminal FXXLF motif that mediates the androgen-dependent N/C interaction with AF2 in the AR ligand binding domain. The molecular interaction between AR and MAGE-11 in the absence and presence of androgen is supported by their intracellular colocalization, coimmunoprecipitation, GST affinity matrix binding, and the MAGE-11-induced increases in AR transcriptional activity and ligand dissociation.

MAGE-11 forms a stable complex with the ligand-free AR that results in increased AR stability. Increased AR stabilization in the absence of androgen raises AR protein levels, which could contribute to the increase in AR transcriptional activity observed in the presence of MAGE-11. In contrast, binding of a strong agonist such as DHT decreases the association between AR and MAGE-11. This is consistent with competition by MAGE-11 for the agonist-induced N/C interaction between the AR FXXLF motif and AF2. At subsaturating concentrations of DHT, increased turnover of AR and MAGE-11 appears to result from this competition. Higher levels of DHT apparently overcome this effect and restore AR stabilization mediated by the N/C interaction.

We observed a persistent association between MAGE-11 and an AR nuclear transport mutant in the presence of DHT that suggests that the N/C interaction alone is not sufficient to destabilize MAGE-11 binding. Our earlier studies with this ARm4 mutant indicate binding kinetics consistent with an N/C interaction (51). Furthermore, persistence of a stable MAGE-11 and AR interaction in the presence of ligands such as estradiol and progesterone that induce AR nuclear trans-

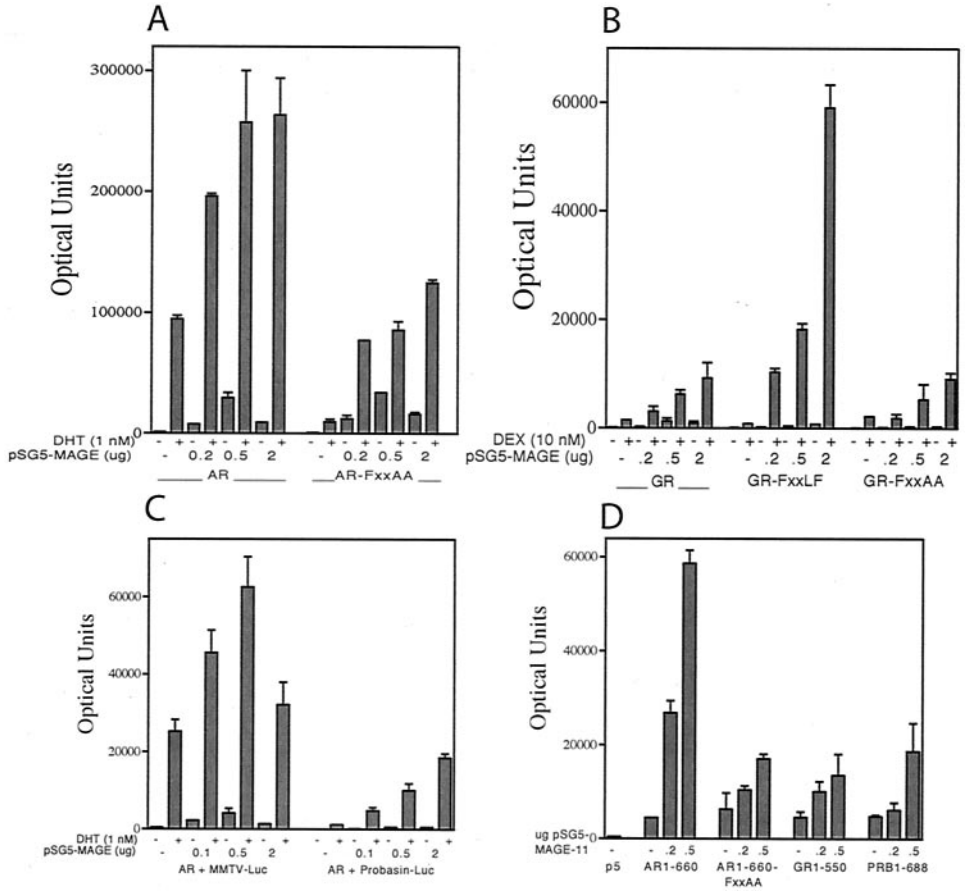

FIG. 11. FXXLF motif-dependent effects of MAGE-11 on receptor mediated transactivation. (A) The effect of MAGE-11 on AR transactivation was tested by transfecting 100 ng of pCMVhAR or pCMVhAR-FXXAA into CV1 cells with 5 μg of PSA-Luc reporter in the absence and presence of 0.2, 0.5, and 2 μg of pSG5-MAGE-11. Luciferase activity was determined in the absence and presence of 1 nM DHT. (B) The effect of MAGE-11 on GR transactivation was tested by transfecting 100 ng of pCMVhGR, pCMVhAR1-132-GR132-777 chimera (GR-FXXLF), and pCMVhAR1-132-FXXAA-GR132-777 (GR-FXXAA) into CV1 cells with 5 μg of PSA-Luc reporter in the absence and presence of 0.2, 0.5, and 2 μg of pSG5-MAGE-11, as indicated. Luciferase activity was determined in the absence and presence of 10 nM dexamethasone (DEX). (C) The effect of MAGE-11 on AR transactivation of the MMTV and probasin enhancer-promoters was tested in CV1 cells transfected with 25 ng of pCMVhAR and 5 μg of MMTV-Luc or with 10 ng of pCMVhAR and 5 μg of probasin $(-244$ to $-96)_3$-Luc in the absence and presence of 0.1, 0.5, and 2 μg of pSG5-MAGE-11. (D) The FXXLF motif dependence of the MAGE-11-induced increase in constitutive activity of NH_2-terminal and DNA binding domain fragments of AR, GR, and PR was tested with CV1 cells transfected with 50 ng of pCMVhAR1-660, pCMVhAR1-660FXXAA, pCMVhGR1-550, p5mPRB-1-688, or pCMV5 empty vector (p5)/6-cm dish with 5 μg of PSA-Luc in the absence and presence of 0.2 and 0.5 μg of pSG5-MAGE-11.

port but do not induce the AR N/C interaction suggests that nuclear targeting of AR is also not sufficient to destabilize the AR and MAGE-11 interaction. The data indicate that both AR nuclear transport and binding of an agonist are required for MAGE-11 and AR AF2 to competitively interact with the AR NH_2-terminal FXXLF motif. We have shown that competition between MAGE-11 binding and the N/C interaction increases AR transactivation of androgen-responsive enhancer-promoters in a manner that is synergistic with the SRC/p160 family of coactivators. MAGE-11 binding and the N/C interaction appear to act in concert with coactivators to modulate AR activity. Binding of MAGE-11 to the AR NH_2-terminal FXXLF motif mimics the effect of an AR-FXXAA mutant (14). Both expose the AF2 site in the AR ligand binding domain that is otherwise inhibited in the presence of androgen by the N/C interaction and allow increased recruitment and activation by the SRC/p160 family of coactivators.

The MAGE gene family. The MAGE gene family consists of 12 homologous proteins coded by a 3.5-Mb segment on the long arm of the X chromosome at human Xq28. MAGE-11 is in a region encoding MAGE-7 and -9 (39). Six other MAGE genes are expressed exclusively in tumors, such as melanomas (hence the family name); lung, colon, and breast cancers; laryngeal tumors; sarcomas; and leukemias (5, 39). Tumor-selective expression of some MAGE family members is attributed to genome-wide demethylation of CpG dinucleotides at promoters (6), a common feature of cancer cells (4). MAGE-11 was previously reported in a variety of tumor cell lines, including HeLa, monkey kidney COS cells, 3T6 mouse fibroblasts, rat glial tumor cells, hamster CHO cells, and human 293 cells (24). MAGE-11 was also detected in testis and placenta (5), suggesting its expression is not limited to cancer cells.

However, there are discrepancies regarding the size of the

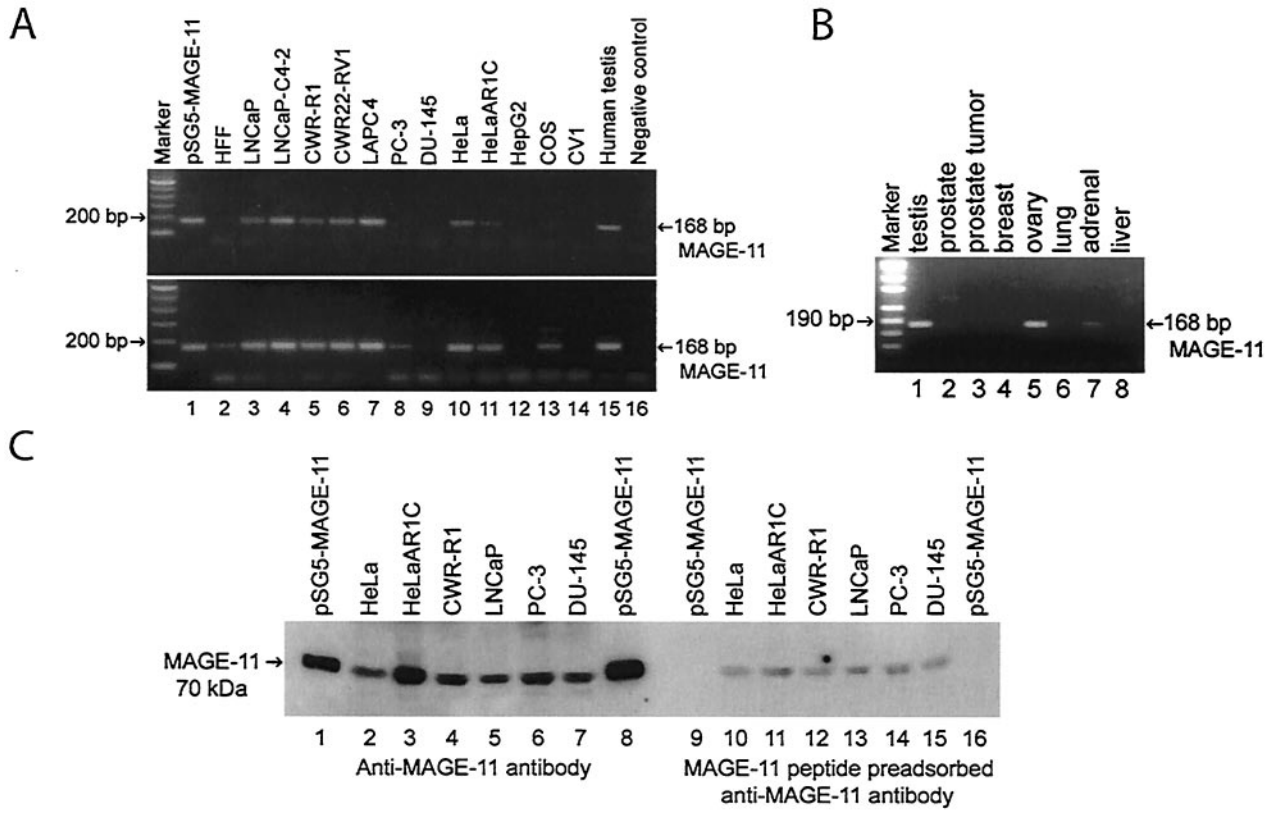

FIG. 12. Endogenous MAGE-11 expression. (A) MAGE-11 mRNA was analyzed by RT-PCR. Total RNA (2 μg) was reverse transcribed, and the resulting cDNAs were amplified by 35 PCR cycles (top). In addition, 2 μl of the first PCRs was used as a template for a second 35-cycle PCR amplification with the same primers (bottom). Amplified MAGE-11 DNA fragments are shown for pSG5-MAGE-11 (lane 1), human foreskin fibroblasts (HFF, lane 2) and prostate cancer cell lines LNCaP (lane 3), LNCaP-C4-2 (lane 4), CWR-R1 (lane 5), CWR22-RV1 (lane 6), LAPC4 (lane 7), PC-3 (lane 8), and DU-145 (lane 9), as well as from HeLa cells (lane 10), HeLaAR1C cell line stably expressing human AR (lane 11), HepG2 (lane 12), COS cells (lane 13), CV1 cells (lane 14), human testis tissue (lane 15), and the no-RNA control (lane 16). The products were analyzed on 2% agarose gels. (B) Total RNA was isolated from adult human tissues with Trizol, reverse transcribed, and PCR amplified as described in Materials and Methods. Shown are the results of 35 PCR cycles with cDNA from human testis (lane 1), prostate (lane 2), a prostate tumor (lane 3), breast (lane 4), ovary (lane 5), lung (lane 6), adrenal gland (lane 7), and liver (lane 8). (C) Endogenous MAGE-11 protein (70 kDa) was detected in immunoblots with the anti-MAGE-11 peptide antibody described in Materials and Methods. The indicated cell lines were cultured to near confluence, and total protein was extracted with radioimmunoprecipitation assay buffer as described in Materials and Methods. Total protein (100 μg) was analyzed in each lane, and immunoblot analyses were performed with the peptide affinity-purified MAGE-11 antibody (2.9 μg/ml) raised in a rabbit. The MAGE-11 antibody was untreated (lanes 1 to 8) or preadsorbed overnight at 4°C by adding 5 μl of 0.5 mg of peptide immunogen/ml to 28 μl of 0.52-mg/ml antibody (lanes 9 to 16). Transiently expressed pSG5-MAGE-11 from COS cells was analyzed with 1 μg (lanes 1 and 9) and 2 μg (lanes 8 and 16) of total protein. The HeLaAR1C cell line expresses a stably integrated Flag-tagged human AR (P. D. Reynolds and E. M. Wilson, unpublished studies). The MAGE-11 antibody was relatively specific to MAGE-11 but also interacted on immunoblots with a ~80-kDa DNA helicase (data not shown).

MAGE-11 protein. Previous studies indicate an apparent molecular mass of 48 kDa (24) that was predicted from a single coding exon (GenBank accession number NM005366) (24, 39). This exon corresponds to the last exon of MAGE-11 shown in Fig. 1A. The previously predicted protein lacked the first 110 NH_2-terminal residues reported here for MAGE-11. This putative truncated form of MAGE-11 would initiate at the third methionine, residue 111 of full-length MAGE-11. We observed a 70-kDa MAGE-11 protein, which agrees with a recent study (23) that identified three additional upstream exons encoding the NH_2-terminal region unique to full-length MAGE-11 (Fig. 1A). When we created the truncated form of MAGE-11 to initiate at the third methionine, it was 52 kDa after in vitro translation and analysis with SDS gels (data not shown). Previous reports of a similarly sized endogenous MAGE-11 made use of an antibody raised against the carboxyl-terminal region of MAGE-11. However, this region is homologous with other members of the MAGE family, raising the possibility of cross-reaction with other family members. Our data nevertheless support the expression of full-length MAGE-11 in human testis, human foreskin fibroblasts, and several human cancer cell lines.

Mechanism of interaction between MAGE-11 and the AR FXXLF motif. The AR FXXLF motif that binds MAGE-11 is identical to the motif that binds AF2 in the AR ligand binding domain mediating the androgen-dependent AR N/C interaction. However, detailed deletion mapping and point mutagenesis studies revealed overlapping yet distinct binding regions. AR binding to MAGE-11 requires an extended 21-amino-acid α-helical region between AR residues 16 to 36 that contains

^{23}FQNLF^{27}. This minimal region is nearly twice as long as the 11-amino-acid AR20-30 α-helical region required to bind AF2 in the AR ligand binding domain. The more-extended AR FXXLF binding region may allow MAGE-11 to compete for the N/C interaction in the presence of an AR agonist. Other regions outside but flanking the AR NH_2-terminal domain FXXLF motif region required for MAGE-11 binding have also been suggested to modulate AR N/C interactions (43).

The entire carboxyl-terminal region of MAGE-11 is required to bind the AR FXXLF motif. This is reminiscent of the carboxyl-terminal region of AR that forms the ligand binding domain and the AF2 hydrophobic cleft that binds FXXLF. Cocrystal structures of the AR ligand binding domain have revealed the hydrophobic AF2 surface that accommodates the amphipathic α-helical regions of the FXXLF and LXXLL motifs (15, 22). The structure of MAGE-11 has not been determined, but analysis using the PONDR Protein Disorder Predictor (http://www.pondr.com/PONDR/pondr.cgi) suggests a highly ordered arrangement of α-helical regions between MAGE-11 residues 220 to 429. It is possible that a similar but unique binding surface on MAGE-11 interacts with the extended α-helical region of the AR FXXLF motif. On the other hand, binding of LXXLL peptides to protein domains other than nuclear receptor ligand binding domains has been reported (37). Binding of the FXXLF motif to MAGE-11 may occur through a mechanism similar to the interaction of the Stat6 transactivation domain LXXLL peptide binding to the PAS-B domain of SRC1 (37).

The stabilizing influence of MAGE-11 on AR in the absence of androgen and androgen-induced AR stabilization that results from the AR N/C interaction raises the possibility that the amphipathic α-helical FXXLF motif region also serves as an AR degradation signal (40). MAGE-11 binding to the FXXLF motif region could mask the putative signal and increase AR stabilization as observed in the absence of hormone. In the presence of DHT, FXXLF motif binding to AF2 could similarly protect against degradation resulting in the well-documented AR stabilization that results from the N/C interaction.

The intracellular association between AR and MAGE-11 is supported by their colocalization in the cytoplasm in the absence of androgen and in the nucleus in the presence of androgen. We also observed that MAGE-11 colocalizes in a prominent punctate cytoplasmic staining pattern, previously reported for this AR nuclear transport mutant (52). Dependence of the punctate pattern on androgen binding argues against nonspecific aggregation and suggests that the AR transport mutant becomes trapped in an as-yet-uncharacterized cytoplasmic substructure on route to the nucleus. For a DNA binding mutant, AR colocalizes with MAGE-11 in prominent subnuclear structures that resemble promyelocytic leukemia (PML) bodies. It was previously reported that agonist, but not antagonist-bound, AR triggers the subnuclear movement of AR and SRC1 out of the PML body into more filamentous nuclear speckles (38). Entrapment of an AR DNA binding domain mutant together with MAGE-11 in PML bodies would reinforce the idea that MAGE-11 facilitates the interaction between AR and the SRC/p160 coactivators.

A competition model. Our search for an FXXLF motif binding protein was based on the premise that a coregulator that binds the AR NH_2-terminal FXXLF motif with high specificity might relieve inhibition of AF2 imposed by the androgen-induced N/C interaction (14). The data presented in this report have led us to propose the model in Fig. 13. DHT binding to AR establishes an equilibrium between the AR N/C interaction (Fig. 13, top right) and AR AF2 binding of the SRC/p160 coactivators (Fig. 13, bottom right). In each instance, MAGE-11 is released in association with AR-mediated gene activation. In the presence of DHT, an AR, MAGE-11, and TIF2 intermediate (Fig. 13, bottom left) is supported by the persistent but reduced association of MAGE-11. The decrease in AR-associated MAGE-11 in the presence of DHT suggests MAGE-11 is released from the AR FXXLF binding site in parallel with formation of the AR N/C interaction or exposure of AF2 to SRC/p160 coactivator binding. This androgen-dependent interrelationship is supported by the synergistic increase in transcriptional activity that occurs in the presence of MAGE-11 and TIF2. It is also supported by the increased association of TIF2 and decreased association of MAGE-11 with the DHT-bound AR. By competing for FXXLF motif binding, MAGE-11 appears to function as an AR coregulator, in part by increasing accessibility of AF2 to SRC/p160 coactivator recruitment. There is also evidence that MAGE-11 acts through additional mechanisms independent of its interaction with the FXXLF motif.

It is well recognized that the AR ligand binding domain expressed as a fragment or fusion protein has little or no transcriptional activity when assayed in mammalian cells (16). This reflects the relatively inefficient recruitment of coactivator LXXLL motifs by AR AF2, even in transformed cell lines where endogenous coactivator levels are typically higher than for normal cells (9). The inherent low activity of the AR ligand binding domain results from the 5- to 10-fold-lower binding affinity of AF2 for the SRC/p160 coactivator LXXLL motifs than the AR NH_2-terminal FXXLF motif (15, 20). Reduced binding affinity for the LXXLL motifs results from sequence changes in AR AF2 that apparently evolved to favor FXXLF motif binding (15). Under conditions of increased SRC/p160 coactivator expression (18) as observed in recurrent prostate cancer (10), AR AF2 can recruit and be activated by this family of endogenous SRC/p160 coactivators (9, 41). The increase in AR transactivation that we observe in response to MAGE-11 without transiently overexpression of the SRC/p160 coactivators suggests that MAGE-11 binding to AR increases the recruitment of endogenous coactivators. Coactivator recruitment by the AR AF2 site in full-length AR is probably more efficient than coactivator recruitment by the AR ligand binding domain fragment alone, since additional interactions are reported to occur between the coactivator and the AR NH_2-terminal region (16).

In the absence of androgen, the predominant binding of MAGE-11 to AR was not surprising, since AR FXXLF motif binding to AF2 that characterizes the AR N/C interaction requires the presence of a high-affinity androgen bound in the ligand binding pocket (51). Isolation of a stable complex between AR and MAGE-11 in the absence of androgen and our observations that MAGE-11 colocalizes with AR in the cytoplasm strongly indicate that binding of MAGE-11 to AR predominates in the absence of androgen. Moreover, in the presence of ligands such as estradiol, progesterone, and hydroxyflutamide that can target AR to the nucleus but do not

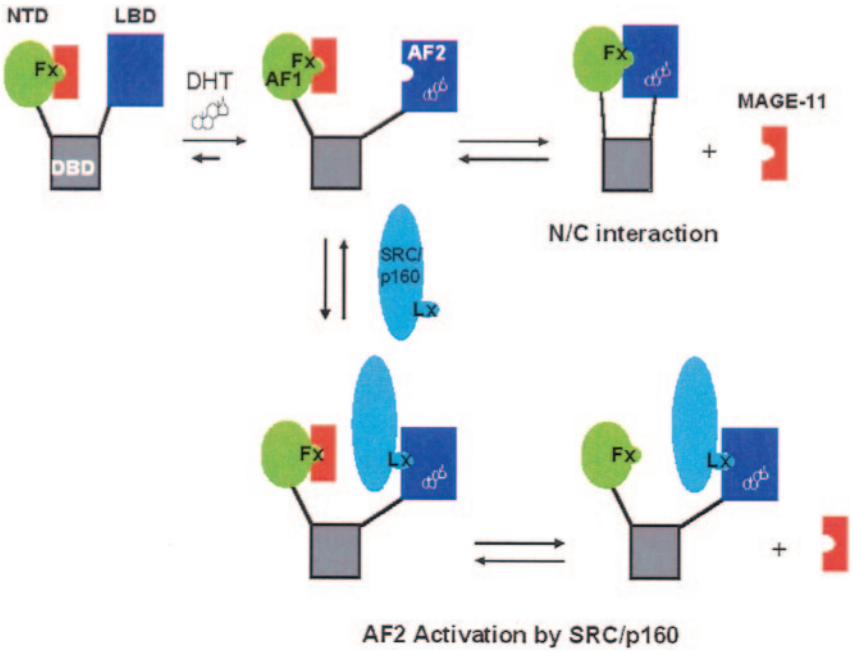

FIG. 13. Model for the effect of MAGE-11 on AR transactivation. In the absence of androgen, MAGE-11 binds the AR NH_2-terminal domain (NTD) FXXLF motif (Fx) and stabilizes the ligand-free AR. Binding of DHT induces AR nuclear transport and a conformational change in AF2 in the ligand binding domain (LBD) that enables FXXLF motif binding in the N/C interaction and release of MAGE-11. Although not depicted, the AR FXXLF motif-AF2 N/C interaction is thought to occur between monomers in an antiparallel AR dimer. The androgen-dependent AR N/C interaction inhibits the activity of AF2, making AF1 the dominant activation domain. In the nucleus, MAGE-11 competes for and relieves the inhibitory effect of the N/C interaction, resulting in increased activation by AF2 binding of the LXXLL motifs (Lx) of the SRC/p160 family of coactivators. The model suggests that MAGE-11 functions as an AR coregulator by occupying the AR FXXLF site and facilitates intermittent binding of coactivators reported to occur at enhancer-promoter regions of androgen-regulated genes.

induce the N/C interaction, a stable interaction with MAGE-11 persists in the nucleus.

On the other hand, MPA at high concentrations does not promote the AR N/C interaction between VP-AR1-660 and GAL-AR624-919 and instead acts as an inhibitor in the presence of DHT (27). In agreement with this, MPA at high concentrations does not stabilize AR (Fig. 5B, lane 6) and is not a strong androgen in vivo (27). However, recently we found that MPA at relatively low concentrations does promote the interaction of GAL-AR20-30 and GAL-AR4-52 with full-length AR (unpublished studies). The discrepancy between the assays is currently not understood. We reported previously that an AR NH_2-terminal WXXLF motif contributes to the N/C interaction, but the influence of specific ligands is not known. Like the AR NH_2-terminal FXXLF motif, the WXXLF motif interacts with AF2 in an androgen-dependent manner (17). The effectiveness of MPA to displace MAGE-11 may contribute to its strong transcriptional effects observed in transient transfection assays (27).

In the presence of DHT, competition between MAGE-11 binding and the AR N/C interaction depends on the DHT concentration and subcellular location of AR. At subsaturating concentrations of androgen ($\leq$10 nM DHT for AR expressed in COS cells), steady-state levels of AR protein were reduced, suggesting that MAGE-11 interferes with the N/C interaction that mediates androgen-induced AR stabilization. However, the AR N/C interaction prevailed at higher androgen levels, and stabilization was restored for wild-type AR but not for the AR-FXXAA mutant defective in the N/C interaction. At androgen levels that fully saturate the AR, the N/C interaction apparently prevailed over MAGE-11 binding.

Even more compelling evidence for the intracellular competition between MAGE-11 and the N/C interaction is that MAGE-11 increases the dissociation rate of bound androgen from AR. Slow androgen dissociation is a hallmark of the AR N/C interaction (14, 17, 51). However, we also found that the nuclear transport mutant that localizes in the cytoplasm in the presence of DHT stably associates with MAGE-11 in the absence and presence of androgen. In the presence of androgen, ARm4 engages in an N/C interaction, based on its stabilization by androgen and by the slow rate of dissociation of bound ligand (51).

Thus, high-affinity agonist binding and AR nuclear transport both appear to be necessary to establish the dynamic relationship between MAGE-11 and AF2 binding at the AR NH_2-terminal FXXLF site. By binding the FXXLF motif, MAGE-11 competes for the androgen dependent N/C interaction, exposing AF2 to activation by coactivators. Increased coactivator binding likely accounts in part for the MAGE-11-induced increase in AR transcriptional activity of androgen-responsive gene promoters, an increase that is synergistic with coactivator expression. Moreover, the studies support multiple protein interactions at a common FXXLF binding site whereby MAGE-11 influences AR turnover, the N/C interaction, and transcriptional activity in the absence and presence of agonist binding. Binding of MAGE-11 may contribute to the intermit-

tent binding of coactivators that has been reported during AR mediated gene activation (41).

In vivo function of MAGE-11 and its role in prostate cancer. Unlike most of the other MAGE family members that are cell surface tumor-associated antigens, MAGE-11 is confirmed by our studies as a cytoplasmic and nuclear protein that is excluded from nucleoli (24). A putative nuclear targeting signal in MAGE-11 was recognized previously (23). Localization of the MAGE family to the X chromosome and homology to a group of proteins in the sex-determining region of the X chromosome support a role for MAGE-11 in AR function during phenotypic sex determination. MAGE-11 is highly conserved in primates, although a cDNA and genomic DNA database homology search indicates MAGE-11 may not exist in lower species. However, a related MAGEB family of genes was recently reported that is ~60% homologous to the MAGE (MAGEA) family (32). The MAGEB gene family maps to the Xp21 region of the X chromosome and is associated with a dose-sensitive sex reversal phenotype (29, 32, 35) and with the *DAX-1* gene, where mutations cause X-linked adrenal hypoplasia congenita and hypogonadotropic hypogonadism (34).

From an evolutionary perspective, the AR AF2 region of the ligand binding domain is more highly conserved among all species that express AR than is the FXXLF motif. This suggests that the AR AF2 region evolved prior to the FXXLF motif. Exclusive expression of MAGE-11 in primates may continue this evolutionary progression in AR regulation, suggesting that mechanisms that control the function of AR, one of the youngest members of the nuclear hormone receptor superfamily, continue to evolve.

It remains to be established in which cell types and under what physiological conditions MAGE-11 influences AR activity. MAGE-11 mRNA was not detectable by Northern blotting and required RT-PCR methods. Endogenous MAGE-11 protein was detected in prostate cancer cells and at higher levels in HeLa cells when the AR was stably expressed. Since MAGE-11 mRNA levels were not higher in HeLaAR1C cells stably expressing AR, the increase in MAGE-11 protein suggests that AR stabilizes MAGE-11 in a reciprocal relationship with the stabilizing effect of MAGE-11 on AR in the absence of androgen. The melanoma gene family of proteins is characterized by expression in cancer cells, but MAGE-11 is also expressed in normal tissues including testis, placenta (5), and (as shown here) ovary and prostate. The presence of MAGE-11 mRNA in a human foreskin fibroblast cell line also supports a role for MAGE-11 in AR transcriptional activity in normal cells.

Our studies further suggest that MAGE-11 may be important in prostate cancer. We found higher levels of expression of MAGE-11 mRNA in prostate cancer cells that express AR and that have been shown to have increased levels of the SRC/p160 family of coactivators (9). The MAGE-11-induced stabilization of AR in the absence of hormone could account for the increased levels of AR frequently observed with recurrent prostate cancer (3, 28, 46) and may contribute to the increased ligand-independent AR transcriptional activity. This, together with increased levels of the coactivators SRC1 and TIF2 (10), could enhance the sensitivity of AR to low androgen levels (11, 12, 33) and to the effects of mitogen signaling (9). The data support that MAGE-11 is a new player in the cellular pathways that mediate AR transactivation in normal and cancer cells.

ACKNOWLEDGMENTS

We thank Frank S. French for reviewing the manuscript, Susan H. Hall for providing human tissues, and Rebecca I. Kalman, John T. Minges, Emily B. Askew, Andrew T. Hnat, Jonathan L. Faggart, K. Michelle Cobb, and De-Ying Zang for excellent technical assistance.

This work was supported by Public Health Service grant HD16910 from the National Institutes of Child Health and Development, by cooperative agreement (U54-HD35041) as part of the Specialized Cooperative Centers Program in Reproductive Research of the National Institutes of Health, and by Fogarty International Center Training and Research in Population and Health grant R03TW001234 awarded to Frank S. French by the National Institute of Health, supporting S.B. and B.H.

REFERENCES

1. **Balk, S. P.** 2002. Androgen receptor as a target in androgen-independent prostate cancer. Urology **60:**132–138.
2. **Callewaert, L., G. Verrijdt, V. Christiaens, A. Haelens, and F. Claessens.** 2003. Dual function of an amino-terminal amphipathic helix in androgen receptor-mediated transactivation through specific and nonspecific response elements. J. Biol. Chem. **278:**8212–8218.
3. **Chen, C. D., D. S. Welsbie, C. Tran, S. H. Baek, R. Chen, R. Vessella, M. G. Rosenfeld, and C. L. Sawyers.** 2004. Molecular determinants of resistance to antiandrogen therapy. Nat. Med. **10:**33–39.
4. **Counts, J. L., and J. I. Goodman.** 1995. Alterations in DNA methylation may play a variety of roles in carcinogenesis. Cell **83:**13–15.
5. **De Plaen, E., K. Arden, C. Traversari, J. J. Gaforio, J. P. Szikora, C. De Smet, F. Brasseur, P. van der Bruggen, B. Lethé, C. Lurquin, R. Brasseur, P. Chomez, O. De Backer, W. Cavenee, and T. Boon.** 1994. Structure, chromosomal localization, and expression of 12 genes of the MAGE family. Immunogenetics **40:**360–369.
6. **De Smet, C., O. De Backer, I. Faraoni, C. Lurquin, F. Brasseur, and T. Boon.** 1996. The activation of human gene MAGE-1 in tumor cells is correlated with genome-wide demethylation. Proc. Natl. Acad. Sci. USA **93:**7149–7153.
7. **Fujimoto, N., S. Yeh, H. Y. Kang, S. Inui, H. C. Chang, A. Mizokami, and C. Chang.** 1999. Cloning and characterization of androgen receptor coactivator, ARA55, in human prostate. J. Biol. Chem. **274:**8316–8321.
8. **Gelmann, E. P.** 2002. Molecular biology of the androgen receptor. J. Clin. Oncol. **20:**3001–3015.
9. **Gregory, C. W., X. Fei, L. A. Ponguta, B. He, H. M. Bill, F. S. French, and E. M. Wilson.** 2004. Epidermal growth factor increases coactivation of the androgen receptor in recurrent prostate cancer. J. Biol. Chem. **279:**7119–7130.
10. **Gregory, C. W., B. He, R. T. Johnson, O. H. Ford, J. L. Mohler, F. S. French, and E. M. Wilson.** 2001. A mechanism for androgen receptor-mediated prostate cancer recurrence after androgen deprivation therapy. Cancer Res. **61:**4315–4319.
11. **Gregory, C. W., R. T. Johnson, J. L. Mohler, F. S. French, and E. M. Wilson.** 2001. Androgen receptor stabilization in recurrent prostate cancer is associated with hypersensitivity to low androgen. Cancer Res. **61:**2892–2898.
12. **Grossmann, M. E., H. Huang, and D. J. Tindall.** 2001. Androgen receptor signaling in androgen-refractory prostate cancer. J. Natl. Cancer Inst. **93:**1687–1697.
13. **He, B., S. Bai, A. T. Hnat, R. I. Kalman, J. T. Minges, C. Patterson, and E. M. Wilson.** 2004. An androgen receptor NH_2-terminal conserved motif interacts with carboxyl terminus of Hsp70-interacting protein CHIP. J. Biol. Chem. **279:**30643–30653.
14. **He, B., N. T. Bowen, J. T. Minges, and E. M. Wilson.** 2001. Androgen-induced NH_2- and COOH-terminal interaction inhibits p160 coactivator recruitment by activation function 2. J. Biol. Chem. **276:**42293–42301.
15. **He, B., R. T. Gampe, A. J. Kole, A. T. Hnat, T. B. Stanley, G. An, E. L. Stewart, R. I. Kalman, J. T. Minges, and E. M. Wilson.** 2004. Structural basis for androgen receptor interdomain and coactivator interactions suggests a transition in nuclear receptor activation function dominance. Mol. Cell **16:**425–438.
16. **He, B., J. A. Kemppainen, J. J. Voegel, H. Gronemeyer, and E. M. Wilson.** 1999. Activation function 2 in the human androgen receptor ligand binding domain mediates interdomain communication with the NH_2-terminal domain. J. Biol. Chem. **274:**37219–37225.
17. **He, B., J. A. Kemppainen, and E. M. Wilson.** 2000. F*XX*LF and W*XX*LF sequences mediate the NH_2-terminal interaction with the ligand binding domain of the androgen receptor. J. Biol. Chem. **275:**22986–22994.
18. **He, B., L. W. Lee, J. T. Minges, and E. M. Wilson.** 2002. Dependence of selective gene activation on the androgen receptor NH_2- and COOH-terminal interaction. J. Biol. Chem. **277:**25631–25639.

19. **He, B., J. T. Minges, L. W. Lee, and E. M. Wilson.** 2002. The F*XX*LF motif mediates androgen receptor-specific interactions with coregulators. J. Biol. Chem. **277:**10226–10235.
20. **He, B., and E. M. Wilson.** 2003. Electrostatic modulation in steroid receptor recruitment of LXXLL and FXXLF motifs. Mol. Cell. Biol. **23:**2135–2150.
21. **Huang, W., Y. Shostak, P. Tarr, C. Sawyers, and M. Carey.** 1999. Cooperative assembly of androgen receptor into a nucleoprotein complex that regulates the prostate-specific antigen enhancer. J. Biol. Chem. **274:**25756–25768.
22. **Hur, E., S. J. Pfaff, E. S. Payne, H. Gron, B. M. Buehrer, and R. J. Fletterick.** 2004. Recognition and accommodation at the androgen receptor coactivator binding interface. PLoS Biol. **2:**e274.
23. **Irvine, R. A., and G. A. Coetzee.** 1999. Additional upstream coding sequences of MAGE-11. Immunogenetics **49:**585.
24. **Jurk, M., E. Kremmer, U. Schwarz, R. Forster, and E. L. Winnacker.** 1998. MAGE-11 protein is highly conserved in higher organisms and located predominantly in the nucleus. Int. J. Cancer **75:**762–766.
25. **Kang, H. Y., S. Yeh, N. Fujimoto, and C. Chang.** 1999. Cloning and characterization of human prostate coactivator ARA54, a novel protein that associates with the androgen receptor. J. Biol. Chem. **274:**8570–8576.
26. **Kemppainen, J. A., M. V. Lane, M. Sar, and E. M. Wilson.** 1992. Androgen receptor phosphorylation, turnover, nuclear transport, and transcriptional activation. Specificity for steroids and antihormones. J. Biol. Chem. **267:**968–974.
27. **Kemppainen, J. A., E. Langley, C. I. Wong, K. Bobseine, W. R. Kelce, and E. M. Wilson.** 1999. Distinguishing androgen receptor agonists and antagonists: distinct mechanisms of activation by medroxyprogesterone acetate and dihydrotestosterone. Mol. Endocrinol. **13:**440–454.
28. **Koivisto, P., J. Kononen, C. Palmberg, T. Tammela, E. Hyytinen, J. Isola, J. Trapman, K. Cleutjens, A. Noordzij, T. Visakorpi, and O. P. Kallioniemi.** 1997. Androgen receptor gene amplification: a possible molecular mechanism for androgen deprivation therapy failure in prostate cancer. Cancer Res. **57:**314–319.
29. **Lalli, E., and P. Sassone-Corsi.** 2003. DAX-1, an unusual orphan receptor at the crossroads of steroidogenic function and sexual differentiation. Mol. Endocrinol. **17:**1445–1453.
30. **Langley, E., Z. X. Zhou, and E. M. Wilson.** 1995. Evidence for an antiparallel orientation of the ligand-activated human androgen receptor dimer. J. Biol. Chem. **270:**29983–29990.
31. **Lubahn, D. B., D. R. Joseph, M. Sar, J. Tan, H. N. Higgs, R. E. Larson, F. S. French, and E. M. Wilson.** 1988. The human androgen receptor: complementary deoxyribonucleic acid cloning, sequence analysis and gene expression in prostate. Mol. Endocrinol. **2:**1265–1275.
32. **Lurquin, C., C. De Smet, F. Brasseur, F. Muscatelli, V. Martelange, E. De Plaen, R. Brasseur, A. P. Monaco, and T. Boon.** 1997. Two members of the human MAGEB gene family located in Xp21.3 are expressed in tumors of various histological origins. Genomics **46:**397–408.
33. **Mohler, J. L., C. W. Gregory, O. H. Ford, D. Kim, C. M. Weaver, P. Petrusz, E. M. Wilson, and F. S. French.** 2004. The androgen axis in recurrent prostate cancer. Clin. Cancer Res. **10:**440–448.
34. **Muscatelli, F., T. M. Strom, A. P. Walker, E. Zanaria, D. Recan, A. Meindl, B. Bardoni, S. Guioli, G. Zehetner, W. Rabl, H. P. Schwarz, J. C. Kaplan, G. Camerino, T. Meitinger, and A. P. Monaco.** 1994. Mutations in the DAX-1 gene give rise to both X-linked adrenal hypoplasia congenita and hypogonadotropic hypogonadism. Nature **372:**672–676.
35. **Muscatelli, F., A. P. Walker, E. De Plaen, A. N. Stafford, and A. P. Monaco.** 1995. Isolation and characterization of a MAGE gene family in the Xp21.3 region. Proc. Natl. Acad. Sci. USA **92:**4987–4991.
36. **Rao, M. A., H. Cheng, A. N. Quayle, H. Nishitani, C. C. Nelson, and P. S. Rennie.** 2002. RanBPM, a nuclear protein that interacts with and regulates transcriptional activity of androgen receptor and glucocorticoid receptor. J. Biol. Chem. **277:**48020–48027.
37. **Razeto, A., V. Ramakrishnan, C. M. Litterst, K. Giller, C. Griesinger, T. Carlomagno, N. Lakomek, T. Heimburg, M. Lodrini, E. Pfitzner, and S. Becker.** 2004. Structure of the NCoA-1/SRC-1 PAS-B domain bound to the L*XX*LL motif of the STAT6 transactivation domain. J. Mol. Biol. **336:**319–329.
38. **Rivera, O. J., C. S. Song, V. E. Centonze, J. D. Lechleiter, B. Chatterjee, and A. K. Roy.** 2003. Role of the promyelocytic leukemia body in the dynamic interaction between the androgen receptor and steroid receptor coactivator-1 in living cells. Mol. Endocrinol. **17:**128–140.
39. **Rogner, U. C., K. Wilke, E. Steck, B. Korn, and A. Poustka.** 1995. The melanoma antigen gene (MAGE) family is clustered in the chromosomal band Xq28. Genomics **29:**725–731.
40. **Sadis, S., C. Atienza, and D. Finley.** 1995. Synthetic signals for ubiquitin-dependent proteolysis. Mol. Cell. Biol. **15:**4086–4094.
41. **Shang, Y., M. Myers, and M. Brown.** 2002. Formation of the androgen receptor transcription complex. Mol. Cell **9:**601–610.
42. **Simental, J. A., M. Sar, M. V. Lane, F. S. French, and E. M. Wilson.** 1991. Transcriptional activation and nuclear targeting signals of the human androgen receptor. J. Biol. Chem. **266:**510–518.
43. **Steketee, K., C. A. Berrevoets, H. J. Dubbink, P. Doesburg, R. Hersmus, A. O. Brinkmann, and J. Trapman.** 2002. Amino acids 3–13 and amino acids in and flanking the ^{23}FxxLF^{27} motif modulate the interaction between the N-terminal and ligand-binding domain of the androgen receptor. Eur. J. Biochem. **269:**5780–5791.
44. **Tan, J. A., S. H. Hall, P. Petrusz, and F. S. French.** 2000. Thyroid receptor activator molecule, TRAM-1, is an androgen receptor coactivator. Endocrinology **141:**3440–3450.
45. **Tork, S., I. Hatin, J. P. Rousset, and C. Fabret.** 2004. The major 5′ determinant in stop codon read-through involves two adjacent adenines. Nucleic Acids Res. **32:**415–421.
46. **Visakorpi, T., E. Hyytinen, P. Koivisto, M. Tanner, R. Keinanen, C. Palmberg, A. Palotie, T. Tammela, J. Isola, and O. P. Kallioniemi.** 1995. In vivo amplification of the androgen receptor gene and progression of human prostate cancer. Nat. Genet. **9:**401–406.
47. **Voegel, J. J., M. J. Heine, M. Tini, V. Vivat, P. Chambon, and H. Gronemeyer.** 1998. The coactivator TIF2 contains three nuclear receptor-binding motifs and mediates transactivation through CBP binding-dependent and -independent pathways. EMBO J. **17:**507–519.
48. **Yang, L., J. Guerrero, H. Hong, D. B. DeFranco, and M. R. Stallcup.** 2000. Interaction of the tau2 transcriptional activation domain of glucocorticoid receptor with a novel steroid receptor coactivator, Hic-5, which localizes to both focal adhesions and the nuclear matrix. Mol. Biol. Cell **11:**2007–2018.
49. **Yeh, S., and C. Chang.** 1996. Cloning and characterization of a specific coactivator, ARA70, for the androgen receptor in human prostate cells. Proc. Natl. Acad. Sci. USA **93:**5517–5521.
50. **Zhou, Z. X., B. He, S. H. Hall, E. M. Wilson, and F. S. French.** 2002. Domain interactions between coregulator ARA(70) and the androgen receptor (AR). Mol. Endocrinol. **16:**287–300.
51. **Zhou, Z. X., M. V. Lane, J. A. Kemppainen, F. S. French, and E. M. Wilson.** 1995. Specificity of ligand-dependent androgen receptor stabilization: receptor domain interactions influence ligand dissociation and receptor stability. Mol. Endocrinol. **9:**208–218.
52. **Zhou, Z. X., M. Sar, J. A. Simental, M. V. Lane, and E. M. Wilson.** 1994. A ligand-dependent bipartite nuclear targeting signal in the human androgen receptor. Requirement for the DNA-binding domain and modulation by NH_2-terminal and carboxyl-terminal sequences. J. Biol. Chem. **269:**13115–13123.

THE JOURNAL OF BIOLOGICAL CHEMISTRY VOL. 281, NO. 10, pp. 6648–6663, March 10, 2006

Probing the Functional Link between Androgen Receptor Coactivator and Ligand-binding Sites in Prostate Cancer and Androgen Insensitivity*

Received for publication, October 31, 2005, and in revised form, December 16, 2005 Published, JBC Papers in Press, December 19, 2005, DOI 10.1074/jbc.M511738200

Bin He[‡1], Robert T. Gampe, Jr.[§], Andrew T. Hnat[‡], Jonathan L. Faggart[‡], John T. Minges[‡], Frank S. French[‡], and Elizabeth M. Wilson[‡2]

From the [‡]Laboratories for Reproductive Biology, Lineberger Comprehensive Cancer Center, Department of Pediatrics, Biochemistry and Biophysics, University of North Carolina, Chapel Hill, North Carolina 27599 and [§]Discovery Research, GlaxoSmithKline, Research Triangle Park, North Carolina 27709

The androgen receptor (AR) is a ligand-activated transcription factor required for male sex development and virilization and contributes to prostate cancer initiation and progression. High affinity androgen binding triggers conformational changes required for AR transactivation. Here we characterized naturally occurring AR gene mutations in the region of activation function 2 (AF2) that decrease or increase AR transcriptional activity by altering the region bounded by AF2 and the ligand binding pocket without affecting equilibrium androgen binding affinity. In the androgen insensitivity syndrome, germ line AR mutations increase the androgen dissociation rate and reduce AR F*XX*LF motif binding and the recruitment of steroid receptor coactivator (SRC)/p160 coactivator L*XX*LL motifs. In prostate cancer, somatic AR mutations in AF2 or near the bound ligand slow androgen dissociation and increase AR stabilization and coactivator recruitment. Crystal structures of the AR ligand binding domain bound to R1881 and F*XX*LF or L*XX*LL motif peptide indicate the mutations are proximal to the AF2 bound peptide, adjacent to the ligand pocket, or in a putative ligand gateway. The results suggest a bidirectional structural relay between bound ligand and coactivator that establishes AR functional potency *in vivo*.

Steroid receptors comprise a subgroup of the nuclear receptor family of transcriptional activators that regulate gene expression by recruiting coactivator proteins (1). Like other steroid receptors, the androgen receptor (AR)[3] mediates transcriptional activation primarily through two domains. Activation function 1 (AF1) in the NH_2-terminal region is the major transactivation domain (2) but is not well conserved across species (3). Activation function 2 (AF2) in the ligand binding domain is a highly conserved hydrophobic surface that is stabilized by agonist binding and required for SRC/p160 coactivator recruitment. AF2 is formed by helices 3, 3′, 4, and 12 and is flanked by clusters of oppositely charged residues (4). AR binding of the biologically active androgens testosterone and dihydrotestosterone (DHT) is thought to stabilize the AF2 helix 12 to complete the coactivator binding surface (5–7).

The human AR gene is expressed at chromosome Xq11-12 as a single allele in the 46,XY genetic male. More than 300 different AR single amino acid mutations or partial gene deletions cause the androgen insensitivity syndrome (AIS). Partial loss of AR function results in male infertility and varying degrees of incomplete masculinization. Complete loss of AR function results in an external female genital phenotype in the genetic male (8, 9). Mutations in the AR gene occur in the human population with a frequency of ~0.002%, with single base changes overwhelmingly positioned in the highly structured ligand binding domain. Mutations in the AF2 region of the ligand binding domain can cause AIS without altering equilibrium androgen binding affinity (10, 11).

For the steroid receptors as a group, AF2 serves as a critical if not essential binding site for the L*XX*LL motifs of SRC/p160 coactivators that have histone acetyltransferase activity (12). However, AR is unique because AF2 displays different affinities for multiple L*XX*LL-related motifs. Like other steroid receptors in the presence of agonist, AR AF2 binds the L*XX*LL motifs of SRC/p160 coactivators but with an affinity 5–10 times weaker than that of the AR NH_2-terminal F*XX*LF motif sequence ^{23}FQNLF^{27} (10, 13, 14). AR F*XX*LF motif binding to AF2 mediates the androgen-dependent NH_2- and carboxyl-terminal (N/C) interaction that has been shown to be important for androgen-regulated gene expression (11, 15). AR has in addition an NH_2-terminal W*XX*LF-binding motif (^{433}WHTLF^{437}) that contributes to the N/C interaction by binding AF2 (14, 16, 17). AR transactivation through AF2 in the presence of agonist appears to be limited not only by the lower binding affinity for the coactivator L*XX*LL motifs but also through competitive inhibition of coactivator binding by the AR F*XX*LF motif.

Beneath the exterior surface of the AR AF2 coactivator-binding site is a shallow interface juxtaposed against the ligand binding pocket. This close structural arrangement provides a platform for potential communication between AF2 and bound ligand in regulating AR transcriptional activity. Support for structural communication at this boundary region is evident from the slower androgen dissociation that results from F*XX*LF motif binding to AF2 (11, 15, 18). Coactivator L*XX*LL motif binding may similarly induce conformational changes in AF2 and impact ligand binding kinetics (13, 16). Here we investigated structural features and functional consequences of the naturally occurring AR germ line and somatic mutations in or near the AF2 site in search of evidence for a structural relay between AF2 and the ligand binding pocket. In the AR-linked disorders of androgen insensitivity and prostate cancer, AR gene mutations have opposite effects on AR activity that

* This work was supported by United States Public Health Service Grant HD16910 from the NICHD, by cooperative agreement U54-HD35041 as part of the Specialized Cooperative Centers Program in Reproductive Research of the National Institutes of Health, and by Fogarty International Center Grant R03TW001234 (to B. H.) Training and Research in Population and Health (to F. S. F.) by the National Institutes of Health. The costs of publication of this article were defrayed in part by the payment of page charges. This article must therefore be hereby marked "*advertisement*" in accordance with 18 U.S.C. Section 1734 solely to indicate this fact.

[1] Present address: M533 DeBakey Bldg., Dept. of Molecular and Cellular Biology, Baylor College of Medicine, One Baylor Plaza, Houston, TX 77030

[2] To whom correspondence should be addressed: Laboratories for Reproductive Biology, CB 7500, University of North Carolina, Chapel Hill NC 27599-7500. Tel.: 919-966-5168; Fax: 919-966-2203; E-mail: emw@med.unc.edu.

[3] The abbreviations used are: AR, androgen receptor; WT, wild type; GST, glutathione *S*-transferase; DHT, dihydrotestosterone; AF, activation function; AIS, androgen insensitivity syndrome; GR, glucocorticoid receptor; N/C, NH_2/carboxyl-terminal interaction; R1881, 17α-methyltrienolone.

involve the N/C interaction, androgen dissociation rates, and coactivator recruitment.

EXPERIMENTAL PROCEDURES

Plasmids—pCMVhAR vectors expressing full-length human AR with the following mutations were described: I737T and F725L (10, 19); V889M (20); E897K and I898T (10); K720A (4, 10); H874Y (21); and T877A (22). Other vectors used were as follows: VP-AR-(1–660) (11, 14); transcriptional intermediary factor 2 (TIF2)-AR fusion protein TIF2(L*XX*LL)$_3$AR-(172–919) (18); pSG5-TIF2 and VP-TIF2-(624–1287) (VP-TIF2.1) (23); wild-type and mutant pcDNA3-AR-(624–919) (10, 14); and 5XGAL4Luc3 (16). GST-SRC1-IV (GST-SRC1-(1139–1441)) was created by digesting GAL-SRC1-(1139–1441) with XbaI (blunt-ended) and BamHI, and the fragment was subcloned into pGEX-3X digested with EcoRI (blunt-ended) and BamHI. GST-AR-(4–52) (GST-AR-F*XX*LF) was created by PCR amplifying pACT2-AR-(4–52), digesting the fragment with EcoRI and XhoI, and subcloning into pGEX-4T-1 digested with the same enzymes. AIS and prostate cancer mutations were introduced into GAL-AR-(624–919) by PCR amplification of the corresponding mutant pCMVhAR and cloning the XbaI and NdeI fragments into GAL-AR-(624–919) digested with the same enzymes. pCMVhAR-(507–919) vectors (2) containing the indicated mutations were created by digesting full-length mutant pCMVhAR with KpnI and BamHI and cloning the fragment into pCMV5 digested with the same enzymes. pCMVhAR vectors containing AIS mutations G743V, Q733A, L712F, and V715M were created using a double PCR strategy. TIF2(L*XX*LL)$_3$AR-(172–919)-A*XX*AA containing the V715M or H874Y mutation was constructed by digesting the corresponding pCMVhAR mutant with HindIII and XbaI. The fragments were subcloned into similarly digested TIF2(L*XX*LL)$_3$AR-(172–919)-A*XX*AA. TIF2(L*XX*LL)$_3$AR-(172–919)-A*XX*AA-T877A was created by digesting GAL-AR-(624–919)-T877A with Csp45I and XbaI and inserting the fragment into TIF2(L*XX*LL)$_3$AR-(172–919)-A*XX*AA digested with the same enzymes. TIF2(L*XX*AA)$_3$AR-(172–919) vectors containing V715M, H874Y, and T877A were created by digesting the corresponding pCMVhAR mutant with Csp45I and XbaI and inserting the fragment into similarly digested TIF2(L*XX*AA)$_3$AR-(172–919). All PCR amplified regions were verified by DNA sequencing.

Crystal Structure Analysis—Coordinates of the wild-type AR ligand binding domain bound with R1881 and either AR-(20–30)-F*XX*LF peptide RGAFQNLFQSV, TIF2 L*XX*LL peptide KENALLRYLLDKDD, or no peptide, Protein Data Bank (www.rcsb.org) access codes 1XOW, 2AO6, and 1XQ3, respectively (13), were examined with regard to the functional data from AR mutations in AIS and prostate cancer. The structures were viewed with QUANTA (Accelrys, Inc.) and rendered and annotated with PyMol version 0.98 (Delano Scientific, www.pymol.org) and Adobe Photoshop.

Cell Transfections—Transcriptional activities of wild-type and mutant full-length human AR (pCMVhAR) were determined in transient cotransfection assays. Monkey kidney CV1 cells were maintained in Dulbecco's modified Eagle's medium containing 10% bovine calf serum, 2 mM L-glutamine, 20 mM Hepes, pH 7.2, penicillin, and streptomycin. CV1 cells (4.2×10^5/6 cm dish) were plated in the same medium except containing 5% bovine calf serum, and the next day the cells were transfected with 0.1 μg of wild-type or mutant pCMVhAR and 5 μg of the PSA-Enh-Luc reporter (Michael Carey, University of California Los Angeles) (4). For the effects of SRC/p160 coactivators, pSG5-TRAM1 (2 μg DNA/6 cm dish) was included. After incubating with the calcium phosphate-DNA precipitate for 4 h at 37 °C, cells were shocked with 15% glycerol-containing medium, washed, and transferred to serum-free medium lacking phenol red in the absence and presence of the indicated steroids. Cells were incubated overnight and the next day placed in serum-free medium with and without the indicated hormones. The medium was exchanged and incubated for an additional 24 h at 37 °C with or without hormone. Cells were washed with phosphate-buffered saline and harvested in 0.5 ml of lysis buffer containing 25 mM Tris phosphate, pH 7.8, 2 mM EDTA, 1% Triton X-100. After 30 min rocking at room temperature, 100-μl aliquots were analyzed for luciferase activity using an automated LumiStar Galaxy (BMG Labtech) multiwell plate reader luminometer.

Two-hybrid interaction assays were performed using human epithelioid cervical carcinoma HeLa cells. HeLa cells were maintained in Eagle's minimum essential medium (Invitrogen) supplemented with 10% fetal bovine serum (Sigma), 2 mM L-glutamine, penicillin, and streptomycin. HeLa cells were plated in 12-well plates (5×10^4 cells/well) and transfected using Effectene (Qiagen) or FuGENE (Roche Applied Science) with 50 ng/well GAL-AR-(624–919), 50 ng/well VP-AR-(1–660), and 0.1 μg of 5XGAL4Luc3 reporter vector. For the Effectene procedure, the DNA transfection mixture contained 50 μl of transfection buffer (Qiagen), 1 μl of Enhancer, and 1 μl of Effectene per well (4). To each DNA mixture was added 0.4 ml of serum-containing medium, and 0.4 ml was added to each well containing 0.8 ml of fresh serum-containing medium. For the FuGENE transfection, 43 μl of serum-free medium and 0.6 μl of FuGENE were combined per well, and after a 15-min incubation with the DNA, 40 μl of the mixture was added per well. After 24 h, cells were washed, and serum-free medium (2 ml) lacking phenol red was added with and without the indicated steroids. Cells were incubated overnight, and 100 μl of the cell lysate was assayed for luciferase activity after harvesting in 0.25 ml of lysis buffer as described above. Transcription assays of AR activity were performed in HeLa cells as described above using per well of 12-well plates the following: 10 ng of wild-type or mutant pCMVhAR, 0.25 μg of PSA-Enh-Luc, in the absence and presence of 50 ng/well pSG5-TIF2.

In Vitro Binding Assays—Competitive binding and ligand dissociation studies were performed at 37 °C in whole cell binding assays by plating 4×10^5 COS cells/well of 6-well plates and transfecting 1 μg of wild-type or mutant pCMVhAR or pCMVhAR-(507–919) per well using DEAE-dextran (4). Cells were incubated for 2 h at 37 °C in 0.6 ml of serum-free medium lacking phenol red and containing 5 nM [^{3}H]R1881 (17α-methyl-[^{3}H]methyltrienolone; 82 Ci/mmol), [1,2,4,5,6,7-^{3}H]dihydrotestosterone (DHT, 124 Ci/mmol), or [1,2,6,7-^{3}H]testosterone (78.5 Ci/mmol) (PerkinElmer Life Sciences). Nonspecific binding was determined by the addition of a 100-fold molar excess of unlabeled androgen. For competitive binding studies, increasing concentrations of unlabeled ligands were added during the 2-h incubation. For ligand dissociation studies, unlabeled androgen was added to the labeling media in 0.1 ml of medium to a final concentration of 50 μM, and ligand dissociation at 37 °C was terminated at increasing time intervals up to 2.5 h. Cells were washed with phosphate-buffered saline, and total bound radioactivity was determined by lysing cells in 0.5 ml of 2% SDS, 10% glycerol, and 20 mM Tris, pH 6.8. Dissociation half-times were determined as the mean ± S.E. of the time required to reduce specific androgen binding activity by 50%.

Equilibrium binding constants were determined by transfecting 2×10^5 COS cells/well of 12-well plates with 0.05 μg of wild-type and mutant pCMVhAR expression vector DNA using DEAE-dextran. Cells were incubated with 0.1, 0.2, 0.4, 0.8, 1.5, and 3 nM [^{3}H]R1881 in the absence and presence of a 100-fold molar excess of unlabeled R1881 to assess nonspecific binding. Free [^{3}H]R1881 was determined after the 2-h incubation by counting an aliquot of the medium. Cells were washed and harvested, and radioactivity was determined. In the *in vitro*

TABLE 1

[^{3}H]R1881 dissociation and affinity constants from AR AF2 mutants

Helix position in the ligand binding domain is indicated for AR AIS and charge clamp mutations. AIS grade is based on a 1–7 scale where grade 1 is mild AIS, and grades 6 and 7 are complete AIS (9). Half-times ($t_{½}$ in min) of [^{3}H]R1881 dissociation were determined at 37 °C in COS cells for full-length wild-type and mutant AR-(1–919) and AR DNA and ligand binding domain fragment AR-(507–919). Equilibrium binding affinities (K_d, nM) for full-length wild-type and mutant AR were determined by Scatchard plot analysis. Shown are the means ± S.E. determined from at least three independent assays. Nucleotide base changes are indicated for AR mutations in AIS. Diss indicates dissociation.

	Helix	AIS grade	Full-length AR		AR-(507–919), Diss $t_{½}$ min	Codon change	Ref.
			Diss $t_{½}$ min	K_d			
				nM			
AR-WT			107 ± 5	0.40 ± 0.20	33 ± 9		
F725L	3/4 loop	3–5	86 ± 5	0.82 ± 0.32	31 ± 2	TTC→CTC	10, 19
I737T	4	1–3	81 ± 3	0.44 ± 0.20	38 ± 0	ATT→ACT	10, 19
G743V	5	4–5	58 ± 6	0.16 ± 0.06	19 ± 3	GGG→GTG	76–78
Q733H	4	3–4	34 ± 3	0.30 ± 0.30	30 ± 4	CAG→CAT	79, 80
L712F	3	3	26 ± 3	0.42 ± 0.17	20 ± 1	CTT→GTT	81
I898T	12	6	21 ± 2	0.34 ± 0.02	6 ± 2	ATT→ACT	10, 80
V889M	11/12 loop	6	9 ± 1	0.46 ± 0.25	4 ± 2	GTG→ATG	82–86
K720A	3		101 ± 14	0.54 ± 0.15	27 ± 4		
E897K	12		38 ± 4	0.52 ± 0.18	34 ± 5		

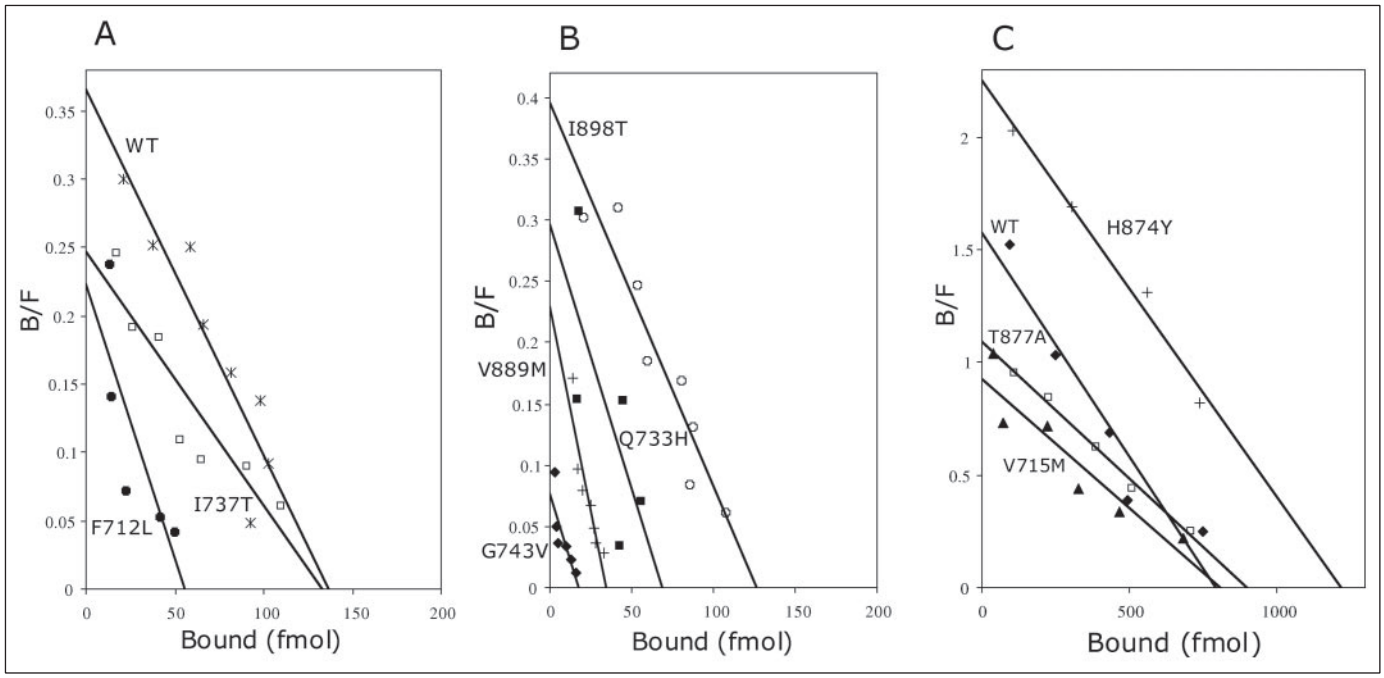

FIGURE 1. **Scatchard plots of [^{3}H]R1881 binding to wild-type AR and AR AIS and prostate cancer mutants.** Equilibrium androgen binding affinities were determined at 37 °C in cultured COS cells transiently expressing wild-type (*WT*) and mutant AR as described under "Experimental Procedures." *A* and *B*, representative data are shown for full-length WT AR and AR AIS mutants I737T, F712L, I898T, Q733H, V889M, and G743V. *C*, representative data are shown for full-length WT AR and AR prostate cancer mutants H874Y, T877A, and V715M. Apparent equilibrium androgen binding affinities (see Table 1) were determined from the means of at least three independent experiments. *B/F*, bound/free.

affinity matrix binding assays, GST fusion proteins were expressed, isolated, and incubated with [^{35}S]methionine-labeled AR ligand binding domain residues 624–919 as described (10, 14).

Degradation Assays—Wild-type and V715M, H874Y, or T877A pCMVhAR (10 μg/10-cm dish) was expressed in COS cells (2×10^6/10-cm dish) plated in Dulbecco's modified Eagle's medium containing 10% bovine calf serum (Hyclone) and transfected using DEAE-dextran. After 24 h, transfected cells were placed in serum-free medium. 48 h from transfection, cells were incubated for 20 min at 37 °C in serum-free medium lacking phenol red and methionine. To the NEG-772 Easytag Express protein labeling mixture, L-[^{35}S]methionine (1175 Ci/mmol; PerkinElmer Life Sciences) was added at 80 μCi/dish, and cells were incubated for 20 min at 37 °C. The medium was changed to serum-free without phenol red and containing 2 mM cold methionine and 1 nM testosterone, and cells were incubated for the indicated times. At each time point the medium was replaced on all plates. At the indicated times, cells were washed and harvested in phosphate-buffered saline and lysed in freshly prepared RIPA buffer (1 ml/dish) containing 1% Triton X-100, 1% deoxycholate, 0.1% SDS, 0.15 M NaCl, 5 mM EDTA, 50 mM Tris-HCl, pH 7.4, proteinase inhibitor mixture (Roche Applied Science), 1 mM dithiothreitol, and 1 mM phenylmethylsulfonyl fluoride (Sigma). Cell extracts were incubated with 25 μg of AR52 IgG antibody and 10 μl of protein A-agarose beads (Sigma) for 2 h at 4 °C. Affinity beads were centrifuged and washed with RIPA buffer, and protein was eluted in 50 μl of sample buffer containing 4% SDS, 20% glycerol, 0.2% 2-mercaptoethanol, and 20 mM Tris-HCl, pH 6.8, and separated on 10% acrylamide gels containing SDS. The gel proteins were transferred to nitrocellulose membranes and exposed to x-ray film. Degradation half-times were determined from semi-logarithmic plots of optical density of the scanned AR bands *versus* time and are expressed as the mean half-time and standard error to reduce AR levels by 50% from three independent experiments.

RESULTS

Rapid Dissociation of Bound Androgen Correlates with Reduced AR Activity in Vivo—The relationship between androgen dissociation rate and AR functional activity was investigated by characterizing naturally occurring ligand binding domain germ line mutations in AF2 and flanking regions that cause partial or complete AIS. AR mutations L712F, F725L, Q733H, I737T, G743V, V889M, and I898T result from single base changes in the coding sequence. Equilibrium binding affinities (K_d) for [^{3}H]R1881 (a synthetic androgen) were similar to that of wild-type AR (Table 1). Representative Scatchard plot analysis of the AR AIS mutants is shown in Fig. 1, *A* and *B*. On an AIS grading scale of 1–7 (9), the 46,XY genetic males had phenotypes that ranged from the mildest grade 1 with normal male external genitalia and gynecomastia (I737T), moderate grades 3–5 with ambiguous genitalia (F725L, I737T, G743V, Q733H, and L712F), and complete AIS grade 6 with external female phenotype (I898T and V889M) (9).

The dissociation half-time ($t_{½}$) of [^{3}H]R1881 for full-length wild-type AR expressed in COS cells at 37 °C was 107 min (Table 1). More rapid androgen dissociation was observed for AR with mutations F725L and I737T ($t_{½}$ = 81–86 min), G743V, Q733H, and L712F ($t_{½}$ = 26–58 min), and I898T and V889M ($t_{½}$ = 9–21 min) (Fig. 2*A*). Mean half-times of [^{3}H]R1881 dissociation (Table 1) suggest that faster androgen dissociation correlates with a more severe AIS phenotype. By comparison, AF2 charge clamp mutation K720A did not alter androgen dissociation, whereas E897K caused more rapid androgen dissociation. Neither charge clamp mutation has been reported in AIS.

Androgen dissociation rates were also measured for AR-(507–919), an AR DNA and ligand binding domain fragment that lacks the NH_2-terminal region. Androgen dissociation from AR-(507–919) ($t_{½}$ = 33 min) is ~3 times faster than from full-length AR (Table 1), reflecting the absence of the N/C interaction (14). Apparent equilibrium binding affinity of AR-(507–919) for [^{3}H]R1881 is nevertheless similar to that of wild-type full-length AR (20). Naturally occurring mutations can therefore alter androgen dissociation kinetics through different mechanisms. Mutations in AF2 can directly interfere with F*XX*LF motif binding in the N/C interaction, alter a ligand entry and exit gateway, or have indirect effects through structural changes in AF2 and the ligand binding pocket. Studies using AR-(507–919) allowed us to distinguish these possibilities.

Androgen dissociation from AR-(507–919) containing F725L, I737T, or Q733H ($t_{½}$ = 30–38 min) was similar to that of wild-type AR-(507–919) (Fig. 2*B* and Table 1), indicating this subgroup of AR mutations in AIS does not directly alter ligand entry or exit from the binding pocket. AR-(507–919) containing G743V or L712F increased androgen dissociation ($t_{½}$ = 19–20 min), and I898T and V889M caused the most rapid rates of androgen dissociation ($t_{½}$= 4–6 min) (Fig. 2*B* and Table 1) (10).

The results suggest that F725L, I737T, and Q733H located in helices 3–5 alter ligand dissociation indirectly in the ligand binding pocket through changes at the AF2 surface that interfere with the N/C interaction. This subgroup of mutations cause partial AIS with phenotypic variation (Table 1). The rapid androgen dissociation rate of AR-(507–919) I898T suggests AF2 residue Ile-898 also impacts the ligand binding pocket from the AF2 surface. The fast androgen dissociation caused by V889M in the 11/12 loop at the base of helix 12 outside the ligand binding pocket suggests Val-889 is involved as gatekeeper for ligand entry and exit. Both I898T and V889M caused grade 6 complete AIS.

AR AF2 Mutations That Cause AIS Interfere with AR FXXLF and Coactivator LXXLL Motif Binding—A mammalian two-hybrid assay revealed that these AR AIS AF2 mutations inhibited F*XX*LF and L*XX*LL binding to a similar extent. GAL-AR-(624–919) containing the AR ligand binding domain was coexpressed with VP-AR-(1–660) containing AR NH_2-terminal F*XX*LF motif sequence ^{23}FQNLF^{27} (Fig. 3*A*) or VP-TIF2-(624–1287) containing the three L*XX*LL motif regions of TIF2 (Fig. 3*B*). Relative to the wild-type AR ligand binding domain interaction, only 5–30% luciferase activity remained for the AIS mutants in the presence of 0.1 and 1 nM DHT. Similarly, charge clamp mutation

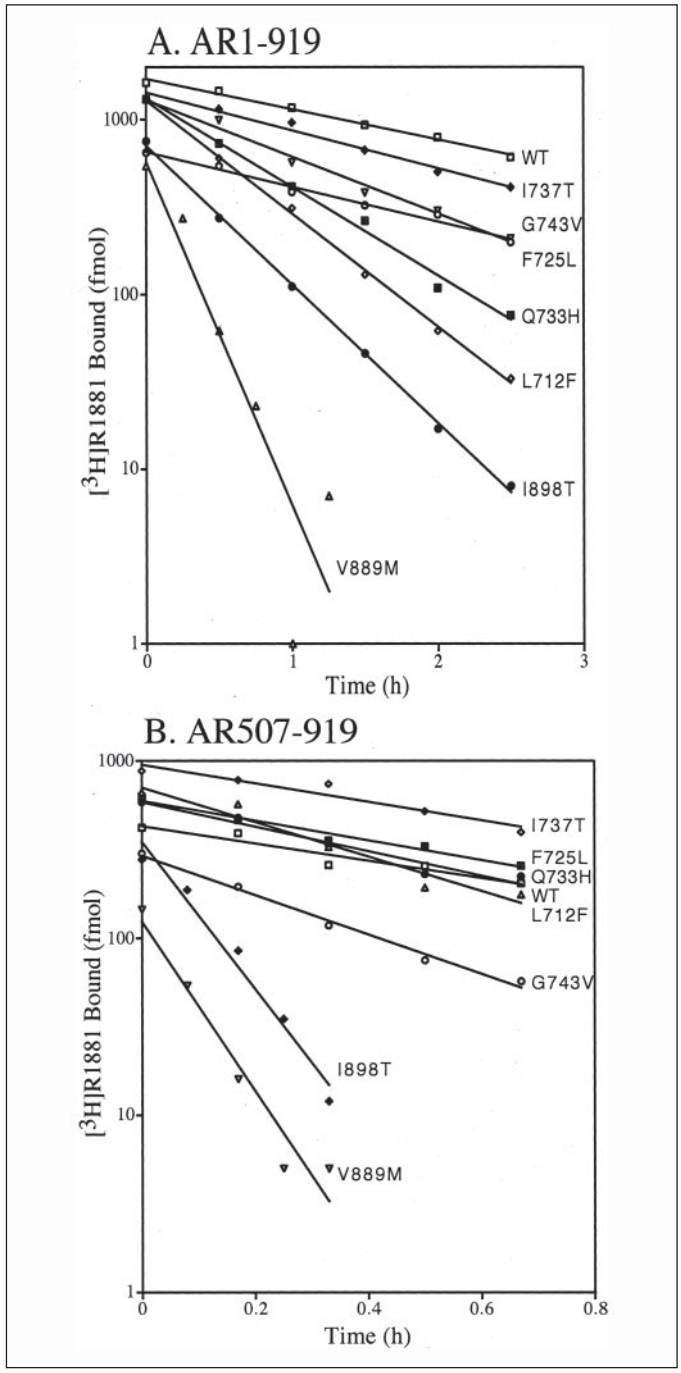

FIGURE 2. **Increased androgen dissociation of AR AIS mutations.** Dissociation rates of [^{3}H]R1881 were measured at 37 °C in cultured COS cells transiently expressing wild-type (*WT*) and mutant AR and AR-(507–919) as described under "Experimental Procedures." *A*, representative data are shown as indicated for full-length WT AR (AR-(1–919)) and AR AIS mutants I737T, G743V, F725L, Q733H, L712F, I898T, and V889M. *B*, representative data are shown as indicated for AR-(507–919), a DNA and ligand binding domain fragment, with WT sequence and AR-(507–919) mutants I737T, F725L, Q733H, L712F, G743V, I898T, and V889M. Dissociation half-times (see Table 1) were calculated from three independent experiments and are the mean times required for 50% reduction in binding activity.

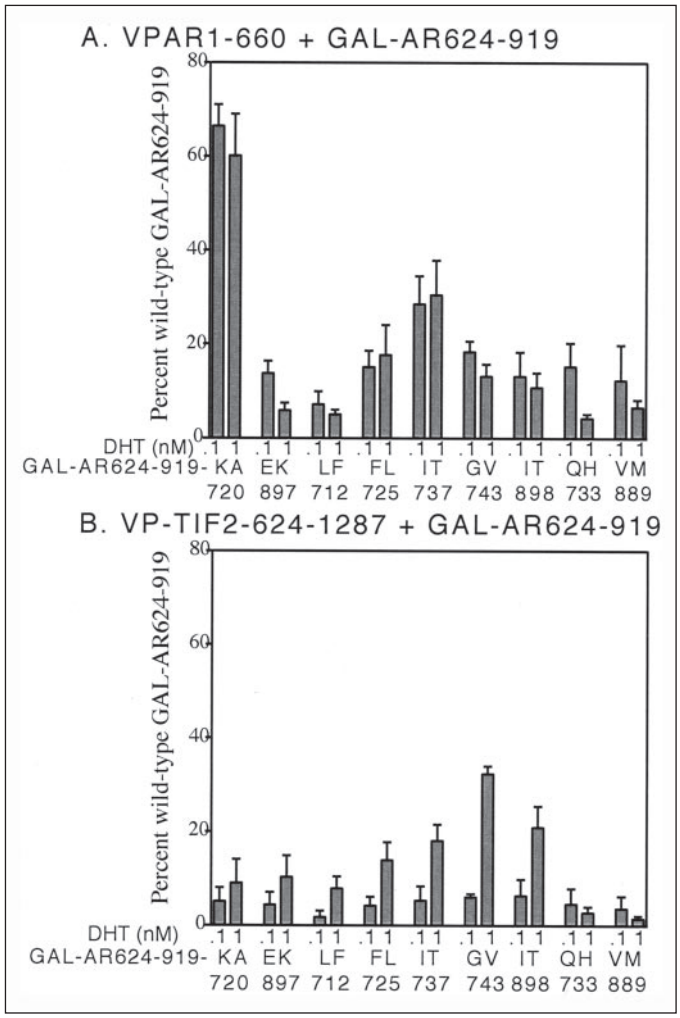

FIGURE 3. **Effect of AIS and charge clamp mutations on AR F*XX*LF and TIF2 L*XX*LL motif binding to AF2 in the AR ligand binding domain.** In two-hybrid interaction assays, HeLa cells (50,000 cells/well of 12-well plates) were transfected using Effectene or FuGENE with 0.1 μg/well 5XGAL4Luc reporter vector. *A*, VP-AR-(1–660) (50 ng/well) containing the VP16 transactivation domain and AR NH_2-terminal and DNA binding domain residues 1–660 was transfected with the indicated GAL-AR-(624–919) mutants (50 ng/well) containing the AR ligand binding domain with wild-type sequence or the indicated mutation. *B*, VP-TIF2-(624–1287) (50 ng/well) containing the VP16 transactivation domain and the TIF2-(624–1287) three L*XX*LL motif region was transfected with the indicated GAL-AR-(624–919) mutants (50 ng/well). Transfected cells were incubated for 24 h in the absence and presence of 0.1 and 1 nM DHT. Shown is the mean percent activity and error of the GAL-AR-(624–929) mutants compared with the activity of wild-type GAL-AR-(624–929) from at least four independent measurements.

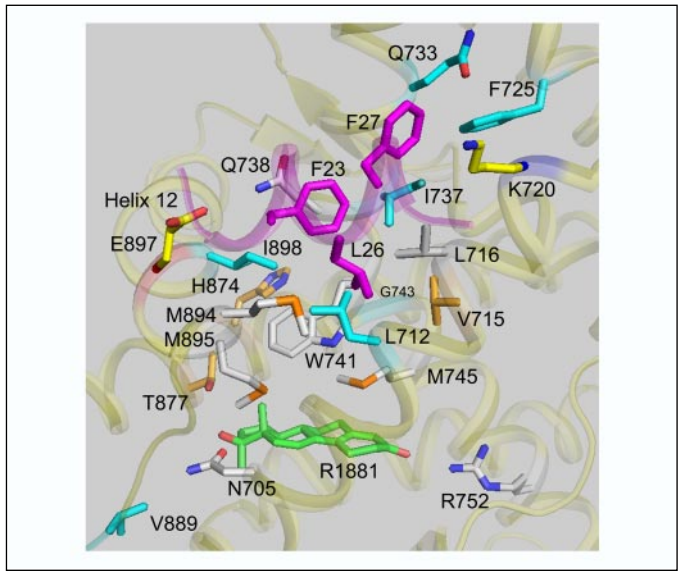

FIGURE 4. **Wild-type AF2 and ligand binding pocket region of the AR ligand binding domain bound with R1881 and AR-(20–30) F*XX*LF peptide (Protein Data Bank access code 1XOW).** Ribbon rendering is used to represent the ligand binding domain (translucent *yellow* backbone) and AR F*XX*LF peptide ^{20}RGAFQNLFQSV^{30} (translucent *magenta* backbone with opaque *magenta* side chains for Phe-23, Leu-26, and Phe-27). Wild-type AR side chains altered in AIS (*cyan*) and prostate cancer (*orange*) are illustrated along with charge clamp residues Glu-897 (translucent *red* backbone, *yellow* side chain, and *red* oxygen) and Lys-720 (translucent *blue* backbone, *yellow* side chain, and *blue* nitrogen), ligand binding pocket residues Asn-705, Trp-741, Met-745, Arg-752 (*gray* side chains, *blue* nitrogen, *red* oxygen, and *orange* sulfur), and R1881 (*green* carbon and *red* oxygen).

E897K disrupted both F*XX*LF and L*XX*LL motif binding, whereas K720A selectively inhibited L*XX*LL motif binding.

Structure Analysis and Predictions for AR Mutations in AIS—Cocrystal structures of the R1881-AR ligand binding domain complex bound to the F*XX*LF or L*XX*LL motif peptide demonstrated similar yet distinctive properties (13). The sites of 5 of the 7 residues mutated in AIS lie in close proximity to the bound F*XX*LF peptide (*magenta* in Fig. 4 and 5) or L*XX*LL peptide (not shown). Interatomic distances between wild-type residues mutated in AIS (*cyan* in Figs. 4 and 5) and the bound F*XX*LF or L*XX*LL peptide motifs are summarized in Table 2.

Our structural analysis began with mutations near the Phe-23 $i + 1$ residue of F*XX*LF that cause a spectrum of AIS phenotypes (Table 1), where $i + 1$ to $i + 5$ designate residues of the F*XX*LF and L*XX*LL motifs. AF2 residues Leu-712 (helix 3, H3), Ile-737 (H4), and Ile-898 (H12) form a close hydrophobic cluster (designated AIS group 1) proximal to $i + 1$ nearest the ligand binding pocket (Figs. 4 and 5*A*). AIS group 1 mutations weakened motif binding and caused faster androgen dissociation kinetics, both of which interfere with AR activity *in vivo* as evidenced by the AIS phenotype.

L712F in helix 3 increased androgen dissociation from full-length AR, with a half-time similar to that of AR-(507–919) with the same mutation. This suggests the principal effect of L712F is to disrupt favorable F*XX*LF motif binding to AF2, with secondary effects in the ligand binding region. Leu-712 is 4.1 Å from Phe-23 and 3.6 Å from a prominent helix 5 residue Trp-741[4] situated above and close to the B-, C-, and D-rings of R1881 (Fig. 5*A*). Leu-712 is surrounded by hydrophobic residues $i + 4$ Leu-26, Val-716 (H3), Ile-737 (H4), and Met-894 (H12). Introduction of the large phenylalanine side chain by L712F potentially disrupts F*XX*LF motif binding by directly altering favorable hydrophobic packing and contacts to Phe-23 and Leu-26, thereby weakening the protection of bound ligand afforded by the N/C interaction. L712F may also influence Met-894, a residue adjacent to helix 12 residues Met-895, Glu-897, and Ile-898, and reduce a stabilizing effect of helix 12 on the bound ligand. Unfavorable interactions between L712F and Trp-741 independent of the N/C interaction may account for the moderately faster ligand dissociation from AR-(507–919) L712F.

In contrast, I898T in helix 12 caused complete AIS and rapid androgen dissociation from full-length AR and AR-(507–919). Ile-898 is 4.4 Å from Phe-23 of the bound peptide, 5.3 Å from Trp-741, and is surrounded by Leu-712 (H3), Gln-738 (H4), Met-895 (H12), and Gln-902 (H12). I898T introduces a polar side chain near residue Gln-738, a side

[4] From our original report (13), a recent report (75), and as shown here, the absence of a C-19 methyl group in R1881 allows the Trp-741 and Met-745 side chains to adopt a conformation that differs from previously reported AR structures bound with DHT that has the C-19 methyl (34, 38). In more recent refinements not detailed here, we found our R1881 crystallographic data to be most consistent with the Trp-741 side chain conformed in roughly equal occupancy with one rotamer very similar to that shown here with R1881 and the other similar to that seen with DHT. This further supports the ligand-dependent dynamic properties of Trp-741 in the ligand binding pocket.

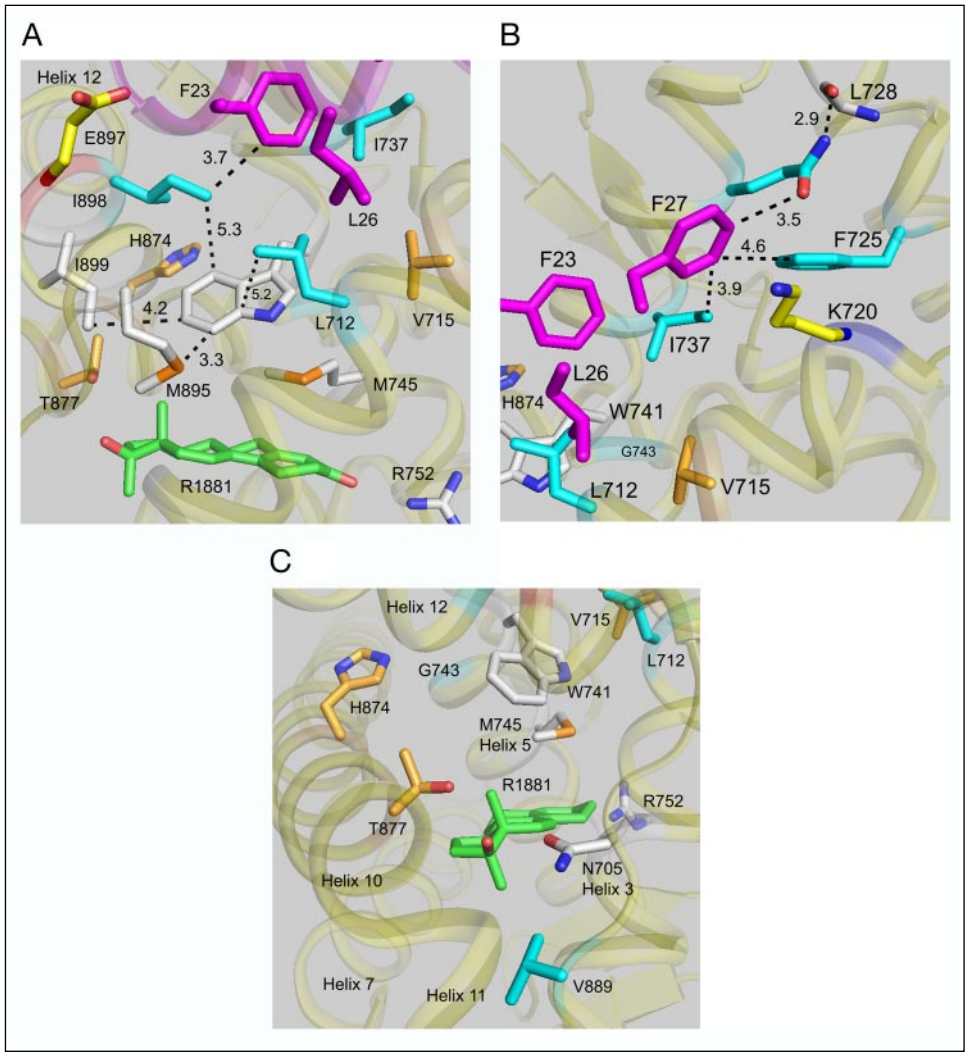

FIGURE 5. **Close up views of wild-type AR AF2 and ligand binding pocket bound with R1881 and AR-(20–30) F*XX*LF peptide (color scheme from Fig. 4).** *A,* wild-type residue side chains for group 1 AIS mutations L712F, I737T, and I898T near $i + 1$ Phe-23 of the ^{23}FQNLF^{27} motif. Leu-712 and Ile-898 are proximal to Trp-741, whereas the more distal Ile-737 lies between Phe-23 and Phe-27 as seen in *B*. Intermolecular distances (Å, *dashed black lines*) are indicated between Trp-741 to Ile-898, Leu-712, Met-895, and Ile-899. *B,* wild-type residue side chains for group 2 AIS mutations F725L, Q733H, and I737T near the $i + 5$ Phe-27 of the ^{23}FQNLF^{27} motif. Phe-725 and Gln-733 are located near the Lys-720 and the carboxyl-terminal end of the F*XX*LF motif, whereas Ile-737 is centered between Phe-23 and Phe-27. *C,* wild-type residue side chains for AIS mutants G743V and V889M. Gly-743 resides in helix 5 close to Trp-741 in the ligand binding pocket core. Val-889 in the helix 11–12 linker may serve a gatekeeper function in a possible ligand gateway near helices 3, 6, 11, and 12.

chain in wild-type AR that rearranges to stack against Phe-23 upon binding the F*XX*LF motif. I898T may contribute to a hydrogen bonding network involving side chains from Gln-738, Gln-902, and Lys-905 (H12) as evident in the peptide-free structure (13). This contribution may influence the helix 12 equilibrium to favor an unbound AF2 with reduced motif binding affinity and thus shorten the lifetime of the bound ligand. Alternatively, I898T may simply disrupt favorable hydrophobic contacts in the region by presenting too much polarity in the region near Phe-23.

In I737T, threonine again replaces isoleucine. However, I737T is less disruptive than I898T based on androgen dissociation kinetics and the AIS phenotype. Unlike Ile-898 and Leu-712, Ile-737 is centered between $i + 1$ and $i + 5$ (3.7 Å from Phe-23 and 3.9 Å from Phe-27) and more distant (6.4 Å) from Trp-741 in the ligand binding pocket compared with Leu-712 (3.6 Å) and Ile-898 (4.2 Å) (Table 2 and Fig. 5, *A* and *B*). I737T in helix 4 introduces a polar side chain into a richly hydrophobic region comprised of Leu-712, Val-715, Val-716, Ala-719, Phe-725, Val-736, Leu-812, Ile-898, and the $i + 1$ Phe-23 and $i + 5$ Phe-27 residues. The near wild-type ligand dissociation half-time for AR-(507–919) I737T but the faster dissociation half-time for full-length AR I737T compared with wild-type AR suggests that I737T interferes with F*XX*LF motif binding at the $i + 1$ and $i + 5$ sites by disrupting local hydrophobic interactions with adjacent AF2 residues rather than greatly disturbing residues in the ligand binding domain interior.

A second AF2 hydrophobic center (designated AIS group 2) is comprised of residues Phe-725 (H3′), Gln-733 (H4), and Ile-737 (H4) from AIS group 1. These residues reside within 4.6 Å of $i + 5$ of either bound peptide near the Lys-720 charge clamp (Figs. 4 and 5*B*), and Gln-733 and Phe-725 are more remote to the ligand-binding site than is Ile-737. AIS group 2 mutations account for reduced motif binding and shorter androgen dissociation half-time, both of which interfere with AR activity *in vivo* evidenced by the AIS phenotype. AR F725L and I737T modestly shortened the R1881 dissociation half-time compared with Q733H. The greater effect of Q733H may arise from a change in the 3 Å hydrogen bond contributed by Gln-733 N-ϵ2 to the Leu-728 backbone carbonyl, as well as the introduction of the polar aromatic imidazole side chain near $i + 5$ Phe-27 and Phe-725 (Fig. 5*B*). F725L preserves the hydrophobic character of the region, even though a large planar phenyl ring is replaced by the smaller branched leucine side chain that would alter the shape complementarity and regional hydrophobic contacts between Phe-725 and the $i + 5$ site. Given their close proximity to $i + 5$ and remote location to the ligand binding pocket and near wild-type ligand dissociation rate of AR-(507–919), AIS mutations F725L and Q733H most likely decrease androgen retention times by directly interfering with F*XX*LF motif binding in the $i + 5$ region.

The remaining two AIS mutations, G743V and V889M, respectively, cause moderately severe and complete AIS in correlation with the ligand dissociation kinetics in Table 1. Gly-743 in helix 5 located just

outside AF2 in the hydrophobic core near Trp-741, Met-745, and the ligand binding pocket (Fig. 5*C*) faces Val-866 in helix 10 and is surrounded by Met-742 (H5), Val-746 (H5), Leu-811 (H8), Val-866 (H10), Gln-867 (H10), and Ala-870 (H10). The 2-fold more rapid androgen dissociation half-time caused by G743V in full-length AR suggests destabilization of the ligand binding pocket and interference with ligand-dependent F*XX*LF motif binding. Replacing a flexible glycine with valine may render helix 5 too rigid to allow neighboring core residues to adjust and contact the ligand optimally or it may simply destabilize the helix 5 coil and/or key packing interactions near helices 10 and 11.

Ligand trafficking through an opening assembled by the NH_2 terminus of helix 3, helix 11, the 11–12 linker, and AF2 helix 12 was supported by the effects of V889M, a mutation that caused complete AIS. Val-889 lies in the linker region preceding the AF2 helix 12 distant from AF2 and the bound peptide motif (Fig. 4 and Fig. 5*C* and Table 2). Val-889 is near the ligand binding pocket, ~6 Å from D-ring substituents of the bound ligand and 3.5 Å from Asn-705, a residue that hydrogen bonds with the ligand C-17 hydroxyl group and is adjacent to Phe-876 (H10), Phe-891, Leu-880 (H11), Leu-701 (H3), and Phe-697 (H3). Methionine residues are notable for their flexible and accommodating side chain. However, in this case it appears that the longer side chain and large sulfur atom of V889M disturbs the largely hydrophobic region and destabilizes the linker region and equilibrium position of the AF2 helix 12. A key interaction between Asn-705 and the steroid D-ring may also be disrupted and reduce the lifetime of the bound ligand without significantly altering the equilibrium binding constant.

TABLE 2

Interatomic distances (in Å) between bound AR FXXLF peptide, TIF2 LXXLL peptide, and AR Trp-741 to AR ligand binding domain residues

Interatomic distances (Å) are from the AR F*XX*LF peptide, the TIF2 third L*XX*LL peptide, or AR Trp-741 to the indicated ligand binding domain atoms. The first residue of the F*XX*LF or L*XX*LL motif is $i + 1$. Atom designations adhere to standard IUPAC nomenclature.

AR ^{23}FXXLF^{27}		i+1			i+4			i+5			AR ^{741}W		
	AR LBD atom	F23	Å	LBD	L26	Å	LBD	F27	Å	LBD	W741	Å	LBD
Androgen Insensitivity Syndrome	F725	CZ	8.0	CZ	CD2	11.9	CE2	CE1	4.6	CE2	CG	12.7	CE1
	Q733	CE1	7.7	CB	CG	12.4	CB	CZ	3.5	OE1	CG	16.4	CD
	I737	CZ	3.7	CG2	CD2	7.5	CG2	CE1	3.9	CD1	CG	6.4	CG2
	L712	CE2	4.1	CE1	CD2	4.6	CG	CD1	8.8	CD1	CD1	3.6	CD1
	I898	CD1	3.7	CD1	CD2	7.2	CD1	CB	9.3	CD1	CE3	4.2	CG2
	V889	CD2	19.0	CG1	CD2	19.4	CG1	CB	24.2	CG1	CH2	11.6	CG1
	G743	CE2	13.7	CA	CD2	16.4	CA	CD1	17.1	CA	CD1	8.0	CA
Charge clamp	K720	CZ	7.7	CD	CG	7.9	CD	CE1	3.8	CD	CG	15.3	CE
								O	2.7	NZ			
	E897	CB	4.6	CD	CB	9.0	CD	CB	10.7	CD	CZ3	11.0	CD
		N	3.2	OE2									
Prostate Cancer	V715	CE2	7.8	CB	CD2	8.0	CB	CG	10.7	CB	CD1	5.2	CG2
	H874	CE2	12.3	NE2	CD2	15.8	NE2	CD1	16.7	NE	CE3	5.5	CD2
	T877	CD2	14.6	CG2	CD2	15.8	NE2	CD1	16.7	NE2	CZ3	5.3	CG2

TIF2 ^{736}LXXLL^{740}		i+1			i+4			i+5			AR ^{741}W		
	AR LBD atom	L745	Å	LBD	L748	Å	LBD	L749	Å	LBD	W741	Å	LBD
Androgen Insensitivity Syndrome	F725	CD2	9.3	CZ	CB	10.6	CE2	CD1	4.3	CE2	CG	12.3	CZ
	Q733	CD2	8.5	CB	CB	11.0	CB	CD2	3.7	OE1	CG	15.7	CD
	I737	CD1	4.8	CG2	CB	8.0	CD1	CD1	4.0	CD1	CG	6.2	CG2
	L712	CD1	4.5	CD1	CD1	6.1	CG	CD1	9.5	CD1	CD1	3.9	CD1
	I898	CD2	4.7	CD1	CD1	9.0	CD1	CD2	11.2	CD1	CZ3	4.1	CG2
	V889	CD1	19.6	CG1	CD1	19.9	CG1	CB	25.6	CG1	CH2	11.7	CG1
	G743	CD2	14.9	CA	CD1	17.9	CA	CD1 1	17.4	CA	CG	7.4	CA
Charge clamp	K720	CD1	8.8	CD	CB	6.4	CD	CD1	3.9	CD	CG	15.6	CE
					O	3.0	NZ	O	2.9	NZ			
	E897	CB	7.4	CD	CD1	12.0	CD	CB	14.0	CD	CZ3	11.4	CD
Prostate Cancer	V715	CD1	7.9	CB	CD1	9.0	CB	CD1	9.4	CB	CD1	4.8	CG2
	H874	CD2	12.7	NE2	CD1	12.3	NE2	CD1	17.7	NE2	CE3	5.9	CD2
	T877	CD2	12.7	CG2	CD1	17.2	OG1	CD1	20.8	CG2	CZ3	5.9	CG2

AR Mutations in Prostate Cancer Slow Androgen Dissociation—Several somatic mutations in prostate cancer occur in the AR AF2 and ligand binding region (24). These include V715M (25), H874Y (21, 26), T877A (22, 27), V730M (25, 28), and R726L (29). These prostate cancer mutations result from single base changes and do not significantly alter the apparent equilibrium binding affinity of [^{3}H]R1881 (Fig. 1*C* and Table 3). Valines 715 and 730 are in the hydrophobic core of AF2; Arg-726 is in the positive charge cluster flanking AF2 (4), and His-874 and Thr-877 are in helix 10 adjacent to AF2 helix 12. Neither V730M nor R726L change the androgen dissociation rate, and no difference from wild-type AR was observed for AR R726L in two-hybrid assays of motif binding (data not shown). R726L was identified as a germ line mutation in the Finnish population (29, 30) and lacks a strict clinical correlation with prostate cancer. V730M selectively increases SRC1 L*XX*LL motif binding (13).

Remarkably, three AR mutations in prostate cancer, V715M, H874Y, and T877A, slowed the dissociation rate of bound androgen relative to wild-type AR (Fig. 6*A*). The half-times of [^{3}H]R1881 dissociation increased 2-fold from $t_{½}$ = 107 min for wild-type AR to $t_{½}$ = 207–212 min for AR V715M, H874Y, and T877A (Table 3). Longer dissociation half-times of [^{3}H]DHT and [^{3}H]testosterone were also observed. Testosterone dissociation from AR H874Y was 4.5-fold slower than from wild-type AR. Normally testosterone dissociates ~3 times faster than DHT from full-length wild-type AR (Table 3) and is a weaker androgen *in vivo* (31).

The effects of the mutations were also evident in the absence of the N/C interaction because they slowed the dissociation of R1881 from AR-(507–919) (Fig. 6*B*). Dissociation half-times of [^{3}H]R1881 from AR-(507–919) containing V715M, H874Y, or T877A were ~2-fold longer ($t_{½}$ = 60–82 min) compared with the wild-type fragment ($t_{½}$ = 31 min) (Table 3). Other AR ligand binding domain mutations reported in prostate cancer retained high affinity equilibrium binding (8) but did not slow dissociation of [^{3}H]R1881. These included G750S ($t_{½}$ = 123 min), S782N ($t_{½}$ = 93 min), A896T ($t_{½}$ = 88 min), and L701H ($t_{½}$ = 28 min). Thus a slower androgen dissociation depends largely on the position of the mutation in the ligand binding domain.

TABLE 3

[^{3}H]Androgen dissociation and affinity constants for AR prostate cancer mutants

Helix position in the ligand binding domain is indicated for the sites of AR prostate cancer mutations. Half-times ($t_{½}$ in min) of [^{3}H]R1881, [^{3}H]DHT, and [^{3}H]testosterone (T) dissociation (Diss) were determined at 37 °C in COS cells for wild-type and mutant full-length AR (amino acid residues 1–919). [^{3}H]R1881 dissociation was determined for wild-type and mutant AR-(507–919). Equilibrium binding affinities (K_d, nM) of [^{3}H]R1881 for wild-type and mutant full-length AR were determined by Scatchard plot analysis. Binding constants are the mean ± S.E. from three independent assays. Nucleotide base changes are indicated for AR mutations in prostate cancer.

AR	Helix	Full-length AR				AR-(507–919), Diss $t_{½}$ min, R1881	Codon change
		Diss $t_{½}$ min			K_d, R1881		
		R1881	DHT	T			
					nM		
Wild-type		107 ± 5	206 ± 30	59 ± 3	0.40 ± 0.20	31 ± 3	
V715M	3	207 ± 43	298 ± 78	101 ± 5	0.79 ± 0.25	70 ± 8	GTG→ATG
H874Y	10	212 ± 53	324 ± 60	266 ± 15	0.56 ± 0.37	60 ± 7	CAT→TAT
T877A	10	208 ± 37	240 ± 48	143 ± 15	0.75 ± 0.30	82 ± 12	ACT→GCT

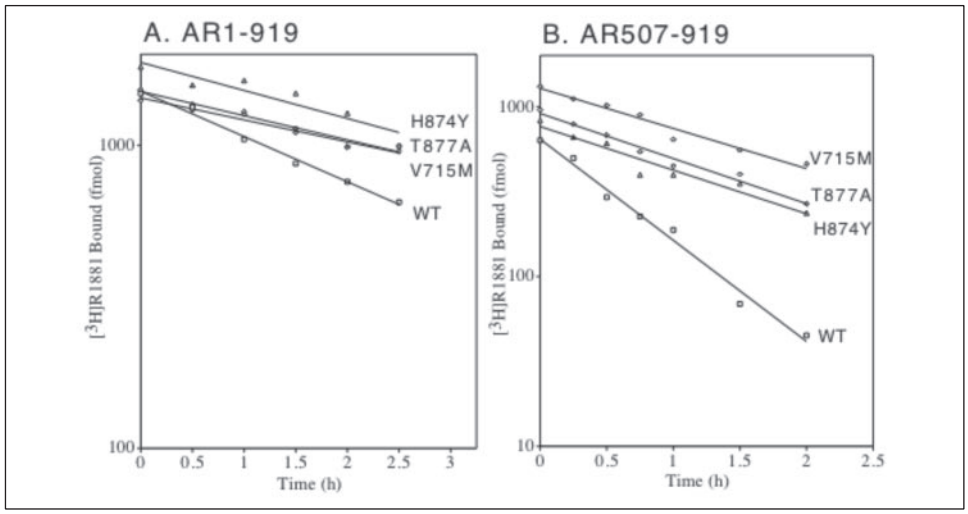

FIGURE 6. **Slower androgen dissociation of three AR prostate cancer mutants.** Dissociation rates of [^{3}H]R1881 were measured at 37 °C in cultured COS cells transiently expressing wild-type (*WT*) and mutant AR and AR-(507–919) as described under "Experimental Procedures." *A,* representative data are shown as indicated for full-length WT AR (AR-(1–919)) and AR AIS mutants H874Y, T877A, and V715M. *B,* representative data are shown as indicated for AR-(507–919) with WT sequence and AR-(507–919) mutants V715M, T877A, and H874Y. Dissociation half-times (see Table 3) were calculated from at least three independent experiments and are the mean times required for 50% reduction in binding activity.

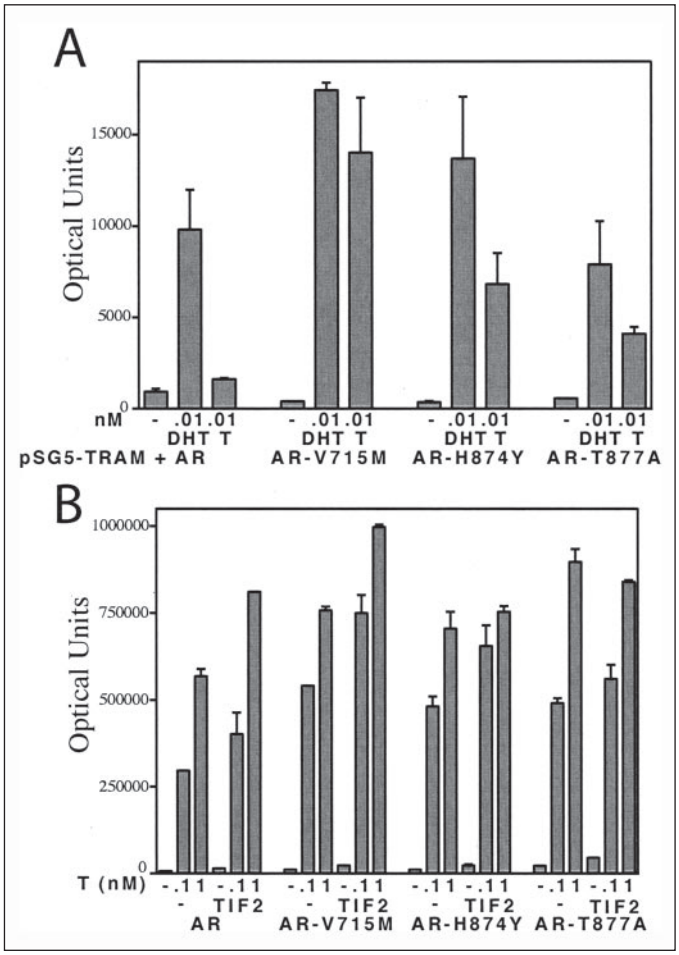

FIGURE 7. **Increased AR transactivation of AR prostate cancer mutants V715M, H874Y, and T877A.** *A,* CV1 cells (4.2×10^5/6-cm dish) were transfected using calcium phosphate DNA precipitation and per dish, 100 ng of pCMVhAR with wild-type or V715M, H874Y, or T877A mutant sequence, 2 μg of pSG5-TRAM1, and 5 μg of PSA-Enh-Luc. Transfected cells were incubated for 40 h in the absence and presence of 0.01 nM DHT or testosterone (*T*). *B,* HeLa cells (5×10^4/well of 12-well plates) were transfected using FuGENE by adding per well, 10 ng of pCMVhAR with wild-type or V715M, H874Y, or T877A mutant sequence, 0.25 μg of PSA-Enh-Luc, in the absence or presence of 50 ng of pSG5-TIF2. Transfected cells were incubated in the absence and presence of 0.1 and 1 nM testosterone (*T*), and luciferase activity was determined. Luciferase activities are representative of three independent experiments.

Increased AR Transcriptional Activity and Coactivator Recruitment—The effects of the prostate cancer mutations on AR transcriptional activity were determined in the absence and presence of SRC/p160 coactivator coexpression. With transient coexpression of p160 coactivator TRAM-1 in CV1 cells, AR V715M, H874Y, and T877A increased transcriptional activity relative to wild-type AR in response to 0.01 nM testosterone (Fig. 7*A*). Transcriptional activity was also greater with the more potent androgen DHT; however, the effects of the mutations were less evident in the presence of DHT. In the absence of transient coactivator expression or at higher levels of androgen, no major differences in AR transcriptional activity were observed in CV1 cells (data not shown). However, in HeLa cells that express higher endogenous levels of SRC/p160 coactivators (32), prostate cancer mutations V715M, H874Y, and T877A increased AR activity in the presence of testosterone (Fig. 7*B*). For AR V715M, transcriptional activity also increased with coexpression of TIF2. Increases in transcriptional activities of the three mutants over wild-type AR were noted in both cell lines in the presence of 1 nM 4-androstene-3,17-dione (data not shown).

The increase in AR transcriptional activity and slower dissociation of bound androgen by two of the mutants was associated with increased binding of the F*XX*LF or L*XX*LL motifs to the AR carboxyl-terminal region in GAL-AR-(624–919). In two-hybrid assays, V715M and H874Y increased F*XX*LF (Fig. 8*A*) and L*XX*LL (Fig. 9*A*) motif binding over that of the wild-type AR in the presence of DHT or testosterone. For the F*XX*LF motif in VP-AR-(1–660), greater increases in binding indicative of the AR N/C interaction were observed using 0.1 nM testosterone or DHT. For the L*XX*LL motif in VP-TIF2-(624–1287), increases in transcriptional activity were apparent in response to low levels of androgen. Increased F*XX*LF and L*XX*LL motif binding by the mutants relative to wild-type AR was also observed in response to the adrenal androgens, 4-androstene-3,17-dione and 5α-androstane-3α,17β-diol (Figs. 8*B* and 9*B*). However, no increase in motif binding was detected with AR T877A in the presence of these androgens (Figs. 8 and 9).

Competitive ligand binding assays confirmed that V715M, H874Y, and T877A did not alter AR binding affinity for R1881, DHT, testosterone, 4-androstene-3,17-dione, or 5α-androstane-3α,17β-diol (Fig. 10). However, as reported previously (21, 27), LNCaP cell line mutant AR T877A increased binding of hydroxyflutamide, estradiol, and progesterone (data not shown).

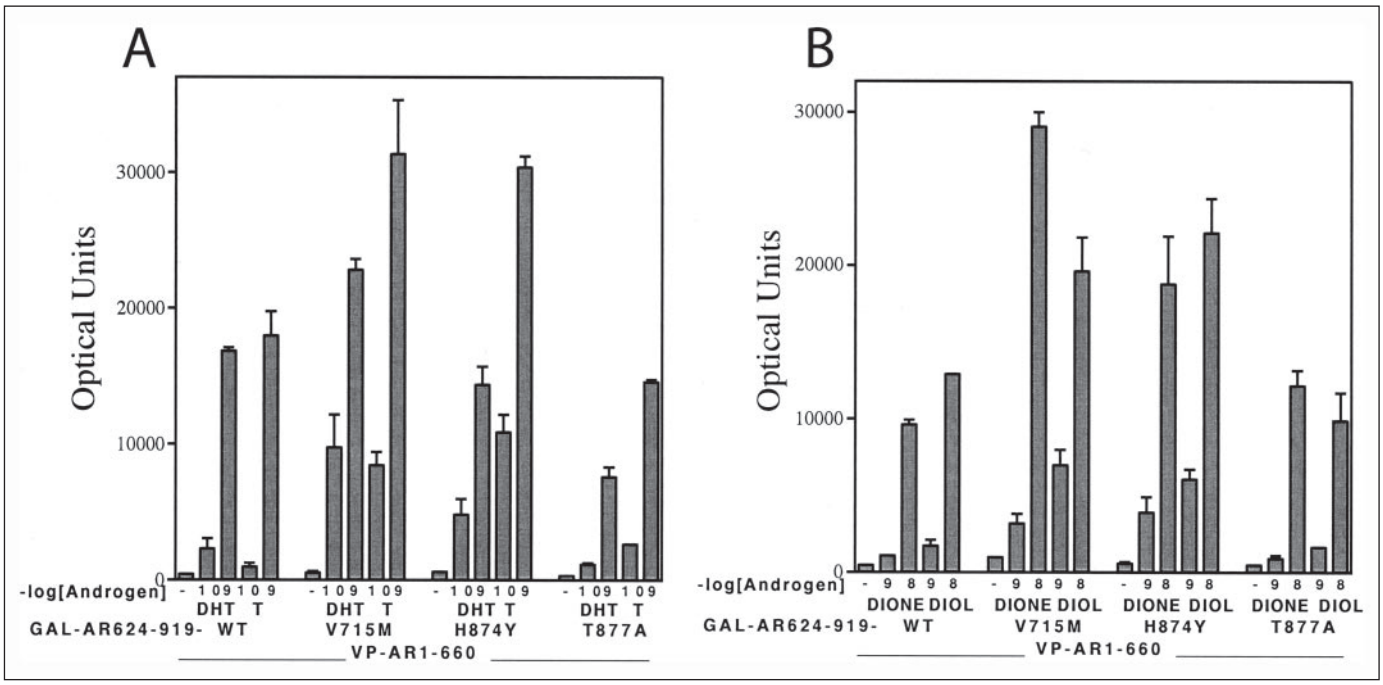

FIGURE 8. **Increase in AR F*XX*LF motif binding by prostate cancer mutations V715M and H874Y.** HeLa cells (5×10^5/well of 12-well plates) were transfected using FuGENE by adding per well, 0.1 μg of 5XGAL4Luc3, 50 ng of GAL-AR-(624–929) containing wild-type or V715M, H874Y, and T877A mutant AR ligand binding domain, and 50 ng of VP-AR-(1–660). Transfected cells were incubated for 24 h in the absence and presence of 0.1 and 1 nM DHT or testosterone (*T*) (*A*), and with 1 and 10 nM 4-androstene-3,17-dione (*DIONE*) or 5α-androstane-3α,17β-diol (*DIOL*) (*B*). Luciferase activity and error are representative of three independent experiments.

AR transcriptional activity can therefore increase as a result of AR mutations in prostate cancer through mechanisms that include increased F*XX*LF and L*XX*LL motif binding and slower dissociation rates of bound androgen. The absence of a prominent increase in F*XX*LF or L*XX*LL motif binding by T877A suggests it was the structural effects imposed by V715M and H874Y rather than the slow androgen dissociation rate *per se* that stabilized motif binding.

TIF2 LXXLL-AR Chimeras—Previously, we showed that the AR N/C interaction between the AR NH_2-terminal F*XX*LF motif and AF2 slows the dissociation of bound androgen. However, slower androgen dissociation does not occur in the presence of the L*XX*LL motif when AR was coexpressed with TIF2 (14) or in L*XX*LL-AR chimeras (18). Because the V715M and H874Y mutations increased AR F*XX*LF and TIF2 L*XX*LL motif binding to the AR carboxyl-terminal fragment, we determined whether L*XX*LL motif binding influences androgen dissociation of these mutants. Dissociation half-times of [^{3}H]R1881 were determined for TIF2-AR chimeras in which the AR NH_2-terminal region (residues 1–171) containing the F*XX*LF motif was replaced by the L*XX*LL motif region of TIF2 (residues 627–780), and the V715M, H874Y, or T877A mutation was introduced into the ligand binding domain (Table 4). For some of the chimeras, L*XX*AA replaced the TIF2 L*XX*LL motifs to establish L*XX*LL motif dependence. In others, A*XX*AA replaced the AR W*XX*LF motif at residues 433–437, a motif that contributes only weakly to the dissociation rate of bound androgen (18).

TIF2-AR chimeras with L*XX*LL or L*XX*AA TIF2 sequence had faster dissociation half-times ($t_{1/2}$ = 40–48 min) compared with full-length AR ($t_{1/2}$ = 107 min) (Table 4). This reflects the absence of the AR N/C interaction and a weaker interaction of L*XX*LL motifs to AR AF2. Introducing each of the prostate cancer mutations, V715M, H874Y, and T877A, slowed androgen dissociation, but this was independent of L*XX*LL motif binding. A notable exception was V715M, which increased binding of L*XX*AA, suggesting this mutation alters motif binding specificity.

Slow dissociation of androgen from the AR prostate cancer mutants therefore appears to result from inherent changes in the ligand binding domain rather than from increased coactivator L*XX*LL motif binding. The mutations influence the AF2 boundary with the ligand binding pocket to stabilize ligand and for two of the mutants, L*XX*LL motif binding.

Increased Motif Binding in Vitro—GST affinity matrix binding assays were used to examine further the effect of the AR prostate cancer mutations on L*XX*LL and F*XX*LF motif binding. In this assay, the fourth L*XX*LL motif of SRC1 was selected because of its relatively strong binding to the AR ligand binding domain compared with other L*XX*LL motifs (33). ^{35}S-Labeled AR ligand binding domain fragments AR-(624–919) with wild-type or V715M, H874Y, and T877A mutant sequences were incubated with GST-SRC1-IV (SRC1 residues 1139–1441) or GST-AR-F*XX*LF (AR residues 4–52) (Fig. 11). In the presence of DHT or testosterone, prostate cancer mutants AR V715M and H874Y bound the L*XX*LL and F*XX*LF motifs to a greater extent than AR T877A or wild-type AR. The data support the increase in intracellular L*XX*LL motif binding shown in Figs. 7–9 and provide further evidence that prostate cancer mutants V715M and H874Y increase L*XX*LL and F*XX*LF motif binding.

Structure Analysis and Predictions for AR Mutations in Prostate Cancer—Structure of the AR ligand binding domain complexed with R1881 and F*XX*LF or L*XX*LL peptide was analyzed in light of the AR prostate cancer mutations. The Val-715 side chain in AF2 helix 3 faces toward the ligand binding pocket and at its closest distance is ~5.2 Å from Trp-741,[4] a hydrophobic residue in helix 5 that lies directly above and contacts the bound ligand (Fig. 12). A hydrophobic space surrounding Val-715 created by residues Leu-712, Trp-718, Ile-737, Trp-741, Leu-744, and Met-745 appears to readily accommodate the V715M mutation. Compared with valine, the longer, flexible methionine side chain may better fill the space and stabilize interactions with Trp-741, possibly strengthening interactions with the ligand that are further

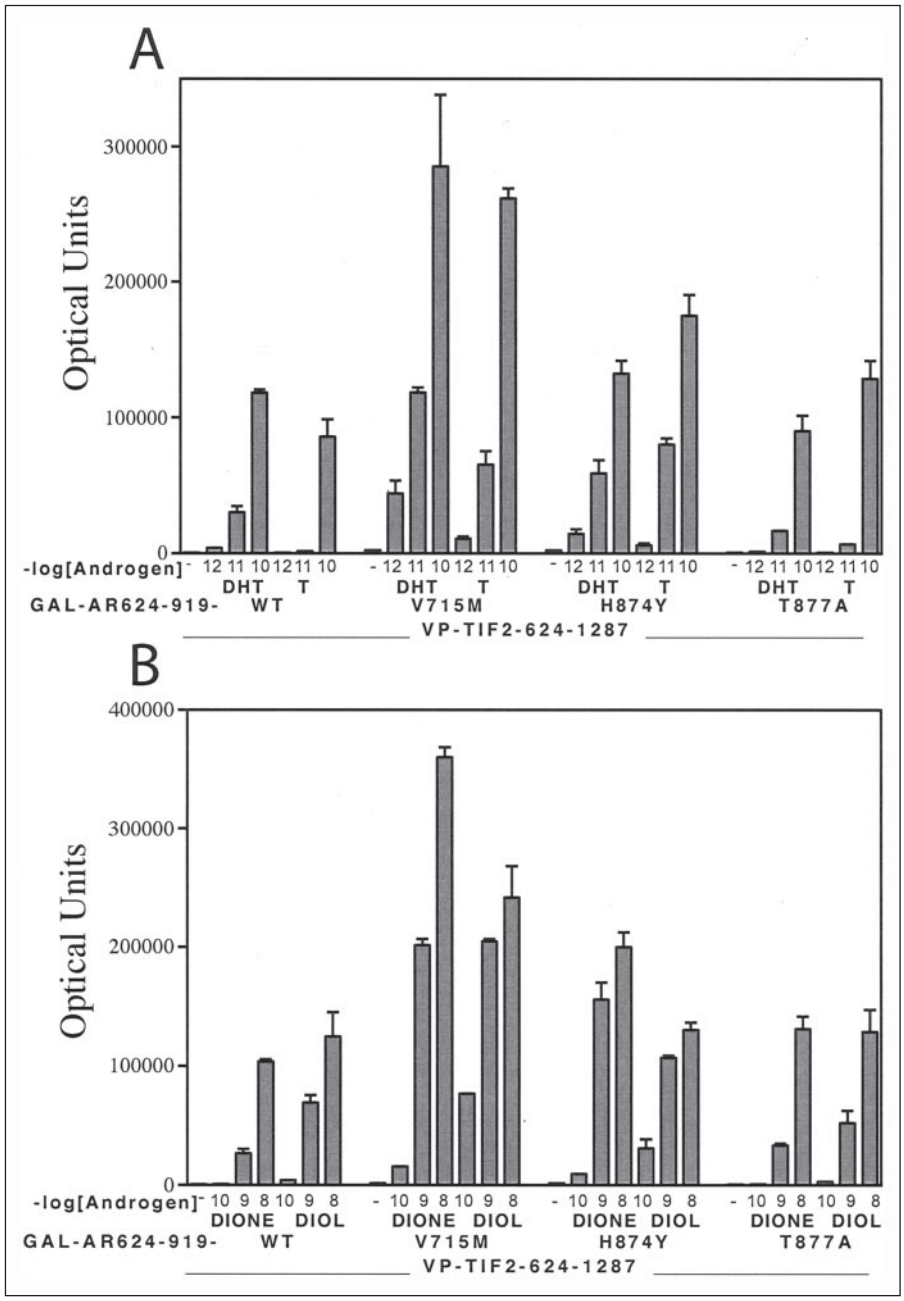

FIGURE 9. **Increase in TIF2 L*XX*LL motif binding by prostate cancer mutations V715M and H874Y.** HeLa cells (5×10^5/well of 12-well plates) were transfected using FuGENE by adding per well, 0.1 μg of 5XGAL4Luc3, 50 ng of GAL-AR-(624–929) containing wild-type or V715M, H874Y, and T877A mutant AR ligand binding domain, and 50 ng of VP-TIF2-(624–1287). Transfected cells were incubated for 24 h in the absence and presence of 0.001, 0.01, and 0.1 nM DHT or testosterone (*T*) (*A*), or 0.1, 1, and 10 nM 4-androstene-3,17-dione (*DIONE*) or 5α-androstane-3α,17β-diol (*DIOL*) (*B*). Luciferase activity and error are representative of three independent experiments.

transmitted toward the AF2 floor through Ile-898. Altered structural changes between Trp-741 and AF2 floor residues may enhance shape complementarity at the AF2 floor and facilitate F*XX*LF and L*XX*LL motif binding.

Located in helix 10, His-874 is on the opposite side of Trp-741 from Val-715 and farther from the bound peptides (Table 2) but about equidistant (5.5 Å) to Trp-741. Through a conserved water, His-874 engages in a solvent-mediated hydrogen bond to the backbone of Trp-741 in helix 5. The H874Y mutation provides more hydrophobicity with a longer hydroxylated phenyl ring that may displace the conserved water and directly hydrogen-bond to a helix 5 backbone atom. Direct hydrogen bonding could stabilize helix 5, strengthen interactions between Trp-741 and the bound ligand, and transmit stabilizing effects to the AF2 floor that enhance F*XX*LF and L*XX*LL motif binding.

Helix 10 residues Thr-877 and His-874 are similar distances from the AF2-bound peptide (Table 2) and like Val-715 are ~5.0 Å from Trp-741. However, in contrast to Val-715 and His-874, Thr-877 has direct contact with the D-ring hydroxyl of bound DHT (34) and R1881 (13) through a 2.9 Å hydrogen bond. In contrast, the slower androgen dissociation rates caused by T877A are associated with a hydrophilic to hydrophobic residue change, loss of a hydrogen bond to the ligand, and no substantial increase in F*XX*LF or L*XX*LL motif binding. It therefore appears that T877A has a different conformational effect on AF2 than that caused by the V715M and H874Y mutations.

The data indicate that all three AR prostate cancer mutations that slow the dissociation rate of bound androgen are positioned near (V715M and H874Y) or in (T877A) the ligand binding pocket and may influence the conformation of Trp-741, a hydrophobic residue that directly contacts the bound ligand. The data suggest that V715M and H874Y impact not only the ligand binding pocket to slow androgen dissociation but also the AF2 binding surface to facilitate L*XX*LL and F*XX*LF motif binding.

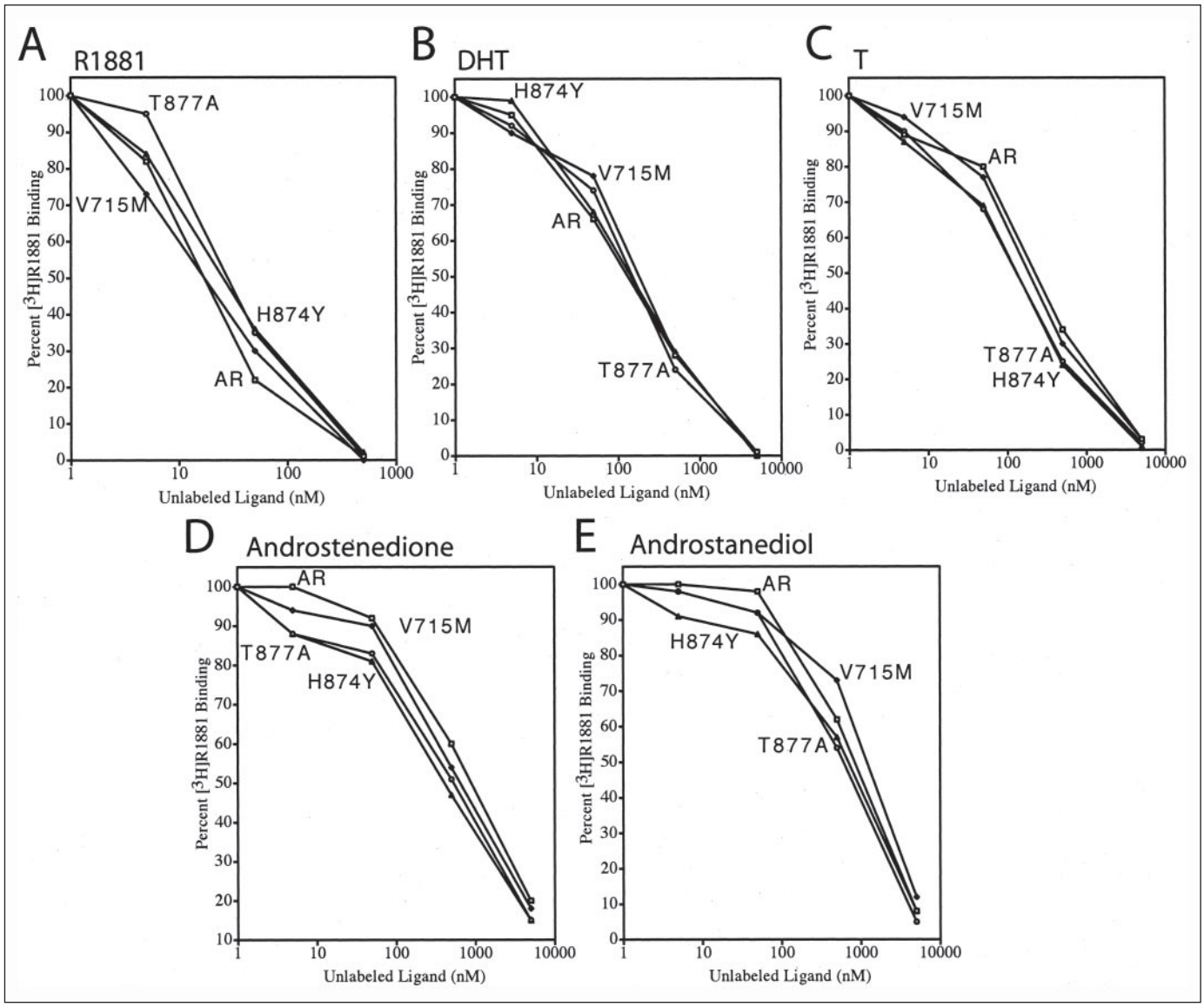

FIGURE 10. **Steroid binding specificity of AR V715M, H874Y, and T877A mutants in prostate cancer.** Competitive binding studies were performed in COS cells (4×10^5/well of 6 well plates) using the DEAE-dextran transfection method as described under "Experimental Procedures" with 2 μg/well pCMVhAR containing wild-type or V715M, H874Y, and T877A mutant sequences. Cells were incubated with 5 nM [^{3}H]R1881 in the absence and presence of increasing concentrations of unlabeled R1881 (*A*), DHT (*B*), testosterone (*T*) (*C*), 4-androstene-3,17-dione (*D*), and 5α-androstane-3α,17β-diol (*E*). Shown are the average percent competitive binding determinations from three independent experiments.

TABLE 4

[^{3}H]R1881 Dissociation of TIF2-AR prostate cancer mutation chimeras

Half-times ($t_{1/2}$ in min) of [^{3}H]R1881 dissociation (Diss) were determined at 37 °C in COS cells for AR and TIF2-AR chimeras containing TIF2-(627–780) L*XX*LL motif region expressed NH_2-terminal in fusion proteins with AR-(172–919), with and without the V715M, H874Y, or T877A mutation. L*XX*AA replaced the three TIF2 L*XX*LL motifs, and AQNAA replaced the WQNLF residues 433–437 AR region. The data are the mean ± S.E. from three independent assays.

	Diss $t_{1/2}$ min
AR	107 ± 5
TIF2(L*XX*LL)$_3$AR-(172–919)-A*XX*AA	48 ± 6
TIF2(L*XX*AA)$_3$AR-(172–919)	40 ± 5
TIF2(L*XX*LL)$_3$AR-(172–919)-A*XX*AA-V715M	77 ± 5
TIF2(L*XX*AA)$_3$AR-(172–919)-V715M	135 ± 24
TIF2(L*XX*LL)$_3$AR-(172–919)-A*XX*AA-H874Y	134 ± 6
TIF2(L*XX*AA)$_3$AR-(172–919)-H874Y	137 ± 18
TIF2(L*XX*LL)$_3$AR-(172–919)-A*XX*AA-T877A	126 ± 16
TIF2(L*XX*AA)$_3$AR-(172–919)-T877A	119 ± 21

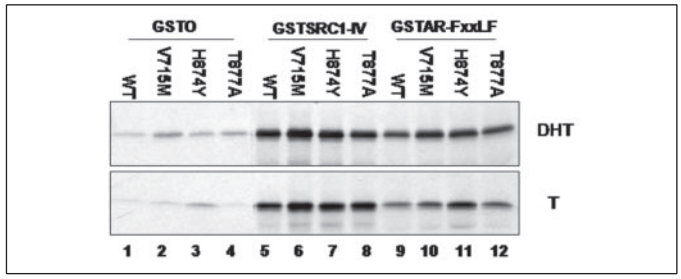

FIGURE 11. **Increased binding of L*XX*LL and F*XX*LF motifs to AR prostate cancer mutants V715M, H874Y, and T877A *in vitro*.** GST affinity matrix binding assays were performed using GST-0 empty parent vector (*lanes 1–4*), GST-SRC1-IV containing the fourth carboxyl-terminal L*XX*LL of SRC1 residues 1139–1441 (*lanes 5–8*), and GST-AR-(4–52) (GST-AR-F*XX*LF) containing the AR F*XX*LF motif in residues 4–52 (*lanes 9–12*). GST-purified extracts were incubated with pcDNA3-HA-AR-(624–919) with wild-type or V715M, H874Y, and T877A mutant sequence in the presence of 1 μM DHT or testosterone (*T*). The bands represent ^{35}S-labeled HA-AR-(624–919) with wild-type or indicated mutant sequence.

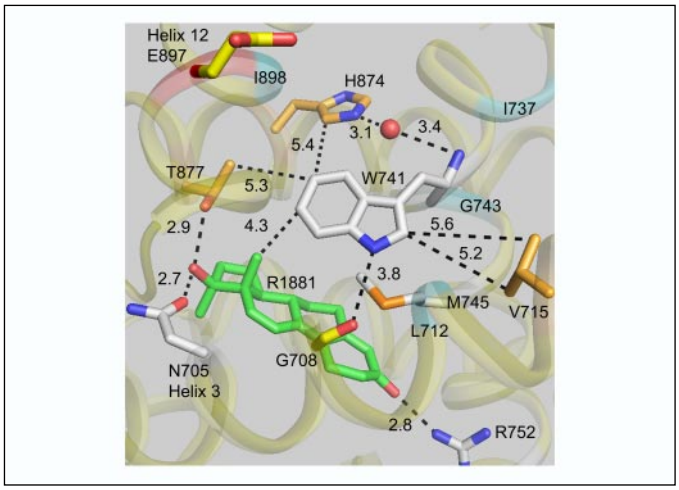

FIGURE 12. **Close up view of the wild-type AR ligand binding pocket region (color scheme from Fig. 4).** Three prostate cancer mutations, V715M, H874Y, and T877A, surround helix 5 residue Trp-741, which lies above R1881 in the steroid-binding site. The V715M mutation contributes a seventh methionine to the predominantly hydrophobic ligand binding pocket. The His-874 side chain engages in a water (*red sphere*)-mediated hydrogen bond to the backbone of Tyr-741. Residue Thr-877 and Asn-705 hydrogen-bond to the C-17 hydroxyl group on the steroid D-ring. Intermolecular distances (Å, *dashed black lines*) are indicated. The backbone of nearby AIS mutations are in *cyan*.

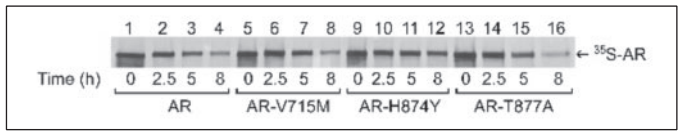

FIGURE 13. **Increased stabilization of AR prostate cancer mutants in the presence of 1 nM testosterone.** Wild-type AR or AR V715M, H874Y, and T877A in pCMVhAR (10 μg/dish) were expressed in COS cells (1.8×10^6 cells/10-cm dish) using the DEAE-dextran transfection method. Cells were placed in serum-free medium without phenol red-free 24 h after transfection, and 24 h after incubation, cells were incubated with 80 μCi of [^{35}S]methionine per plate for 20 min in the presence of 1 nM testosterone. Cells were transferred to serum-free medium containing 2 mM cold methionine and 1 nM testosterone and incubated at 37 °C for 0, 2.5, 5, or 8 h as indicated. Cells were harvested, and AR was immunoprecipitated. Mean AR degradation half-times were determined as described under "Experimental Procedures." The x-ray film was exposed for 3 days and is representative of three independent experiments.

Increased AR Stability—The F*XX*LF motif-mediated AR N/C interaction slows the dissociation rate of bound androgen and stabilizes AR (11, 18, 35). This link between androgen dissociation rate and AR stability is evident with potent androgens such as DHT (20) compared with weaker androgens such as testosterone. AR nevertheless binds testosterone with an equilibrium affinity similar to DHT, but testosterone dissociates more rapidly and is a less effective androgen *in vivo* (20, 31). We therefore investigated whether slower dissociation of testosterone from the AR prostate cancer mutants increased AR stabilization.

AR degradation rates were determined in COS cells at 37 °C by [^{35}S]methionine pulse-chase labeling in the presence of 1 nM testosterone (Fig. 13). The half-time of degradation of wild-type AR ($t_{½}$ = 1.8 ± 0.3 h) was faster than that of AR V715M ($t_{½}$ = 2.8 ± 0.4 h) and AR H874Y ($t_{½}$ = 3.2 ± 0.4 h) but similar to AR T877A ($t_{½}$ = 2.0 ± 0.5 h). The results indicate that even though all three mutations prolonged the androgen dissociation half-time, only V715M and H874Y increased AR stability in the presence of testosterone.

DISCUSSION

Naturally Occurring Mutations Alter the AR AF2 and Ligand Binding Interface—We have characterized naturally occurring AR mutations in the region of the ligand binding pocket and AF2 binding surface for AR F*XX*LF and coactivator L*XX*LL motifs. The mutations increased or decreased AR functional activity *in vivo* without causing significant changes in equilibrium androgen binding affinity. Germ line mutations in AF2 that cause a phenotypic spectrum of AIS increased the androgen dissociation rate and decreased AR F*XX*LF and SRC/p160 coactivator L*XX*LL motif binding to AF2. Conversely, three AR somatic mutations in prostate cancer slowed the dissociation rate of R1881 by 2-fold and testosterone by up to 4.5-fold. Slower androgen dissociation by the prostate cancer mutants was associated with increased AR transcriptional activity, and for AR V715M and H874Y with increased F*XX*LF and L*XX*LL motif binding to AF2. The location and effect of AIS mutation V889M on ligand dissociation suggest a hormone gateway at the base of AF2 helix 12 between helices 3, 6, 10, and 12, where Val-889 serves as gatekeeper. Moreover, the effects of the AIS and prostate cancer mutations implicate Trp-741 as a critical residue in a structural interplay between AF2, bound ligand, and residues neighboring the ligand.

FXXLF and LXXLL Motif Binding to AF2—The AF2 site in steroid receptors is a hydrophobic surface in the ligand binding domain required for hormone-dependent SRC/p160 coactivator L*XX*LL motif binding (4, 5). AR AF2 has a higher affinity for the AR NH_2-terminal F*XX*LF motif than the coactivator L*XX*LL motifs (13). Differences in the apparent relative AR binding affinities for these helical motifs are attributed in part to flanking residues that interfere with motif binding depending on peptide length (4, 36, 37).

Structural studies have shown subtle induced fit differences between the AR AF2 binding surfaces with bound F*XX*LF and L*XX*LL peptides (13). The $i + 1$ motif side chains contact nearly the same side chains in AF2, as do the $i + 5$ side chains, even with the ~2-Å shift in relative position of the two bound peptides. It was therefore not unexpected that AR mutations in AIS and prostate cancer studied here had similar effects on the two motifs, *i.e.* AIS mutations decreased F*XX*LF and L*XX*LL binding, and two of the prostate cancer mutations increased binding of these motifs.

Despite similarities in the AF2 binding surface, it is F*XX*LF motif binding that slows androgen dissociation (18). This is evident by the ~3 times faster androgen dissociation rate of AR-(507–919) compared with full-length AR. AR-(507–919) retains high affinity equilibrium androgen binding but lacks the AR NH_2-terminal region and thus lacks an N/C interaction. Disrupting the AR N/C interaction by mutations in the NH_2-terminal F*XX*LF motif (14) or F*XX*LF motif binding of melanoma antigen gene protein MAGE-11 (36) also increases intracellular androgen dissociation.

The inability of coactivator L*XX*LL motif binding to slow androgen dissociation from AR was evident in previous studies where TIF2 and AR were coexpressed (14) and from the TIF2-AR chimera studies reported here. TIF2-AR chimeras with wild-type AR ligand binding domain had androgen dissociation rates similar to AR-(507–919) and ~2.5 faster than full-length AR. Prostate cancer mutations V715M, H874Y, and T877A slowed androgen dissociation in the chimeras but not in an L*XX*LL motif-dependent manner.

Slower androgen dissociation resulting from F*XX*LF motif binding to AF2 suggests that structural changes are transmitted from AF2 to the ligand binding pocket. However, induced fit conformational changes noted for the side chains of AF2 charge clamp residues Glu-897 and Lys-720, along with Met-734 and Met-894 (13, 38), do not visibly alter the structure of the ligand binding domain core. Clues that Leu-712 and Ile-898 serve as a conduit for transmission of F*XX*LF binding to the ligand binding pocket exist in the ligand dissociation and structural data. Both L712F and I898T in full-length AR and AR-(509–919) increase androgen dissociation. Leu-712 is located 4.0 Å and Ile-898 5.8 Å from the Met-894 sulfur atom in helix 12. The fully engaged charge

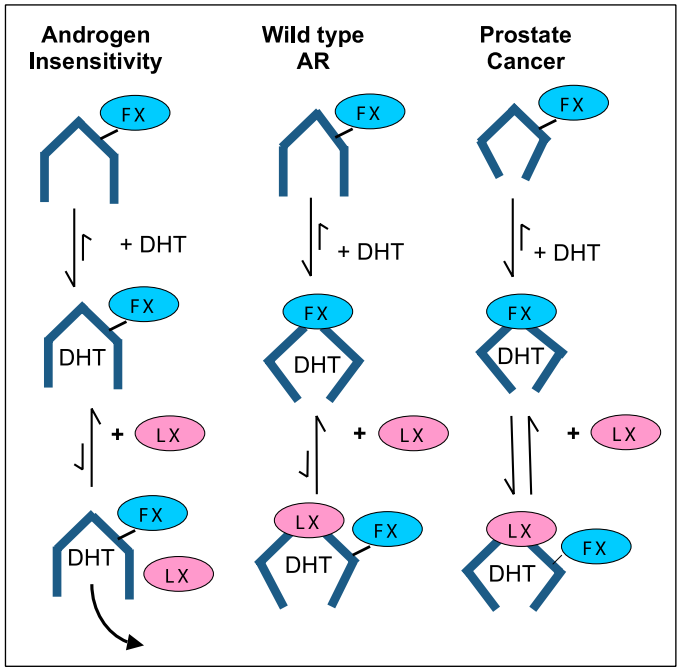

FIGURE 14. **Two-state model of steroid receptor ligand binding and coactivator recruitment.** High affinity agonist binding induces subtle conformational changes in the ligand binding domain that allow for F*XX*LF or L*XX*LL motif binding to AF2. A full agonist effect requires slow ligand dissociation, which is achieved as a result of inherent properties of the ligand (*e.g.* DHT for AR) and is increased by high affinity motif binding to AF2. In the two-state model, high affinity slow dissociating ligands stabilize the active closed state. Faster dissociating ligands that are weaker agonists or antagonists favor the open state. Steroid receptor activity depends on an equilibrium between open and closed states. Naturally occurring AR AF2 mutations impact AR activity *in vivo* by shifting the equilibrium between open and closed states without altering equilibrium agonist binding affinity. AF2 mutations that decrease AR transcriptional activity and cause the androgen insensitivity syndrome (*AIS*) favor the open state, causing more rapid androgen dissociation through effects at the AF2 surface, at the boundary between AF2 and the ligand binding pocket, or more directly at the ligand gateway at the base of AF2 helix 12. In contrast, prostate cancer mutations can increase AR transcriptional activity by favoring the closed state, slowing ligand dissociation and improving F*XX*LF (*FX*) and L*XX*LL (*LX*) motif binding. The effect of AIS and prostate cancer mutations demonstrate ligand-dependent structural communication between AF2 and the ligand binding pocket mediated by subtle changes that the inherent stability of the ligand binding domain. The model suggests steroid receptor activity *in vivo* increases by prolonged retention time of bound ligand.

clamp residues with higher affinity F*XX*LF motif binding may provide a greater stabilizing influence on helix 12 residues such as Met-894 than the more weakly bound L*XX*LL motif that lacks an NH_2-terminal hydrogen bond to charge clamp residue Glu-897 (13, 38). Stabilizing effects passed from helix 12 to Leu-712 and Ile-898 may propagate to Trp-741, which lies above the ligand pocket, resulting in slower ligand dissociation.

In contrast, residues Phe-725, Gln-733, and Ile-737 (group 2) mutated in AIS are situated near Lys-720 in AF2 and $i + 5$ of F*XX*LF and are more remote to the ligand binding pocket. AIS mutations F725L, Q733H, and I737T increase androgen dissociation from full-length AR but not from AR-(507–919), in agreement with two-hybrid assays that the AIS group 2 mutations interfere with F*XX*LF motif binding. Aside from the notable rearrangement of Lys-720, no remarkable structural differences are seen between the $i + 5$ region and the ligand binding pocket when F*XX*LF is bound. This result and their more remote location from the ligand binding pocket suggest that these residues, particularly Phe-725 and Gln-733, stabilize AR primarily by maintaining the bound F*XX*LF motif, which in turn stabilizes the ligand binding core. Residue Ile-737 lies closer to Trp-741 and may more directly influence the ligand binding pocket in response to higher affinity F*XX*LF motif binding. F*XX*LF motif binding also influences the position of the Met-895 side chain that lies close to the steroid D-ring, providing another link in the signal conduit between bound peptide and ligand binding core.

The results from AR and other steroid receptors indicate that motif binding must be high affinity to prolong the half-time of ligand dissociation. The AR F*XX*LF motif peptide binds AF2 with higher affinity than the L*XX*LL motif peptide (13), and it is F*XX*LF motif binding that slows ligand dissociation from AR (14). High affinity coactivator L*XX*LL motif binding to estrogen receptor-α AF2 or in a TIF2-glucocorticoid receptor chimera also slows ligand dissociation (18, 39). This suggests a reciprocal relationship in which ligand binding stabilizes AF2 for motif binding, and high affinity motif binding slows ligand dissociation. The lack of large, defining motif-specific structural differences in the intervening region between AF2 and ligand binding pocket supports the hypothesis that high affinity motif binding imparts subtle stabilizing changes that favor ligand retention, the N/C interaction, coactivator binding, and ultimately receptor activity *in vivo*. Some of the subtle dynamic changes may not be resolved in crystal structures due to rapid kinetics or to the limitations of resolution, precision accuracy in the structure data, and superpositions.

Slow androgen dissociation caused by AR V715M and H874Y in prostate cancer is associated with increased binding of the L*XX*LL and F*XX*LF motifs. T877A, on the other hand, slows androgen dissociation without increasing motif binding. This apparent disconnect for T877A indicates that androgen dissociation slower than that of wild-type AR is not sufficient to increase L*XX*LL motif binding. The structural changes from T877A appear to be limited to the local environment of the ligand binding pocket and are not transmitted to neighboring regions. Similarly, the previously described effects of V730M positioned in AF2 were limited predominantly to the AF2 surface because coactivator L*XX*LL motif binding increased but V730M did not alter androgen dissociation (13). On the other hand, V715M and H874Y are positioned between AF2 and the ligand binding pocket and have bidirectional stabilizing effects on ligand and motif binding. Each of these four mutations increases AR activation in response to the weaker adrenal androgens. Ligand binding domain mutations in prostate cancer can therefore increase AR transcriptional activity through subtle structural changes that favor ligand binding and/or coactivator recruitment.

Structures of the AR ligand binding domain bound to R1881 and F*XX*LF or L*XX*LL motif peptides suggest an induced fit mechanism whereby changes are limited predominantly to side chains in the coactivator binding surface (13). Equilibrium androgen binding affinity was maintained by the AIS and prostate cancer mutants in this study, indicating absence of major structural changes in the interior of the ligand binding domain. We nevertheless observed effects on ligand retention, coactivator recruitment, and receptor activity. A recent computer simulation of the glucocorticoid receptor (GR) investigated the effects of V571M, a residue in GR positioned three residues NH_2-terminal relative to V715M in AR. GR V571M increased transcriptional activity and binding specificity for aldosterone (40). Like V715M and H874Y in AR, V571M is positioned between the coactivator and ligand binding surfaces in GR. The *in silico* molecular dynamic studies of GR V571M predicted changes of less than 0.03 nm, supporting increased coactivator recruitment through subtle structural remodeling in AF2.

A model (Fig. 14) is suggested whereby different functional states of the receptor arise from global changes in structural stability of the ligand binding domain. Ligand binding increases AR stability that is necessary for motif binding to AF2. Receptor activity is augmented by AR mutations such as V715M and H874Y in AF2 and ligand binding boundary region that favor a more stable structural state and slower ligand disso-

ciation and improved AR F*XX*LF or coactivator L*XX*LL motif binding. The active state is achieved by agonist binding and favored by mutations that lend stability through mechanisms such as reduced backbone fluctuations and improved anchoring of helices 3 and 12 as suggested for GR V571M (40). If similar to GR V571M, methionine in the AR prostate cancer mutant V715M might be better accommodated and improve van der Waals interactions that increase overall stability of the ligand binding domain. Increased inherent stability of the ligand binding domain by prostate cancer mutations enhance the AR response to weaker or lower concentrations of androgens. Mutations that decrease structural stability of the ligand binding domain reduce receptor activity in response to circulating androgens and cause AIS. Single amino acid substitutions alter the equilibrium between the active closed state and inactive open state that impacts ligand and coactivator binding and ultimately receptor activity.

Increased Coactivator Recruitment in Prostate Cancer—A number of mechanisms have been proposed to account for AR-mediated increases in cell growth in prostate cancer. These include AR gene amplification (41), increased cross-talk through growth factor signaling pathways (32), increased SRC/p160 coactivator expression (42), and AR mutations. The reported AR mutation rate in prostate cancer varies (43–47) with recent studies suggesting a frequency of ~5% (43, 48–52) that increases in later stages of the disease following androgen withdrawal or anti-androgen therapy (48, 53–55). The low incidence of AR mutations in early stage clinical specimens argues against their role in prostate cancer initiation (54). On the other hand, functional mutations that arise during tumor progression associated with genetic instability suggest positive selection for tumor cell survival (21, 56). Most AR mutants in prostate cancer retain AR transcriptional activity in response to testosterone or DHT, and nearly half the reported mutants are active in response to a range of ligands, including adrenal steroids (21, 25, 28, 52, 57, 58). AR mutations described here can contribute to increased AR functional activity and favor prostate cancer cell survival and expansion through mechanisms that include increased retention time of bound androgen or other steroids, increased SRC/p160 coactivator recruitment, and increased AR stability.

The prostate cancer mutations studied in this report were identified previously in prostate cancer specimens and cell lines (21, 22, 25, 27, 28, 44, 52, 59). T877A occurs in the LNCaP cell line (22, 27) and in multiple specimens of prostate cancer (52). Thr-877 is in the linker region before AF2 helix 12 and in the ligand pocket close to rings C and D of the bound steroid. The T877A mutation increases the space around the steroid D-ring to accommodate other steroids, consistent with the promiscuous ligand binding properties of this mutant (34, 57, 59–62). His-874 in helix 10 is between AF2 and the ligand binding pocket (61, 63) above rings C and D of the bound steroid. H874Y was identified in the CWR22 human prostate cancer xenograft and also displays reduced ligand specificity (21). V715M is in helix 3 at the boundary between AF2 and the steroid A-ring side of the binding pocket and was identified in a poorly differentiated recurrent late stage prostate cancer (25).

The similar effects of H874Y and V715M on androgen dissociation and F*XX*LF and L*XX*LL motif binding may result from different structural influences. H874Y would displace a conserved structural water shown in Fig. 12, which might allow direct hydrogen bonding to the helix 5 backbone. V715M may increase hydrophobic interactions to stabilize ligand binding. It is noteworthy that 6 other methionine residues reside directly in the ligand binding pocket and that His-874 and Val-715 are on opposite sides of AF2, each within ~5 Å of Trp-741, a hydrophobic residue that contacts the ligand and has a role in retaining ligand (10). H874Y and V715M introduce extended hydrophobic side chains that improve interactions with Trp-741 that may prolong ligand retention time by stabilizing Trp-741 and optimizing contacts between Trp-741 and the ligand. T877A also lies ~5 Å from Trp-741. The surprisingly well compensated alanine substitution of T877A forfeits a hydrogen bond to the D-ring of testosterone and DHT (34, 64), supporting the importance of hydrophobic interactions in stabilizing bound ligand. Interactions between Trp-741 and bound ligand may have a role in establishing the DHT and testosterone dissociation rates from wild-type AR.

Prostate cancers are initially androgen-dependent, regress after androgen deprivation therapy, and resume growth after a period of remission despite low circulating androgen (48, 49, 65). AR is expressed in most recurrent prostate cancers (66) and likely contributes to recurrent tumor growth (67, 68). Recent studies have shown DHT levels decline in recurrent prostate cancer tissue following androgen deprivation therapy, whereas testosterone persists at tissue levels similar to benign prostatic hyperplasia (69). AR mutations that slow dissociation of testosterone or weaker adrenal androgens may stabilize the ligand binding domain and facilitate growth of recurrent prostate cancer through AR mechanisms in concert with enhanced mitogen signaling.

Why DHT Is a More Potent Androgen than Testosterone—Our characterization of AIS and prostate cancer AR mutants indicates a functional link between androgen dissociation rate and AR activity that parallels the known physiological potencies of testosterone and DHT. AR binds these two biologically active androgens with similar equilibrium binding affinity (K_d) determined from the ratio of association and dissociation rate constants (31). Yet testosterone dissociates ~3 times faster than DHT. Dissociation of both androgens is slowed by the AR N/C interaction mediated by F*XX*LF motif binding to AF2, which decreases AR degradation and increases androgen-dependent gene activation (11, 16). The importance of prolonged ligand retention for steroid receptor activity is also applicable to estrogen receptor-α, which binds estriol and 17β-estradiol with similar high affinity, but like the relationship between testosterone and DHT, estriol dissociates more rapidly and is a weaker estrogen than 17β-estradiol (70). More recent evidence indicates that removal of the ligand-bound estrogen receptor-α from chromatin through degradation in a transcription-coupled manner is another important mechanism of transcriptional control (71, 72).

A full or amplified agonist response mediated by AR and perhaps other steroid receptors appears to depend on sufficient ligand retention time to maintain structural stability in the ligand binding domain. The human 5α-reductase deficiency syndrome indicates that DHT is required for AR functional activity during embryonic development. Naturally occurring mutations in the human 5α-reductase type 2 gene reduce the conversion of testosterone to DHT, cause ambiguous external sex phenotypes, and reduce prostate size in 46,XY genetic males (73). AR mutations in prostate cancer can slow the dissociation of testosterone to a rate similar to that of DHT, which increases AR stability and transcriptional activity in response to testosterone or other weaker androgens in this disease. Ligand retention time as a key determinant of AR functional activity is supported by the rapid dissociation rates of high affinity AR antagonists (35).

Requirements for AR Stabilization—Most steroid receptors are degraded subsequent to agonist-induced gene activation, presumably as a feedback mechanism to limit the hormone response. AR appears an exception because it is degraded more slowly in the presence of bound androgen (74), and stabilization is linked to increased transcriptional activity *in vivo*. AR degradation increases in response to mutations that increase androgen dissociation and cause AIS (20). Conversely, AR

mutations in prostate cancer can further slow androgen dissociation, stabilize AR, and contribute to increased androgen-dependent and -independent AR activity in prostate cancer. The cancer-testis protein MAGE-11 selectively binds the AR NH_2-terminal F*XX*LF motif and competes for the AR N/C interaction. Binding of MAGE-11 relieves the competitive inhibition of SRC/p160 coactivator L*XX*LL motif binding to AF2 caused by AR F*XX*LF motif binding in the N/C interaction, thereby increasing androgen dissociation and AR turnover. As a result, AR functional activity increases by way of greater SRC/p160 coactivator recruitment (36).

A number of mechanisms involving increased SRC/p160 coactivator recruitment appear to contribute to greater AR activity in clinically recurrent prostate cancer. These include increased expression levels of TIF2 and SRC1 (42) and a broader spectrum of active androgens resulting from mutations like T877A (21, 27) and H874Y (21, 26) and mutations such as V730M that increase coactivator L*XX*LL motif binding without altering the androgen dissociation rate (13). Here we report that AR mutations can provide inherent structural stability to the ligand binding domain, slow androgen dissociation, and improve SRC/p160 coactivator recruitment. SRC/p160 coactivator binding increases receptor-mediated gene activation through the recruitment of CBP/p300 and PCAF for histone acetylation and chromatin remodeling.

Acknowledgment—We thank K. Michelle Cobb for excellent technical assistance.

REFERENCES

1. Glass, C. K., and Rosenfeld, M. G. (2000) *Gene Dev.* **14,** 121–141
2. Simental, J. A., Sar, M., Lane, M. V., French, F. S., and Wilson, E. M. (1991) *J. Biol. Chem.* **266,** 510–518
3. He, B., Bai, S., Hnat, A. T., Kalman, R. I., Minges, J. T., Patterson, C., and Wilson, E. M. (2004) *J. Biol. Chem.* **279,** 30643–30653
4. He, B., and Wilson, E. M. (2003) *Mol. Cell. Biol.* **23,** 2135–2150
5. Darimont, B. D., Wagner, R. L., Apriletti, J. W., Stallcup, M. R., Kushner, P. J., Baxter, J. D., Fletterick, R. J., and Yamamoto, K. R. (1998) *Genes Dev.* **12,** 3343–3356
6. Feng, W., Ribeiro, R. C., Wagner, R. L., Nguyen, H., Apriletti, J. W., Fletterick, R. J., Baxter, J. D., Kushner, P. J., and West, B. L. (1998) *Science* **280,** 1747–1749
7. Moras, D., and Gronemeyer, H. (1998) *Curr. Opin. Cell Biol.* **10,** 384–391
8. Gottlieb, B., Beitel, L. K., Wu, J. H., and Trifiro, M. (2004) *Hum. Mutat.* **23,** 527–533
9. Quigley, C. A., De Bellis, A., Marschke, K. B., El-Awady, M. K., Wilson, E. M., and French, F. S. (1995) *Endocr. Rev.* **16,** 271–321
10. He, B., Kemppainen, J. A., Voegel, J. J., Gronemeyer, H., and Wilson, E. M. (1999) *J. Biol. Chem.* **274,** 37219–37225
11. Langley, E., Kemppainen, J. A., and Wilson, E. M. (1998) *J. Biol. Chem.* **273,** 92–101
12. Spencer, T. E., Jenster, G., Burcin, M. M., Allis, C. D., Zhou, J., Mizzen, C. A., McKenna, N. J., Onate, S. A., Tsai, S. Y., Tsai, M. J., and O'Malley, B. W. (1997) *Nature* **389,** 194–198
13. He, B., Gampe, R. T., Kole, A. J., Hnat, A. T., Stanley, T. B., An, G., Stewart, E. L., Kalman, R. I., Minges, J. T., and Wilson, E. M. (2004) *Mol. Cell* **16,** 425–438
14. He, B., Kemppainen, J. A., and Wilson, E. M. (2000) *J. Biol. Chem.* **275,** 22986–22994
15. Langley, E., Zhou, Z. X., and Wilson, E. M. (1995) *J. Biol. Chem.* **270,** 29983–29990
16. He, B., Lee, L. W., Minges, J. T., and Wilson, E. M. (2002) *J. Biol. Chem.* **277,** 25631–25639
17. He, B., and Wilson, E. M. (2002) *Mol. Gen. Metab.* **75,** 293–298
18. He, B., Bowen, N. T., Minges, J. T., and Wilson, E. M. (2001) *J. Biol. Chem.* **276,** 42293–42301
19. Quigley, C. A., Tan, J. A., He, B., Zhou, Z. X., Mebarki, F., Morel, Y., Forest, M., Chatelain, P., Ritzen, E. M., French, F. S., and Wilson, E. M. (2004) *Mech. Ageing Dev.* **125,** 683–695
20. Zhou, Z. X., Lane, M. V., Kemppainen, J. A., French, F. S., and Wilson, E. M. (1995) *Mol. Endocrinol.* **9,** 208–218
21. Tan, J., Sharief, Y., Hamil, K. G., Gregory, C. W., Zang, D. Y., Sar, M., Gumerlock, P. H., DeVere White, R. W., Pretlow, T. G., Harris, S. E., Wilson, E. M., Mohler, J. L., and French, F. S. (1997) *Mol. Endocrinol.* **11,** 450–459
22. Harris, S. E., Harris, M. A., Rong, Z., Hall, J., Judge, S., French, F. S., Joseph, D. R., Lubahn, D. B., Simental, J. A., and Wilson, E. M. (1991) in *Molecular and Cellular Biology of Prostate Cancer* (Karr, J. P., Coffey, D. S., Smith, R. G., and Tindall, D. J., eds) pp. 315–330, Plenum Publishing Corp., New York
23. Voegel, J. J., Heine, M. J., Tini, M., Vivat, V., Chambon, P., and Gronemeyer, H. (1998) *EMBO J.* **17,** 507–519
24. Feldman, B. J., and Feldman, D. (2001) *Nat. Rev. Cancer* **1,** 34–45
25. Culig, Z., Hobisch, A., Cronauer, M. V., Cato, A. C., Hittmair, A., Radmayr, C., Eberle, J., Bartsch, G., and Klocker, H. (1993) *Mol. Endocrinol.* **7,** 1541–1550
26. Duff, J., and McEwan, I. J. (2005) *Mol. Endocrinol.* **19,** 2943–2954
27. Veldscholte, J., Ris-Stalpers, C., Kuiper, G. G., Jenster, G., Berrevoets, C., Claassen, E., van Rooij, H. C., Trapman, J., Brinkmann, A. O., and Mulder, E. (1990) *Biochem. Biophys. Res. Commun.* **173,** 534–540
28. Peterziel, H., Culig, Z., Stober, J., Hobisch, A., Radmayr, C., Bartsch, G., Klocker, H., and Cato, A. C. (1995) *Int. J. Cancer* **63,** 544–550
29. Mononen, N., Syrjakoski, K., Matikainen, M., Tammela, T. L., Schleutker, J., Kallioniemi, O. P., Trapman, J., and Koivisto, P. A. (2000) *Cancer Res.* **60,** 6479–6481
30. Gruber, S. B., Chen, H., Tomsho, L. P., Lee, N., Perrone, E. E., and Cooney, K. A. (2003) *Prostate* **54,** 306–309
31. Wilson, E. M., and French, F. S. (1976) *J. Biol. Chem.* **251,** 5620–5629
32. Gregory, C. W., Fei, X., Ponguta, L. A., He, B., Bill, H. M., French, F. S., and Wilson, E. M. (2004) *J. Biol. Chem.* **279,** 7119–7130
33. Needham, M., Raines, S., McPheat, J., Stacey, C., Ellston, J., Hoare, S., and Parker, M. (2000) *J. Steroid Biochem. Mol. Biol.* **72,** 35–46
34. Sack, J. S., Kish, K. F., Wang, C., Attar, R. M., Kiefer, S. E., An, Y., Wu, G. Y., Scheffler, J. E., Salvati, M. E., Krystek, S. R., Weinmann, R., and Einspahr, H. M. (2001) *Proc. Natl. Acad. Sci. U. S. A.* **98,** 4904–4909
35. Kemppainen, J. A., Langley, E., Wong, C. I., Bobseine, K., Kelce, W. R., and Wilson, E. M. (1999) *Mol. Endocrinol.* **13,** 440–454
36. Bai, S., He, B., and Wilson, E. M. (2005) *Mol. Cell. Biol.* **25,** 1238–1257
37. Estebanez-Perpina, E., Moore, J. M., Mar, E., Delgado-Rodrigues, E., Nguyen, P., Baxter, J. D., Buehrer, B. M., Webb, P., Fletterick, R. J., and Guy, R. K. (2005) *J. Biol. Chem.* **280,** 8060–8068
38. Hur, E., Pfaff, S. J., Payne, E. S., Gron, H., Buehrer, B. M., and Fletterick, R. J. (2004) *PLoS Biol.* **2,** 1303–1312
39. Gee, A. C., Carlson, K. E., Martini, P. G., Katzenellenbogen, B. S., and Katzenellenbogen, J. A. (1999) *Mol. Endocrinol.* **13,** 1912–1923
40. Carlsson, P., Koehler, K. F., and Nilsson, L. (2005) *Mol. Endocrinol.* **19,** 1960–1977
41. Koivisto, P., Hyytinen, E., Palmberg, C., Tammela, T., Visakorpi, T., Isola, J., and Kallioniemi, O. P. (1995) *Am. J. Pathol.* **147,** 1608–1614
42. Gregory, C. W., He, B., Johnson, R. T., Ford, O. H., Mohler, J. L., French, F. S., and Wilson, E. M. (2001) *Cancer Res.* **61,** 4315–4319
43. Newmark, J. R., Hardy, D. O., Tonb, D. C., Carter, B. S., Epstein, J. I., Isaacs, W. B., Brown, T. R., and Barrack, E. R. (1992) *Proc. Natl. Acad. Sci. U. S. A.* **89,** 6319–6323
44. Taplin, M. E., Bubley, G. J., Shuster, T. D., Frantz, M. E., Spooner, A. E., Ogata, G. K., Keer, H. N., and Balk, S. P. (1995) *N. Engl. J. Med.* **332,** 1393–1398
45. Taplin, M. E., and Ho, S. M. (2001) *J. Clin. Endocrinol. Metab.* **86,** 3467–3477
46. Terouanne, B., Nirde, P., Rabenoelina, F., Bourguet, W., Sultan, C., and Auzou, G. (2003) *Mol. Pharmacol.* **63,** 791–798
47. Tilley, W. D., Buchanan, G., Hickey, T. E., and Bentel, J. M. (1996) *Clin. Cancer Res.* **2,** 277–285
48. Balk, S. P. (2002) *Urology* **60,** 132–138
49. Gelmann, E. P. (2002) *J. Clin. Oncol.* **20,** 3001–3015
50. Heinlein, C. A., and Chang, C. (2004) *Endocr. Rev.* **25,** 276–308
51. Koivisto, P., Kolmer, M., Visakorpi, T., and Kallioniemi, O. P. (1998) *Am. J. Pathol.* **152,** 1–9
52. Shi, X. B., Ma, A. H., Xia, L., Kung, H. J., and de Vere White, R. W. (2002) *Cancer Res.* **62,** 1496–1502
53. Hara, T., Miyazaki, J., Araki, H., Yamaoka, M., Kanzaki, N., Kusaka, M., and Miyamoto, M. (2003) *Cancer Res.* **63,** 149–153
54. Marcelli, M., Ittmann, M., Mariani, S., Sutherland, R., Nigam, R., Murthy, L., Zhao, Y., DiConcini, D., Puxeddu, E., Esen, A., Eastham, J., Weigel, N. L., and Lamb, D. J. (2000) *Cancer Res.* **60,** 944–949
55. Taplin, M. E., Bubley, G. J., Ko, K. J., Small, E. J., Upton, M., Rajeshkumar, B., and Balk, S. P. (1999) *Cancer Res.* **59,** 2511–2515
56. Lengauer, C., Kinzler, K. W., and Vogelstein, B. (1998) *Nature* **396,** 643–649
57. Chang, C. Y., Walther, P. J., and McDonnell, D. P. (2001) *Cancer Res.* **61,** 8712–8717
58. Elo, J. P., Kvist, L., Leinonen, K., Isomaa, V., Henttu, P., Lukkarinen, O., and Vihko, P. (1995) *J. Clin. Endocrinol. Metab.* **80,** 3494–3500
59. Matias, P. M., Carrondo, M. A., Coelho, R., Thomaz, M., Zhao, X. Y., Wegg, A., Crusius, K., Egner, U., and Donner, P. (2002) *J. Med. Chem.* **45,** 1439–1446
60. Krishnan, A. V., Zhao, X. Y., Swami, S., Brive, L., Peehl, D. M., Ely, K. R., and Feldman, D. (2002) *Endocrinology* **143,** 1889–1900
61. Steketee, K., Timmerman, L., Ziel-van der Made, A. C., Doesburg, P., Brinkmann, A. O., and Trapman, J. (2002) *Int. J. Cancer* **100,** 309–317
62. Zhao, X. Y., Malloy, P. J., Krishnan, A. V., Swami, S., Navone, N. M., Peehl, D. M., and Feldman, D. (2000) *Nat. Med.* **6,** 703–706
63. McDonald, S., Brive, L., Agus, D. B., Scher, H. I., and Ely, K. R. (2000) *Cancer Res.* **60,** 2317–2322

64. Matias, P. M., Donner, P., Coelho, R., Thomaz, M., Peixoto, C., Macedo, S., Otto, N., Joschko, S., Scholz, P., Wegg, A., Basler, S., Schafer, M., Egner, U., and Carrondo, M. A. (2000) *J. Biol. Chem.* **275,** 26164–26171
65. Aquilina, J. W., Lipsky, J. J., and Bostwick, D. G. (1997) *J. Natl. Cancer Inst.* **89,** 689–695
66. van der Kwast, T. H., Schalken, J., Ruizeveld de Winter, J. A., van Vroonhoven, C. C. J., Mulder, E., Boersma, W., and Trapman, J. (1991) *Int. J. Cancer* **48,** 189–193
67. Gregory, C. W., Hamil, K. G., Kim, D., Hall, S. H., Pretlow, T. G., Mohler, J. L., and French, F. S. (1998) *Cancer Res.* **58,** 5718–5724
68. Zegarra-Moro, O. L., Schmidt, L. J., Huang, H., and Tindall, D. J. (2002) *Cancer Res.* **62,** 1008–1013
69. Mohler, J. L., Gregory, C. W., Ford, O. H., Kim, D., Weaver, C. M., Petrusz, P., Wilson, E. M., and French, F. S. (2004) *Clin. Cancer Res.* **10,** 440–448
70. Anderson, J. N., Peck, E. J., and Clark, J. H. (1975) *Endocrinology* **96,** 160–167
71. Shang, Y., Hu, X., DiRenzo, J., Lazar, M. A., and Brown, M. (2000) *Cell* **103,** 843–852
72. Lonard, D. M., Nawaz, Z., Smith, C. L., and O'Malley, B. W. (2000) *Mol. Cell* **5,** 939–948
73. Imperato-McGinley, J., Guerrerro, J. L., Gautier, T., and Peterson, R. E. (1974) *Science* **186,** 1213–1215
74. Kemppainen, J. A., Lane, M. V., Sar, M., and Wilson, E. M. (1992) *J. Biol. Chem.* **267,** 968–974
75. Bohl, C. E., Miller, D. D., Chen, J., Bell, C. E., and Dalton, J. T. (2005) *J. Biol. Chem.* **280,** 37747–37754
76. Georget, V., Terouanne, B., Lumbroso, S., Nicolas, J. C., and Sultan, C. (1998) *J. Clin. Endocrinol. Metab.* **83,** 3597–3603
77. Nakao, R., Yanase, T., Sakai, Y., Haji, M., and Nawata, H. (1993) *J. Clin. Endocrinol. Metab.* **77,** 103–107
78. Poujol, N., Lumbroso, S., Terouanne, B., Lobaccaro, J. M., Bourguet, W., and Sultan, C. (2002) *J. Clin. Endocrinol. Metab.* **87,** 5793–5800
79. Hiort, O., Huang, Q., Sinnecker, G. H., Sadeghi-Nejad, A., Kruse, K., Wolfe, H. J., and Yandell, D. W. (1993) *J. Clin. Endocrinol. Metab.* **77,** 262–266
80. Hiort, O., Sinnecker, G. H., Holterhus, P. M., Nitsche, E. M., and Kruse, K. (1998) *J. Pediatr.* **132,** 939–943
81. Holterhus, P. M., Sinnecker, G. H., and Hiort, O. (2000) *J. Clin. Endocrinol. Metab.* **85,** 3245–3250
82. Ahmed, S. F., Cheng, A., Dovey, L., Hawkins, J. R., Martin, H., Rowland, J., Shimura, N., Tait, A. D., and Hughes, I. A. (2000) *J. Clin. Endocrinol. Metab.* **85,** 658–665
83. De Bellis, A., Quigley, C. A., Marschke, K. B., El-Awady, M. K., Lane, M. V., Smith, E. P., Sar, M., Wilson, E. M., and French, F. S. (1994) *J. Clin. Endocrinol. Metab.* **78,** 513–522
84. Essawi, M., Gad, Y. Z., El-Rouby, O., Temtamy, S. A., Sabour, Y. A., and El-Awady, M. K. (1997) *Dis. Markers* **13,** 99–105
85. MacLean, H. E., Ball, E. M., Rekaris, G., Warne, G. L., and Zajac, J. D. (2004) *Hum. Mutat.* **23,** 287
86. Pinsky, L., Trifiro, M., Kaufman, M., Beitel, L. K., Mhatre, A., Kazemi-Esfarjani, P., Sabbaghian, N., Lumbroso, R., Alvarado, C., Vasiliou, M., and Gottlieb, B. (1992) *Clin. Investig. Med.* **15,** 456–472